To the Graduate Council:

I am submitting herewith a dissertation written by Junwu Liu entitled "A Study of Polymer Electrolyte Membranes and Associated Interfacial Systems via Molecular Dynamics Simulations." I have examined the final electronic copy of this dissertation for form and content and recommend that it be accepted in partial fulfillment of the requirements for the degree of Doctor of Philosophy with a major in Chemical Engineering.

_____
David J. Keffer, Major Professor

_____
Stephen J. Paddison, Major Professor

We have read this dissertation
and recommend its acceptance:

_____
Shengting Cui

_____
Brian J. Edwards

_____
James R. Morris

Accepted for the Council:

_____
Carolyn R. Hodges
Vice Provost and Dean of the Graduate School

A STUDY OF POLYMER ELECTROLYTE MEMBRANES AND ASSOCIATED INTERFACIAL SYSTEMS VIA MOLECULAR DYNAMICS SIMULATIONS

A Dissertation
Presented for the
Doctor of Philosophy
Degree
The University of Tennessee, Knoxville

Junwu Liu

December 2009

Acknowledgments

My heartfelt thanks go to Dr. David Keffer, my major advisor, for his guidance, perceptive counsel, and invaluable advice. He always challenged me to learn, think, question, and analyze with patience and persistence. I wish to thank my three knowledgeable and wonderful co-advisors, Dr. Brian Edwards, Dr. Stephen Paddison, and Dr. Shengting Cui, each of whom contributed important and unique perspectives throughout the research development. I sincerely thank their assistance, advice, and willingness to provide thoughtful and detailed feedback at various stages of this research. I express my gratitude to Dr. James Morris for serving on my committee. I would like to thank the Department of Chemical and Biomolecular Engineering for the financial support which made this work possible. I am also grateful to the former department secretaries, Ms. Betty Frazier and Ms. Susan Seymour, for their excellent assistance in the official matters and responsiveness to my information needs. I would like to thank my family and friends, whose suggestions and encouragement were very valuable on the research path. Lastly, I am thankful to all those who helped me complete my Doctor of Philosophy Degree in Chemical Engineering.

Abstract

The development of novel polymer electrolyte membrane (PEM) materials which operate at high temperature (i.e. > 100˚C) and low humidity conditions and efficiently transport protons has been a major focus for PEM fuel cell technology. The motivation behind a high temperature PEM fuel cell is based on the fact that, at high temperature, the catalysts used in the fuel cell are more active and less susceptible to poisoning due to impurities in the feed stream. The challenge lies in the fact that as the temperature is increased, the membrane loses water and its ability to transport protons. The successful design and synthesis of high-performance PEMs would benefit from a fundamental, molecular-scale understanding of how polymer chemistry, hydration levels, and morphology affect proton mobility within the membrane.

Additionally, substantially less work has concentrated on the molecular-level details of proton transport at the multi-phase interfaces among the PEM, vapor, water, electrodes, and catalyst surface. The electrochemical processes occurred at such interfaces dictate the performance of the PEM fuel cells. Understanding the structural and dynamic properties at these interfaces is, therefore, crucial for the optimization of current energy devices. All such information cannot come from experimental investigations alone, but requires knowledge of multiscale simulations which are successful in bridging distinct time and length scales, providing insights into the morphology and structure through analysis of the molecular processes.

The first objective of this work is to use molecular dynamic (MD) simulations to investigate the nanophase-segregated structure in the PEM as a function of polymer chemistry and hydration levels. The variables probed to define polymer chemistry include (1) side chain length, (2) equivalent weight, and (3) molecular weight. We examine the structure in attempts to establish a relationship between the polymer chemical composition and the hydrated morphology and transport properties. The second objective is to use MD simulations to generate the structure of the interfaces involving the PEM within the Membrane-Electrode Assemblies (MEAs). These interfaces include (1) the PEM/vapor interface, (2) the PEM/vapor/catalyst interface, and (3) the PEM/vapor/carbon electrode interface. We examine these interfaces in order to establish an understanding of the structure of these interfaces as a function of water content.

Table of Contents

List of Tables

List of Figures

Chapter 1

Introduction

The electrolyte is a key component of polymer electrolyte membrane (PEM) fuel cells. It functions as a separator between anode and cathode while facilitating proton conduction. When hydrated, such polymeric materials exhibit a nanophase-segregated morphology in which hydrophilic clusters, consisting of sulfonic acid groups, water molecules and other hydrophilic components, are percolated through the hydrophobic phase consisting primarily of polytetrafluoroethylene (PTFE) backbone of the polymer. It is within this hydrophilic domain that ionic conductivity happens: protons dissociate from the sulfonic acid groups, become hydrated and diffuse in the confined water within the hydrophobic matrix.

Clearly, the presence of water is essential for the proton transport. The maintenance of hydration levels is typically through the humidifying of incoming gas streams. The serious problems relevant for the gas humidification include the range of operating temperature and parasitic power losses due to electro-osmotic drag. High temperature operation would improve the kinetics of the fuel cell reactions and catalyst resistance to the poisoning of carbon monoxide and other gas impurities. However, because only at high humidity conditions are these PEMs able to transport protons for the operation of PEM fuel cells[1], the temperatures must be below about 100°C, otherwise it is difficult to keep water inside the membrane. In addition, high humidification can cause flooding of the electrodes and limit access of gases to the catalyst layer. The so-called electro-osmosis involves the transport of one or two water molecules with the protons moving from the anode to the cathode [2]. This can cause a water depleted zone near the anode which hinders the efficient proton conduction, thus creating the power losses in the cell. Although this drawback is compensated partly by hydraulic permeation or backward diffusion, the water management is still a serious problem for the design and synthesis of novel electrolyte materials.

Tremendous efforts have already been expended to improve the fuel cell performance, especially some attempts towards the R & D of polymer materials which can operate at high temperatures and low humidity conditions. The present focus is on Nafion clearly because of its good chemical and mechanical stability, high proton conductivity and widespread application in fuel cell technology. Even though a wealth of theoretical and experimental work has been done to investigate the morphological information of Nafion [3-29], its precise morphology is still of considerable debate. Several morphological models for Nafion have been proposed: micelles of

spherical water clusters [8], lamellar structures[30], sandwich-like structures[31], cylindrical channels[32], and polymer bundles [33]. All these models investigate different structural features but are still difficult to identify conclusively the morphology of the hydrated membranes. Thus, it is difficult to perform only experiments to collect all the required information. At this point, the computational multi-scale modeling and simulations, which are successful in bridging distinct time and length scales, can be a valuable tool to probe the local microscopic structure of the hydrated morphology and the dependence on the hydration levels. Several groups have already studied the system. For example, Vishnyakov and Neimark [34] studied alkali ion transport in hydrated Nafion membranes. They reported the existence of hydrophilic subphase with short-lived bridging mechanism to conduct protons and water. Urata et al. [35] investigated the morphology of hydrated Nafion and found that a continuous aqueous phase existed at 10 wt% water content. Although numerous theoretical and experimental studies have advanced our understanding of the morphology of hydrated membranes, it is still complex and elusive. But undoubtedly, the hydrated morphology is affected by the chemical structure of the polymer materials. Thus, a fundamental, molecular-scale understanding of the relationship between the chemical composition of the PEM and the hydrated morphology would significantly aid in the development of novel, high-performance materials.

Substantial studies of molecular modeling [34-61] have been presented to understand the relationship between polymer structure and diffusion properties of various species such as water and protons. For example, how the side chain length affects the membrane properties was early reported by Dow Chemical which originally synthesized the short side-chain (SSC) PFSA membrane with similar polymeric backbone to Nafion but disparate side chain -$OCF_2CF_2SO_3H$ to investigate the effects of side chain length on the hydrated morphology and proton mobility. The comparison revealed that these two membranes have similar morphology[62, 63] but SSC PFSA membrane has the improved performances such as superior proton conductivity and lower bulk resistance at low to intermediate hydration levels [64, 65]. Our MD simulations in the present work indicated that the SSC PFSA membranes tend to produce a more dispersed cluster distribution at low to intermediate hydration levels and these distinctions will become smaller at higher water contents. The flexibility difference of the sulfonic acid terminated side chains

clearly gives rise to the qualitative differences of the hydrated morphology and the proton conduction.

In addition to the variation in the side-chain length between Nafion and SSC PFSA membranes, there are other features of the polymer structure exploited to improve membrane properties. For example, Jalani and Datta[66] probed the effects of water activity on water sorption behavior through the comparison of Nafion membranes of three different equivalent weights (EWs): 960, 1100, and 1200. They observed that the membrane will absorb more water as EW is decreased and the difference becomes greater at higher relative humidity. In electronic structure calculations of two side chain fragments of the SSC ionomer, Paddison and Elliott[42] found that the separation distance of sulfonic acid groups on the polymeric backbone affects the minimum amount of water necessary to facilitate the proton(s) transfer to the first hydration shell and the character of the hydrated proton. Two extreme cases were reported by Jang et al.[51] to study the effects of monomeric sequence on the polymer structure and the ionic transport. One case has the side chains evenly spaced on the backbone; the other has all the side chains aggregated at one end of the polymer. They found that the transport of water molecules with the latter case is larger than with the former, consistent with their observation that the latter blocky case leads to larger aqueous clusters.

One of challenges for MD simulations is to ensure a fully equilibrated configuration, since the timescales required for equilibration of long polymers is prohibitive or beyond the timescale accessible to MD. The molecular weight distributions for the Nafion polymer in real membranes has been given in the $10^5 – 10^6$ g/mol range [67]. This molecular weight translates into a degree of polymerization (DP) between about DP = 90 - 900 for a typical Nafion membrane of EW 1100. But due to computational limits, all MD simulations chose system much smaller than those used in real applications, such as that of Vishnyakov and Neimark, and that of Urata *et al.*, both using oligomers containing 10 monomers [35, 46]. Hristov and Paddision *et al.* [61], in their recent paper, used one macromolecule with forty monomer units. In the present work, we modeled two different Nafion chains, i.e. Nafion with three side chains (trimer) and with 15 side chains, which will allow us to evaluate the effect of molecular weight (MW) at least in this small chain limit.

In the present work, MD simulations were performed to investigate the relationship between the chemical composition of the PEMs and the resulting proton and water diffusion properties, since the chemical composition affects the hydrated morphology, thus controlling the proton and water conduction. The differences in the hydrated morphology resulting from the variation of the PEM chemical composition and the effects of these changes on proton transport are probed through the variation of three parameters: (i) side chain length, (ii) equivalent weight (EW measured in grams of dry polymer per mole of SO_3^- ion exchange functional groups), and (iii) polymeric molecular weight (MW).

Another achievement of this work is the characterization and analysis of the structural and dynamic properties at the interfaces present in the Membrane-Electrode Assemblies (MEAs) through MD simulations. Improving the performance of PEM fuel cells requires molecular-scale understanding of the physical, electrochemical, and electrocatalytical phenomena at these interfaces and relating these processes to the performance of MEAs.

In a typical PEM fuel cell, the anode and cathode of the Membrane-Electrode Assembly (MEA) are composed of electrically conductive carbon particles packed together into a porous diffusion layer. The molecular H_2 (O_2) diffuses through the anode (cathode) to a "catalyst layer". The catalyst layer is composed of catalyst nano-particles deposited on either the outer layer of the electrode or the outer surface of the PEM. A film of ionomer is also present in the catalyst layer to provide paths for proton transport from the catalyst nano-particles to the PEM. This ionomer can be low molecular weight oligomers of the same polymer electrolyte that composes the PEM. Key to the functioning of PEM fuel cell is the presence and careful management of water. The PEM only conducts protons when hydrated. In all likelihood, the ionomer film in the catalyst layer also requires water to conduct protons. Therefore there are a variety of interfaces involving the ionomer/polymer electrolyte that can be present in the MEA, depending upon where one looks and the amount of water in the system. The PEM can have an interface with a vapor phase at low water contents or a liquid water phase at high water contents. The PEM has an interface with the catalyst particles and with the carbon electrode themselves.

Understanding the processes occurred at the interfaces between the hydrated membrane and the electrodes (carbon-supported Pt nanoparticles) is one of the challenges to optimize the fuel cell performance. However, less work has concentrated on the molecular and atomistic-level

details of proton transport at the interfaces and how proton conduction is affected by the distribution of water at the interfaces. In aqueous solution, a relatively clear molecular-level picture of water close to a catalyst-containing electrode was given through a combination of experiment and simulation [68, 69]. Lamas *et al.* [70], by using MD simulation, investigated the configurational and dynamic properties of water near the catalyst surface as a function of Nafion content.

We simulated two interfaces in the present work. The first is the three-phase interface between the hydrated membrane, the vapor, and the surface of the catalyst support. The second is the three-phase interface between the hydrated membrane, the vapor, and the surface of the catalyst particle. We reported on the structure and dynamics of these two interfaces, which include the solid surfaces.

The proton transport across these interfaces is anticipated to be dependent on a pathway bridging the catalyst surface and hydrated membrane. Thus, one parameter we investigated in the present work is the critical gap size in the pathway beyond which efficient proton transport can not occur.

In summary, the overall focus of this work is to investigate the effects of chemical composition and structure of PEMs on the membrane hydrated morphology and the associated interfaces within the MEAs of PEM fuel cells. Chapters 2, 3, and 4 describe the effects of modified polymer structure on the hydrated morphology and proton conduction through classical MD simulation methodology. Chapters 5 and 6 probe the structural and dynamic properties of the interfacial systems present in the PEM fuel cells and give the critical gap size between the hydrated membrane and the catalyst surface through which the efficient proton transport will occur.

In chapter 2, we performed MD simulations to investigate the hydrated morphology and proton diffusion properties of Nafion with three monomer units (trimer) as a function of different hydration levels. It has been demonstrated that the water cluster size strongly depends on the water contents.

In chapter 3, we performed MD simulations to probe the effects of the length of the side chain on the proton transport by comparing Nafion and SSC PFSA membranes with the same backbone. This serves to isolate the effect of the differing side chain lengths. The differences of

the hydrated morphology and of the cluster size and intercluster connectivity for Nafion and SSC membrane have been observed. Such qualitative differences are due to the flexibility difference of the pendant side chains of the PFSA materials.

In chapter 4, we performed MD simulations to explore the effects of polymer structure (side chain length, equivalent weight and molecular weight) on the hydrated morphology and proton diffusion at different hydration levels by using Nafion and SSC ionomers, each ionomer containing 15 monomer units. Through the analysis of snapshots of the system, pair correlation functions, histograms of hydronium ion hydration, cumulative probability distributions for water cluster size, and self-diffusivities, etc., a complete and consistent picture of how the structure and chemistry of the PEM membrane affect the hydrated morphology and proton diffusion is provided.

In chapter 5, MD simulations were conducted to probe the structural and dynamic properties of the interfacial systems present in the PEM fuel cells: the interfaces at the membrane/vapor/carbon electrode, and the interface at the membrane/vapor/catalyst. The difference of wetting ability between catalyst and graphite surfaces is illustrated and the structural and dynamic properties of water on the catalyst surface are also presented.

In chapter 6, we performed MD simulations to find the critical gap size between the hydrated membrane and the catalyst surface through which the protons can traverse. The smallest gap size through which the efficient transport can occur is provided. The implication is that catalyst particles that are not within a certain distance from either the proton exchange membrane or recast ionomer in the electrode leading to the membrane do not possess a path for efficient proton transport to the membrane and consequently do not contribute significantly to power production in the fuel cell.

Finally, in chapter 7, the main conclusions are summarized for each work described in this dissertation.

References

(1) K. D. Kreuer, *ChemPhysChem*, **2002**. 3, 771-775.

(2) M. Ise, K. D. Kreuer, and J. Maier, *Solid State Ionics*, **1999**. 125, 213-223.

(3) A. Eisenberg, *Macromolecules*, **1970**. 3, 147-154.

(4) K. D. Kreuer, *J. Membr. Sci.*, **2001**. 185, 29-39.

(5) M. Falk, *Can. J. Chem.*, **1980**. 58, 1495-1501.

(6) R. Duplessix, M. Escoubes, B. Rodmacq, F. Volino, E. Roche, A. Eisenberg, and M. Pineri, in *Water in Polymers*, S. P. Rowland, Editor; American Chemical Society: Washington DC, 1980.

(7) B. Rodmacq, J. M. Coey, M. Escoubes, E. Roche, R. Duplessix, A. Eisenberg, and M. Pineri, in *Water in Polymers*, S. P. Rowland, Editor; American Chemical Society: Washington DC, 1980.

(8) T. D. Gierke, G. E. Munn, and F. C. Wilson, *J. Polym. Sci.: Polym. Phys. Ed.*, **1981**. 19, 1687-1704.

(9) W. Y. Hsu and T. D. Gierke, *J. Membr. Sci.*, **1983**. 13, 307-326.

(10) H. L. Yeager and A. Steck, *J. Electrochem. Soc.*, **1981**. 128, 1880-1884.

(11) M. W. Verbrugge and R. F. Hill, *J. Electrochem. Soc.*, **1990**. 137, 886-893.

(12) G. Gebel, *Polymer*, **2000**. 41, 5829-5838.

(13) P. J. James, J. A. Elliott, T. J. McMaster, J. M. Newton, A. M. S. Elliott, S. Hanna, and M. J. Miles, *J. Mater. Sci.*, **2000**. 35, 5111-5119.

(14) A. L. Rollet, G. Gebel, J. P. Simonin, and P. Turq, *J. Polym. Sci. B-Polym. Phys.*, **2001**. 39, 548-558.

(15) M. Fujimura, T. Hashimoto, and H. Kawai, *Macromolecules*, **1981**. 14, 1309-1315.

(16) M. Fujimura, T. Hashimoto, and H. Kawai, *Macromolecules*, **1982**. 15, 136-144.

(17) M. D. Heaney and J. Pellegrino, *J. Membr. Sci.*, **1989**. 47, 143-161.

(18) A. Lehmani, S. Durand-Vidal, and P. Turq, *J. Appl. Polym. Sci.*, **1998**. 68, 503-508.

(19) Z. Porat, J. R. Fryer, M. Huxham, and I. Rubinstein, *J. Phys. Chem.*, **1995**. 99, 4667-4671.

(20) M. Eikerling, A. A. Kornyshev, and U. Stimming, *J. Phys. Chem. B*, **1997**. 101, 10807-10820.

(21) V. K. Datye, P. L. Taylor, and A. J. Hopfinger, *Macromolecules*, **1984**. 17, 1704-1708.

(22) K. A. Mauritz, C. J. Hora, and A. J. Hopfinger, in *Ions in Polymers*, A. Eisenberg, Editor; American Chemical Society: Washington DC, 1980.

(23) K. A. Mauritz and C. E. Rogers, *Macromolecules*, **1985**. 18, 483-491.

(24) B. Dreyfus, *Macromolecules*, **1985**. 18, 284-292.

(25) J. A. Elliott, S. Hanna, A. M. S. Elliott, and G. E. Cooley, *Macromolecules*, **2000**. 33, 4161-4171.

(26) Y. K. Tovbin, *Zhurnal Fizicheskoi Khimii*, **1998**. 72, 55-59.

(27) Y. K. Tovbin and N. F. Vasyatkin, *Colloid Surf. A*, **1999**. 158, 385-397.

(28) S. K. Young, S. F. Trevino, and N. C. Beck Tan, *J. Polym. Sci.*, **2002**. 40, 387-400.

(29) E. J. Roche, M. Pineri, R. Duplessix, and A. M. Levelut, *J. Polym. Sci., Part B: Polym. Phys.*, **1981**. 19, 1-11.

(30) M. H. Litt, *Polym. Prepr.*, **1997**. 38, 80.

(31) H. G. Haubold, T. Vad, H. Jungbluth, and P. Hiller, *Electrochimica Acta*, **2001**. 46, 1559-1563.

(32) K. Schmidt-Rohr and Q. Chen, *Nat. Mater.*, **2008**. 7, 75-83.

(33) L. Rubatat, A. L. Rollet, G. Gebel, and O. Diat, *Macromolecules*, **2002**. 35, 4050-4055.

(34) A. Vishnyakov and A. V. Neimark, *J. Phys. Chem. B*, **2001**. 105, 9586-9594.

(35) S. Urata, J. Irisawa, A. Takada, W. Shinoda, S. Tsuzuki, and M. Mikami, *J. Phys. Chem. B*, **2005**. 109, 4269-4278.

(36) A. Venkatnathan, R. Devanathan, and M. Dupuis, *J. Phys. Chem. B*, **2007**. 111, 7234-7244.

(37) S. J. Paddison and T. A. Zawodzinski, *Solid State Ionics*, **1998**. 113–115, 333-340.

(38) S. J. Paddison, L. R. Pratt, and T. A. Zawodzinski, *J. New Mater. Electrochem. Syst.*, **1999**. 2, 183-188.

(39) S. J. Paddison, R. Paul, and T. A. Zawodzinski, *J. Electrochem. Soc.*, **2000**. 147, 617-626.

(40) S. J. Paddison and R. Paul, *Phys. Chem. Chem. Phys.*, **2002**. 4, 1158-1163

(41) S. J. Paddison, R. Paul, and K. D. Kreuer, *Phys. Chem. Chem. Phys.*, **2002**. 4, 1151-1157.

(42) S. J. Paddison and J. A. Elliott, *J. Phys. Chem. A*, **2005**. 109, 7583-7593.

(43) S. J. Paddison and J. A. Elliott, *Phys. Chem. Chem. Phys.*, **2006**. 8, 2193-2203.

(44) S. J. Paddison and J. A. Elliot, *Solid State Ionics*, **2007**. 178, 561-567.

(45) J. A. Elliott, S. Hanna, A. M. S. Elliott, and G. E. Cooley, *Phys. Chem. Chem. Phys.*, **1999**. 1, 4855-4863.

(46) A. Vishnyakov and A. V. Neimark, *J. Phys. Chem. B*, **2000**. 104, 4471-4478.

(47) A. Vishnyakov and A. V. Neimark, *J. Phys. Chem. B*, **2001**. 105, 7830-7834.

(48) E. Spohr, P. Commer, and A. A. Kornyshev, *J. Phys. Chem. B*, **2002**. 106, 10560-10569.

(49) P. Commer, A. G. Cherstvy, E. Spohr, and A. A. Kornyshev, *Fuel Cells*, **2002**. 2, 127-136.

(50) M. Eikerling, S. J. Paddison, and T. A. J. Zawodzinski, *J. New Mater. Electrochem. Syst.*, **2002**. 5, 15-23.

(51) S. S. Jang, V. Molinero, T. Cagin, and W. A. Goddard, *J. Phys. Chem. B*, **2004**. 108, 3149-3157.

(52) R. Paul and S. J. Paddison, *J. Phys. Chem. B*, **2004**. 108, 13231-13241.

(53) S. I. J. Urata, A. Takada, W. Shinoda, S. Tsuzuki, and M. Mikami, *J. Phys. Chem. B*, **2005**. 109, 17274.

(54) R. Paul and S. J. Paddison, *J. Chem. Phys.*, **2005**. 123, 224704.

(55) M. K. Petersen and G. A. Voth, *J. Phys. Chem. B* **2006**. 110, 18594-18600.

(56) S. J. Paddison, *J. New Mater. Electrochem. Syst.*, **2001**. 4, 197-207.

(57) N. P. Blake, M. K. Petersen, G. A. Voth, and H. Metiu, *J. Phys. Chem. B* **2005**. 109, 24244.

(58) S. J. Paddison and J. A. Elliott, *Solid State Ionics*, **2006**. 177, 2385.

(59) R. Devanathan, A. Venkatnathan, and M. Dupuis, *J. Phys. Chem. B*, **2007**. 111, 8069-8079.

(60) R. Devanathan, A. Venkatnathan, and M. Dupuis, *J. Phys. Chem. B*, **2007**. 111, 13006-13013.

(61) I. H. Hristov, S. J. Paddison, and R. Paul, *J. Phys. Chem. B*, **2008**. 112, 2937-2949.

(62) J. Halim, F. N. Buchi, O. Haas, M. Stamm, and G. G. Scherer, *Electrochim. Acta*, **1994**. 39, 1303-1307.

(63) G. Gebel and R. B. Moore, *Macromolecules*, **2000**. 33, 4850-4855.

(64) C. A. Edmondson, P. E. Stallworth, M. E. Chapman, J. J. Fontanella, M. C. Wintersgill, S. H. Chung, and S. G. Greenbaum, *Solid State Ionics*, **2000**. 135, 419-423.

(65) K. Prater, *J. Power Sources*, **1990**. 29, 239-250.

(66) N. H. Jalani and R. Datta, *J. Membr. Sci.*, **2005**. 264, 167-175.

(67) D. E. Curtin, R. D. Lousenberg, T. J. Henry, P. C. Tangeman, and M. E. Tisack, *J. Power Sources*, **2004**. 131, 41-8.

(68) H. Ogasawara, B. Brena, D. Nordlund, M. Nyberg, A. Pelmenschikov, L. G. M. Pettersson, and A. Nilsson, *Phys. Rev. Lett*, **2002**. 89, 276102.

(69) I. Benjamin, *Modern Aspects of Electrochemistry*, **1997**. 31, 115-179.

(70) E. J. Lamas and P. B. Balbuena, *Electrochim. Acta*, **2006**. 51, 5904-5911.

Chapter 2

A molecular dynamics study of a Nafion polyelectrolyte membrane and the aqueous phase structure for proton transport

This part is a slightly revised version of a paper by the same title published in the *Journal of physical Chemistry B* in 2007 by Shengting Cui, Junwu Liu, Myvizhi Esai Selvan, David Keffer, Brian Edwards, William Steele:

S.T. Cui; J.W. Liu; M.E. Selvan; D.J. Keffer; B.J. Edwards, and W.V. Steele, "A Molecular Dynamics Study of a Nafion Polyelectrolyte Membrane and the Aqueous Phase Structure for Proton Transport", *J. Phys. Chem. B*, **111**(9) 2007 p. 2208-2218.

The use of "we" in this part refers to the co-authors and the author of this dissertation. My primary contributions to this paper include (1) running all of the simulations, and (4) preparing almost all the plots and the tables.

Abstract

A molecular dynamics simulation study of hydrated Nafion at water contents ranging from 5 to 20 wt % was performed to examine the structure and dynamics of the hydrated polyelectrolyte system. The simulations show that the system forms segregated hydrophobic regions consisting primarily of the polymer backbone and hydrophilic regions with an inhomogeneous water distribution. We find that the water clustering strongly depends on the water content. At low water content, only isolated small water clusters are formed. As the water content increases, it becomes increasingly possible that a predominant majority of water molecules form a single cluster, suggesting that the hydrophilic regions become connected. We characterize the atomic structures formed within the system by various atomic pair correlation functions. The water structure factor shows a peak at q values corresponding to an intercluster distance about 2.5 nm and greater. With increasing water content, the distance moves to larger values, consistent with findings from scattering experiments. We find that the degree of solvation of hydronium ions by water molecules is a strong function of water content. At 5 wt %, a majority of the hydronium ions are hydrated by no more than two water molecules, prohibiting structural diffusion. As water content increases, the hydronium ions continue to become increasingly hydrated, resulting in structures capable of forming eigen ions, a necessary step in structural diffusion. Addressing the experimentally observed fact that conductivity in these

membranes abruptly drops near 5 wt %, we find that both the local structure of the poorly hydrated hydronium ions and the disconnected nature of the global morphology of the water nanonetwork at low water content should contribute to poor conductivity.

2.1 Introduction

Proton transport through polyelectrolyte exchange membranes is an important practical issue in fuel cell design. In recent years, there has been an increased interest in understanding the fundamental processes of proton transport in these membranes [1, 2]. Many experimental studies, including neutron scattering, X-ray scattering, and other methods, have been carried out in attempts to understand the transport processes from structural and dynamical perspectives [3-25]. In hydrated Nafion membranes, the morphology of the membrane consists of segregated hydrophobic (consisting of the backbone of the polymer) and hydrophilic (consisting of water and the charged side groups of the polymer) regions. However, despite the abundance of literature on the topic, there still does not exist a clear consensus on the molecular-level morphology of hydrated Nafion and its dependence on such parameters as degree of hydration. The morphology of the latter structure is closely related to the proton-transfer process.

On the basis of experimental findings, various models [7-9, 26-32] have been proposed to describe the proton transport mechanism. In the cluster-network model of Gierke and Hsu [7, 8], water organizes into spherical clusters of ~3−5 nm in diameter, which are connected by cylindrical channels ~1 nm in diameter. In the three-dimensional model of Tovbin and Vasyatkin [31, 32] the sulfonate groups of the polymer organize into bilayers, which form pores where the water clusters reside. However, the long-range organization of the pores remains an open question. Spherical cluster formation is also assumed in the three-phase model of Yeager and Steck [9] which consists of the fluorocarbon, the side-chain interface, and the water phases. Central among the models is the formation of water clusters [4]. Less clear is how the clusters connect and form a continuous network to accomplish the transfer of protons.

In recent years, a number of molecular simulation studies of hydrated polymer electrolyte membranes have been published [4, 33-45], however, a clear picture regarding the cluster morphology and its connectivity has not been attained. For example, Vishnyakov and Neimark [33] studied water clustering for hydrated Nafion and found that at 12.5 wt % water and a cutoff

distance of 4.5 Å, the aqueous subphase consisted of disconnected clusters of about 100 molecules in size. On the basis of the observation, the authors suggested the water and ion transport is accomplished by short-lived dynamic bridges instead of the channels between clusters. In contrast, Urata et al. [42] studied the morphology of the hydrated Nafion membrane and found using the same cutoff that a continuous aqueous phase existed at 10 wt % hydration. These authors, however, did not report the distribution of the cluster size. In this study, we investigate the hydrated Nafion membrane morphology with a quantitative cluster size distribution as a function of water content.

For the bulk aqueous solution, there has been significant progress toward understanding the proton transport process through both experiment and quantum mechanical computational studies. It has been generally established that the Zundel ion and Eigen ion complexes induced by proton sharing in aqueous solutions significantly enhance the proton transport process [46, 47] via the Grotthuss Mechanism [48] also referred to as structural diffusion, proton shuttling, and proton hopping. These works indicate the critical importance of the local hydrogen bonding between the hydronium ions and water molecules in facilitating the transport of protons in bulk aqueous systems.

In Nafion membranes, proton hopping can still take place, but the bulk water mechanism is perturbed by a lack of a bulklike water structure. It is known that proton transport strongly depends on water content, perhaps as a result of water cluster formation and the increased probability of Zundel and Eigen ion formation [1, 2]. It is thus clearly important to understand the local structure of the hydronium ion hydration and the global structure of water cluster formation in the Nafion membrane materials. For this aim, we carried out molecular dynamics simulations on systems consisting of Nafion polymer chains, hydronium ions, and water. We examine in detail the hydration of the polymers and the hydronium ions and the formation of water clusters. We discuss in this context the implication of the hydronium hydration on the possibility of the formation the Zundel and Eigen ion complexes. By examination of the cluster distribution and the dependence on the degree of hydration, we hope to shed some light on the issue of cluster networks and connectivity in polyelectrolyte membranes.

In short, while the hydrated Nafion system has been extensively studied, the contribution of this work is to provide a comprehensive analysis of the global morphology and the local

structure and describe the consequences of these configurations on both the vehicular and structural diffusion of hydronium ions. The various measures that are evaluated in this manuscript include configuration snapshots, pair correlation functions, structure factors, cluster histograms, hydronium ion hydration histograms, hydronium ion hydration lifetimes, and mean square displacements.

2.2 Molecular Models and Method

The chemical formula for a monomer of the Nafion polyelectrolyte molecule is [49]

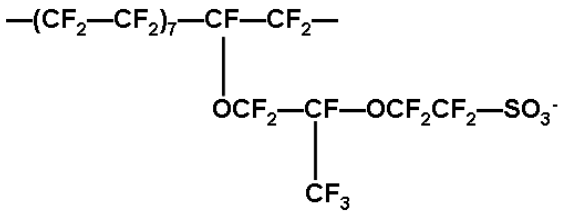

The monomer unit of the molecule consists of a backbone of CF_X groups and a side chain with two ether linkages ending in a sulfonate group. In our simulations, the polyelectrolyte molecules are composed of three monomers. Thus, each molecule has 3 side groups and 48 CF_X groups along the backbone. The backbone is terminated by CF_3 groups at the ends.

For computational efficiency, we used the united atom model for all CF_X groups in the Nafion polyelectrolyte molecules. The potential model for Nafion has been published in previous studies by other authors [35, 37, 43, 50-53]. Consistent with the united atom model for the CF_X groups, we used the Lennard-Jones parameters developed for the CF_X groups by Cui et al. [50, 51]. The backbone does not carry electric charge and interacts only via Lennard-Jones and intramolecular interactions. The bond lengths, bond angles, and partial charges for the side group are given in ref 37. The force constants for bond stretching and bond angle bending are taken from Gejji et al. [52] and Cornell et al. [53]. The torsional potential is from ref 43. Intramolecular sites on the same molecule separated by more than three bonds, and sites on different molecules also interact via nonbonded interactions, including the Lennard-Jones and the electrostatic (between charged sites) interactions.

The water is modeled using the TIP3P model [54, 55] with a flexible OH bond [53]. The model for hydronium ions, H_3O^+, is similar to that of Urata et al. [42]. In particular, the partial charges for the oxygen and hydrogen atoms are taken from Urata et al. [42]. The bond distance,

bond angles, and the force constants are the same as in the TIP3P model and are from refs 53−55. In the calculation of nonbonded interactions, the Lennard-Jones interaction is treated using a cutoff distance of 10 Å. The electrostatic interaction is treated with a site−site reaction field method that has been proven to be accurate [56, 57]. In this method, the Coulombic interaction between charged sites is calculated within a distance of 10 Å, and the reaction field contribution is treated with a uniform background counter charge. This method has been demonstrated to be accurate for modeling aqueous ionic solutions [56, 57]. We have chosen to use a relatively short Nafion polymer (3 monomers as compared to, for example, 10 monomers in Urata et al. [42], because the fluorinated backbone of Nafion makes it a stiff polymer. As a result, it has a relatively long relaxation time compared to a hydrocarbon of the same backbone length, which increases dramatically with chain length. Because of finite computational resources, we cannot simulate for even one relaxation time of a polymer with ten monomers. Faced with this fact, one must make a choice between insufficient sampling of a longer chain and more reliable sampling of a shorter chain. Our choice to model the shorter chain is based on the approach that the model necessarily approximates reality, but the method should be reliable and reproducible. Regardless, we have thoroughly compared our results with published simulation work, such as that of Urata et al. [42], to determine the effect of chain length, before we decided that 3 monomers was adequate.

In this study of hydrated Nafion, we included 64 polyelectrolyte molecules (192 monomers) and 192 H_3O^+, which are required to neutralize the charges. We examined the properties of the system for water contents of 5, 10, 15, and 20% of the Nafion polyelectrolyte, which correspond to the λ ratio (defined as the number of water molecules to the number of SO_3^- groups) of 4.44, 6.42, 9.63, and 12.83, respectively. This resulted in 660, 1040, 1656, and 2272 water molecules, corresponding to 7932, 9072, 10920, and 12768 total interaction sites in the simulations. The densities and water contents were chosen based on experimentally measured values [58]. For the four levels of hydration, the experimentally determined overall densities of the system are 1.95, 1.87, 1.80, and 1.74 g/cm^3. All simulations were carried out at a temperature of 300 K, and the production runs were at least 2 ns in length.

We carried out constant NVT simulations for this system. The equations of motion were integrated using the r-RESPA method [59] with a time step of 2.0 fs for the large time step and

0.2 fs for the intramolecular motions. The temperature was maintained at a constant value using the Nosé−Hoover thermostat [60-62].

The initial configurations were created by placing molecular centers of all the molecules in the system on cubic lattice points within the simulation volume. All the atoms were initially given zero size by setting their corresponding Lennard-Jones parameters to zero. A molecular dynamics simulation was performed for 10 000 time steps in which the Lennard-Jones size parameters were gradually increased to their full values. In this way, initial configurations with non-overlapping atoms were created efficiently. Equilibration using these initial configurations was then carried out for at least 2 ns before any production runs were begun.

2.3 Results and Discussion

In this work, we examine the structure and dynamics of hydrated Nafion. The various measures that are evaluated in this manuscript include configuration snapshots, pair correlation functions, structure factors, cluster histograms, hydronium ion hydration histograms, hydronium ion hydration lifetimes, and mean square displacements. We begin the discussion with snapshots of equilibrated configurations. In parts a−d of Figure 2.1 (see Appendix A, page31), we show the snapshots of typical configurations of the hydrated Nafion for water contents of 5, 10, 15, and 20%, respectively. These snapshots generally confirm the hypothesis that the hydrated Nafion is segregated into hydrophobic and hydrophilic regions. The hydrophobic regions are constituted by the backbones of the Nafion polymer, and the hydrophilic regions are constituted by water molecules and the hydronium ions, as well as the head group of the side chains. The figures clearly show that the sulfonate groups tend to be located at the interface between the clusters and the hydrophobic regions. The hydronium ions, as displayed in green, are essentially always associated with water molecules. (See Table 2.1 (see Appendix A, page 28) for the average hydration number per hydronium ion). Visual inspection suggests that at low water content, 5% by weight, the water molecules are dispersed as clusters of a few water molecules and the connectivity between the clusters is poor. As the water content increases, the cluster size increases, as does the connectivity. We defer more detailed quantitative analysis of the clusters to section 2.3.6.

We next present various pair correlation functions (PCF) in the hydrated Nafion system. These pair correlation functions are important for several reasons. They provide information on polymer configuration (S−S correlations), on hydration of the sulfonic acid group ($S-O_{H2O}$), on the water network ($O_{H2O}-O_{H2O}$), and on the hydration of hydronium ions ($O_{H3O+}-O_{H2O}$). This last PCF is particularly interesting since proton motion via structural diffusion is closely tied to the hydration structure of the hydronium ion.

We note that previously, Urata et al. [42] studied the sulfur−sulfur, sulfur−water, water−water, and ether oxygen−water correlation functions. In this study, we conducted a more extensive examination of the atomic pair correlation functions in order to gain insight into the structure of hydrated Nafion membranes, and in particular, we examined the sulfonate−hydronium and water−hydronium correlation functions. These additional PCFs shed some light on the structural characteristics of Zundel and Eigen ions, which are essential for proton transfer. Where possible, we have compared our PCFs with those of Urata et al. [42] in order to evaluate the effect of our shorter chains.

2.3.1 Pair Correlation Functions of the Sulfonate Group with Water and Hydronium.

Parts a and b of Figure 2.2 show the pair correlation functions for the oxygen atoms on the sulfonate group and the oxygen on H_2O and H_3O^+, respectively. We see two peaks at the interatomic distances of 2.9 and 5.2 Å for H_2O and 2.7 and 5.0 Å for H_3O^+, respectively. The first peak corresponds to the closest contact (the first hydration shell) between the oxygen atoms. The second peak corresponds to the second hydration shell. For the first peak, its magnitude for H_3O^+ is more than twice that of water. This can be explained by the strong electrostatic interaction between the positively charged H_3O^+ and negatively charged sulfonate oxygen. There is also a second peak between the oxygen of the sulfonate group and the oxygen of H_3O^+, corresponding to the oxygen atoms of the two groups being separated by a layer of water molecules. The existence of the second hydration peak between the sulfur and the H_3O^+ suggests that the hydronium ions are not completely bound to the sulfonate groups at all times, even though they are oppositely charged. Solvent separation of the hydronium and sulfonate ions have been previously suggested from statistical mechanical models of proton transport in Nafion [63, 64]. Solvent separation has also been observed in quantum mechanical calculations of hydrated

Nafion [65]. Similar solvent separated ion pair second peak was observed in previous MD work [44]. In ref 44, it is suggested that it is essential to have a reactive potential in order to describe solvent separation. In this work, we do not have a reactive potential and we observe solvent separation. We do not observe the "artificial peak" attributed to nonreactive potentials cited in ref 44. The hydronium ion can dissociate from the sulfonate group and is surrounded by water molecules.

The correlation functions between the sulfur atom of the sulfonate group and the oxygen atom of the H_2O and H_3O^+ are related to those for the oxygen of the sulfonate group and are shown in parts c and d of Figure 2.2. The first peaks occur at about 4 Å, and the sulfur atoms cannot be in direct contact with H_2O and H_3O^+ because of the oxygen atoms of the sulfonic acid group. In Table 2.1, we list the average hydration number around the sulfonate group. It shows that the average number of H_3O^+ in the first hydration shell (contact ions) decreases with water content, while the number of water molecules increases with the water content. The increased water content increases the average number of water molecules around a sulfonate group and augments the solvation power of water and is thus more likely to pull the hydronium ion away from the sulfonate anion site. The magnitude of the peaks in Figure 2.2 varies from one water content value to the next. These magnitudes in part reflect a bias inherent in the pair correlation function, in that, for example, the $S-O_{H2O}$ $g(r)$ is normalized by the average water density, which changes with water content. One way to eliminate this bias is to integrate the pair correlation function up to a given distance, showing the number of molecules within that distance. The hydration shell of H_2O and H_3O^+ about the S atom is shown in Figure 2.3. Here we see that as one increases the water content in the system, the number of H_2O hydrating a sulfur atom steadily increases, while the number of H_3O^+ near the sulfur atom steadily decreases. Thus, the ions become more separated by the solvent, as more H_2O hydrates both the SO_3^- and the H_3O^+ ions.

2.3.2 H_2O-H_2O Pair Correlation Functions.

Figure 2.4 shows the water oxygen−oxygen correlation function. The first peak occurs at 2.8 Å, corresponding to the closest contact of the two oxygen atoms. There is also a small second peak for the 5% water content, occurring at an interatomic distance of 3.7 Å. As the water

content increases, the second peak becomes a shoulder and almost completely disappears. Similar behavior was also seen in the study of Urata et al. [42]. The peak positions are consistent with published bulk simulation predictions for the TIP3P model [54, 55].

Many experiments have been carried out to study the characteristics of water clusters and cluster distribution. Using the calculated $g(r)$ value for water, we estimated the structure factor based on the expression

$$S(q) = 1 + \frac{4\pi N}{V} \int [g(r) - 1] \frac{\sin qr}{q} r dr \qquad (1)$$

The results are shown in Figure 2.5 for the water content values studied. A peak in the structure factor represents a "characteristic length scale" in the system, in this case, the "intercluster spacing" or the average distance between centers of clusters. For 5 wt % water, we observe a peak in the structure factor for 5 wt % water at a value of q corresponding to approximately 24 Å. Our data suggests that, for increasing water content, the peak shifts to lower q values. At 10 wt % water, for example, the peak occurs at a q value corresponding to a characteristic length of 26 Å, and for higher water contents the peak continues to move to smaller q (corresponding to larger intercluster distances, in agreement with established experimental findings by scattering experiments). Since our system is roughly 60 Å in each dimension, we are limited to modeling clusters up to half that size (30 Å) in this study and thus cannot say whether it is due to a complete phase segregation or a cluster of the same size.

It is important to understand that this characteristic length of twenty-odd Å does not translate into a model in which the aqueous subphase is composed of spheres of 24 or 26 Å in diameter. Rather this length scale is composed of a characteristic aqueous subphase size plus the spacing of hydrophobic phase between them. Thus the actual water clusters can be much smaller than this, as shown in parts a and b of Figure 2.1.

2.3.3 H_2O−H_3O^+ Pair Correlation Function.

Parts a−c of Figure 2.6 show the pair correlation functions between the H_2O and H_3O^+ at various water contents. In Figure 2.6a, we show the oxygen−oxygen correlation function between water and hydronium. The first peak occurs at about 2.6 Å, and the second peak occurs at a distance of 5.0 Å. There is also a slight peak at 7.6 Å. The first peak height decreases with

water content, suggesting a decreased binding of water molecules to the hydronium ion caused by increased solvation effect when more water molecules are present. The solvent effect has been understood from potential of mean force theory [57, 66]. Parts b and c of Figure 2.6 show the pair correlation function between oxygen and hydrogen of H_2O and H_3O^+; Figure 2.6b for water oxygen and hydronium hydrogen and Figure 2.6c for water hydrogen and hydronium oxygen. Although the atomic species are the same, the two pair correlation functions are clearly different. In Figure 2.6b, the two prominent peaks occur at distances of about 1.6 and 2.9 Å. In Figure 2.6c, the two peaks occur at 3.3 and 5.5 Å. The peak heights are also dramatically different. The pair correlation functions suggest that the water molecules around a hydronium ion are oriented in such a way that the oxygen atom is pointed toward the hydronium, while the hydrogen atoms are pointed away from the hydronium. This rules out the configuration where the oxygen of the hydronium forms a hydrogen bond with the hydrogen of the water molecules, which would produce a peak at 1.6 Å. This can be understood from the electrostatics: since the hydronium ion is positively charged, and the hydrogen of the water molecule carries a positive partial charge, the hydrogen atoms of the water molecules are pushed away from the hydronium.

2.3.4 Hydration of the Hydronium Ions.

Since the hydronium ions are the counterions of the sulfonate group of the polymer, they tend to be near the sulfonate ions. At the same time, these ions can also be hydrated by highly polar water molecules. The hydration numbers for some of the atoms in the polymer and the hydronium are listed in Table 2.1. It is seen that the hydration number increases with the water content. This simply reflects the fact that there are more water molecules available as the water content increases. By comparison of the sulfonate group and the hydronium, the hydration peak of the hydronium is much higher. One reason is that the hydronium, being a free molecule, is accessible by water molecules in all directions, whereas part of the surrounding volume of sulfur is exclusive to water molecules due to intramolecular connectivity. The other is due to the tighter binding of water molecules at the shorter distance to the hydronium, which is reflected in the narrower distribution of the hydronium−water oxygen distribution (Figure 2.6a).

In Figure 2.7a, we show the probability of finding a fixed number of water molecules around a hydronium ion with a radial distance less than 3.2 Å, which includes most of the first

peak in the pair correlation function. Several features are notable from this histogram. This figure clearly shows that there is a shift in the hydration distribution to higher values as the water content is increased. The probability of finding a H_3O^+ with only 1 or 2 waters within this radius strictly decreases with increasing water content. This histogram has relevance to the process of structural diffusion, which relies on the presence of an Eigen ion, requiring at least 3 waters within a 3.2 Å radius. In other words, all of the H_3O^+ with 2 or fewer waters around them are incapable of structural diffusion. In the case of 5% water, 56% of the hydronium ions have 2 or fewer waters around them. This structure can explain in part the low proton conductivity experimentally observed near 5% water. We also see that, regardless of the global morphology of the water nanonetwork, the pair correlation function can provide direct information relevant to the process of structural diffusion.

Figure 2.7b shows the lifetime of the hydrated hydronium complexes with none to greater than three water molecules. The monotonic decrease of the lifetime of the complex with increased hydration can be interpreted through the decreased binding energy of the water molecules to the hydronium. The hydration time is roughly in the range of picoseconds, which is sufficiently long for proton transfer to occur between the hydronium and a hydration water molecule. Experiments suggest that the lifetime of Zundel and Eigen ions is less than about 0.1 ps [67]. We do not see the strong dependence of the dynamics of hydronium hydration on water content as we did for the structure of the hydronium hydration in Figure 2.7a.

2.3.5 Sulfur−Sulfur Correlation Function.

The sulfur−sulfur correlation functions are displayed in parts a−c of Figures 2.8. Figure 2.8a shows the total correlation functions, and parts b and of Figure 2.8 show the intramolecular and intermolecular components of the correlation function. As shown, the correlation function displays a peak at approximately 4.0 Å. From parts b and c of Figure 2.8, it is seen that the peak is largely due to the intramolecular sulfur−sulfur correlation. At low water content, the sulfur−sulfur intermolecular correlation function shows that the sulfur atoms have a tendency to stay closer together, probably due to the higher population of smaller water clusters, as discussed below.

The non-monotonic trend of the intramolecular component of the S−S pair correlation function is the sole qualitative discrepancy between this work and the previous work of Urata et al. [42]. We attribute this difference to the fact that our chains contained 3 monomers, while those of Urata et al. [42] contained 10 monomers. In our case, we have far fewer intramolecular interactions, resulting in a larger degree of statistical uncertainty in this specific property. In these simulations, we found no other property significantly affected by chain length.

2.3.6 Water Cluster Distribution.

For a clear visualization of the clusters and their connectivity, we show in parts a−d of Figure 2.9 the snapshots of Figure 2.1 without the polymers. Interactive structures are available on the web [68], where the ability to rotate the structure enables the eye to appreciate more fully the nature of the structure. In all cases, the water network is composed of many narrow, interconnecting nanochannels. For 5% water content, these figures show that the water molecules are dispersed and that there are many voids. At high water content, there are fewer voids and the water molecules in the clusters appear to be more densely packed. To characterize the clusters quantitatively, we calculated the cluster size distribution using cutoff distances of 3.5, 4.5, and 5.5 Å. Two water molecules (including the hydronium ions) are deemed to belong to the same cluster if their intermolecular distance is determined to be smaller than the cutoff distance. These are displayed in parts a−d of Figure 2.10. The 3.5-Å distance roughly includes all water molecules in the first hydration shell, and the 4.5 Å distance also includes the second hydration shell. In the figures, we plotted the number of clusters vs the cluster size. The inset shows the total number of molecules (including both water and hydronium) corresponding to the particular cluster size. We include the inset because the histogram itself shows large peaks at small cluster sizes. This is misleading in terms of the distribution of molecules among clusters, since small clusters contain very few molecules. The insets show the distribution on a molecular basis.

At 15 and 20% water content, we see from the insets in parts c and d of Figure 2.10 that, regardless of cutoff distance in the cluster definition, the vast majority of the molecules exist in a single sample-spanning cluster. The few remaining molecules are in small isolated clusters of less than 20 molecules. At 10% water content, the same is true only for the 4.5 and 5.5 Å cutoffs. For the small cutoff, most of the molecules are now in small clusters of 20 or less. At 5 wt %

water content, a single large cluster only for the 5.5-Å cutoff. For the two smaller cutoffs, we see numerous small clusters.

The trend is clear. If we focus on the 4.5-Å cutoff we see a single large cluster for 10, 15, and 20% water content. However, at 5 wt % we do not. This morphology can explain in part the experimentally observed drop in proton conductivity near 5 wt % water.

By combining the information in Figures 2.9 and 2.10, we come to the following description of the morphology of the water nanonetwork in this hydrated Nafion membrane. At low water content, 5 wt %, there are many small isolated water clusters in the membrane. At higher water contents, there is generally a single large water cluster. Smaller clusters dynamically detach and coalesce with the larger cluster. By the definition of cluster used in this study, the fact that the water (and hydronium) essentially form a single cluster reflects the connectivity of water channel networks in the system. There is, however, a significant amount of inhomogeneity in terms of water density distribution. In connection with experiment, the high-density regions would contribute more to the scattering. The average distance between the high-density regions corresponds to the experimentally observed peak in the structure factor.

We should also point out that our results for the cluster distribution are qualitatively different than those of Vishnyakov and Neimark [33]. They found small clusters at 12.5 wt % using the 4.5 Å cutoff. One explanation for the difference may be that they used potassium as the cation, rather than a hydronium ion. The stronger electrostatic interaction of the potassium ion may have served to localize the water around them.

2.3.7 Diffusion.

We calculated the diffusion coefficient of water and the hydronium ions based on the Einstein relation. The results are presented in Table 2.3. Since our model for hydronium ions does not include the transfer of protons between the hydronium ions and the water molecules, the diffusion coefficient for hydronium does not include the Grotthuss mechanism. Here we simply report the vehicular diffusivities. A more accurate determination of the hydronium diffusion will be addressed in a future publication. Without the structural diffusion effect, the hydronium diffusion is significantly slower than that of the water molecules, because the hydrated water molecules around the hydronium ions significantly increase the effective size of the hydronium

ions. Another factor is the relatively immobile sulfonate groups, which tend to bind to the hydronium and thus slow down the diffusion of the ion. The diffusion coefficient calculated for water molecules compares very well with that measured in experiment [69]. The water diffusion coefficient is significantly smaller than in bulk water, caused by the existence of the barriers in the membrane between clusters and the constraint of the boundary at the interface between the water cluster and the polyelectrolyte. The diffusivities of both water and the hydronium ion increase with increasing degree of hydration.

2.4 Conclusions

We have performed a molecular dynamics simulation study of hydrated Nafion at water contents ranging from 5 to 20 wt % to examine the structure and dynamics of the hydrated polyelectrolyte system. The simulations showed that the system forms segregated hydrophobic regions consisting primarily of the polymer backbone and hydrophilic regions with an inhomogeneous water distribution. We found that the water clustering strongly depended on the water content. At low water content, only isolated small water clusters were formed. As the water content increased, it became increasingly possible that a predominant majority of water molecules formed a single cluster, suggesting that the hydrophilic regions became connected. The morphology of the aqueous nanonetwork showed an interconnecting matrix of thin water channels. We characterized the atomic structures formed within the system by various atomic pair correlation functions. We found that the degree of solvation of hydronium ions by water molecules was a strong function of water content. At 5 wt %, a majority of the hydronium ions were hydrated by 2 or fewer water molecules, prohibiting structural diffusion. As water content increased, the hydronium ions continued to become increasingly hydrated, resulting in structures capable of forming eigen ions, a necessary step in structural diffusion. Addressing the experimentally observed fact that conductivity in these membranes abruptly drops near 5 wt %, we found that both the local structure of the poorly hydrated hydronium ion and the disconnected nature of the global morphology of the water nanonetwork at low water content can be contributing factors to poor conductivity.

2.5 Acknowledgment

The work is supported by a grant from the U.S. Department of Energy (DOE) BES under Contract No. DE-FG02-05ER15723. This research used resources of the Center for Computational Sciences at Oak Ridge National Laboratory, which is supported by the Office of Science of the DOE under Contract DE-AC05-00OR22725.

References

(1) K. D. Kreuer, S. J. Paddison, E. Spohr, and M. Schuster, *Chem. Rev.*, **2004**. 104, 4637-4678.

(2) S. J. Paddison, *Annu. Rev. Mater. Res.*, **2003**. 33, 289-319.

(3) M. Falk, *Can. J. Chem.*, **1980**. 58, 1495-1501.

(4) A. Eisenberg, *Macromolecules*, **1970**. 3, 147-154.

(5) R. Duplessix, M. Escoubes, B. Rodmacq, F. Volino, E. Roche, A. Eisenberg, and M. Pineri, in *Water in Polymers*, S. P. Rowland, Editor; American Chemical Society: Washington DC, 1980.

(6) B. Rodmacq, J. M. Coey, M. Escoubes, E. Roche, R. Duplessix, A. Eisenberg, and M. Pineri, in *Water in Polymers*, S. P. Rowland, Editor; American Chemical Society: Washington DC, 1980.

(7) T. D. Gierke, G. E. Munn, and F. C. Wilson, *J. Polym. Sci.: Polym. Phys. Ed.*, **1981**. 19, 1687-1704.

(8) W. Y. Hsu and T. D. Gierke, *J. Membr. Sci.*, **1983**. 13, 307-326.

(9) H. L. Yeager and A. Steck, *J. Electrochem. Soc.*, **1981**. 128, 1880-1884.

(10) M. W. Verbrugge and R. F. Hill, *J. Electrochem. Soc.*, **1990**. 137, 886-893.

(11) G. Gebel, *Polymer*, **2000**. 41, 5829-5838.

(12) P. J. James, J. A. Elliott, T. J. McMaster, J. M. Newton, A. M. S. Elliott, S. Hanna, and M. J. Miles, *J. Mater. Sci.*, **2000**. 35, 5111-5119.

(13) P. J. James, T. J. McMaster, J. M. Newton, and M. J. Miles, *Polymer*, **2000**. 41, 4223-4231.

(14) K. D. Kreuer, *J. Membr. Sci.*, **2001**. 185, 29-39.

(15) H. G. Haubold, T. Vad, H. Jungbluth, and P. Hiller, *Electrochimica Acta*, **2001**. 46, 1559-1563.

(16) A. L. Rollet, G. Gebel, J. P. Simonin, and P. Turq, *J. Polym. Sci. B-Polym. Phys.*, **2001**. 39, 548-558.

(17) A. L. Rollet, O. Diat, and G. Gebel, *J. Phys. Chem. B*, **2002**. 106, 3033-3036.

(18) S. K. Young, S. F. Trevino, and N. C. B. Tan, *J. Polym. Sci. B-Polym. Phys.*, **2002**. 40, 387-400.

(19) M. Fujimura, T. Hashimoto, and H. Kawai, *Macromolecules*, **1981**. 14, 1309-1315.

(20) M. Fujimura, T. Hashimoto, and H. Kawai, *Macromolecules*, **1982**. 15, 136-144.

(21) E. J. Roche, M. Pineri, R. Duplessix, and A. M. Levelut, *J. Polym. Sci. B-Polym. Phys.*, **1981**. 19, 1-11.

(22) M. D. Heaney and J. Pellegrino, *J. Membr. Sci.*, **1989**. 47, 143-161.

(23) J. A. Elliott, S. Hanna, A. M. S. Elliott, and G. E. Cooley, *Macromolecules*, **2000**. 33, 4161-4171.

(24) A. Lehmani, S. Durand-Vidal, and P. Turq, *J. Appl. Polym. Sci.*, **1998**. 68, 503-508.

(25) Z. Porat, J. R. Fryer, M. Huxham, and I. Rubinstein, *J. Phys. Chem.*, **1995**. 99, 4667-4671.

(26) M. Eikerling, A. A. Kornyshev, and U. Stimming, *J. Phys. Chem. B*, **1997**. 101, 10807-10820.

(27) V. K. Datye, P. L. Taylor, and A. J. Hopfinger, *Macromolecules*, **1984**. 17, 1704-1708.

(28) K. A. Mauritz and C. E. Rogers, *Macromolecules*, **1985**. 18, 483-491.

(29) K. A. Mauritz, C. J. Hora, and A. J. Hopfinger, in *Ions in Polymers*, A. Eisenberg, Editor; American Chemical Society: Washington DC, 1980.

(30) B. Dreyfus, *Macromolecules*, **1985**. 18, 284-292.

(31) Y. K. Tovbin, *Zhurnal Fizicheskoi Khimii*, **1998**. 72, 55-59.

(32) Y. K. Tovbin and N. F. Vasyatkin, *Colloid Surf. A*, **1999**. 158, 385-397.

(33) A. Vishnyakov and A. V. Neimark, *J. Phys. Chem. B*, **2001**. 105, 9586-9594.

(34) X. D. Din and E. E. Michaelides, *AIChE J.*, **1998**. 44, 35-47.

(35) J. A. Elliott, S. Hanna, A. M. S. Elliott, and G. E. Cooley, *Phys. Chem. Chem. Phys.*, **1999**. 1, 4855-4863.

(36) A. Vishnyakov and A. V. Neimark, *J. Phys. Chem. B*, **2000**. 104, 4471-4478.

(37) A. Vishnyakov and A. V. Neimark, *J. Phys. Chem. B*, **2001**. 105, 7830-7834.

(38) R. Jinnouchi and K. Okazaki, *J. Electrochem. Soc.*, **2003**. 150, E66-E73.

(39) E. Spohr, P. Commer, and A. A. Kornyshev, *J. Phys. Chem. B*, **2002**. 106, 10560-10569.

(40) P. Commer, A. G. Cherstvy, E. Spohr, and A. A. Kornyshev, *Fuel Cells*, **2002**. 2, 127-136.

(41) S. S. Jang, V. Molinero, T. Cagin, and W. A. Goddard, *J. Phys. Chem. B*, **2004**. 108, 3149-3157.

(42) S. Urata, J. Irisawa, A. Takada, W. Shinoda, S. Tsuzuki, and M. Mikami, *J. Phys. Chem. B*, **2005**. 109, 4269-4278.

(43) D. Rivin, G. Meermeier, N. S. Schneider, A. Vishnyakov, and A. V. Neimark, *J. Phys. Chem. B*, **2004**. 108, 8900-8909.

(44) M. K. Petersen, F. Wang, N. P. Blake, H. Metiu, and G. A. Voth, *J. Phys. Chem. B*, **2005**. 109, 3727-3730.

(45) M. K. Petersen and G. A. Voth, *J. Phys. Chem. B* **2006**. 110, 18594-18600.

(46) M. Tuckerman, K. Laasonen, M. Sprik, and M. Parrinello, *J. Chem. Phys.*, **1995**. 103, 150-161.

(47) M. Tuckerman, K. Laasonen, M. Sprik, and M. Parinello, *J. Phys. Chem.* , **1995**. 99, 5749-5752.

(48) C. J. T. Grotthuss, *Annales de Chimie (Paris)*, **1806**. 58, 54.

(49) Nafion, DuPont. **http://www1.dupont.com/NASApp/dupontglobal/** corp/index.jsp.

(50) S. Cui, J. I. Siepmann, H. D. Cochran, and P. T. Cummings, *Fluid Phase Equilib.*, **1998**. 146, 51-61.

(51) H.-C. Li, C. McCabe, S. Cui, P. T. Cummings, and H. D. Cochran, *Mol. Phys.*, **2003**. 101, 2157-2169.

(52) S. P. Gejji, K. Hermansson, and J. Lindgren, *J. Phys. Chem.*, **1993**. 97, 3712-3715.

(53) W. D. Cornell, P. Cieplak, C. I. Bayly, I. R. Gould, K. M. Nerz, D. M. Ferguson, D. C. Spellmeyer, T. Fox, J. W. Caldwell, and P. A. Kollman, *J. Am. Chem. Soc.* , **1995**. 117, 5179.

(54) W. L. Jorgensen, J. Chandrasekhar, J. D. Madura, R. W. Impey, and M. L. Klein, *J. Chem. Phys.*, **1983**. 79, 926-935.

(55) D. J. Price and C. L. Brooks, *J. Chem. Phys.*, **2004**. 121, 10096-10103.

(56) G. Hummer, D. M. Soumpasis, and M. Neumann, *Mol. Phys.*, **1992**. 77, 769-785.

(57) S. Cui and J. G. Harris, *Chem. Eng. Sci.*, **1994**. 49, 2749-2763.

(58) D. R. Morris and X. Sun, *J. Appl. Polym. Sci.*, **1993**. 50, 1445-1452.

(59) M. Tuckerman, B. J. Berne, and G. J. Martyna, *J. Chem. Phys.*, **1992**. 97, 1990-2001.

(60) S. Nosé, *Mol. Phys.*, **1984**. 52, 255-268.

(61) S. Nosé, *J. Chem. Phys.*, **1984**. 81, 511-519.

(62) W. G. Hoover, *Phys. Rev. A*, **1985**. 31, 1695-1697.

(63) S. J. Paddison, R. Paul, and T. A. Zawodzinski, *J. Electrochem. Soc.*, **2000**. 147, 617-626.

(64) S. J. Paddison, R. Paul, and T. A. Zawodzinski, *J. Chem. Phys.*, **2001**. 115, 7753-7761.

(65) S. J. Paddison and J. A. Elliott, *J. Phys. Chem. A*, **2005**. 109, 7583-7593.

(66) D. A. McQuarrie, *Statistical Mechanics*. Harper's Chemistry Series, Harper & Row, 1976.

(67) S. Woutersen and H. J. Bakker, *Phys. Rev. Lett.*, **2006**. 96, 138305.

(68) D. J. Keffer, M. Esai Selvan, and J. Liu, Nafion Structures on the Web: **http://clausius.engr.utk.edu/atoms/nafion/MainPage.html**.

(69) X. Gong, A. Bandis, A. Tao, G. Meresi, Y. Wang, P. T. Inglefield, A. A. Jones, and W. Y. Wen, *Polymer*, **2001**. 42, 6485-6492

Appendix A

Table 2. 1 Hydration number around various atomic groups.

atomic types	distance	Hydration number for different water content			
		5 wt%	10 wt%	15 wt%	20 wt%
sulfur-O(H_2O)	0~5.0Å	5.47	6.87	7.68	8.19
sulfur-O(H_3O^+)	0~4.8Å	1.71	1.26	1.14	0.89
O(SO_3^-)-O(H_2O)	0~4.0Å	2.38	2.96	3.23	3.42
O(SO_3^-)-O(H_3O^+)	0~3.5Å	0.55	0.39	0.36	0.27
O(H_3O^+)-O(H_2O)	0~3.2Å	2.25	2.76	2.97	3.15

Table 2. 2 Number of water molecules in small and large clusters.

	cluster size											
	<100 Rc(Å)			>100 Rc(Å)			<200 Rc(Å)			>200 Rc(Å)		
water content	3.5	4.5	5.5	3.5	4.5	5.5	3.5	4.5	5.5	3.5	4.5	5.5
5 wt %	732	331	74	120	521	778	832	439	107	20	413	745
10 wt %	261	45	4	971	1187	1228	372	51	4	860	1181	1228
15 wt %	28	8	2	1820	1840	1846	28	8	2	1820	1840	1846
20 wt %	25	5	0	2439	2459	2464	25	5	0	2439	2459	2464

Table 2. 3 Diffusion coefficients for water and hydronium.

water content	water D (10^{-6} cm^2/s)	hydronium (H_3O^+)D (10^{-6} cm^2/s)
5 wt %	1.387	0.297
10 wt %	3.755	0.636
15 wt %	7.365	1.473
20 wt %	9.405	2.523

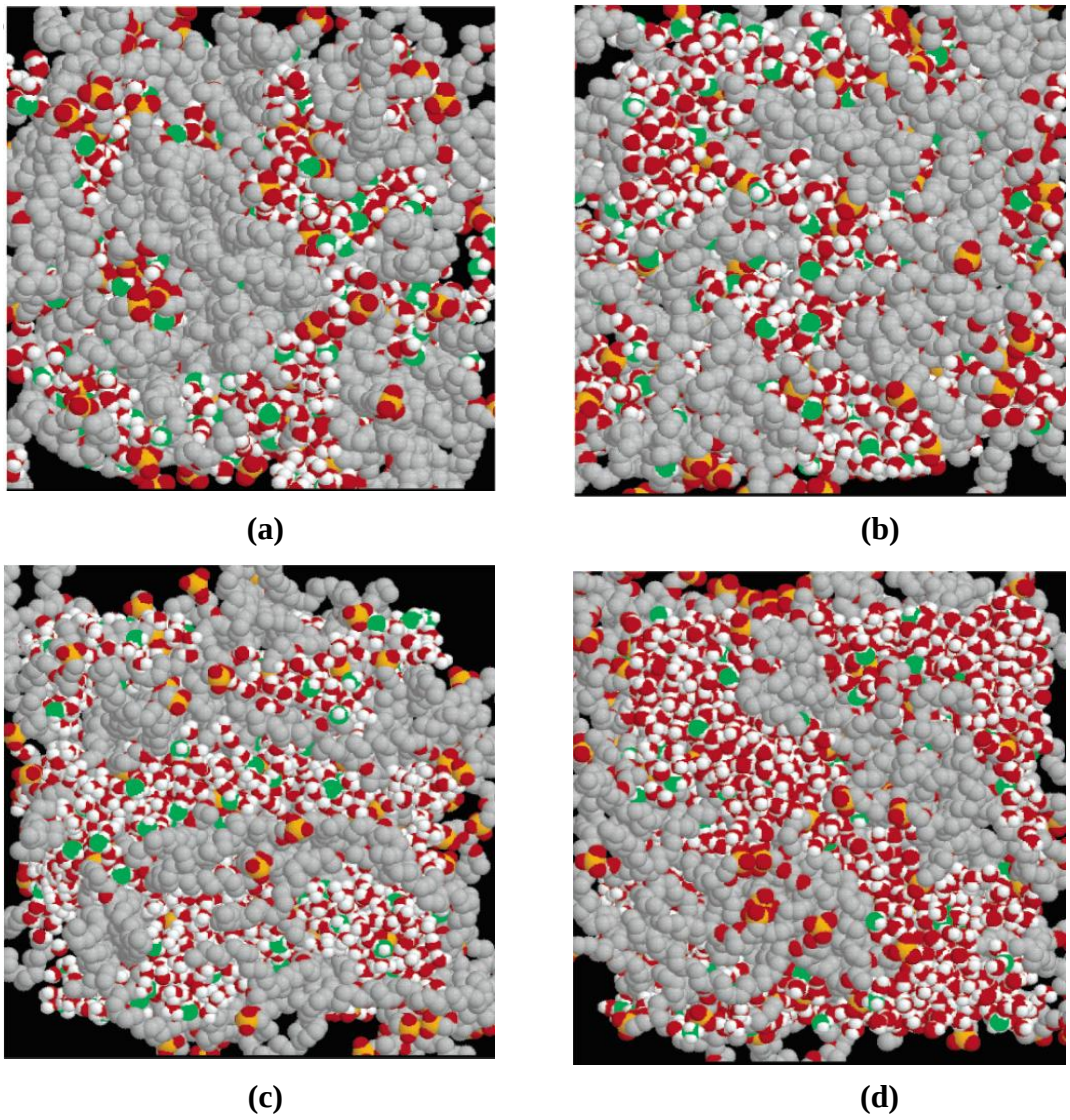

Figure 2. 1 (a) Snapshot of the configuration at 5% water content at the end of the production run. Gray, CF_X groups; orange, sulfur; red, oxygen atom of H_2O or SO_3^-; green, oxygen atom of H_3O^+; white, hydrogen. (b) The same as (a) but at 10% water content. (c) The same as (a) but at 15%water content. (d) The same as (a) but at 20% water content.

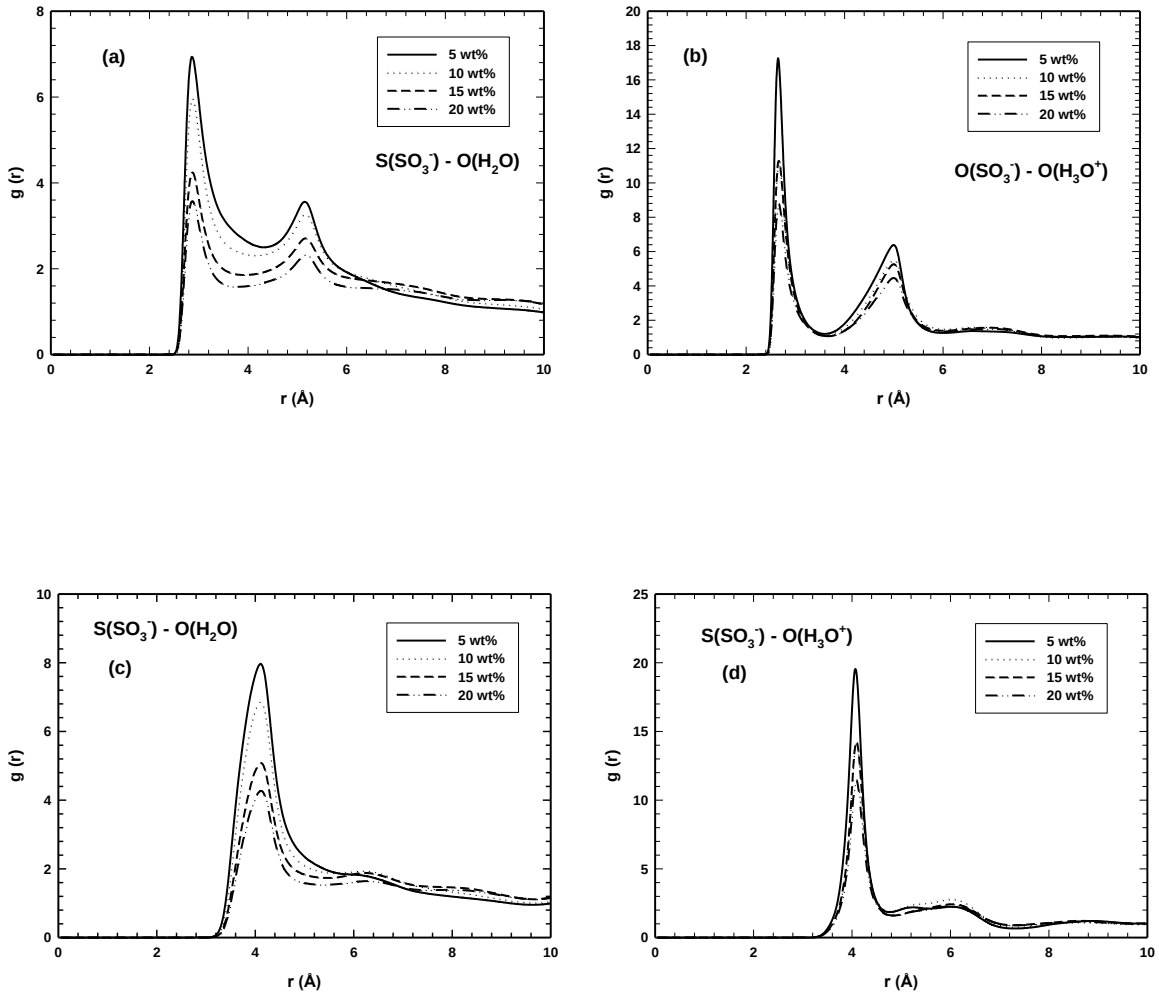

Figure 2. 2 (a) The PCFs between the oxygen of the sulfonate group and the oxygen of water molecules. (b) The PCFs for oxygen of the sulfonate group and oxygen of hydronium. (c) The PCFs for sulfur of sulfonate group and oxygen of water. (d) The PCFs for sulfur of sulfonate group and oxygen of hydronium.

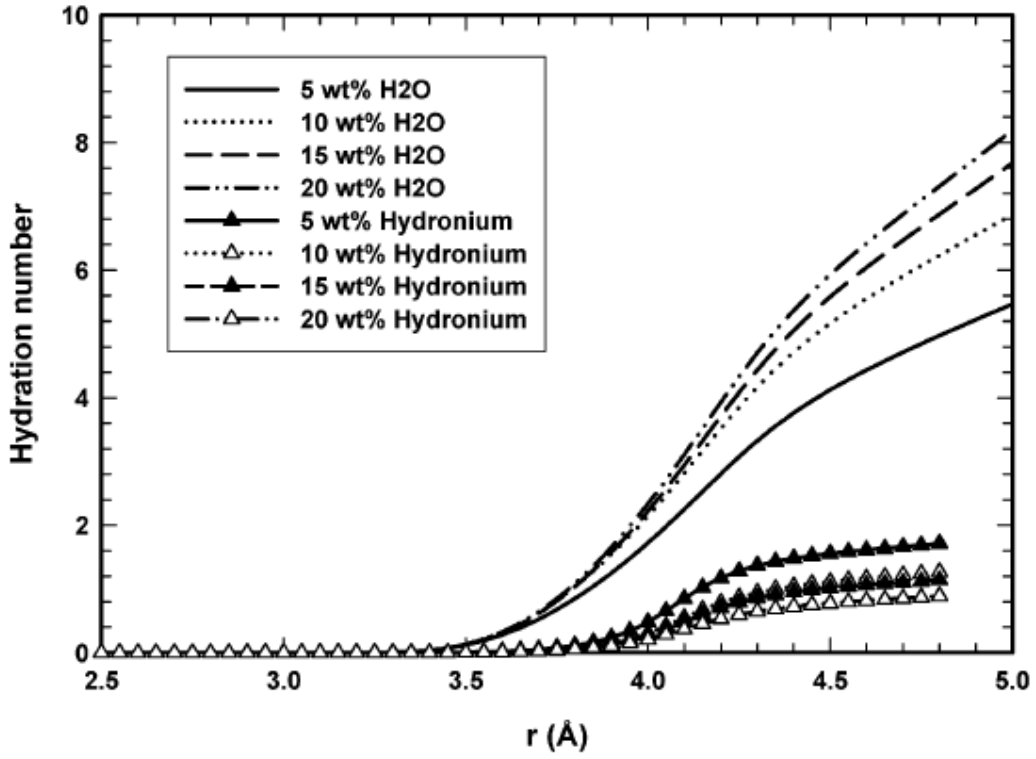

Figure 2. 3 The number of water molecules (hydronium) around an S atom of the sulfonate. Lines, water; lines with symbols, hydronium.

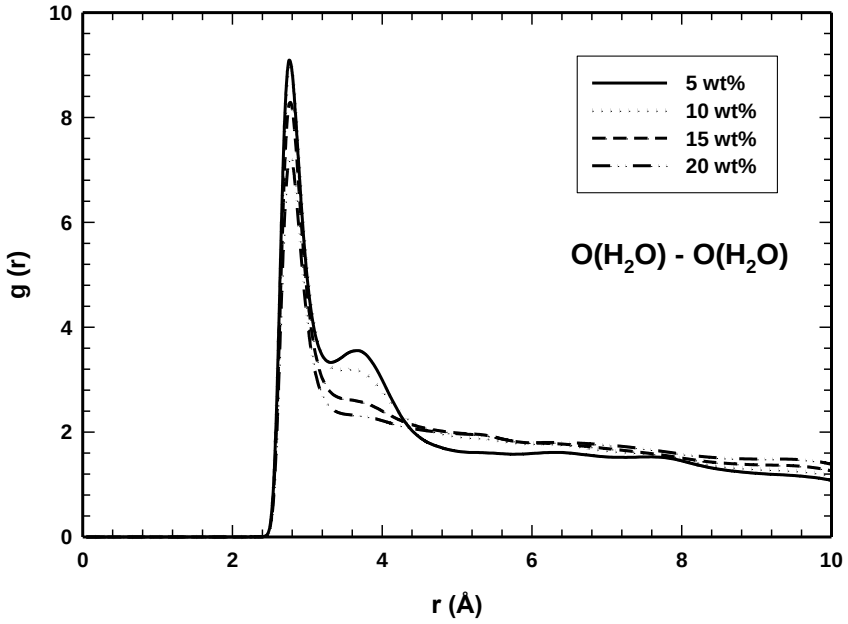

Figure 2. 4 Water oxygen-oxygen pair correlation function.

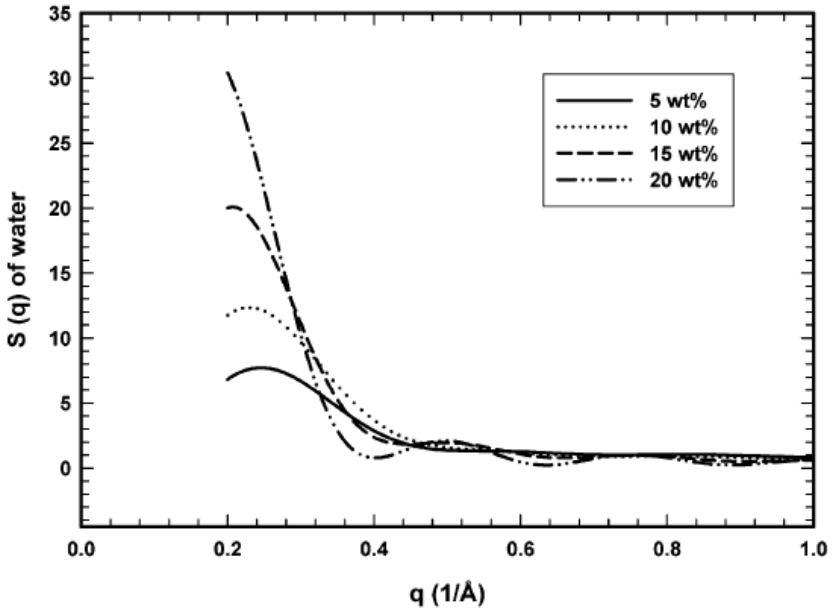

Figure 2. 5 The structure factor $S(q)$ obtained from eq 1 for water oxygen-oxygen pair correlation function.

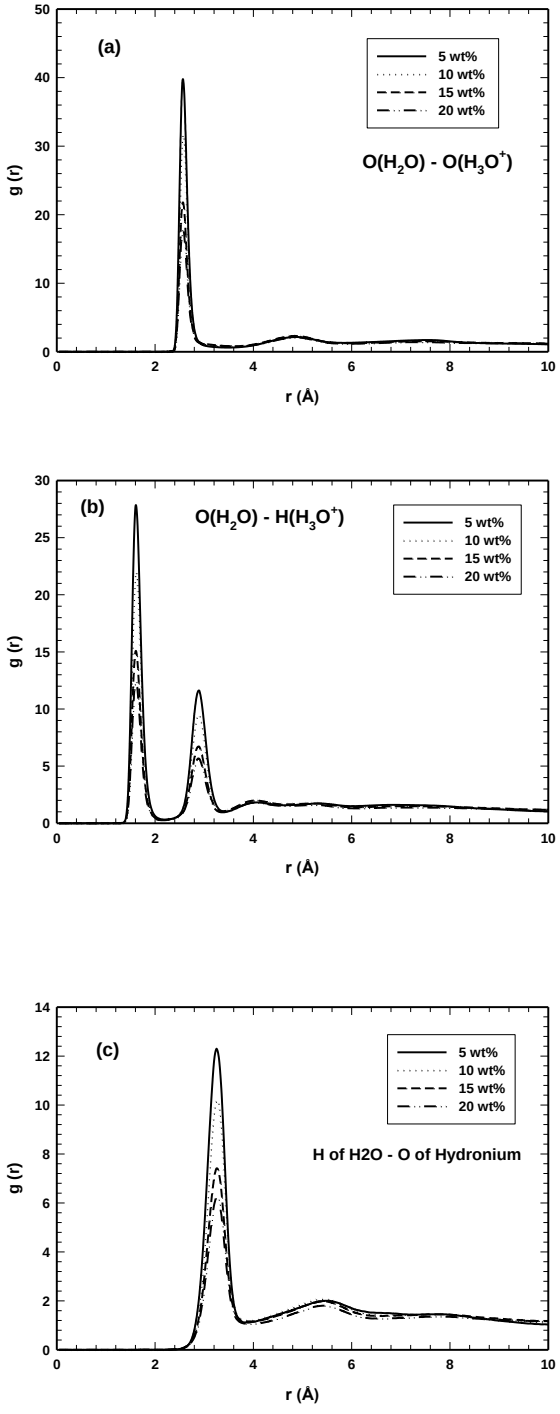

Figure 2. 6 (a) The PCFs for the oxygen of water and the oxygen of hydronium. (b) The PCFs for the oxygen of water and the hydrogen of hydronium. (c) The PCFs for the hydrogen of water and the oxygen of hydronium.

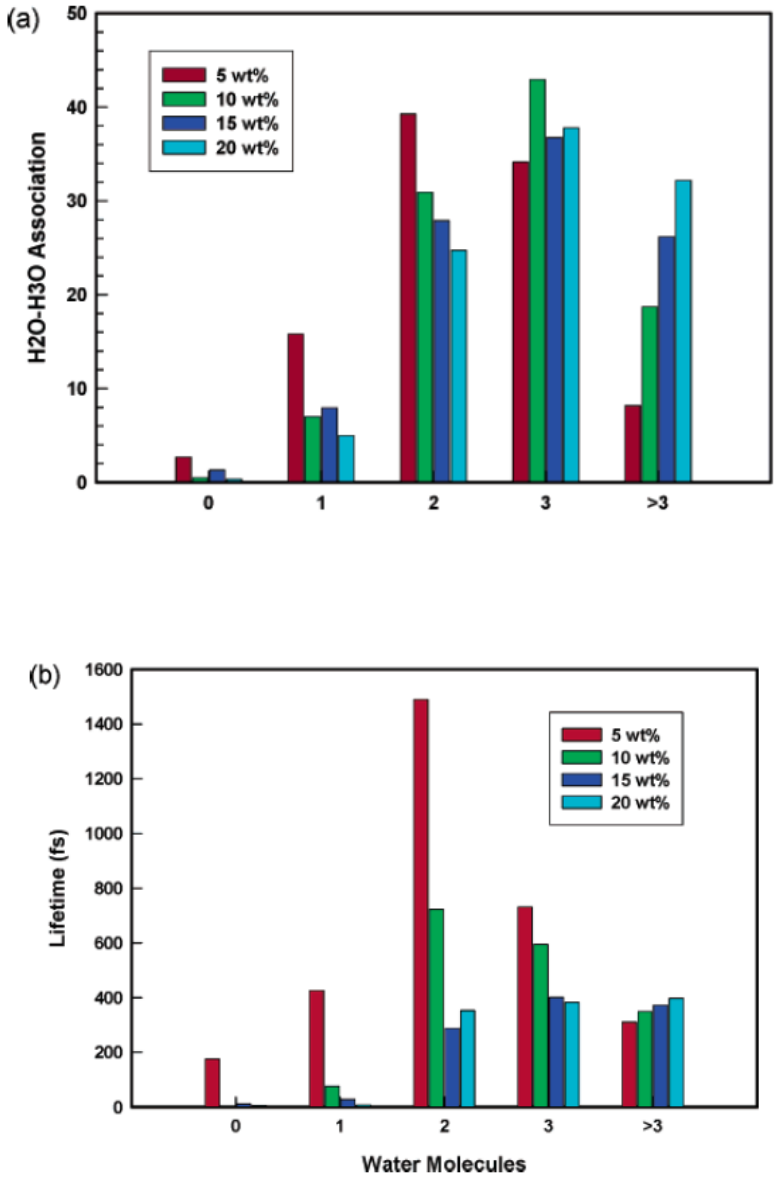

Figure 2. 7 (a) Distribution of hydrated hydronium complexes as a function hydration number. (b) The dependence of lifetime of various hydrated hydronium complexes on the hydration number around the hydronium.

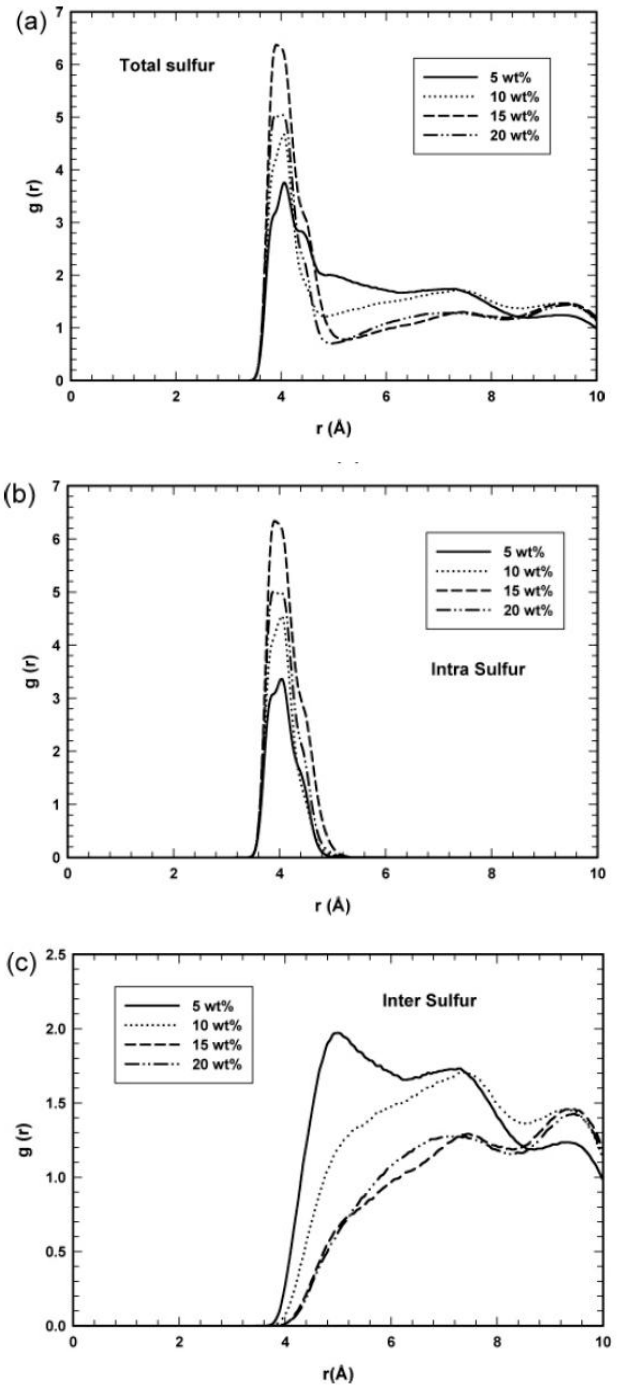

Figure 2. 8 (a) The total sulfur-sulfur PCFs at various water contents. (b) The intramolecular component sulfur-sulfur PCFs. (c) The intermolecular component sulfur-sulfur PCFs.

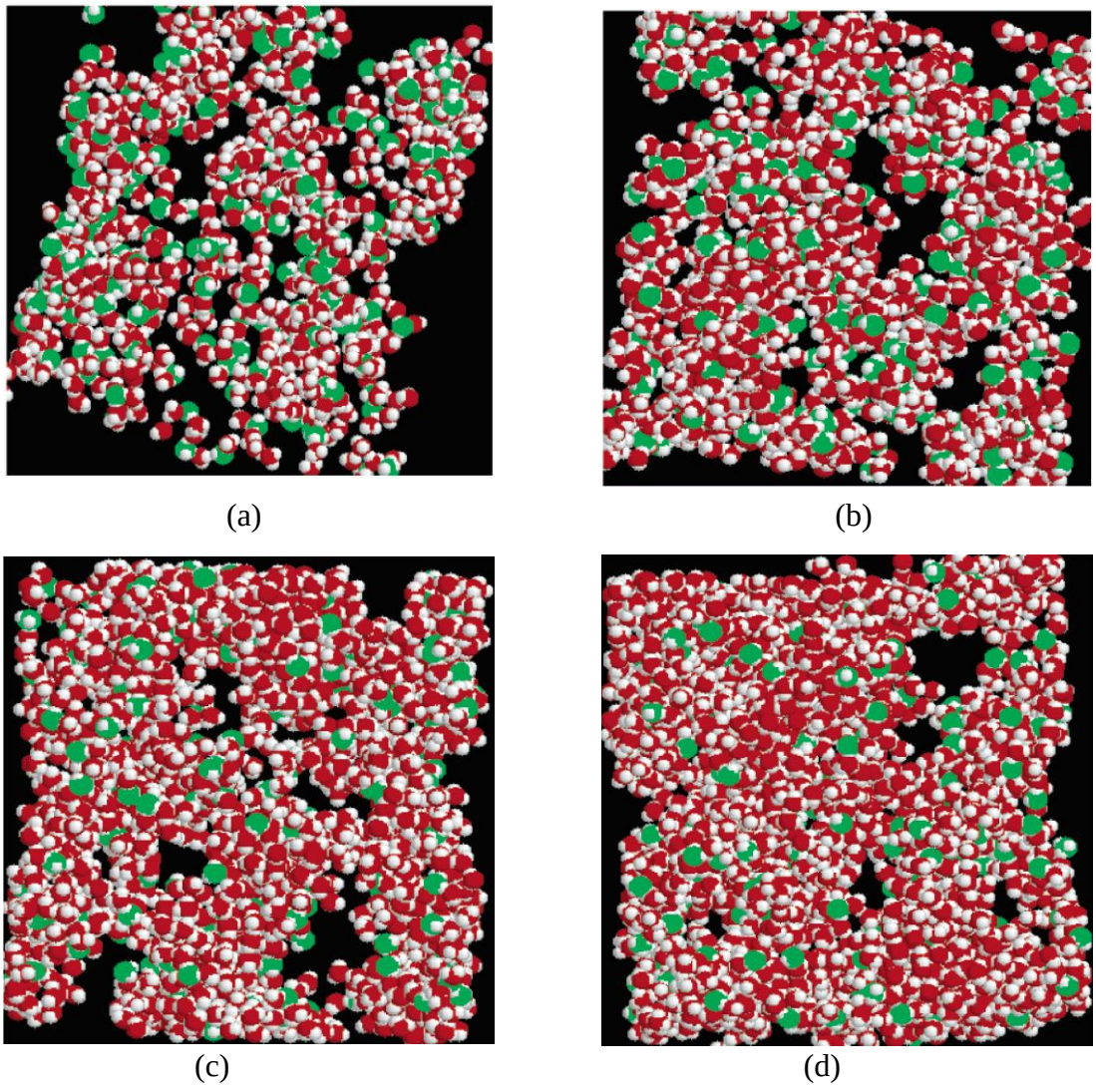

Figure 2. 9 (a) The same configuration as in Figure 2.1a without showing the polymer. The color code is the same as in Figure 2.1a. (b) The same as in (a) but for 10% water content. (c) The same as in (a) but for 15% water content. (d) The dame as in (a) but for 20% water content.

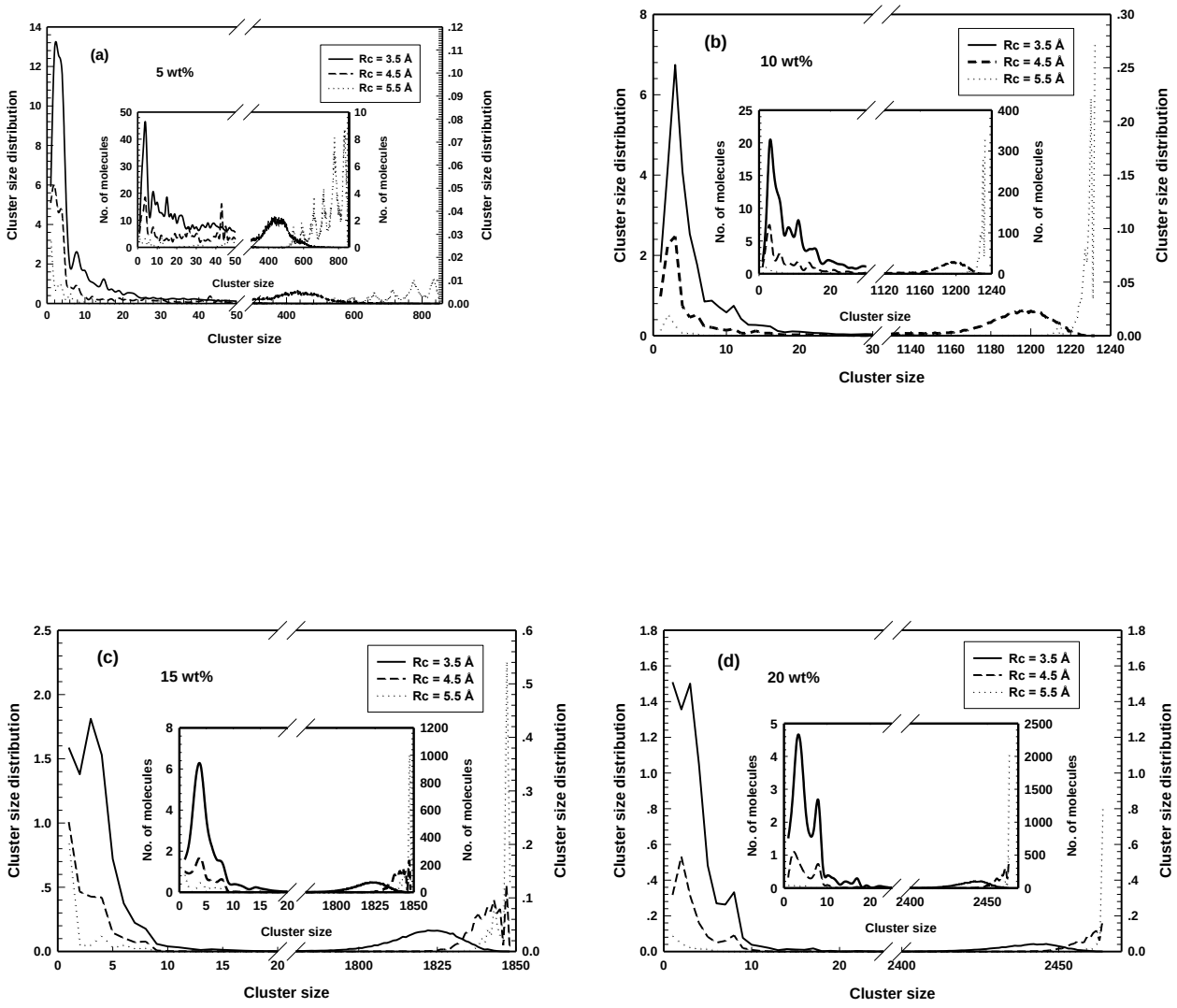

Figure 2. 10 (a) Water cluster distribution for 5% water content averaged over 2 ns duration. Inset: the average number of water molecules in a particular cluster size. (b) The same as (a) but for 10% water content. (c) The same at (a) but for 15% water content. (d) The same as (a) but for 20% water content.

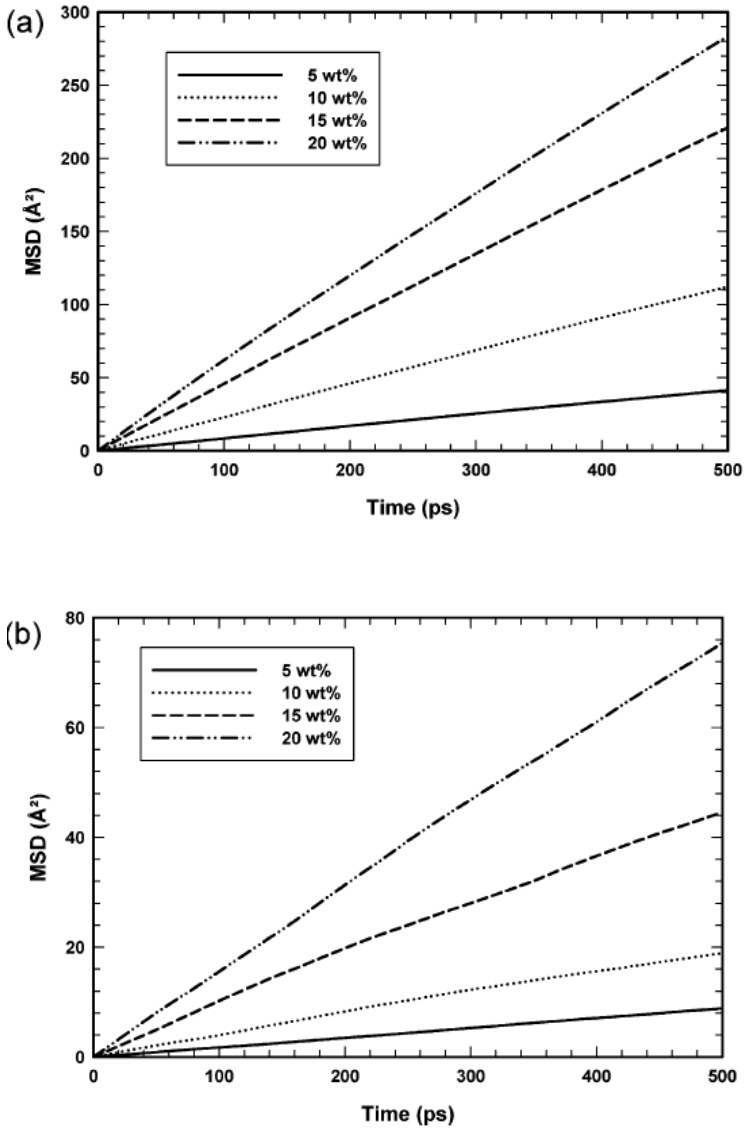

Figure 2. 11 (a) Mean square displacement of water molecules in hydrated Nafion for water contents between 5 and 20 w t%. (b) Mean square displacement of hydronium ions in hydrated Nafion for water content between 5 and 20 wt %.

Chapter 3

Comparison of the hydration and diffusion of protons in perfluorosulfonic acid membranes with molecule dynamics simulations

This part is a slightly revised version of a paper by the same title published in the *Journal of Physical Chemistry B* in 2008 by Shengting Cui, Junwu Liu, Myvizhi Esai Selvan, Stephen Paddision, David Keffer, Brian Edwards:

S.T. Cui; J.W. Liu; M.E. Selvan; S.J. Paddison, D.J. Keffer; and B.J. Edwards, "Comparison of the Hydration and Diffusion of Protons in Perfluorosulfonic Acid Membranes with Molecular Dynamics Simulations", *J. Phys. Chem. B,* **112**, 2008, 13273-13284.

The use of "we" in this part refers to the co-authors and the author of this dissertation. My primary contributions to this paper include (1) part of the simulation work, and (2) preparation of almost all the plots and tables.

Abstract

Classical molecular dynamics (MD) simulations were performed to determine the hydrated morphology and hydronium ion diffusion coefficients in two different perfluorosulfonic acid (PFSA) membranes as functions of water content. The structural and transport properties of 1143 equivalent weight (EW) Nafion, with its relatively long perfluoroether side chains, are compared to the short-side-chain (SSC) PFSA ionomer at an EW of 977. The separation of the side chains was kept uniform in both ionomers consisting of $-(CF_2)_{15}-$ units in the backbone, and the degree of hydration was varied from 5 to 20 weight % water. The MD simulations indicated that the distribution of water clusters is more dispersed in the SSC ionomer, which leads to a more connected water-channel network at the low water contents. This suggests that the SSC ionomer may be more inclined to form sample-spanning aqueous domains through which transport of water and protons may occur. The diffusion coefficients for both hydronium ions and water molecules were calculated at hydration levels of 4.4, 6.4, 9.6, and 12.8 H_2O/SO_3H for each ionomer. When compared to experimental proton diffusion coefficients, this suggests that as the water content is increased the contribution of proton hopping to the overall proton diffusion increases.

3.1 Introduction

The polymer electrolyte in proton exchange membrane (PEM) fuel cells has been the focus of research aimed at improving the performance of the device to function under hot (i.e., >100 °C) and dry conditions [1-3]. Novel PEMs that possess good chemical and mechanical stability, low gas permeability, and high proton conductivity are needed, and the route to successful implementation into these power sources is tied to acquiring a systematic understanding of how proton mobility is determined by polymer structure and chemistry, water content, and choice of the protogenic group [4]. Some guidance may be inferred from what is understood concerning the transport of protons in bulk water: a combination of vehicular and structural diffusion processes, with the latter being the more dominant [5-8]. The regions of a hydrated PEM that contain the water, however, are exceedingly more complex than bulk water. The two diffusion mechanisms are thought to contribute to proton mobility in hydrated PEMs, but their relative contributions are not fully understood and are highly dependent on the water content and morphology of the membrane [9].

Nafion, the archetypical PEM, is a perfluorosulfonic acid (PFSA) ionomer with pendant $-OCF_2CFCF_3OCF_2CF_2SO_3H$ side chains (see Figure 3.1a).When hydrated, this PFSA exhibits phase separation on a nanometer scale into regions consisting of the hydrophobic polytetrafluoroethylene (PTFE) backbone and domains consisting of tethered sulfonate groups, hydrated protons, and water molecules. Neutron diffraction studies have characterized the size of the water clusters in this aqueous phase to be of the order of 2−5 nm [10]. The morphology of the aqueous phase has been modeled as micelles of spherical water clusters [11, 12], layered structures [13, 14], polymer bundles [15, 16], or cylindrical channels [17, 18]. The precise morphology of hydrated PFSA membranes is not definitively characterized despite extensive experimental and theoretical studies [10, 11, 17, 19-43]. We refer to distinct portions of the aqueous region as clusters but do so without any implication as to the geometry. This terminology allows us to make contact with the percolation literature, in which the notion of a sample-spanning cluster (SaSC) is typical.

It is clear from percolation theory that there must be a sample-spanning cluster (SaSC) in order for there to be a net flux of species in a system with a static connectivity. If static aqueous phase morphology was present in a PFSA membrane, then there would have to be a

sample-spanning aqueous region across the entire width of the material. However, in these electrolytes, the molecules undergo at least Brownian motion, resulting in relaxation of both the side chains and backbone of the polymer and the water molecules. This relaxation translates into a dynamic morphology which, along with vehicular and structural diffusion of protons, determines the proton conductivity of the membrane. The time scale associated with the morphology relaxation is certainly larger than that associated with the diffusional processes. Vehicular diffusion occurring within a cluster may be estimated from molecular dynamics (MD) simulations, in which long-time behavior of the mean-square displacement (MSD) as a function of time is linear (as dictated by the Einstein relation), and on the order of 1−10 ns [44]. The proton hopping time is ~1.5 ps and is significantly faster than the time associated with vehicular diffusion [45, 46]. The time scale associated with the aqueous cluster dynamics is equivalent to the relaxation time of the polymer in the system because the two nanophases, together, are space-filling. It is more difficult to estimate the time scale associated with the relaxation of a polymer in a hydrated ionomer, but the typical time scale for a polymer is at least on the order of seconds [47]. Clearly, the time scale associated with aqueous cluster morphology dynamics is orders of magnitude slower than that for vehicular or structural diffusion of protons within a cluster.

We can conceive of a system in which protons move relatively rapidly within a cluster but are confined to remain within a given cluster until, on a longer time scale, "bridges" form between the clusters and the connectivity of the aqueous phase changes. Hence, the SaSC within the hydrated membrane consists of regions of dense aqueous clusters interconnected by irregular, less well-packed regions of water which act as channels. Efficient migration of protons through the membrane is therefore dependent on the existence of SaSCs. The morphology of hydrated membranes, as indicated earlier, is complex and irregular, and thus difficult to characterize through only a simple theory. Obviously, the morphology of the aqueous domains is influenced by the chemistry and crystallinity of the ionomer. Thus, a better understanding of the relationship between polymer architecture, along with the resulting hydrated morphology, will be critical for the development of novel high performance membranes.

A great variety of different PEMs have been synthesized [48, 49] and characterized in an attempt to improve upon the unsatisfactory proton conductivity of Nafion at low water contents.

These novel ionomers include the following: PFSA ionomers [50] with differing side chain, lengths and equivalent weights (EWs); nonfluorinated [51] aromatic polymers such as polysulfones, poly(ether ketones), poly(phosphazenes), and polyimides; composites [52, 53] such as conventional ionomers containing silica, titania, heteropolyacids, layered metal phosphonates, etc. Although several of these materials show improvements over Nafion in certain respects, such as long-time thermal stability at $T > 130$ °C and conductivities that are quite a bit higher at very low water contents, no membrane has been developed that is superior in all respects and meets the requirements for fuel cells operating without external humidification [54].

An early indication that side chain length affected membrane properties (e.g., proton conductivity) was observed with the short-side-chain (SSC) PFSA ionomer (i.e., a membrane with a PTFE backbone similar to Nafion but $-OCF_2CF_2SO_3H$ side chains) [55-57] first synthesized by the Dow Chemical Company [58]. Although SAXS and SANS measurements [2, 56, 57, 59] revealed that the hydrated morphology (i.e., relative position of the ionomer peak) was quite similar to Nafion, the proton conductivity was determined to be significantly higher for membranes with EWs of approximately 800 when compared to Nafion 117 [2, 59-61]. This superiority was confirmed in fuel cell testing with current densities observed nearly 3 times higher at a potential of 0.5 V [62]. Recently, the SSC ionomer has experienced a resurgence of interest due to the much simpler synthesis of the base monomer by Solvay Solexis, and is thus commercially available, at a more reasonable cost than previously available, under the trade name Hyflon [63-65]. Other PFSA membranes have been synthesized that show higher proton conductivities than Nafion 117; of significance is the membrane developed by the 3M company with $-O(CF_2)_4SO_3H$ side chains using an electrochemical fluorination process [66, 67]. The observed higher proton conductivities in PFSA membranes with shorter side chains than Nafion are undoubtedly linked to the higher exchange capacity but perhaps also to subtle changes to the hydrated morphology [2, 68].

There is now a substantial body of literature describing molecular modeling studies [69-97] seeking to understand the relationship between polymer architecture and transport of various species (e.g., water, protons, etc.) important to the performance of the ionomer in a fuel cell [54]. Of relevance to the current work, efforts have been aimed at elucidating how the chemistry of the

side chain [69, 71, 80, 89, 91, 92] affects the aggregation of the acidic groups and the dissociation and mobility of the protons. Paddison and Elliot [89, 91] performed *ab initio* self-consistent field molecular orbital calculations on a single short-side-chain perfluorinated sulfonic acid segment carrying two side sulfonic acid groups, hydrated by a few additional water molecules. They investigated the effect of the spacing between the side sulfonic acid groups on the backbone of the segment on the ability of water molecules to form continuous hydrogen bonds along the segment. Their work suggests the importance of sulfonic group separation in the formation of the hydrogen bonding network in PEMs; however, they did not carry out quantitative analysis of water cluster distribution. Jang et al. [83] performed molecular dynamics to study the effect of molecular architectural variance of Nafion 117. One variance has the side chains evenly distributed along the backbone; the other has 10 side chains all placed at one end of the polymer. Their MD study showed that the PEM consisting of the end-weighted molecules gives rise to larger clusters, whereas the molecules with regularly spaced side chains give rise to smaller but more dispersed clusters.

We report on classical molecular dynamics simulations of Nafion and the SSC membrane in an effort to identify differences in hydrated morphology and the connections between morphology and the rates and mechanism of proton diffusion. The latter is, of course, limited to diffusion of hydronium ions, as our simulations do not allow for the breaking of any covalent bonds. Nevertheless, these simulations are useful in understanding how vehicular diffusion changes as a function of ionomer chemistry and hydration. Furthermore, insight is obtained on how the length of the pendant side chains affects the intracluster diffusion of water and hydronium ions, as well as the connectivity of the domains containing the water molecules and ions (i.e., H_3O^+ and $-SO_3^-$). This should prove helpful in identifying specific features of PFSA membranes that may be modified to enhance proton transport.

3.2 Molecular Models and Simulations

The chemical structures of the repeat unit (i.e., monomer) of both Nafion and the SSC PFSA membrane are shown in Figure 3.1. We selected a polymeric structure with the side chains separated by seven tetrafluoroethylene (i.e., $-CF_2CF_2-$) units in the backbone for both ionomers, thus allowing direct comparison with previous MD simulations involving Nafion [98-100]. This

results in similar equivalent weights for each polymer: an EW of 1143 for Nafion and an EW of 977 for the SSC ionomer. This choice allows assessment of the effect of side chain length on two systems with similar backbone structure. While this choice corresponds directly to the readily available Nafion 117 (i.e., EW ~1100 g/mol), the SSC ionomer in our simulations is significantly higher in EW than commonly utilized in fuel cells (e.g., EW ~800 g/mol). However, a recent extensive characterization study of SSC membranes allows comparison of structural and transport data with Dow membranes of 1084 EW [2]. Furthermore, the molecular-level trends observed in our simulations should be applicable to other equivalent weights.

Force fields have been developed for both Nafion [70, 74, 83] and the SSC PFSA membrane [97]. Both PFSA ionomers were modeled in this study as oligomers consisting of only three monomer units, resulting in fragments with 48 CF_X groups along the backbone, similarly to previous work [98]. Although these molecules are considerably shorter than those in a real ionomer (e.g., for Nafion, there are at least 90 monomer units per macromolecule), previous work [98] revealed little difference to simulations involving fragments consisting of 10 monomers. Furthermore, the oligomers have short relaxation times and are therefore easier to equilibrate. It is computationally intractable to fully relax the fragments with macromolecules of realistic molecular weight [97]. Consequently, a united atom model for the CF_X groups on both the backbone and side chains was implemented for computational efficiency using Lennard-Jones parameters developed by Cui et al. [101, 102]. The backbone does not carry electric charge, save for the united atom at which the side chain is attached, and interacts only via Lennard-Jones and intramolecular interactions. Bond lengths, bond angles, and partial charges were determined for the side chains from the parameters of Vishnyakov and Neimark [74]. The charge assigned to a united atom is the sum of charges from the atomistic model. The force constants for bond stretching and bond angle bending were taken from Gejji et al. [103] and Cornell et al.[104]. The torsional potential was taken from Rivin et al.[105].

Intramolecular sites on the same molecule separated by more than three bonds, and sites on different molecules, also interact via nonbonded interactions, including the Lennard-Jones and electrostatic (between charged sites) interactions. Previous simulations of hydrated Nafion [98] did not include electrostatic intramolecular interactions; however, presently, they are included.

The effect is slight in most cases, and the essential features of pair correlation functions are very small, except for the sulfur−sulfur pair correlation function (PCF), $g(r)$. Thus, we have included the results for the sulfur−sulfur PCFs in the present work. The other PCFs, which are only slightly modified, however, are provided in the Supporting Information.

The water was modeled using the TIP3P model [106, 107] with a flexible OH bond [104]. Similar bond distances, bond angles, and the force constants were employed for the hydronium ions, H_3O^+, as were used for the water molecules, with partial charges for the oxygen and hydrogen atoms taken from Urata et al.[85]. In the calculation of nonbonded interactions, the Lennard-Jones interaction was truncated using a cutoff distance of 10 Å. The electrostatic interaction was implemented with a site−site reaction field method that has proven to be accurate for modeling aqueous ionic solutions [108, 109]. In this method, Coulombic interactions between charged sites were calculated within a distance of 10 Å, and the reaction field contribution was implemented with a uniform background counter charge.

The simulated systems for both PFSA membranes consisted of 64 macromolecules (i.e., a total of 192 monomers), with 192 hydronium ions (H_3O^+), the latter to ensure overall charge neutrality. The properties of each ionomer were examined for water contents corresponding to λ (defined as the number of water molecules per $-SO_3H$ group) values of 4.4, 6.4, 9.6, and 12.8. This resulted in 660, 1040, 1656, and 2272 water molecules, corresponding to 7164, 8304, 10152, and 12000 total interaction sites in the simulations. The densities and water contents were chosen on the basis of experimentally measured values for Nafion [110]. For the four levels of hydration, the experimentally determined overall densities of the system are 1.95, 1.87, 1.80, and 1.74 g/cm^3. We used a molecular volume for the SSC PFSA systems, appropriately scaled, based on the number of atoms relative to that of Nafion, keeping the molecular volume of the water and hydronium ions the same as for Nafion. All simulations were carried out at a temperature of 300 K, and data collection was performed over at least 2 ns.

Constant NVT simulations were performed for this system. The equations of motion for the interaction sites were integrated using the r-RESPA method [111] with a time step of 2.0 fs for the large time step and 0.4 fs for the intramolecular interactions. The temperature was maintained at a constant value using the Nosé-Hoover thermostat [112-114], with a thermostat frequency of 10^{-4} fs^{-1}. The initial configurations were created by randomly placing molecular centers of all

the molecules in the system on cubic lattice points within the simulation volume. Hydronium ions were initially placed without regard for the position of the sulfonate groups so as not to bias their equilibrium position. All atoms were initially assigned an infinitesimal volume by setting their corresponding Lennard-Jones parameters to null values. An MD simulation was performed for 10000 time steps in which the Lennard-Jones size parameters were gradually increased to their assigned values. Initial configurations with nonoverlapping atoms were thereby created efficiently. Equilibration using these initial configurations was then performed for at least 500 ps before any data collection was begun.

3.3 Results and Discussion

3.3.1 Visualization of the Hydrated Morphology.

The morphologies of the SSC PFSA and Nafion membranes are shown in Figures 3.2 and 3.3, respectively. The snapshots are for each system at the end of the simulation at water contents corresponding to $\lambda = 4.4$ and 9.6 for parts a and b, respectively. The atoms of each ionomer have been omitted in the snapshots in order to show clearly the clustering of the water molecules. Qualitatively, the general feature for both the SSC PFSA and Nafion membranes is that of water clusters consisting of networks (either mostly disconnected, $\lambda = 4.4$ water, or mostly connected by irregularly shaped channels, $\lambda = 9.6$). At water content $\lambda = 4.4$, these figures show that the water clusters are quite small and the connectivity is poor, consistent with the findings of other authors [94, 97]. The clusters are also less densely packed in the interior. At high water content, the clusters become larger and connecting channels exist between the clusters; furthermore, the water molecules in the clusters appear to be more densely packed. Both characteristics will have important effects on the long-range transport of protons and water molecules. Careful examination of the clusters also shows that most hydronium ions appear to be exposed to the exterior of the clusters, suggesting that they are lining the surface of the clusters as a result of the interaction with the oppositely charged sulfonate groups of the ionomers. However, it is also worth pointing out that both sum-frequency generation [115-117] (i.e., SFG) and second harmonic generation [118, 119] (i.e., SHG) spectroscopy experiments and *ab initio* MD

simulations of neat water clusters [120] and clusters of methanol and water [121] indicate the preference of hydrated protons for the surface or interface. It has been reasoned that this increased concentration of hydronium ions (or hydrated protons) is due to a dielectric mismatch at an interface which is certainly the case with hydrated PFSA membranes [122, 123]. Notwithstanding, a more detailed quantitative analysis of the preferential location of the hydrated protons as a function of hydration is warranted in both membranes.

3.3.2 Cluster Size Distribution and Channel Connectivity.

It has been suggested from a survey of both experimental and theoretical studies of PFSA membranes that the important ingredients of proton conduction are complexity, cooperativity, and connectivity [124]. The last involves not only hydrogen bonding between the water molecules and the sulfonic acid groups and with other water molecules but importantly also hydrogen bonding between the water and ion containing domains in the polymeric matrix. Proton transport occurs through the membrane due to migration of the protons across distances several orders of magnitude larger than the size of typical clusters; thus, intercluster proton transfer has to occur, which could constitute a bottleneck in morphologies where the clusters are poorly connected. To characterize this connectivity quantitatively, we examined the cluster size distribution for water contents from λ = 4.4 to 12.8 using various critical cutoff distances, denoted by Rc. The cluster distributions were calculated by sampling the presence of certain sized clusters using a cutoff distance during the MD simulation and performing a time average. Note from the outset that the cluster distributions depend on the choice of the cutoff distance, which is somewhat arbitrary, but a comparison of the cluster structure at the same cutoff distance will show the relative tendency for cluster formation in any pair of systems. Furthermore, water molecules within the first hydration shell of a hydronium ion (i.e., less than ~3.5 Å) can make direct contact with the hydronium ions, and it is therefore possible for proton transport to occur quickly after simple ballistic motion. Thus, a cutoff distance of Rc = 3.5 Å is a reasonable critical distance based on considerations relevant to proton transport. We have also examined other critical distances to obtain a more complete picture of the cluster connectivity.

Figures 3.4 and 3.5 display the cluster size distribution for the SSC and Nafion membranes, respectively, each at four distinct hydration levels and for three representative critical cutoff

distances: Rc = 2.8 Å (corresponding to the first peak position of the water−-hydronium ion $g_{O–O}(r)$, see Figure 3.9 below); Rc = 3.5 Å (slightly larger than the first minimum of $g_{O–O}(r)$, inclusive of all molecules in the first hydration shell); and Rc = 4.5 Å (inclusive of the second hydration shell). The cluster size distribution represents the average number of clusters present in the system corresponding to a particular cluster size. Figure 3.4 indicates the presence of only small water clusters in the morphology of the SSC PFSA membrane at all water contents when a cutoff of Rc = 2.8 Å is applied. As the water content is increased, clusters of increasing size are formed, with the largest cluster size consisting of 25, 50, 100, and 200 molecules for water contents of 4.4, 6.4, 9.6, and 12.8, respectively. For Nafion with Rc = 2.8 Å, similar behavior was observed, with a maximum cluster size similar to that of the SSC PFSA membrane.

With Rc = 3.5 Å, the SSC ionomer at a water content of $\lambda = 4.4$ (Figure 3.4a) is composed of only small clusters, with maximum cluster size consisting of about 250 water molecules. At the next higher hydration (Figure 3.4b), far fewer small clusters are present, and also a small magnitude distribution around 1123 molecules is observed. Although the probability is small, the number of molecules involved is larger, representing the vast majority of the water molecules and hydronium ions in the system. Such clusters, as indicated earlier, are sample-spanning clusters (SaSC) due to the formation of connected water channels or domains throughout the system. At water contents of $\lambda = 9.6$ and 12.8, a decrease is observed both in size and in number of small clusters, while at the same time an increase is evident in the height of the peak corresponding to the SaSC.

A continuous distribution for all cluster sizes with some significant peaks for cluster sizes less than about 20 molecules is observed in the SSC PFSA ionomer at the lowest hydration for Rc = 4.5 Å. At the next higher hydration level (i.e., $\lambda = 6.4$), the appearance of the SaSC peak and at larger cluster size is again observed. Further increase of the water content to $\lambda = 9.6$ and 12.8 leads to higher peaks and a shift of the peak position to even larger clusters. There is also an observed reduction in both the number and size of the small clusters for increasing water content. This reflects the increased probability that a water molecule will find a near neighbor with increasing water content. The formation of a SaSC indicates that the entire membrane is likely to be connected with water channels that enable efficient proton conductivity. We note that a cutoff of 4.5 Å would include the second hydration shell of the water or hydronium ion. The molecules

would then have to undergo vehicular diffusion to move within the first hydration shell to be in direct contact with the next molecule in the cluster, which is a slower process than the ballistic motion of molecules in the first hydration shell. Proton transfer through this route is slower.

The cluster distribution and connectivity for Nafion are qualitatively similar to that observed in a SSC PFSA membrane, as inferred from Figure 3.5. The differences are mostly quantitative, and are more easily recognized from the cumulative number of molecules in the cluster discussed below.

The global picture of the cluster distribution and connectivity is explored in Figure 3.6, which displays the cumulative probability of finding a molecule in a cluster of a specific size for both PFSA membranes across the various hydration levels. The cumulative probability has been normalized for ease of comparison. For the SSC PFSA with Rc = 2.8 Å, the cumulative probability reaches a plateau at rather small cluster sizes, consistent with the fact that only small clusters are present. Hence, for both Nafion and the SSC PSFA membrane at λ = 4.4, nearly 100% of the water molecules and hydronium ions are in clusters of not more than 20 molecules. As the water content is increased, there is a clear tendency for the curves to shift to the right, reaching plateaus at the maximum cluster size, suggesting that the clusters become larger with increasing water content. In Figure 3.6b, where Rc = 3.5 Å, the behavior is quite different. At the lowest water content, the cumulative probability distribution reaches a plateau at about 250 molecules. At a hydration level where λ = 6.4, there is an initial rise to about 0.1 in the cumulative probability, then an extended region of slow increase, and a rapid rise at around 1100 molecules in cluster size. This is related to the fact that a majority of the water molecules and hydronium ions are in a large cluster spanning the entire system (i.e., a SaSC). At the higher two water contents (λ = 9.6 and 12.8), the contributions to cumulative probability are essentially due to the rise in the amount of water in the large SaSC. In Figure 3.6c, with Rc = 4.5 Å, water clusters become more connected. At a water content where λ = 4.4, there is a continuous rise in the cumulative probability, suggesting the presence of clusters of all sizes. However, only a small contribution in the cumulative probability due to small clusters and a sharp rise for the SaSC is observed at the intermediate hydration level (λ = 6.4). Finally, at the two highest water contents (λ = 9.6 and 12.8), the number of molecules in small clusters is negligible and the vast majority of the molecules are in the SaSC, as reflected by the sharp lines in Figure 3.6c.

The rise in the cumulative probability curve for Nafion is more gradual than that for the SSC PFSA membrane for cutoffs at hydration levels where $\lambda = 4.4$ and 6.4 when cutoffs of Rc = 3.5 and 4.5 Å are used, respectively (see parts b and c of Figure 3.6). This would suggest that there is a greater contribution in the hydrated morphology due to small and intermediate sized water clusters in Nafion than in the SSC PFSA ionomer at these water contents. The latter has the tendency to form larger, more connected clusters, and this may be due to the stiffness of the shorter side chain [71, 91]. As a result, the sulfonate groups are more widely separated in the SSC PFSA ionomer, which results in a dispersed aqueous phase. Dispersion of the $-SO_3^-$ groups can bridge the connection between clusters which would otherwise be isolated. This hypothesis is further supported through examination of the S−S pair correlation functions, discussed below.

The main characteristics of the water clusters in the two hydrated systems are summarized in Table 3.1. The difference is most obvious at the low water contents: for $\lambda = 4.4$ and 6.4, it is apparent that the percentage of water and hydronium ions in the SaSC is significantly higher in the SSC PFSA membrane. It is also evident that the general feature of water cluster distribution in PFSA membranes can be characterized by SaSC and its connectivity. The morphology of the aqueous phase is affected by the architecture of the PFSA ionomer. When a short cutoff distance (2.8 Å) is applied, both membranes exhibit disconnected morphologies at all water contents. For longer cutoff distances (e.g., 4.5 Å), both ionomers exhibit a single aqueous SaSC at all water contents, except the very lowest. At $\lambda = 4.4$, the water clusters in the SSC PFSA ionomer are slightly more connected than in Nafion. At intermediate cutoff distances (3.5 Å), both membranes exhibit a single aqueous SaSC at the two highest water contents and exhibit disconnected morphologies at the lowest water content. At the intermediate water content ($\lambda =$ 6.4), the aqueous phase in the ionomer with the shorter side chains is again better connected than in Nafion.

3.3.3 Pair Correlation Functions.

The sulfonate sulfur−water oxygen pair correlation functions are presented in Figure 3.7. For both PFSA membranes, the sulfur−oxygen PCF shows a strong first peak and a weak, barely visible second peak. With increasing hydration, the height of the first peak decreases. The height of the prominent peak in the PCF for the two ionomers is slightly different. For the SSC

ionomer, the height of the peak is 8.2, 7.0, 5.2, and 4.4, and for Nafion, it is 9.1, 7.8, 5.9, and 4.8 at water contents of λ = 4.4, 6.4, 9.6, and 12.8, respectively. Thus, the peak is generally higher for Nafion than for the SSC PFSA membrane.

The sulfur−hydronium ion PCFs for both membranes are displayed in Figure 3.8 and may be compared with those for sulfur−water. The peak positions are roughly similar to those in the sulfur−water PCFs, but the heights are much greater. The dependence on water content is similar to sulfur−water; i.e., the peak height decreases with increasing water content. The height of the first peak for SSC is 15.1, 9.9, 7.0, and 5.6, and for Nafion, it is 14.2, 7.9, 5.5, and 4.4 for water contents where λ = 4.4, 6.4, 9.6, and 12.8, respectively. Thus, the height of the first peak is generally higher for the SSC ionomer than for Nafion, suggesting that the hydronium ions are, on average, more likely to be found in close proximity to the sulfonate groups in the PFSA membrane with the short side chains. This is consistent with the higher water peak in the hydrated Nafion systems, as the greater density of water molecules results in increased screening of the sulfonate anions [88].

The sulfur−sulfur PCFs for the SSC PFSA and Nafion membranes are displayed in Figures 3. 9 and 3.10, respectively. As mentioned earlier, the inclusion of an intramolecular electrostatic interaction was expected to have only a noticeable effect on the sulfur−sulfur PCFs, mostly via the intramolecular correlation function. Comparison of the total sulfur−sulfur PCFs shows that the first peak at 4.8 Å is about 2.5 for the SSC ionomer and about 3.1 for Nafion at the lowest water content. This peak is always greater in Nafion and, as the water content is increased, broadens and eventually flattens. This suggests that the sulfonate groups in the ionomer with the longer side chains tend to aggregate closer to one another than those in the SSC membrane, perhaps due to the greater flexibility in the longer side chains. The total sulfur−sulfur PCFs are decomposed into intramolecular and intermolecular components in Figures 3.9b,c and 3.10b,c. It is apparent that, except at the lowest water content (λ = 4.4), the pair correlation function is dominated by the contribution from the intermolecular correlation. Also, for both the intermolecular and intramolecular PCFs, the first peak is higher for Nafion than for the SSC ionomer. This would again underscore the increased rigidity of the shorter side chains.

Figure 3.11 displays the hydronium ion−hydronium ion PCFs in relation to the sulfur−sulfur PCFs. Since the hydronium ions are the counterions of the sulfonate anions, it is expected that

they will be associated with the latter at low water contents, a fact that has been observed in previous classical MD simulations [88, 93, 94, 97]. However, as the water content is increased, the hydronium ions become more separated from the sulfonate groups. The general feature of the hydronium−hydronium PCFs is that they peak at relatively large distances (i.e., >6 Å). The probability for close contact (at about 3 Å) is extremely small, and peaks in the PCFs occur at roughly about 7 and 9 Å. Clearly, repulsion prevents any close association of the hydronium ions, and due to their association with the sulfonate groups, their correlations occur at relatively great distances. The position of the peak may in some way reflect the character or size of the aqueous clusters. Small clusters (e.g., those at $\lambda = 4.4$) apparently are more likely to concentrate the hydronium ions in a small spatial region and cause stronger correlation. Furthermore, "pinning" of the H_3O^+ to one or more $-SO_3^-$ groups is likely to occur when little water is available to solvate the fixed anions [97].

Diffusion coefficients calculated from the mean-square displacement of H_2O and H_3O^+ for both PFSA membranes at all four hydration levels are plotted in Figure 3.12. The results were derived from simulations of at least 2 ns in length, with a sampling time of at least 1 ns following equilibration. The numerical results are collected in Table 3.2, along with experimental values taken from Kreuer et al.[2, 125]. The simulated hydronium ion diffusion coefficients for Nafion are consistently higher than those for the SSC PFSA membranes across the entire range of hydration. The simulated values are all lower, in comparison to the experimental values, though only slightly lower at the lowest hydration level (i.e., $\lambda = 4.4$) with the SSC ionomer. This would seem to support the findings of others that, as the water content is increased, the contribution of proton hopping to the overall proton diffusion increases. The agreement seen in the hydronium ion diffusion coefficients with measured proton diffusion coefficients does not rule out proton hopping at very low water contents, and although it has been suggested that under minimal hydration the mechanism may be vehicular (i.e., as H_3O^+) [3], it is probably more complicated than simply *en masse* diffusion. The water diffusion coefficients are also lower in the SSC ionomer at the various water contents, with the exception of $\lambda = 9.6$, where they are essentially equal. The calculated H_2O diffusion coefficients are consistently much higher than the experimental values, in contrast to the hydronium ion diffusion coefficients. This is a trend

observed in the classical MD simulations of Dupuis et al.[93, 95] using both a different model for Nafion and the water.

3.4 Conclusions

Molecular dynamics simulations were performed to analyze the effect of the length of the side chain on hydrated morphology and hydronium ion diffusion in Nafion and the SSC PFSA membranes. The cluster distributions displayed distinctive differences at the lower water contents (λ = 4.4 and 6.4); i.e., hydration of the SSC PFSA membrane tends to produce a more dispersed cluster distributions. At higher water content, the cluster differences between the two systems become very small, even though the SSC PFSA appears to show a slight tendency to be more connected. Since the hydrated membrane is inherently a heterogeneous system, even when the average water concentration is high, there are fluctuations where the local water concentration is low so that the mechanism considered here at lower water concentration is in operation. It is recognized that consideration of connectivity based on a molecular distance alone (which is the criterion used here for inclusion in a cluster) may not be discriminative enough to characterize the connectivity of a water-channel network; the channel width, for example, may also be important. A more complete method for characterizing the connectivity of a water-channel network, and a much larger system, is needed to understand completely the origin of the conductance behavior of these membrane materials. Nevertheless, an initial step has been taken in that direction, and the insight gained in this work provides a useful basis for understanding such systems. We are currently developing better methods for characterizing the water cluster-channel network and for directly calculating proton conductivity in the framework of reactive molecular dynamics.

The simulations indicate that the SSC PFSA tends to induce more dispersed water cluster distribution, and thus enhance the connectivity of the clusters by water channels, whereas the Nafion, with a longer and more flexible side chain, is more amenable to aggregate and form clusters that are more disconnected than the SSC PFSA. We also examined various pair correlation functions of which the most relevant are the ones that involve the sulfonic acid group and the hydronium ion. The pair correlation functions also suggest a more dispersed water distribution in the SSC PFSA membranes than Nafion, as indicated by lower peaks in the

sulfur−sulfur and hydronium−hydronium PCFs, consistent with cluster distribution analysis. The diffusion coefficient of water and hydronium ions are both slightly lower in the SSC PFSA membrane when compared to Nafion, suggesting that structural diffusion by proton hopping may account for the observed higher conductivities in the SSC PFSA membrane.

3.5 Acknowledgment

This work was supported by a grant from the U. S. Department of Energy BES program under contract number DE-FG02-05ER15723. Resources of the Center for Computational Sciences at Oak Ridge National Laboratory, which is supported by the Office of Science of the DOE under Contract DE-AC05-00OR22725 was used through the University of Tennessee Computational Science Initiative.

References

(1) S. J. Paddison, *Annu. Rev. Mater. Res.*, **2003**. 33, 289-319.

(2) K. D. Kreuer, M. Schuster, B. D. Obliers, O., U. Traub, A. Fuchs, U. Klock, S. J. Paddison, and J. Maier, *J.Power Sources*, **2008**. 178, 499-509.

(3) K. D. Kreuer, S. J. Paddison, E. Spohr, and M. Schuster, *Chem. Rev.*, **2004**. 104, 4637-4678.

(4) J. A. Elliott and S. J. Paddison, *Phys. Chem. Chem. Phys.*, **2007**. 9, 2602-2618.

(5) M. Tuckerman, K. Laasonen, M. Sprik, and M. Parrinello, *J. Phys. Chem.* , **1995**. 99, 5749-5752.

(6) D. Marx, M. E. Tuckerman, J. Hutter, and M. Parrinello, *Nature*, **1999**. 397, 601-604.

(7) N. Agmon, *Chem. Phys. Lett.*, **1995**. 244, 456-62.

(8) H. Lapid, N. Agmon, M. K. Petersen, and G. A. Voth, *J. Chem. Phys.*, **2005**. 122, 014506/1-014506/11.

(9) K. D. Kreuer, *Solid State Ionics*, **2000**. 136-137, 149-160.

(10) A. Eisenberg, *Macromolecules*, **1970**. 3, 147-154.

(11) T. D. Gierke, G. E. Munn, and F. C. Wilson, *J. Polym. Sci.: Polym. Phys. Ed.*, **1981**. 19, 1687-1704.

(12) G. Gebel and J. Lambard, *Macromolecules*, **1997**. 30, 7914-7920.

(13) M. H. Litt, *Polym. Prepr.*, **1997**. 38, 80.

(14) H. G. Haubold, T. Vad, H. Jungbluth, and P. Hiller, *Electrochimica Acta*, **2001**. 46, 1559-1563.

(15) A. L. Rollet, O. Diat, and G. Gebel, *J. Phys. Chem. B*, **2002**. 106, 3033-3036.

(16) L. Rubatat, A. L. Rollet, G. Gebel, and O. Diat, *Macromolecules*, **2002**. 35, 4050-4055.

(17) K. D. Kreuer, *J. Membr. Sci.*, **2001**. 185, 29-39.

(18) K. Schmidt-Rohr and Q. Chen, *Nat. Mater.*, **2008**. 7, 75-83.

(19) M. Falk, *Can. J. Chem.*, **1980**. 58, 1495-1501.

(20) R. Duplessix, M. Escoubes, B. Rodmacq, F. Volino, E. Roche, A. Eisenberg, and M. Pineri, in *Water in Polymers*, S. P. Rowland, Editor; American Chemical Society: Washington DC, 1980.

(21) B. Rodmacq, J. M. Coey, M. Escoubes, E. Roche, R. Duplessix, A. Eisenberg, and M. Pineri, in *Water in Polymers*, S. P. Rowland, Editor; American Chemical Society: Washington DC, 1980.

(22) T. D. Gierke, G. E. Munn, and F. C. Wilson, *J. Polym. Sci., Part B: Polym. Phys.*, **1981**. 19, 1687.

(23) W. Y. Hsu and T. D. Gierke, *J. Membr. Sci.*, **1983**. 13, 307-326.

(24) H. L. Yeager and A. Steck, *J. Electrochem. Soc.*, **1981**. 128, 1880-1884.

(25) M. W. Verbrugge and R. F. Hill, *J. Electrochem. Soc.*, **1990**. 137, 886-893.

(26) G. Gebel, *Polymer*, **2000**. 41, 5829-5838.

(27) P. J. James, J. A. Elliott, T. J. McMaster, J. M. Newton, A. M. S. Elliott, S. Hanna, and M. J. Miles, *J. Mater. Sci.*, **2000**. 35, 5111-5119.

(28) A. L. Rollet, G. Gebel, J. P. Simonin, and P. Turq, *J. Polym. Sci. B-Polym. Phys.*, **2001**. 39, 548-558.

(29) S. K. Young, S. F. Trevino, and N. C. B. Tan, *J. Polym. Sci. B-Polym. Phys.*, **2002**. 40, 387-400.

(30) M. Fujimura, T. Hashimoto, and H. Kawai, *Macromolecules*, **1981**. 14, 1309-1315.

(31) M. Fujimura, T. Hashimoto, and H. Kawai, *Macromolecules*, **1982**. 15, 136-144.

(32) E. J. Roche, M. Pineri, R. Duplessix, and A. M. Levelut, *J. Polym. Sci. B-Polym. Phys.*, **1981**. 19, 1-11.

(33) M. D. Heaney and J. Pellegrino, *J. Membr. Sci.*, **1989**. 47, 143-161.

(34) A. Lehmani, S. Durand-Vidal, and P. Turq, *J. Appl. Polym. Sci.*, **1998**. 68, 503-508.

(35) Z. Porat, J. R. Fryer, M. Huxham, and I. Rubinstein, *J. Phys. Chem.*, **1995**. 99, 4667-4671.

(36) M. Eikerling, A. A. Kornyshev, and U. Stimming, *J. Phys. Chem. B*, **1997**. 101, 10807-10820.

(37) V. K. Datye, P. L. Taylor, and A. J. Hopfinger, *Macromolecules*, **1984**. 17, 1704-1708.

(38) K. A. Mauritz, C. J. Hora, and A. J. Hopfinger, in *Ions in Polymers*, A. Eisenberg, Editor; American Chemical Society: Washington DC, 1980.

(39) K. A. Mauritz and C. E. Rogers, *Macromolecules*, **1985**. 18, 483-491.

(40) B. Dreyfus, *Macromolecules*, **1985**. 18, 284-292.

(41) J. A. Elliott, S. Hanna, A. M. S. Elliott, and G. E. Cooley, *Macromolecules*, **2000**. 33, 4161-4171.

(42) Y. K. Tovbin, *Zhurnal Fizicheskoi Khimii*, **1998**. 72, 55-59.

(43) Y. K. Tovbin and N. F. Vasyatkin, *Colloid Surf. A*, **1999**. 158, 385-397.

(44) S. Cui, J. Liu, M. Esai Selvan, D. J. Keffer, B. J. Edwards, and W. V. Steele, *J. Phys. Chem. B*, **2007**. 111, 2208-2218.

(45) M. Tuckerman, K. Laasonen, M. Sprik, and M. Parrinello, *J. Chem. Phys.*, **1995**. 103, 150-161.

(46) U. W. Schmitt and G. A. Voth, *J. Chem. Phys.*, **1999**. 111, 9361-9381.

(47) M. Doi and S. F. Edwards, *The Theory of Polymer Dynamics*, Oxford University Press, 1986.

(48) O. Savadogo, *J. New Mater. Electrochem. Syst.*, **1998**. 1, 47-66.

(49) J. A. Kerres, *J. Membrane Sci.*, **2001**. 185, 3.

(50) R. Souzy and B. Ameduri, *Progress in Polymer Science*, **2005**. 30, 644-687.

(51) J. Roziere and D. J. Jones, *Annu. Rev. Mater. Res.*, **2003**. 33, 503.

(52) G. Alberti and M. Casciola, *Ann. Rev. Mater. Res.*, **2003**. 33, 129-154.

(53) O. Savadogo, *J. Power Sources*, **2004**. 127, 135-161.

(54) S. J. Hamrock and M. A. Yandrasits, *J. Macromol. Sci. C: Polym. Rev.*, **2006**. 46, 219-244.

(55) M. R. Tant, K. P. Darst, K. D. Lee, and C. W. Martin, *Multiphase Polymers: Blends and Ionomers*; ACS Proceedings Series; American Chemical Society: Washington, DC, 1989.

(56) R. B. I. Moore and C. R. Martin, *Macromolecules*, **1989**. 22, 3594-9.

(57) G. Gebel and R. B. Moore, *Macromolecules*, **2000**. 33, 4850-4855.

(58) B. R. Ezzell, W. P. Carl, and W. A. Mod, *Sulfonic acid electrolyte cell having fluorinated polymer membrane with hydration product less than 22,000*; The Dow Chemical Company: U.S., 1982.

(59) J. Halim, F. N. Buchi, O. Haas, M. Stamm, and G. G. Scherer, *Electrochim. Acta*, **1994**. 39, 1303-1307.

(60) T. A. Zawodzinski, T. A. Springer, J. Davey, R. Jestel, C. Lopez, J. Valerio, and G. Shimshon, *J. Electrochem. Soc.*, **1993**. 140, 1981-1985.

(61) C. A. Edmondson and J. J. Fontanella, *Solid State Ionics*, **2002**. 152, 355.

(62) K. Prater, *J. Power Sources*, **1990**. 29, 239-250.

(63) V. Arcella, A. Ghielmi, and G. Tommasi, *Ann. N. Y. Acad. Sci.*, **2003**. 984, 226-244.

(64) V. Arcella, C. Troglia, and A. Ghielmi, *Ind. Eng. Chem. Res.*, **2005**. 44, 7646.

(65) A. Ghielmi, P. Vaccarono, C. Troglia, and V. Arcella, *J. Power Sources*, **2005**. 145, 108.

(66) S. J. Hamrock, L. M. Rivard, G. I. Moore, and H. T. Freemeyer, *Polymer Electrolyte Membranes*; US Patent, 2004.

(67) M. Emery, M. Guerra, G. Haugen, K. Hintzer, K. H. Lochhaas, P. P. Pham, D., M. T. Schaberg, A., M. Yandrasits, and S. Hamrock, *ECS Trans.* , **2007**. 11, 3.

(68) D. Wu, S. J. Paddison, and J. A. Elliott, *Energy Environ. Sci.* , **2008**. 1, 284-293.

(69) S. J. Paddison and T. A. Zawodzinski, *Solid State Ionics*, **1998**. 113–115, 333-340.

(70) J. A. Elliott, S. Hanna, A. M. S. Elliott, and G. E. Cooley, *Phys. Chem. Chem. Phys.*, **1999**. 1, 4855-4863.

(71) S. J. Paddison, L. R. Pratt, and T. A. Zawodzinski, *J. New Mater. Electrochem. Syst.*, **1999**. 2, 183-188.

(72) S. J. Paddison, R. Paul, and T. A. Zawodzinski, *J. Electrochem. Soc.*, **2000**. 147, 617-626.

(73) A. Vishnyakov and A. V. Neimark, *J. Phys. Chem. B*, **2000**. 104, 4471-4478.

(74) A. Vishnyakov and A. V. Neimark, *J. Phys. Chem. B*, **2001**. 105, 7830-7834.

(75) A. Vishnyakov and A. V. Neimark, *J. Phys. Chem. B*, **2001**. 105, 9586-9594.

(76) S. J. Paddison, R. Paul, and T. A. Zawodzinski, *J. Chem. Phys.*, **2001**. 115, 7753-7761.

(77) S. J. Paddison, *J. New Mater. Electrochem. Syst.*, **2001**. 4, 197-207.

(78) E. Spohr, P. Commer, and A. A. Kornyshev, *J. Phys. Chem. B*, **2002**. 106, 10560-10569.

(79) P. Commer, A. G. Cherstvy, E. Spohr, and A. A. Kornyshev, *Fuel Cells*, **2002**. 2, 127-136.

(80) M. Eikerling, S. J. Paddison, and T. A. J. Zawodzinski, *J. New Mater. Electrochem. Syst.*, **2002**. 5, 15-23.

(81) S. J. Paddison, R. Paul, and K. D. Kreuer, *Phys. Chem. Chem. Phys.*, **2002**. 4, 1151-1157.

(82) S. J. Paddison and R. Paul, *Phys. Chem. Chem. Phys.*, **2002**. 4, 1158-1163

(83) S. S. Jang, V. Molinero, T. Cagin, and W. A. Goddard, *J. Phys. Chem. B*, **2004**. 108, 3149-3157.

(84) R. Paul and S. J. Paddison, *J. Phys. Chem. B*, **2004**. 108, 13231-13241.

(85) S. Urata, J. Irisawa, A. Takada, W. Shinoda, S. Tsuzuki, and M. Mikami, *J. Phys. Chem. B*, **2005**. 109, 4269-4278.

(86) S. I. J. Urata, A. Takada, W. Shinoda, S. Tsuzuki, and M. Mikami, *J. Phys. Chem. B*, **2005**. 109, 17274.

(87) N. P. Blake, M. K. Petersen, G. A. Voth, and H. Metiu, *J. Phys. Chem. B* **2005**. 109, 24244.

(88) R. Paul and S. J. Paddison, *J. Chem. Phys.*, **2005**. 123, 224704.

(89) S. J. Paddison and J. A. Elliott, *J. Phys. Chem. A*, **2005**. 109, 7583-7593.

(90) M. K. Petersen and G. A. Voth, *J. Phys. Chem. B* **2006**. 110, 18594-18600.

(91) S. J. Paddison and J. A. Elliott, *Phys. Chem. Chem. Phys.*, **2006**. 8, 2193-2203.

(92) S. J. Paddison and J. A. Elliott, *Solid State Ionics*, **2006**. 177, 2385.

(93) A. Venkatnathan, R. Devanathan, and M. Dupuis, *J. Phys. Chem. B*, **2007**. 111, 7234-7244.

(94) R. Devanathan, A. Venkatnathan, and M. Dupuis, *J. Phys. Chem. B*, **2007**. 111, 8069-8079.

(95) R. Devanathan, A. Venkatnathan, and M. Dupuis, *J. Phys. Chem. B*, **2007**. 111, 13006-13013.

(96) S. J. Paddison and J. A. Elliot, *Solid State Ionics*, **2007**. 178, 561-567.

(97) I. H. Hristov, S. J. Paddison, and R. Paul, *J. Phys. Chem. B*, **2008**. 112, 2937-2949.

(98) S. T. Cui, J. W. Liu, M. E. Selvan, D. J. Keffer, B. J. Edwards, and W. V. Steele, *J. Phys. Chem. B* **2007**. 111, 2208.

(99) M. E. Selvan, J. Liu, D. J. Keffer, S. Cui, B. J. Edwards, and W. V. Steele, *J. Phys. Chem. C* **2008**. 112, 1975.

(100) J. Liu, M. E. Selvan, S. Cui, B. J. Edwards, D. J. Keffer, and W. V. Steele, *J. Phys. Chem. C* **2008**. 112, 1985.

(101) S. Cui, J. I. Siepmann, H. D. Cochran, and P. T. Cummings, *Fluid Phase Equilib.*, **1998**. 146, 51-61.

(102) H.-C. Li, C. McCabe, S. Cui, P. T. Cummings, and H. D. Cochran, *Mol. Phys.*, **2003**. 101, 2157-2169.

(103) S. P. Gejji, K. Hermansson, and J. Lindgren, *J. Phys. Chem.*, **1993**. 97, 3712-3715.

(104) W. D. Cornell, P. Cieplak, C. I. Bayly, I. R. Gould, K. M. Nerz, D. M. Ferguson, D. C. Spellmeyer, T. Fox, J. W. Caldwell, and P. A. Kollman, *J. Am. Chem. Soc.* , **1995**. 117, 5179.

(105) D. Rivin, G. Meermeier, N. S. Schneider, A. Vishnyakov, and A. V. Neimark, *J. Phys. Chem. B*, **2004**. 108, 8900-8909.

(106) W. L. Jorgensen, J. Chandrasekhar, J. D. Madura, R. W. Impey, and M. L. Klein, *J. Chem. Phys.*, **1983**. 79, 926-935.

(107) D. J. Price and C. L. Brooks, *J. Chem. Phys.*, **2004**. 121, 10096-10103.

(108) G. Hummer, D. M. Soumpasis, and M. Neumann, *Mol. Phys.*, **1992**. 77, 769-785.

(109) S. Cui and J. G. Harris, *Chem. Eng. Sci.*, **1994**. 49, 2749-2763.

(110) D. R. Morris and X. Sun, *J. Appl. Polym. Sci.*, **1993**. 50, 1445-1452.

(111) M. Tuckerman, B. J. Berne, and G. J. Martyna, *J. Chem. Phys.*, **1992**. 97, 1990-2001.

(112) S. Nosé, *Mol. Phys.*, **1984**. 52, 255-268.

(113) S. Nosé, *J. Chem. Phys.*, **1984**. 81, 511-519.

(114) W. G. Hoover, *Phys. Rev. A*, **1985**. 31, 1695-1697.

(115) C. Radüge, V. Pflumio, and Y. R. Shen, *Chem. Phys. Lett.*, **1997**. 274, 140.

(116) P. B. Miranda and Y. R. Shen, *J. Phys. Chem. B* **1999**. 103, 3292.

(117) M. S. Shultz, S. Baldelli, C. Schnitzer, and D. Simonelli, *J. Phys. Chem. B*, **2002**. 106, 5313.

(118) P. B. Petersen and R. J. Saykally, *J. Phys. Chem. B*, **2005**. 109, 7976.

(119) P. B. Petersen and R. J. Saykally, *Chem. Phys. Lett.* , **2008**. 458, 255.

(120) S. S. Iyengar, T. J. F. Day, and G. A. Voth, *Int. J. Mass Spectrosc.*, **2005**. 241, 197.

(121) J. A. Morrone, K. E. Haslinger, and M. E. Tuckerman, *J. Phys. Chem. B*, **2006**. 110, 3712-3720.

(122) S. J. Paddison, G. Bender, K. D. Kreuer, N. Nicoloso, and T. A. Zawodzinski, *J. New Mater. Electrochem. Syst.*, **2000**. 3, 291.

(123) R. Paul and S. J. Paddison, *Solid State Ionics*, **2004**. 168, 245-248.

(124) *Device and Materials Modeling in PEM Fuel Cells*. S. J. Paddison, Promislow, K. S., Eds., Springer: New York, 2008.

(125) K. D. Kreuer, *Solid State Ionics*, **1997**. 97, 1.

Appendix B

Table 3. 1 Aqueous cluster characteristics as functions of cluster cut-off distance.

	Rc = 2.8 Å		Rc = 3.5 Å		Rc = 4.5 Å	
	Nafion	SSC	Nafion	SSC	Nafion	SSC
$\lambda = 4.4$ presence of SaSC	N	N	N	N	Y	Y
peak position/ range	N/A	N/A	N/A	N/A	Continuous distribution	Continuous distribution
% of molecules in SaSC	0.0	0.0	0.0	0.0	13.06	23.00
$\lambda = 6.4$ presence of SaSC	N	N	Y	Y	Y	Y
peak position/ range	N/A	N/A	1107/ 986-1232	1123/ 0-1190	1232/ 1159-1232	1215/ 1128-1232
% of molecules in SaSC	0.0	0.0	41.0	74	98.36	98.21
$\lambda = 9.6$ presence of SaSC	N	N	Y	Y	Y	Y
peak position/ range	N/A	N/A	1833/ 1793-1848	1825/ 1748-1848	1848/ 1832-1848	1848/ 1820-1848
% of molecules in SaSC	0.0	0.0	96.80	98.4	99.28	99.78
$\lambda = 12.8$ presence of SaSC	N	N	Y	Y	Y	Y
peak position/ range	N/A	N/A	2464/ 2425-2464	2453/ 2377-2464	2464/ 2445-2464	2464/ 2440-2464
% of molecules in SaSC	0.0	0.0	99.05	99.3	99.55	99.92

Table 3. 2 Diffusion coefficients[a] for water and hydronium ions in hydrated SSC PFSA and Nafion membranes at various water contents.

water content	SSC PFSA		Nafion	
λ	H_2O	H_3O^+	H_2O	H_3O^+
4.4	0.91 (0.4)[b]	0.11 (0.1)[b]	1.02 (0.5)[c]	0.20 (0.4)[c]
6.4	2.78 (1.0)	0.41_5 (0.6)	3.56 (1.0_5)	0.97 (1.1_5)
9.6	6.50 (2.0)	1.34 (3.5)	6.39 (4.0)	1.96 (3.5)
12.8	7.86 (4.0)	2.12 (8.0)	9.66 (4.5)	3.20 (7.0)

[a] Calculated from mean square displacements. All values $\times 10^{-6}$ cm^2 s^{-1}.

[b] Values in parentheses for both water and hydrated proton for the SSC PFSA membrane are experimental values for the Dow membrane with an EW of 1150 [3].

[c] Values in parentheses for both water and hydrated proton for the Nafion membrane are experimental values for Nafion 117 [118].

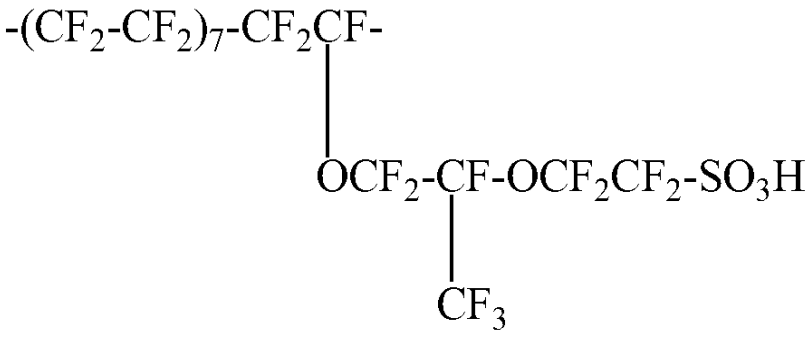

(a)

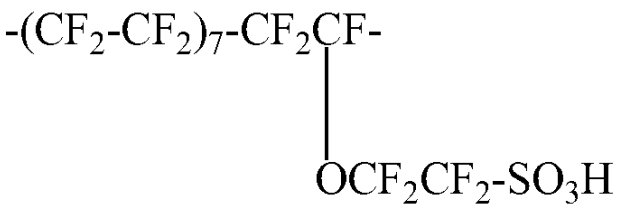

(b)

Figure 3. 1 Chemical structures of the monomers used in the simulations with side chain separation of $–(CF_2)_{15}–$ in the PTFE backbone: (a) 1143 EW Nafion; and (b) 977 EW SSC PFSA ionomer.

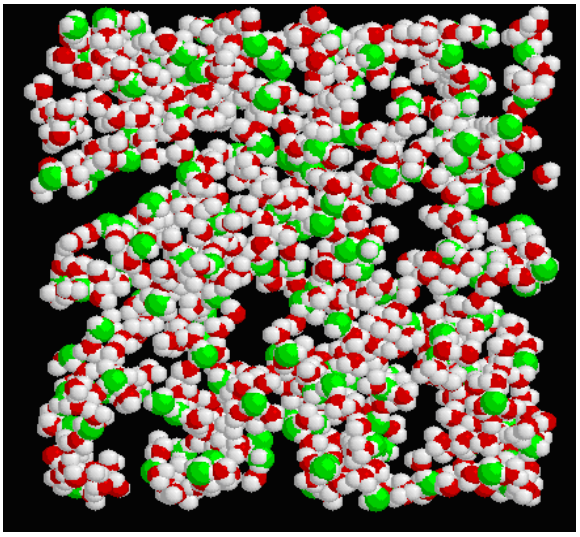

(a)

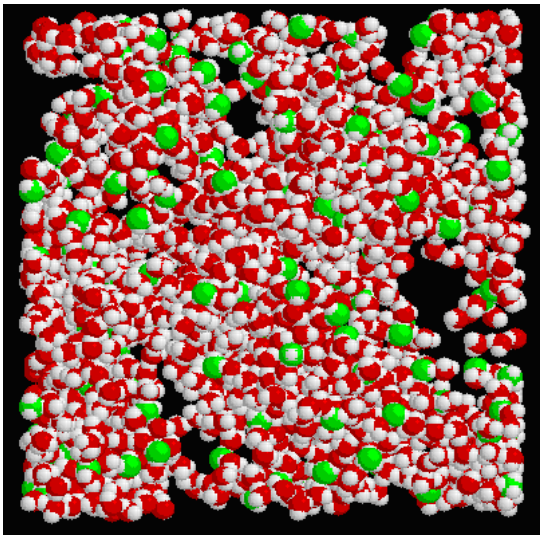

(b)

Figure 3. 2 Snapshots of the final configurations of the SSC PFSA ionomer at hydration levels of (a) $\lambda = 4.4$, and (b) $\lambda = 9.6$. Atoms of the ionomer are not shown. Red atoms are oxygen atoms of water molecules, green atoms are oxygen atom of hydronium ions, and white atoms are hydrogen atoms.

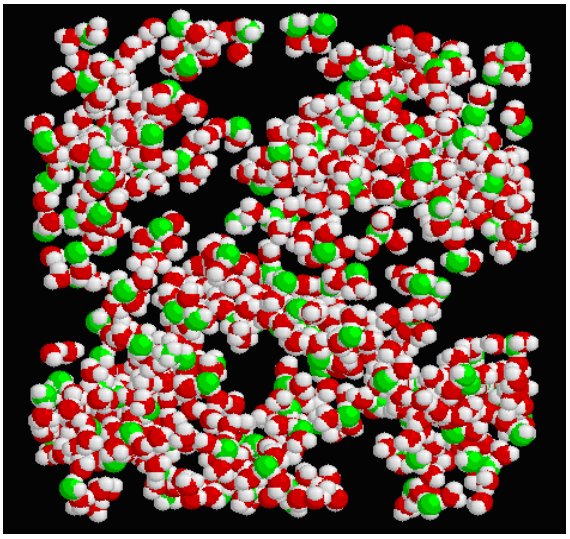

(a)

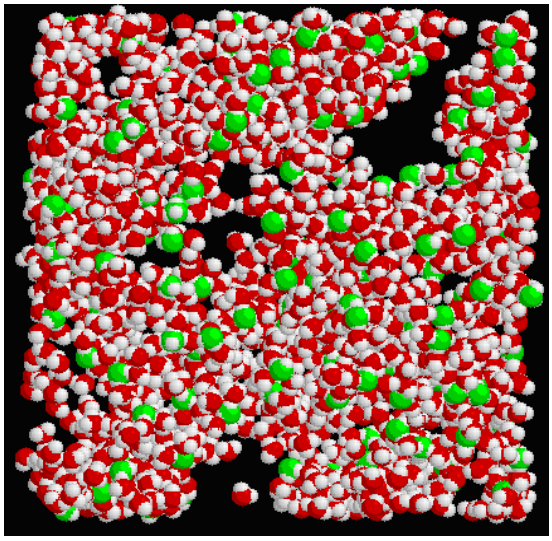

(b)

Figure 3. 3 Snapshots of the final configurations of hydrated Nafion at hydration levels of (a) λ = 4.4 and (b) λ = 9.6. Atoms of the ionomer are not shown. Atomic color scheme is as in Figure 3.2.

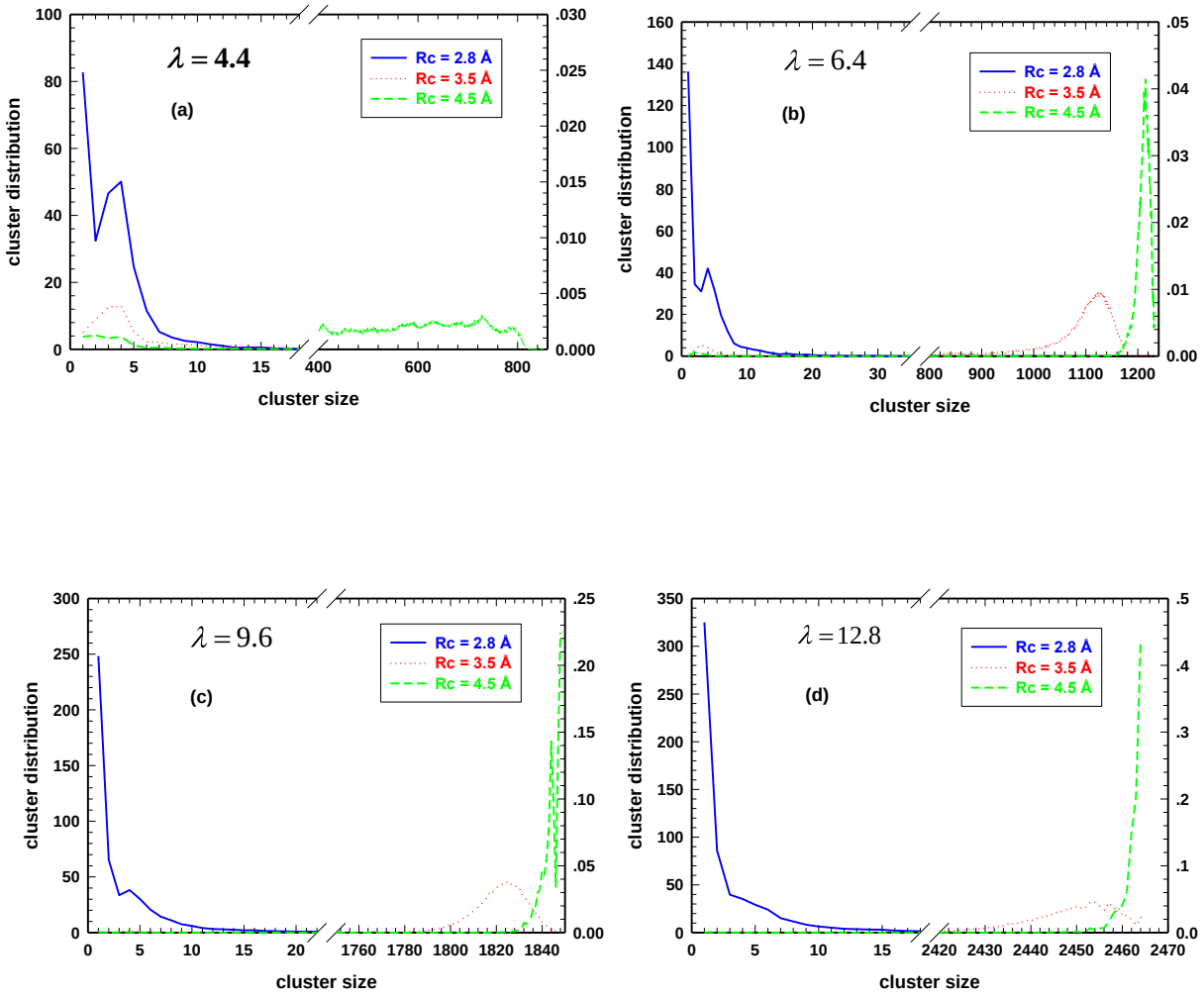

Figure 3. 4 Cluster size distribution for hydrated SSC PFSA at water contents corresponding to (a) λ = 4.4; (b) λ = 6.4; (c) λ = 9.6; and (d) λ = 12.8.

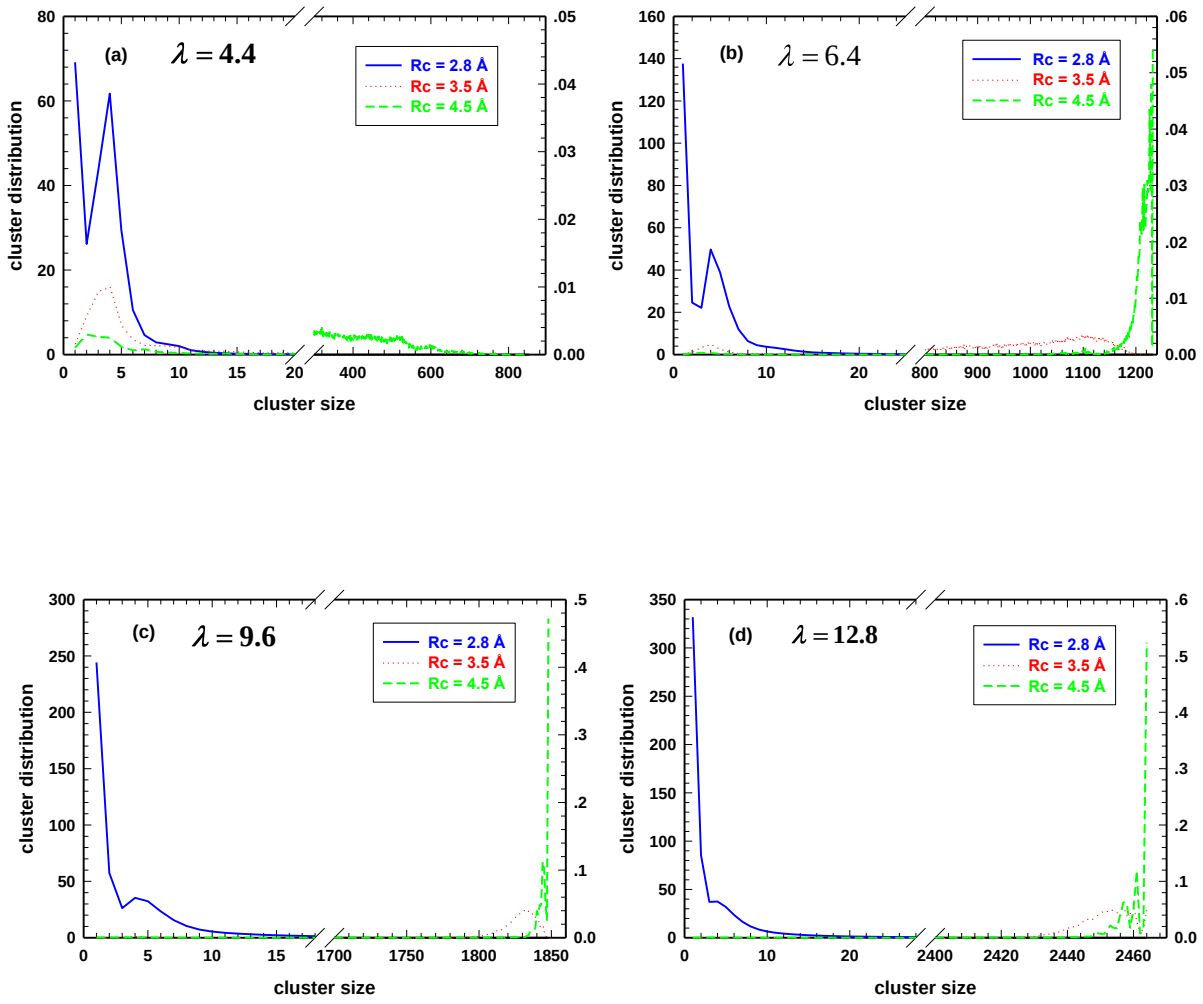

Figure 3. 5 Cluster size distribution for hydrated Nafion at water contents corresponding to (a) λ = 4.4; (b) λ = 6.4; (c) λ = 9.6; and (d) λ = 12.8.

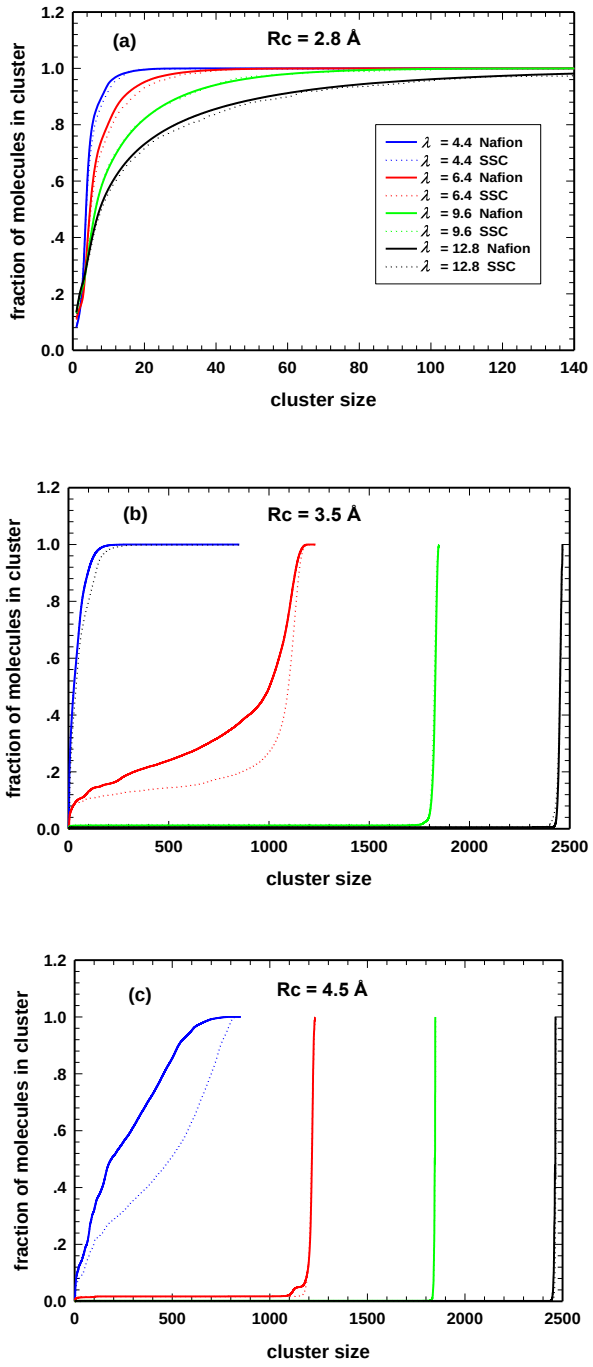

Figure 3. 6 Cumulative number of molecules in clusters in hydrated SSC PFSA ionomer and Nafion for Rc of (a) 2.8 Å; (b) 3.5 Å; and (c) 4.5 Å. Line types in (b) and (c) are the same as in (a).

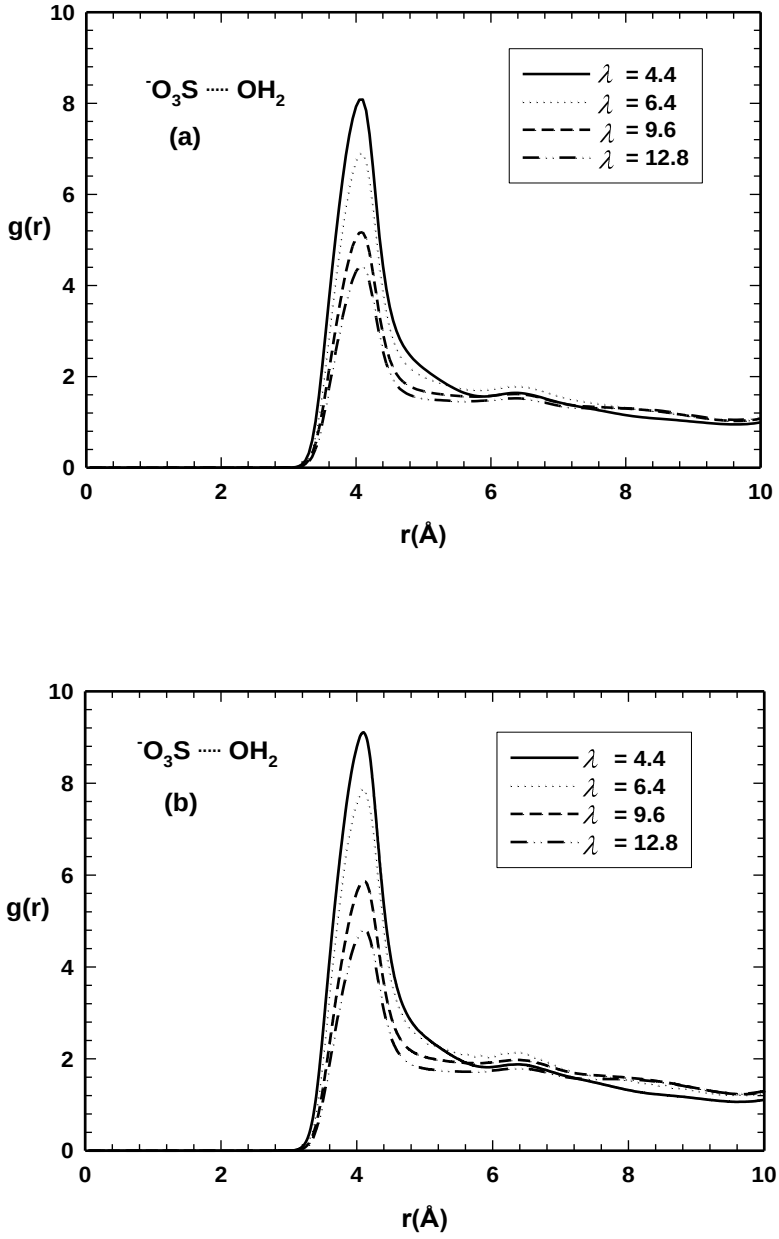

Figure 3. 7 Sulfur-water (oxygen atom of water molecule) pair correlation functions: (a) SSC PFSA; and (b) Nafion.

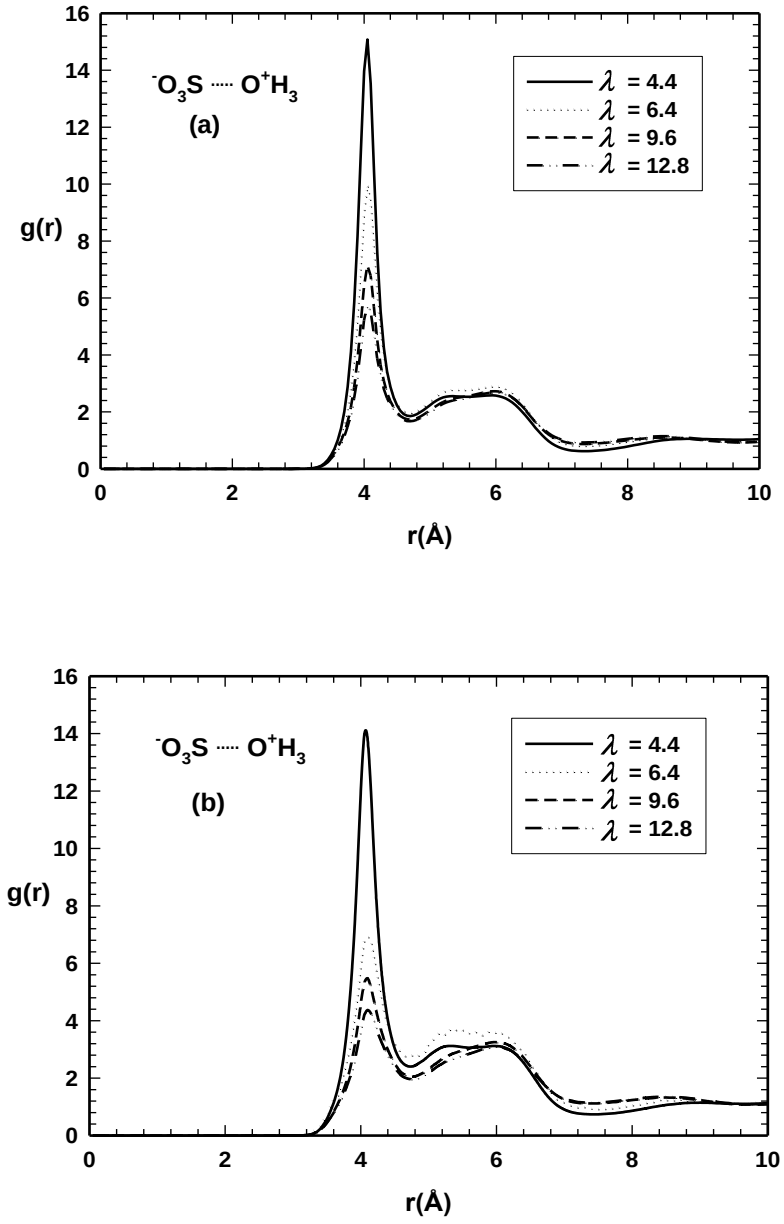

Figure 3. 8 Sulfur-hydronium (oxygen atom of hydronium ion) pair correlation function: (a) SSC-PFSA; (b) Nafion.

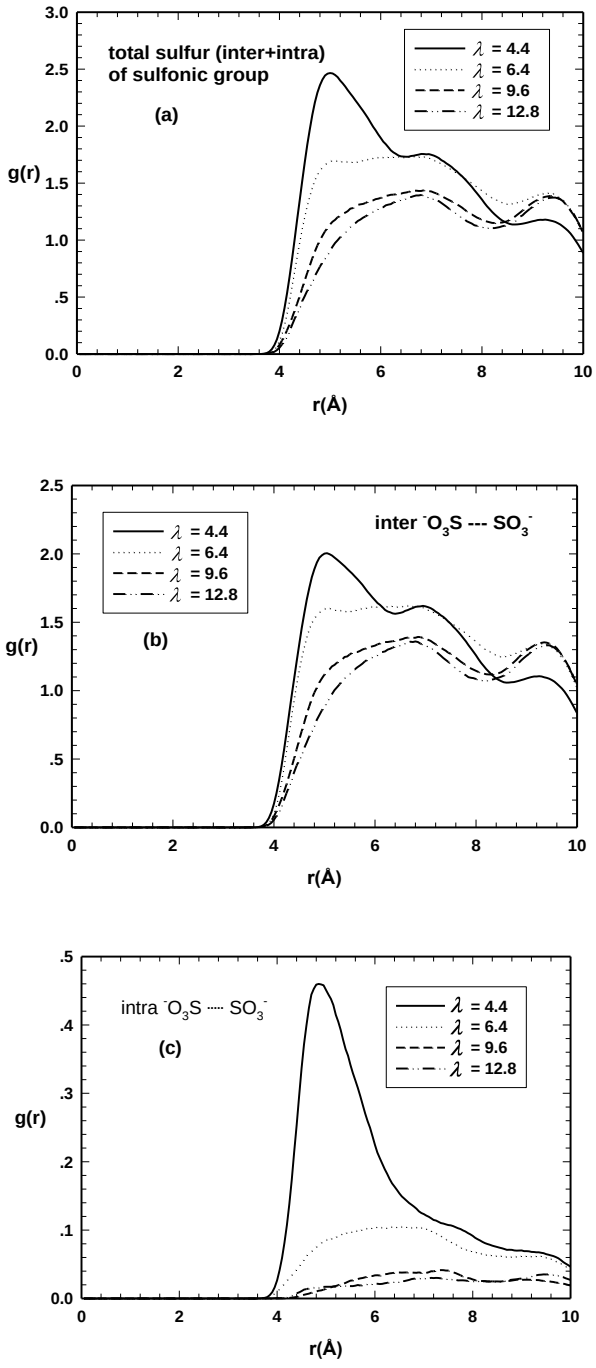

Figure 3. 9 Sulfur-sulfur pair correlation functions for hydrated SSC PFSA ionomer: (a) total; (b) intermolecular; and (c) intramolecular.

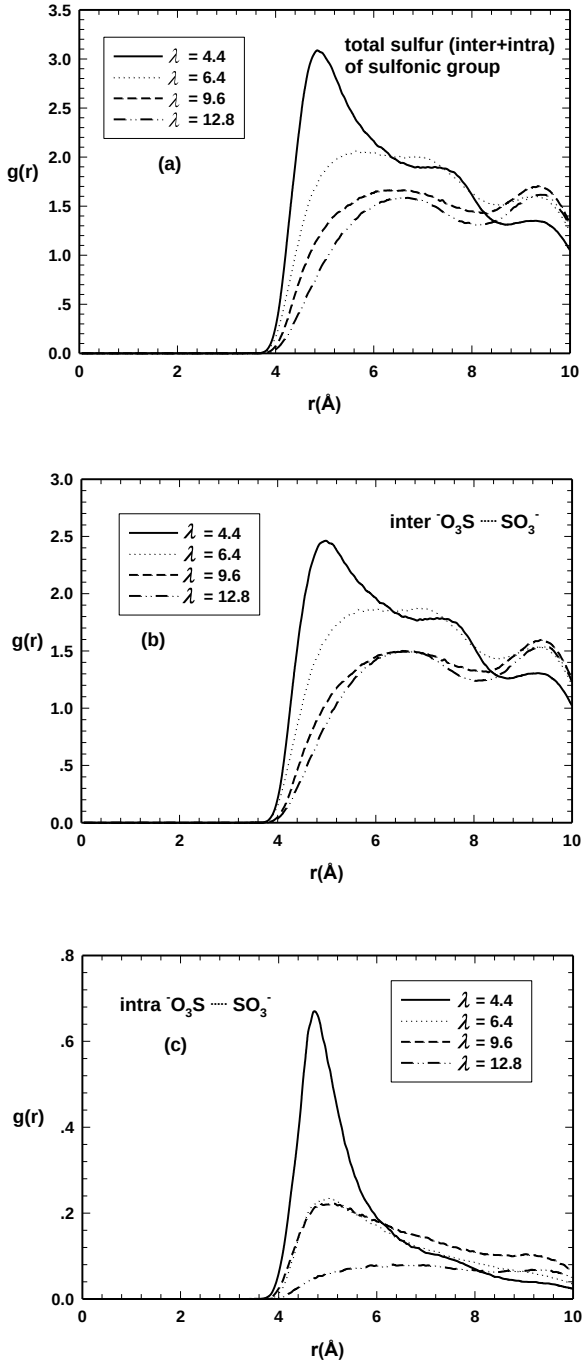

Figure 3. 10 Sulfur-sulfur pair correlation functions for hydrated Nafion: (a) total; (b) intermolecular; and (c) intramolecular.

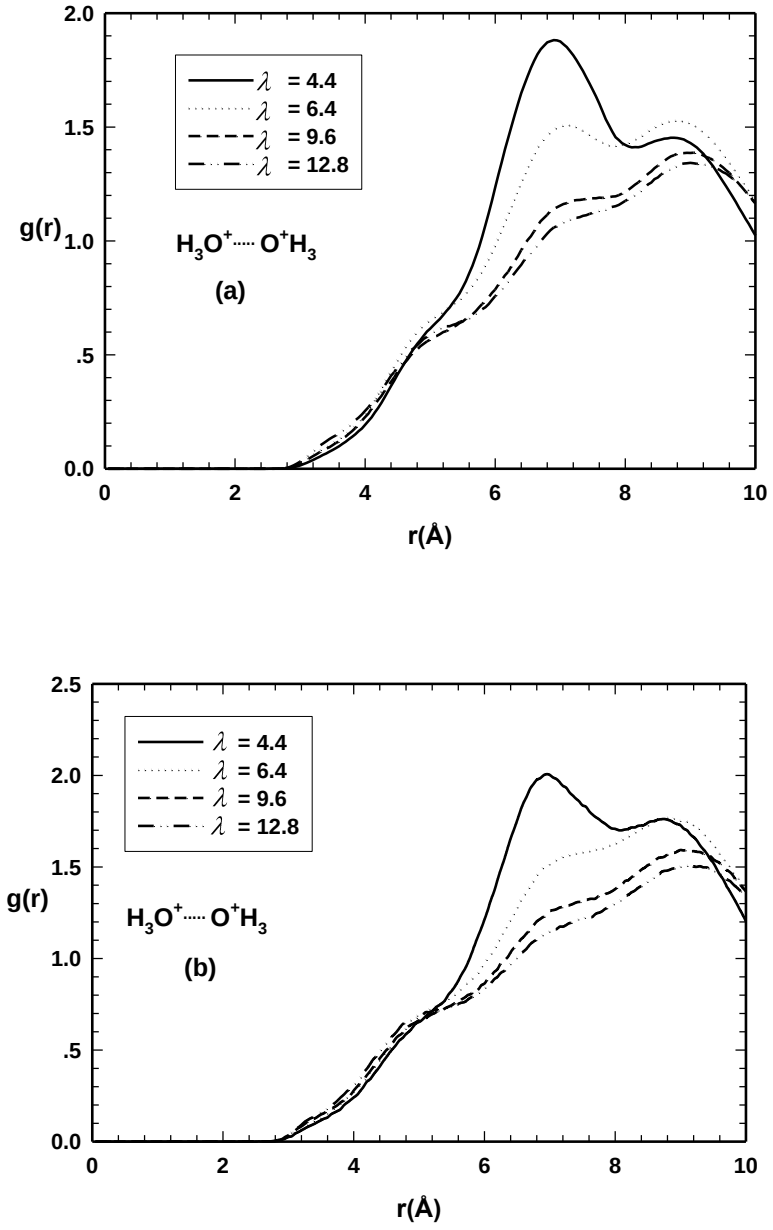

Figure 3. 11 Hydronium ion-hydronium ion pair correlation functions for: (a) SSC PFSA ionomer; and (b) Nafion.

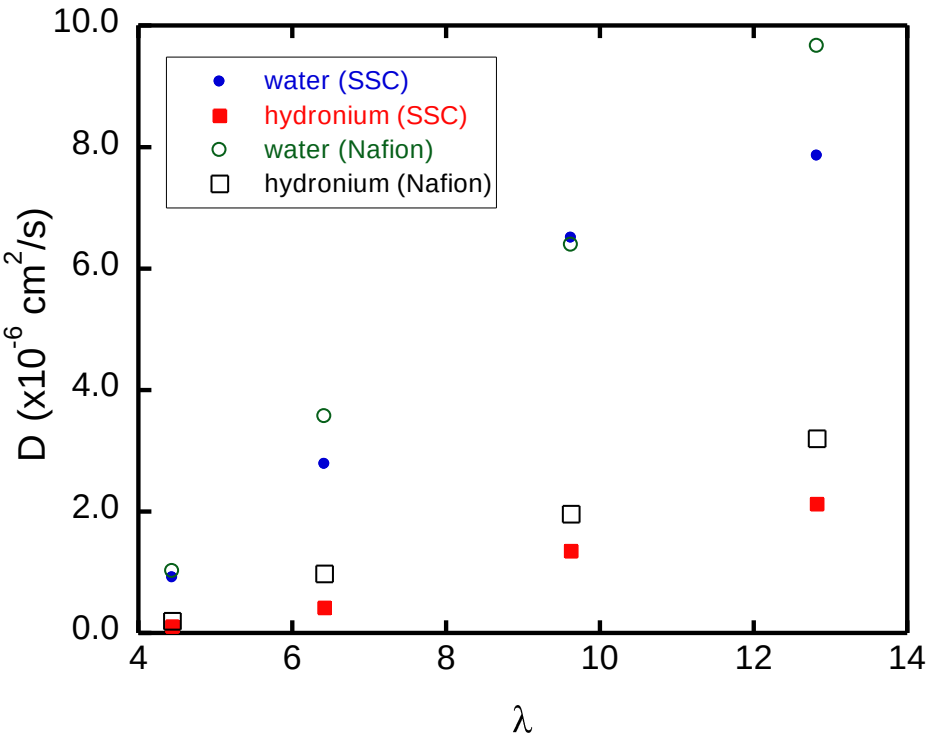

Figure 3. 12 Water and hydronium ion diffusion coefficients of hydrated Nafion and SSC PFSA ionomers.

Chapter 4

The relationship between perfluorosulfonic acid polymer electrolyte structure and hydrated membrane morphology

This part is a slightly revised version of a paper under preparation by Junwu Liu, David J. Keffer, Shengting Cui, Stephen J. Paddison:

J.W. Liu, D.J. Keffer, C.T. Cui, and S.J. Paddison, "The relationship between perfluorosulfonic acid polymer electrolyte structure and hydrated membrane morphology", *under preparation.*

The use of "we" in this part refers to the co-authors and the author of this dissertation. My primary contributions to this paper include (1) implementation of simulation methodology, (2) all of the simulation work and analysis, (3) most of the gathering and interpretation of literature, and (4) most of the writing.

Abstract:

Molecular dynamics simulations were performed to investigate the relationship between the molecular-level structure of perfluorosulfonic acid (PFSA) polymer electrolytes and the nanoscale morphology of the hydrated membranes. Three architectural features are examined including (i) the length of the side-chain to which the sulfonic acid group is attached, (ii) the equivalent weight (EW) of the electrolyte ionomer, and (iii) the molecular weight (MW) of the polymer electrolyte. Membrane morphologies are studied from the water content $\lambda = 3$ (λ represents number of water molecules per sulfonate group) to saturation ($\lambda = 22$). An increase in side-chain length results in a larger characteristic dimension of the aqueous domain, less local confinement for aqueous species, a more poorly connected global aqueous domain. A decrease in EW results in a larger characteristic dimension of the hydrophobic domain, less local confinement for aqueous species, and a better connected aqueous domain. Connectivity enhances and confinement reduces water mobility. A decrease in EW changes both factors (connectivity and confinement) to favor an increase in diffusivity. An increase in side-chain length changes the connectivity to decrease diffusivity but the confinement to increase diffusivity, which together result in little change in the observed water diffusivity. For the short chains studied, we find these results to be independent of MW.

4.1 Introduction

Perfluorosulfonic acid (PFSA) polymeric materials are widely used in polymer electrolyte membrane (PEM) fuel cells as the electrolyte positioned between two porous, catalyst-containing electrodes to facilitate the transport of protonic charges while preventing the transfer of reactant fuels. Many such PFSA materials are commercially available, such as Nafion® (Dupont), Flemion® and Aciplex® (Asahi Chemical), and the short side-chain (SSC) membrane synthesized by Solvay-Solexis as Hyflon®. Particularly, Nafion, the archetypal PFSA membrane, has been studied extensively exhibiting good thermal, mechanical stability and favorable proton conductivity. Some authors have focused on characterizing and investigating the properties of Nafion and other PEMs [1-4]. It is generally accepted that Nafion, when hydrated, exhibits a morphology with nanophase-segregation. There is a hydrophobic matrix, consisting of the fluorinated polymer backbone, within which a hydrophilic domain, consisting of sulfonate groups, water molecules and other hydrophilic components, is distributed. A wealth of experimental and theoretical work has been carried out to elucidate the hydrated morphology of Nafion [5-33], but the local microscopic structure and the transport mechanism for protons, water, and other organic species unfortunately remain elusive, largely due to the inhomogeneous nature of the polymeric materials.

Nafion has drawbacks restricting it as a direct substitute for current energy demands including high production cost, poor protonic conduction at high temperatures and low humidity conditions, and complex water management issues. While substantial research has been devoted in recent years to mitigate these restraints, which affect directly and negatively the performance of PEM fuel cells, the ultimate solution to these efficiency-limiting factors should be addressed through the synthesis and development of novel materials. A fundamental, molecular-scale understanding of the relationship between the chemical composition of the PEM and the resulting transport properties would significantly aid in this direction, since the chemical composition of the PEM affects the membrane morphology, which in turn dictates the connectivity and confinement of the aqueous phase, thus controlling the transport of protons and water.

To understand the effect of side-chain length, one can compare the short side-chain (SSC) PFSA with Nafion. Dow Chemical originally synthesized the short side-chain (SSC) PFSA

membrane with similar polymeric backbone but disparate side chain -$OCF_2CF_2SO_3H$ to investigate the differences of proton conduction [34]. Solvay Solexis used a simpler and more efficient manufacturing method to synthesize a polymer with the same structure as Hyflon® [35]. When compared with Nafion, the SSC PFSA membrane has been reported to have the similar morphology[36, 37] but improved performances such as superior proton conductivity at low to intermediate hydration levels and lower bulk resistance [38, 39]. A theoretical study found that at a low water content, Nafion tends to form isolated water domains, whereas SSC forms a more uniformly distributed water network. At a high hydration level, the situation was reverse [40]. The flexibility difference of the sulfonic acid terminated side chains clearly gives rise to the qualitative differences of the hydrated morphology and the proton conduction. Another important difference is the SSC PFSA membrane has a higher glass transition temperature which is an advantage for high temperature operation of fuel cells [41]. We recently performed classical molecular dynamic (MD) simulations to identify the differences of the hydrated morphology and proton diffusion coefficients in Nafion and SSC with the same backbone but different side-chain length and found that the SSC PFSA membranes tend to produce a more dispersed cluster distribution at low to intermediate hydration levels and these distinctions will become smaller at higher water contents [43]. In a recent paper, Hristov and Paddison *et al.*[43] performed classical MD simulations to characterize the hydrated morphology and hydrionium ion conductivity of low equivalent weight (EW of 580) SSC PFSA membranes. The hydrated morphology reveals the formation of hydrogen bond 'bridges' between distant sulfonate groups. At the lowest hydration level ($\lambda = 3$), there is the presence of ion cages consisting of hydronium ions hydrogen-bonded to three sulfonate groups. Still, the effect of side-chain length on the morphology and proton conduction is a complex area. Taken together, all of the current knowledge is somewhat contradictory. On one hand, experimental data shows that SSC PFSA membrane has superior proton conductivities, such as the finding of Eisman [34], which presented the better performance of the Dow material of EW 800 compared to Nafion 117 of EW 1100. On the other hand, theoretical studies suggest that the more flexible side chains of Nafion contribute to a higher proton mobility, since the flexibility of the side chains will reduce the surface tension of the narrow water channels, hence lowering the activation energy barriers of

proton conduction [44]. A meaningful conclusion will come from a thorough and accurate investigation and characterization of the molecular-based phenomena.

In addition to the variation in the side-chain length between Nafion and SSC PFSA membranes, there are other features of the polymer structure exploited to improve membrane properties. The equivalent weight (EW) is one of them. The effects of EW on the fuel cell performance were investigated experimentally [45]. They reported that 800 EW Nafion ionomers significantly improve the cell performance at 120˚C/35% relative humidity (RH) compared to 1100 EW Nafion, whereas, at 80˚C/100% RH, the difference is not apparent. Jalani and Datta[46] probed the effects of water activity on water sorption behavior through the comparison of Nafion membranes of three different EWs: 960, 1100, and 1200. They observed that the membrane will absorb more water as EW is decreased and the difference becomes greater at higher RH. In electronic structure calculations of two side chain fragments of the SSC ionomer, Paddison and Elliott[47] found that the separation distance of sulfonic acid groups on the polymeric backbone affects the minimum amount of water necessary to facilitate the proton(s) transfer to the first hydration shell and the character of the hydrated proton. Two extreme cases were reported by Jang et al.[48] to study the effects of monomeric sequence on the polymer structure and the ionic transport. One case has the side chains evenly spaced on the backbone; the other has all the side chains aggregated at one end of the polymer. They found that the transport of water molecules with the latter case is larger than with the former, consistent with their observation that the latter blocky case leads to larger aqueous clusters.

Classical MD simulations are successful in providing insights into the PFSA membrane morphology and their consequent effects on proton transport. But due to computational limits, all MD simulations chose systems much smaller than those used in real applications. The challenge is to ensure a fully equilibrated configuration, since the timescales required for equilibration of long polymers is beyond the timescale accessible to MD. Regardless, useful information can be obtained from the examination of shorter chains. We previously modeled Nafion with three side chains (trimer)[49] and obtained consistent simulation results with those of published work, such as that of Vishnyakov and Neimark, and that of Urata *et al.*, both using oligomers containing 10 monomers [50, 51]. Hristov and Paddision *et al.* [43], in their recent paper, used

one macromolecule with forty monomer units. In the present work, we used 40 Nafion ionomers, each with 15 side chains, which will allow us to evaluate the effect of molecular weight (MW) at least in this small chain limit.

Proton transport in the hydrated membrane remains a challenging process to model at the molecular level. There remains much to be understood regarding how the conformational changes of the polymeric backbone, flexibility of side-chain, hydration levels, and molecular weight of the polymer collectively determine the proton translocation process. It is recognized as a sequential concerted two mechanisms: "Grotthuss shuttling" in the form of hydrogen-bonded proton-water network [52] and the vehicular diffusion of hydronium cations (H_3O^+), the solvated form of excess proton [16]. However, their relative contributions are not fully understood. Petersen *et al.* [53], by using a self-consistent multistate empirical valence bond (SCI-MS-EVB) model, suggested that the vehicular and structural diffusions are of similar magnitude yet negatively correlated to facilitate proton mobility. Devanathan and Dupuis [54, 55], using MD simulations, found that at low hydration levels, the sulfonic groups around hyronium ions impede structure diffusion and the mean residence time of H_2O molecules near sulfonate groups decreases with increasing hydration level from ~1 ns at $\lambda = 5$ to ~75 ps at $\lambda = 20$.

The characterization of the differences in the hydrated morphology resulting from the variation of the polymer electrolyte architecture and the effects of these differences on proton transfer and transport will be vital for future materials development and optimization. The focus of this work is to probe the effects of changes in polymer electrolyte architecture on the morphology and transport properties of the resulting membranes. We will discuss (i) the variation of side-chain length, (ii) the variation of equivalent weight (EW), and (iii) the variation of polymeric molecular weight (MW). We pursued this understanding through classical MD simulations at 5 different hydration levels corresponding to $\lambda(H_2O/SO_3H) = 3$, 6, 9, 15, and 22.

4.2 Simulation Methods

4.2.1 Simulation Systems

The chemical formulae for Nafion and SSC PFSA ionomers are shown in Figure 4.1. Two groups of NVT simulations are performed by adopting Nafion and SSC respectively at

temperature 300 K for five different hydration levels ($\lambda = H_2O/SO_3H$) of 3, 6, 9, 15, and 22. λ = 3 represents the dry condition of the PFSA membranes used in the simulations. Based on experimental studies of PFSA membranes equilibrated next to liquid water at room temperature and pressure, λ = 22 corresponds to the saturated membrane [56].

In Figure 4.1, the subscript n determines the EW of the monomeric unit and the separation between side-chains. In this work, we examine four Nafion cases, n = 3, 4, 5, and 7, corresponding to backbones composed of 8, 10, 12, and 16 carbon atoms and EW (in acid form) of 744, 844, 944, and 1144. Four SSC PFSA cases were also studied, n = 4, 5, 6, 7, corresponding to backbones composed of 10, 12, 14, and 16 carbon atoms and EW (in acid form) of 678, 778, 878, and 978. These choices of structures are conducive to cross comparison between different PFSA materials and cover the range of materials that could function as membranes. Thus the effect of EW for Nafion and SSC on structure can be evaluated independently. The effect of side-chain length, when materials with the same separation between side chains are compared, can also be evaluated. Therefore, these simulations reveal how the side-chain length and degree of separation between the side chains affect the PFSA membrane properties.

The molecular weight distributions for the Nafion polymer in real membranes has been given in the 10^5 – 10^6 g/mol range [57]. This molecular weight translates into a degree of polymerization (DP) between about DP = 90 - 900 for a typical Nafion membrane of EW 1100. In our simulations the DP is 15. We have previously reported results from simulations for Nafion and SSC PFSA for n=7 with DP=3 [42]. Thus we can examine the effect of MW, at least in this short chain range, which is admittedly shorter than the polymer electrolytes used in reality.

4.2.2 Interaction Potentials

The potential models for Nafion and SSC PFSA are unaltered from the previous work on the short chains (DP=3) [42, 49, 58, 59]. It is an explicit atom model with the exception of the the CF_X groups, which are treated as united atoms. The potential includes bond stretching, bond bending and bond torsion modes. It also includes non-bonded interactions using the Lennard-Jones potential and a Coulombic interaction. The details of the potential model have

been published in previous studies by other authors [60-66]. Consistent with the united atom model for the CF_X groups, we used the Lennard-Jones parameters developed for the CF_X groups by Cui *et al.*[63, 64]. The backbone does not carry electric charge and interacts only via Lennard-Jones and intramolecular interactions. The bond lengths, bond angles, and partial charges for the side group are given in ref. [67]. The force constants for bond stretching and bond angle bending are taken from Gejji *et al.*[65] and Cornell *et al.*[66]. The torsional potential is from ref. [62].

Water is simulated using the TIP3P model [68, 69] with a flexible OH bond [66]. The model for hydronium ions, H_3O^+, is similar to that of Urata *et al.*[51]. In particular, the partial charges for the oxygen and hydrogen atoms are taken from Urata *et al.*[51]. The bond distance, bond angles, and the force constants are the same as in the TIP3P model [66, 68]. In the calculation of non-bonded interactions, the Lennard-Jones interaction is treated using a cut-off distance of 10 Å. The electrostatic interaction is treated with a site-site reaction field method [70, 71]. In this method, the Coulombic interaction between charged sites is calculated within a distance of 10 Å, and the reaction field contribution is treated with a uniform background counter charge. This method has been demonstrated to be accurate for modeling aqueous ionic solutions [70, 71].

4.2.3 Simulation Techniques and Parameters

In this study of hydrated Nafion and SSC PFSA, we included 40 polymer electrolyte molecules, all of DP=15, and 600 H_3O^+, which are required to neutralize the charges. We examined the properties of the system for water contents corresponding to the λ ratio of 3, 6, 9, 15, and 22, respectively. This resulted in 1200, 3000, 4800, 8400, and 12600 water molecules. Table 4.1 shows the number of each component in the simulated system at the different hydration levels.

The NVT simulations require a density as input. The mass density, ρ, of the hydrated Nafion membranes, based on experimental data, is given by[72]

$$\rho = \frac{EW + M_0\lambda}{\overline{V_m} + \lambda\overline{V_0}} \qquad (1)$$

where EW is the equivalent weight of the PFSA membrane, M_0 is the molecular weight of water, $\overline{V_m}$ is the partial molar volume of the dry membrane and $\overline{V_0}$ is the partial molar volume of water. The partial molar volumes are estimated as $\overline{V_m} = \frac{EW}{\rho_{m,0}}$ and $\overline{V_0} = \frac{M_0}{\rho_0}$, where $\rho_{m,0}$ is the density of the dry membrane (2 g/cm^3) and ρ_0 is the density of water at the operating temperature.

For the density of the hydrated SSC PFSA membranes, we used a molecular volume for the SSC PFSA component appropriately scaled, based on the number of atoms on the molecule relative to that of Nafion, while keeping the molecular volume of the water the same as for Nafion. Table 4.2 shows the densities in the hydrated SSC PFSA and Nafion membranes. All simulations were carried out at temperature 300 K.

We carried out constant NVT simulations for these systems. The equations of motion were integrated using the r-RESPA method[73] with a time step of 2.0 fs for the large time step and 0.2 fs for the intramolecular interactions. The temperature was maintained at a constant value using the Nosé-Hoover thermostat [74-76].

The initial configurations were created by placing molecular centers of all the molecules in the system on cubic lattice points within the simulation volume. All the atoms were initially given zero size by setting their corresponding Lennard-Jones parameters to zero. A molecular dynamics simulation was performed for 10,000 time steps in which the Lennard-Jones size parameters were gradually increased to their full values. In this way, initial configurations with non-overlapping atoms were created efficiently. Equilibration using these initial configurations was then carried out for 2 ns before production runs were begun. The production runs were at least 2 ns in length.

4.3 Results and Discussion

The morphology of the hydrated membrane can be characterized by using a variety of techniques. In this work, we present snapshots of the system, pair correlation functions, histograms of hydronium ion hydration, cumulative probability distributions for water cluster

size, and self-diffusivities. Each measure provides different information. Together they provide a complete and consistent picture of the structure of the hydrated membrane.

4.3.1 Snapshots of Hydrated Morphology

In the measures that follow, including pair correlation functions and water cluster probability distributions, one may wonder if the differences in morphology that are identified are also visible to the eye. To this end we show snapshots of hydrated membranes. The atoms of the PFSA polymers are not shown to clarify the size of water clusters and the intercluster connectivity. The morphologies of the SSC PFSA and Nafion membranes at the end of the simulation for the hydration level corresponding to $\lambda = 6$ are shown in Figures 4.2 and 4.3, respectively. We choose this intermediate level of water content because this is where we see significant difference in morphology. Once the water content is high, the differences in morphology are more difficult to observe. The snapshots of the SSC PFSA in Figures 4.2(a) and 4.2(b) are presented for EW 678 and 978 respectively, the highest and lowest EW for SSC PFSA in this study. The snapshots of Nafion in Figures 4.3(a) and 4.3(b) are presented for EW 844 and 1144 respectively, which correspond to the same backbone separation as the SSC PFSA systems in Figure 4.2.

The movement of protons and water in the hydrated membrane occurs in the aqueous domain. Therefore, the connectivity of the aqueous domains is important. In the language of percolation theory, if there is no sample-spanning cluster present, then there is no net flux. In all four of the snapshots in Figures 4.2 and 4.3, there is an inhomogeneous distribution of water. However, comparison of Figure 4.2 (a) and (b) shows that the water molecules are more uniformly distributed in the low EW SSC PFSA than in the high EW material. A similar conclusion can be reached for Nafion, by comparison of Figures 4.3 (a) and (b). However, the effect of the side-chain length on the distribution of water, via comparison of Figures 4.2(a) with 4.3(a) or Figures 4.2(b) with 4.3(b), is not easily assessed with the naked eye alone. It does appear that at both low and high EW, the water is slightly more uniformly distributed in the SSC PFSA than in Nafion, but it is not unambiguous. Therefore, we turn to quantitative measures of structure to provide additional insight.

4.3.2 Pair Correlation Functions

4.3.2.1 $S(SO_3^-) – S(SO_3^-)$

The sulfur-sulfur pair correlation functions (PCFs) of SSC PFSA and Nafion are presented in Figures 4.4 and 4.5, respectively. This correlation includes both intermolecular and intramolecular contributions to the PCF. Each plot is normalized by dividing its respectively distinct system density, as given in Table 4.2. Hence, even though the comparison of the four plots in Figure 4.4 (SSC) shows that the height of the first peak becomes greater as the EW is increased at the lower water contents (λ = 3 and 6), this alone cannot be used to understand the effects of EW. Here we used coordination number of sulfur to illustrate the effects of EW (Table 4.3). The coordination number is defined as the number of neighboring sulfur atoms that is found within the distance of 8 Å from any given sulfur. This 8 Å cutoff distance approximately corresponds to the first minimum of $S(SO_3^-) – S(SO_3^-)$ PCFs (see Figures 4.4 and 4.5). For the four SSC PFSA membranes, Table 4.3 shows that the coordination number of each sulfur atom decreases with increasing EW at the low and intermediate hydration levels (λ = 3, 6, and 9) and the difference becomes smaller at the higher water contents. This reveals that the sulfonate groups in the ionomer with lower EW (i.e. shorter separation distance between side chains) tend to aggregate more closely to one another than those with higher EW. It is also noted that the coordination numbers become smaller with increasing water content and are almost always higher in Nafion than in the SSC PFSA of corresponding backbone separation.

The PCFs contain much more information than the coordination numbers. At low and intermediate loadings, the first peak height, located at about 4.8 Å, increases with EW for both the SSC PFSA and Nafion. The first peak height is also higher in Nafion than in the corresponding SSC PFSA. In the case of side chain length, this peak height does translate into a higher coordination number. However, in the case of EW, this enhancement in very short range structure does not yield a higher coordination number. Thus, one cannot use peak height alone as a measure of the aggregation of sulfonate groups. This is in part due to the fact that the positions of the first peaks, especially for λ > 6, are smaller for Nafion than for the SSC PFSA. Virtually all of the PCFs have an additional peak at 9.4 Å.

One can evaluate the effect of side-chain length when holding the separation between side chains constant by comparison of Figure 4.4(a) with Figure 4.5(b), Figure 4.4(b) with Figure 4.5(c), and Figure 4.4(d) with Figure 4.5(d). With the same spacing between side chains, the S-S PCFs show that the first peak is always greater in Nafion at the low and intermediate hydration levels, which suggests that the longer side chains of Nafion allow more flexibility causing the sulfonate groups to tend to aggregate to one another more easily relative to those of SSC PFSA. The fact that the Nafion peak at 6.2 Å has moved out to 6.8 Å in SSC PFSA also provides evidence for tighter S-S clustering in Nafion. This is also observed in Table 4.3 which presents that the coordination number for the hydrated Nafion is generally greater than that for the SSC PFSA at the low and intermediate water contents.

Figure 4.6 here displays the comparison of PEMs with different MW. We present results from Nafion (EW=1144) and SSC PFSA (EW=978) for DP = 15 (this work) and DP = 3 from previous work [42]. The hydration levels used for trimer membranes (λ = 4.4, 6.4, 9.6, and 12.8) are different from those adopted in the present paper (λ = 3, 6, 9, 15, and 22). Thus, we put the approximate hydration levels together in an attempt to explore the MW effects. Comparison of the long chains at λ = 6 with trimers at λ = 6.4 shows that the trimers have a broader peak for both SSC PFSA and Nafion. The broader peaks in the trimers are expected, since the water content is slightly higher. All the four curves have a peak at 9.4 Å. For both the long chains and short chains, we find that the S-S PCF shows more clustering in Nafion than in the SSC PFSA, indicating that the enhancement for S-S clustering is independent of MW, at least in the range studied here.

4.3.2.2 $S(SO_3^-) – O(H_2O)$

In Figures 4.7 and 4.8, we show the PCFs between the sulfur atom of the sulfonate groups and the oxygen of water molecules. In Figure 4.7, the PCFs for SSC PFSA at the lowest (678) and highest (978) EW are shown. In Figure 4.8, the PCFs for Nafion at a low (844) and the highest (1144) EW are shown. All figures, Nafion and SSC PFSA irrespective of EW, show that the height of the first peak (at 4.0 Å) decreases as the water content increases. For all water contents greater than λ = 3, the peak at 6.4 Å also decreases with increasing water content. In other words, the water molecules are less tightly bound with increasing water content.

First, we estimate the hydration number of sulfur atoms that is calculated from the PCFs within the distance of 4.8 Å to illustrate the effects of EW (Table 4.4). The distance 4.8 Å was chosen to correspond with the end of the first peak. The hydration number of sulfur for the four SSC PFSA shows that the hydration probability decreased with increasing EW at all water contents, indicating that more water is able to surround the sulfonate group with low EW. The hydration number difference is not pronounced for the hydrated Nafion but it still shows that low EW membrane tends to aggregate more water molecules (see the comparison between EW 744 and EW 1144). Via comparison of SSC EW 678 with Nafion EW 844, SSC EW 778 with Nafion EW 944, and SSC EW 978 with Nafion EW 1144, we see that hydration number for Nafion is greater than that for SSC PFSA at the low and intermediate hydration levels (λ = 3, 6 and 9), which suggests that more water molecules tend to surround the sulfonate group with the longer side-chain. But the situation is opposite at the high hydration levels (λ = 15 and 22), where SSC PFSA membranes appear to have more closely packed water molecules around each sulfur.

In order to explore the effect of MW, we plot the $S(SO_3^-) – O(H_2O)$ PCF in Figure 4.9 for Nafion (EW=1144) and SSC PFSA (EW=978) for DP=15 and DP=3. Again, we see that the enhancement of water clustering around the sulfonate group in Nafion is apparent for both MW. We used Nafion trimers in our previous work and obtained consistent conclusions with those of other groups who used Nafion with DP = 10 [50, 51]. Again, we note that we are well short of industrially relevant MWs, but we do show that the trends established between Nafion and SSC PFSA are consistent for the range of MW studied here.

4.3.2.3 $S(SO_3^-)$-$O(H_3O^+)$

The PCFs between the sulfur and the oxygen of the hydronium ions are shown in Figure 4.10 for SSC PFSA (EW=678 & 978) and in Figure 4.11 for Nafion (EW=844 & 1144). For both SSC PFSA and Nafion membranes, the first peak position is nominally 4.0 Å. The height of the first peak decreases with water content, as the water molecules better solvate both the sulfonate ion and the hydronium ion. The height of the second peak at 6.0 Å is relatively constant for all λ greater than 3. In Table 4.5, the hydronium ion coordination number of the sulfur atoms is calculated from the $S(SO_3^-)$-$O(H_3O^+)$ PCFs within the distance of 4.8 Å. For both SSC PFSA and Nafion, the difference of the coordination number is small and irregular, hence it

is hard to make quantitative comparisons on the effects of EW. However, at the lowest water content ($\lambda = 3$), there are two hydronium ions near each sulfur. Clearly a realistic picture of the structure at low hydration level cannot include the individual pairing off of sulfonate groups and hydronium ions, since that would result in a coordination number of unity. We do see coordination numbers less than unity for high hydration since the hydronium ions are moving further from the sulfonate group into the aqueous phase.

The effect of side-chain length on the association of hydronium ions and sulfonate groups can also be observed. With the same separation distance between side chains, the SSC PFSA has a higher degree of association than does Nafion, at virtually all hydration levels, as shown in Table 4.5. Examining the $S(SO_3^-)$-$O(H_3O^+)$ PCFs in Figures 4.10 and 4.11 directly, there is a noticeable shoulder on the inside of the first peak in the Nafion PCFs that is absent for SSC PFSA. This shoulder broadens the peak in Nafion, but does not impact the coordination number significantly. The closer association of hydronium ions with sulfonate groups in the SSC PFSA likely reflects that in Nafion the aqueous domains are more localized, thus the hydronium ions see a higher effective local water content. It is clear that the association of S and hydronium ions decreases with increasing water content in all systems. Thus the hydronium ions behave in Nafion as if they are in a higher effective local water content.

Figure 4.12 displays the effects of MW on the $S(SO_3^-)$-$O(H_3O^+)$ PCFs. The behavior for the long chains (DP=15) and the short chains (DP=3) is qualitatively similar. Furthermore, the fact that the hydronium ions are more correlated with the S position in SSC PFSA versus Nafion is observed at both MWs.

4.3.2.4 $O(H_2O)$ - $O(H_3O^+)$

The PCFs between the oxygen of the water molecules and the oxygen of the hydronium ions are shown in Figure 4.13 for SSC PFSA (EW=678 & 978) and in Figure 4.14 for Nafion (EW=844 & 1144). In all systems, the first peak is located at about 2.6 Å and decreases in height with increasing water content. This decrease in height is not associated with a decrease in solvation of the hydronium ion. We shall see in the hydronium ion hydration histograms to follow that the number of water molecules around each hydronium ion increases with increasing

water content, as it must. However, the PCFs are normalized by the average density, which itself increases in water content, causing a lowering of the peak height, all other things equal.

The water coordination number of hydronium ions presented in Table 4.6 is obtained from the PCFs within the distance of 3.2 Å. It reveals that a decrease in EW results in slightly more hydration of the hydronium ion. A comparison of SSC EW 678 with Nafion EW 844, SSC EW 778 with Nafion EW 944, and SSC EW 978 with Nafion EW 1144, shows that an increase in side-chain length results in more hydration of the hydronium ion. This is consistent with the picture that the longer side chain of Nafion enhances the formation of localized aqueous domains, which in turn again enhances hydration of the hydronium ions.

We plot the $O(H_2O)$-$O(H_3O^+)$ PCF in Figure 4.15 for Nafion (EW=1144) and SSC PFSA (EW=978) for DP=15 and DP=3 to explore the effect of MW. The shape of the PCFs is similar for both MWs. We also see that the enhancement of water clustering around the hydronium ion in Nafion is apparent for both MWs.

4.3.2.5 $O(H_2O)$-$O(H_2O)$

The PCFs between the oxygen of the water molecules are shown in Figure 4.16 for SSC PFSA (EW=678 & 978) and in Figure 4.17 for Nafion (EW=844 & 1144). In all systems, the first peak is located at about 2.8 Å. The second peak is located at about 3.8 Å and decreases in height with increasing water content, until it almost vanishes. The behavior of the height of the first peak with water content is more complicated and has a maximum at λ = 6 or 9. Presumably this maximum at an intermediate water content is due to the fact that the second peak height has also dropped quickly, allowing some water to redistribute into the first peak.

Table 4.7 presents the coordination number of each water molecule calculated from the PCFs within the distance of 5.2 Å. A comparison of the four SSC PFSA shows that a decrease in EW results in an increase in coordination number, or more association of the water, which is most readily apparent at low and intermediate hydration levels. The difference of coordination number for the Nafion is not pronounced but still shows that the lower EW membrane tends to aggregate more water molecules compared with the high EW membrane.

A comparison of the four SSC PFSA and the four Nafion membranes, shows that an increase in side-chain length also results in an increase in the water association. This too is

consistent with the picture that the longer side chain of Nafion provides greater flexibility, which enhances the formation of localized aqueous domains.

The $O(H_2O)$-$O(H_2O)$ PCF in Figure 4.18 is presented to illustrate the effect of MW for Nafion (EW=1144) and SSC PFSA (EW=978) for DP=15 and DP=3. The shape of the PCFs is similar for both MW. We also see that the enhancement of water clustering in Nafion is apparent for both MWs.

4.3.3 Hydronium Ion Hydration Histograms

In Figures 4.19 and 4.20, we show histograms for hydration of the hydronium ion. This histogram provides the probability that any given hydronium ion has n water molecules around it within a given radial cut-off distance. In this study, as in previous studies, we use a cut-off of 3.2 Å. As a comparison, the average number of water molecules within 3.2 Å of a hydronium ion in bulk water is 3.8 [77]. In Figure 4.19(a) and (b), we provide histograms for SSC PFSA (EW=678 & 978) and Nafion (EW=844 & 1144) at three intermediate values of λ, respectively. For both SSC PFSA and Nafion, one observes an increase in fully hydrated hydronium ions ($n>3$) with an increase in water content, as one must. For SSC PFSA, the low EW material has better hydration at all water contents, as judged by the fact that the probability of finding poorly hydrated hydronium ions ($n<3$) is always lower for the low EW material and the probability of finding fully hydrated hydronium ions ($n>3$) is always higher for the low EW material. An analogous statement can be made for Nafion; lower EW results in better hydration.

In Figure 4.20(a), we provide histograms for SSC PFSA and Nafion (low EW) at three intermediate values of λ. In Figure 4.20(b), we provide histograms for SSC PFSA and Nafion (high EW) at three intermediate values of λ. This re-plotting of the data in Figure 4.19 allows for direct analysis of the effect of side chain length. We see for both the low EW and high EW comparisons that hydronium ions are more likely to be fully hydrated in Nafion that in SSC PFSA. This is consistent with the observation that the additional flexibility in the side chain allows the sulfonate groups to better cluster, resulting in more localized aqueous domains and better hydration of the ions within that domain.

4.3.4 Water Cluster Distributions

Proton transport across a PEM is dependent on the nanophase-segregated morphological structures of hydrated PFSA membranes, in which the aqueous domains provide the path for transport. It has been suggested [67] that these hydrophilic clusters are not a continuous subphase but isolated clusters with the formation and cleavage of temporary bridges between the clusters even at the high hydration levels. Thus, it is reasonable to believe that water and proton mobilities are affected by the size and connectivity of these aqueous clusters. To illustrate these effects quantitatively, we presented here the water cluster distributions at various water contents using the cut-off distance 3.5 Å, which is denoted by Rc. This Rc is arbitrary but includes roughly all the water molecules within the first hydration shell of hydrionium ion (see the PCF of $O(H_2O)$-$O(H_3O^+)$). We used the average statistics at this cut-off distance to illustrate the relative tendency of water cluster formation between comparable systems.

In Figure 4.21, we display the cumulative probability distribution function (PDF) for water cluster size for SSC PFSA and Nafion at two different hydration levels (λ = 6 and 9). Interpreting these cumulative distributions is aided by the asymptotes between which they are bound. A hypothetical poorly connected system in which all water molecules were in clusters of size one would rise to unity at one and remain there. A hypothetical perfectly connected system in which all water molecules were in one large cluster would remain zero until the cluster size contained all the atoms in the simulation. Thus in Figure 4.21, one can examine curves at a given hydration level and see that the distributions move from the poorly connected toward the perfectly connected asymptote as EW is decreased. This is true for both the SSC PFSA and for Nafion, at both water contents shown. This statistical measure confirms the visual observation of the snapshots in Figures 4.2 and 4.3 that an increase in EW resulted in a more heterogeneous system.

In Figure 4.22, we plot cumulative water distributions for SSC PFSA and Nafion (DP=15) with similar backbone spacing between side chains. We see that for the same backbone spacing (EW= 678 & 844 or EW=978 & 1144), that the SSC PFSA has more distributed water domain and better connectivity. Hence, greater side chain length allows greater flexibility, which allows sulfonate groups to cluster, which creates more localized aqueous domains.

The $S(SO_3^-) - O(H_2O)$ PCF is shown in Figure 4.23 for Nafion (EW=1144) and SSC PFSA (EW=978) to explore the effect of MW for DP=15 and DP=3 at λ =6 and 6.4. The x-axis is normalized to account for differences in system size. While there are quantitative differences in the curves, both the long chain and short chain systems maintain the same trend, namely that as the side-chain length increases, the connectivity decreases.

These cluster distributions give an idea of the connectivity of the aqueous phase but do not directly provide information on the geometry of the channels or their characteristic dimensions. In fact, a well-connected membrane spread through the same volume may result in a characteristic channel width that is smaller than a system of large but poorly connected aqueous domains.

In order to provide support for this idea that a better connected network corresponds to smaller channels, we obtained from structure factor (S(q)) calculated as the Fourier transform of the water-water PCFs,

$$S(q) = 1 + 4\pi \frac{N}{V} \int [g(r) - 1)] \frac{\sin(qr)}{q} r dr \qquad (2)$$

It is important to understand that a peak in the structure factor represents the distance between the centers of clusters ($l = 2\pi / q$ Å) and corresponds to a characteristic dimension with periodicity in the system. It does not correspond to the characteristic dimension of the aqueous phase or the hydrophobic phase, but rather the sum of the two characteristic dimensions. Thus a change in characteristic dimension must be carefully interpreted.

The characteristic dimensions are presented in Table 4.8. We are able to obtain the characteristic dimension associated with periodicity in the system if that dimension is smaller than half of our simulation box size. Thus we are limited calculating this result for the SSC PFSA up to λ = 9 and Nafion up to λ = 6. Beyond that, our simulation box is too small to determine the characteristic dimension.

For the data we do have, we observe that Nafion has a larger characteristic dimension than the SSC PFSA at the same backbone separation. This is the origin of the idea that an increase in connectivity results in a commensurate increase in confinement. If one distributes the water in a more uniform manner in the SSC PFSA, then by the fact that the density of the aqueous

phase is virtually constant, the characteristic dimension of the water channels must decrease, resulting in greater confinement.

We also observe that the characteristic dimension increases with EW for both SSC and Nafion (with the exception of Nafion at λ =3). The higher EW materials are more poorly connected and have a bigger characteristic dimension. However, things are not as simple as they seem; an increase in EW results in more hydrophobic material in the membrane. This results in greater spacing of the hydrophobic phase. Thus we suggest that the increase in the characteristic dimension as a result of the increase in EW is a result of the hydrophobic domain size increasing.

One can justify this suggestion as follows. The water-water PCFs and the hydration numbers in Table 4.7 indicate that, within 5.2 Å, the degree of association of water increases as EW decreases. At the same time, the structure factor indicates that the characteristic dimension decreases as EW decreases. If one believes that the association of water should be greatest in the bulk state, when there is the least confinement, then there is an apparent contradiction here. The contradiction is removed if one assumed that the increase in characteristic dimension is associated with an increase in the hydrophobic domain size.

Although the origin remains a suggestion, there are two clear trends that emerge from this work. Compared to the SSC PFSA, Nafion has worse connectivity, a bigger characteristic dimension, and *more* local water-water association, which makes intuitive sense. However, as a function of increasing EW, both materials show a worse connectivity, a bigger characteristic dimension and *less* local water-water association. This is a fundamental difference of the effect of side chain length and EW on structure and implies that the connectivity of the aqueous phase can be impacted not only by the characteristic size of the aqueous phase but also by the characteristic size of the hydrophobic domain.

Thus the idea that an increase in connectivity results in a commensurate increase in confinement is not necessarily true. It is true for a change in side chain length, in which the size of the aqueous domain changes. It is not true for a change in EW, in which the size of the hydrophobic phase changes.

4.3.5 Self-Diffusivities

In this work, we have examined two architectural features of polymer electrolytes that affect the spacing between sulfonic acid groups: backbone spacing between side chains and side-chain length. We have shown that the combined analyses of snapshots, PCFs, hydration histograms, and water cluster distributions yield a consistent picture of the relationship between morphology of the hydrated membrane and architectural features. It is no surprise that these changes in morphology will affect the transport properties of protons and water in the hydrated membrane.

Experimentally, it has been shown that the overall proton conductivity in Nafion increases with decrease of EW up to a point, beyond which high humidity conditions cause a reduction in conductivity due to dilution [45, 46]. Moreover, some theoretical investigations also showed that the separation distance between the sufonic acid groups could affect the transport properties [79-82].

The effect of side-chain length is somewhat complicated. Theoretical study reported that the SSC PFSA tends to form a better distributed aqueous domains compared to the hydrated Nafion at the low hydration levels, whereas the situation becomes opposite at the high hydration levels [40]. Some experiments also presented that the SSC PFSA has higher proton conductivity than Nafion at low to intermediate hydration levels [38, 82]. However, in their recent paper, Kreuer *et al.* [83] concluded that no distinct differences in water and proton transport as a function of water volume fraction were observed for SSC and Nafion of the same EW.

Irrespective of the origins of the morphology change, there are a few intuitive expectations that one may have. First, the diffusivity of water should increase with increasing water content because the aqueous domains are larger, giving rise to more "bulk like" water, in which the transport is faster. Second, more confinement, i.e. smaller channels, should result in a lower diffusivity for the same reason as given above. Third, better connectivity of the aqueous domain should result in a higher diffusivity. The complication in these simple rules is that, while better connectivity may enhance diffusion, an increase in confinement will reduce it. The balance between these two competing forces is difficult to predict.

There is one additional factor to consider in understanding the self-diffusivities that are obtained from MD simulations. As we have previously noted, the timescale of the MD simulations is several ns. In this time span, the water molecules travel a few nanometers (Table 4.9). This distance traveled during the course of the simulation is smaller than the characteristic dimension of the system obtained from the structure factor. Thus, what we observe in the MD simulations is largely diffusion within a single cluster. It is outside the capability of these simulations to measure the long time diffusivity associated with the macroscopic degree of connectivity of the network. For this, the intracluster diffusivities from MD would have to be integrated with a coarse-grained percolation model.

In Figure 4.24(a), the self-diffusivity of water is plotted as a function of water content for all 8 membranes studied in this work. In Figure 4.24(b), the vehicular component of the self-diffusivity of hydronium ions is plotted as a function of water content for all 8 membranes studied in this work. The self-diffusivities are also provided in Tables 4.10 and 4.11. We observe, as we must, that all self-diffusivities increase with increasing water content.

For water, the self-diffusivity generally increases with decreasing EW in both SSC PFSA and Nafion. This effect diminishes as the water content is lowered. We have suggested that the self-diffusivity should increase with connectivity. In this case, this trend is followed, since the connectivity is also increased as the EW is decreased. We have suggested that the diffusivity should increase with a decrease in confinement. If we use the water-water hydration numbers in Table 4.7 as a measure of local confinement (higher hydration equals less confinement), then this trend is also followed. A decrease in EW results in better connectivity and less local confinement and consequently a higher diffusivity. This is consistent with recent experimental observations [83, 84].

The water self-diffusivity does not vary much when comparing the SSC PFSA and Nafion with similar backbone separations. This is consistent with recent experimental observations [83]. We have suggested that the self-diffusivity should increase with connectivity, which would favor the SSC PFSA. We have also suggested that the self-diffusivity should decrease with confinement, which using water-water hydration numbers as a basis, would favor Nafion. Since the two contributing terms are in opposition to each other, the net effect on the diffusivity is small.

In Figure 4.24(b) and Table 4.11, we present the vehicular component of the self-diffusivity of the hydronium ion. There is little dependence on EW at low and intermediate loadings. We see slightly higher self-diffusivities for both SSC PFSA and Nafion at the highest water content as EW is lowered. The effect of side-chain length is more pronounced for the hydronium ion than for water. The hydronium ion self-diffusivities in Nafion are uniformly higher than those for the SSC PFSA across all hydration levels and all comparable backbone separations. This is consistent with the trend found in the Nafion and SSC trimer [42]. As was previously found [42], comparison of the self-diffusivities of the hydronium ion with experimental measurements of proton self-diffusivities shows that the simulated values are all lower but the difference becomes more remarkable with increasing hydration levels. We expect these differences are mainly due to our omission in the simulation of the contribution to the self-diffusivity from the proton-hopping mechanism.

4.4 Conclusions

Classical NVT simulations were performed to investigate the effects of the side chain length, equivalent weight (EW), and the polymeric molecular weight (MW) on the hydrated morphology and diffusion properties of water and hydronium ions in the SSC PFSA and Nafion membranes with each ionomer containing 15 side chains.

In the comparison of the SSC PFSA and Nafion with comparable backbone separations between side chains, we find that in Nafion, there is

- more clustering of the sulfonate groups
- more clustering of water around the sulfonate groups at low water contents, but less clustering of water around the sulfonate groups at high water contents
- less clustering of the hydronium ions around the sulfonate groups
- more clustering of water around the hydronium ions
- more local water-water clustering
- more poorly connected aqueous domain
- a larger characteristic dimension from the structure factor

Taken collectively, these observations paint a picture of the morphology of the hydrated membrane in which an increase in side chain length results in larger but more poorly connected

aqueous domains. The larger aqueous domains allow for better clustering of the species (sulfonate groups, water and hydronium ions) in the aqueous phase. These changes in morphology due to the difference in side chain length do not yield an appreciable difference in water diffusivity. We do observe a slightly higher diffusivity for the hydronium ion in Nafion than in the SSC PFSA.

When one decreases the equivalent weight (EW) in either SSC PFSA or Nafion, there is

- more clustering of the sulfonate groups
- more clustering of water around the sulfonate groups
- little change in the clustering of the hydronium ions around the sulfonate groups
- more clustering of water around the hydronium ions
- more local water-water clustering
- a better connected aqueous domain
- a smaller characteristic dimension from the structure factor

These changes in morphology due to the difference in EW result in a higher diffusivity for water at lower EW. We also observe higher diffusivities for the hydronium ion at lower EW for intermediate and high water contents.

The diffusivity of water is controlled by a balance between connectivity and confinement. The lower EW enhances connectivity and reduces confinement, both of which favor an increase in diffusivity. The longer side chain reduces connectivity and reduces confinement, which are in opposition to each other, and result in no significant change in the diffusivity.

Finally, we compared SSC PFSA and Nation chains composed of 3 and 15 monomeric units and found that the qualitative observations given above are independent of the MW, at least in the low range studied herein.

4.5 Acknowledgments

The work is supported by a grant from the U. S. Department of Energy BES under the contract number DE-FG02-05ER15723. This research used resources of the Center for Computational Sciences at Oak Ridge National Laboratory, which is supported by the Office of Science of the DOE under Contract DE-AC05-00OR22725. This work also used resources of

the National Institute for Computational Sciences (NICS), supported by NSF with agreement number: OCI 07-11134.

References

(1) K. A. Mauritz and R. B. Moore, *Chem. Rev.*, **2004**. 104, 4535-4585.

(2) S. J. Hamrock and M. A. Yandrasits, *J. Macromol. Sci. C: Polym. Rev.*, **2006**. 46, 219-244.

(3) M. F. H. Schuster and W. H. Meyer, *Annu. Rev. Mater. Res.*, **2003**. 33, 233-261.

(4) M. A. Hickner and B. S. Pivovar, *Fuel Cells (Weinheim, Germany)* **2005**. 5, 213.

(5) K. D. Kreuer, S. J. Paddison, E. Spohr, and M. Schuster, *Chem. Rev.*, **2004**. 104, 4637-4678.

(6) M. Falk, *Can. J. Chem.*, **1980**. 58, 1495-1501.

(7) A. Eisenberg, *Macromolecules*, **1970**. 3, 147-154.

(8) R. Duplessix, M. Escoubes, B. Rodmacq, F. Volino, E. Roche, A. Eisenberg, and M. Pineri, in *Water in Polymers*, S. P. Rowland, Editor; American Chemical Society: Washington DC, 1980.

(9) B. Rodmacq, J. M. Coey, M. Escoubes, E. Roche, R. Duplessix, A. Eisenberg, and M. Pineri, in *Water in Polymers*, S. P. Rowland, Editor; American Chemical Society: Washington DC, 1980.

(10) T. D. Gierke, G. E. Munn, and F. C. Wilson, *J. Polym. Sci.: Polym. Phys. Ed.*, **1981**. 19, 1687-1704.

(11) W. Y. Hsu and T. D. Gierke, *J. Membr. Sci.*, **1983**. 13, 307-326.

(12) H. L. Yeager and A. Steck, *J. Electrochem. Soc.*, **1981**. 128, 1880-1884.

(13) M. W. Verbrugge and R. F. Hill, *J. Electrochem. Soc.*, **1990**. 137, 886-893.

(14) G. Gebel, *Polym.*, **2000**. 41, 5829-5838.

(15) P. J. James, J. A. Elliott, T. J. McMaster, J. M. Newton, A. M. S. Elliott, S. Hanna, and M. J. Miles, *J. Mater. Sci.*, **2000**. 35, 5111-5119.

(16) K. D. Kreuer, *J. Membr. Sci.*, **2001**. 185, 29-39.

(17) H. G. Haubold, T. Vad, H. Jungbluth, and P. Hiller, *Electrochimica Acta*, **2001**. 46, 1559-1563.

(18) A. L. Rollet, G. Gebel, J. P. Simonin, and P. Turq, *J. Polym. Sci. B-Polym. Phys.*, **2001**. 39, 548-558.

(19) S. K. Young, S. F. Trevino, and N. C. B. Tan, *J. Polym. Sci. B-Polym. Phys.*, **2002**. 40, 387-400.

(20) M. Fujimura, T. Hashimoto, and H. Kawai, *Macromolecules*, **1981**. 14, 1309-1315.

(21) M. Fujimura, T. Hashimoto, and H. Kawai, *Macromolecules*, **1982**. 15, 136-144.

(22) E. J. Roche, M. Pineri, R. Duplessix, and A. M. Levelut, *J. Polym. Sci. B-Polym. Phys.*, **1981**. 19, 1-11.

(23) M. D. Heaney and J. Pellegrino, *J. Membr. Sci.*, **1989**. 47, 143-161.

(24) A. Lehmani, S. Durand-Vidal, and P. Turq, *J. Appl. Polym. Sci.*, **1998**. 68, 503-508.

(25) Z. Porat, J. R. Fryer, M. Huxham, and I. Rubinstein, *J. Phys. Chem.*, **1995**. 99, 4667-4671.

(26) M. Eikerling, A. A. Kornyshev, and U. Stimming, *J. Phys. Chem. B*, **1997**. 101, 10807-10820.

(27) V. K. Datye, P. L. Taylor, and A. J. Hopfinger, *Macromolecules*, **1984**. 17, 1704-1708.

(28) K. A. Mauritz, C. J. Hora, and A. J. Hopfinger, in *Ions in Polymers*, A. Eisenberg, Editor; American Chemical Society: Washington DC, 1980.

(29) K. A. Mauritz and C. E. Rogers, *Macromolecules*, **1985**. 18, 483-491.

(30) B. Dreyfus, *Macromolecules*, **1985**. 18, 284-292.

(31) J. A. Elliott, S. Hanna, A. M. S. Elliott, and G. E. Cooley, *Macromolecules*, **2000**. 33, 4161-4171.

(32) Y. K. Tovbin, *Zh. Fiz. Khim.*, **1998**. 72, 55-59.

(33) Y. K. Tovbin and N. F. Vasyatkin, *Colloids Surf. A Physicochem. Eng. Asp.*, **1999**. 158, 385-397.

(34) G. A. Eisman, *J. Power Sources*, **1990**. 29, 389-98.

(35) A. Ghielmi, P. Vaccarono, and C. Troglia, *J. Power Sources*, **2005**. 145, 108–115.

(36) J. Halim, F. N. Buchi, O. Haas, M. Stamm, and G. G. Scherer, *Electrochim. Acta*, **1994**. 39, 1303-1307.

(37) G. Gebel and R. B. Moore, *Macromolecules*, **2000**. 33, 4850-4855.

(38) C. A. Edmondson, P. E. Stallworth, M. E. Chapman, J. J. Fontanella, M. C. Wintersgill, S. H. Chung, and S. G. Greenbaum, *Solid State Ionics*, **2000**. 135, 419-423.

(39) K. Prater, *J. Power Sources*, **1990**. 29, 239-250.

(40) D. Brandel, J. Karo, A. Liivat, and J. O. Thomas, *J. Mol. Model*, **2007**. 13, 1039-1046.

(41) M. Yoshitake and A. Watakabe, *Adv. Polym. Sci.*, **2008**. 215, 127-155.

(42) S. Cui, J. Liu, M. E. Selvan, S. J. Paddison, D. J. Keffer, and B. J. Edwards, *J. Phys. Chem. B*, **2008**. 112, 13273-13284.

(43) I. H. Hristov, S. J. Paddison, and R. Paul, *J. Phys. Chem. B*, **2008**. 112, 2937-2949.

(44) S. J. Paddison, *Top. Appl. Phys.*, **2009**. 113, 385-412.

(45) H. Xu, H. R. Kunz, L. J. Bonville, and J. M. Fenton, *J. Electrochem. Soc.*, **2007**. 154, B271-B278.

(46) N. H. Jalani and R. Datta, *J. Membr. Sci.*, **2005**. 264, 167-175.

(47) S. J. Paddison and J. A. Elliott, *J. Phys. Chem. A*, **2005**. 109, 7583-7593.

(48) S. S. Jang, V. Molinero, T. Cagin, and W. A. Goddard, *J. Phys. Chem. B*, **2004**. 108, 3149-3157.

(49) S. Cui, J. Liu, M. Esai Selvan, D. J. Keffer, B. J. Edwards, and W. V. Steele, *J. Phys. Chem. B*, **2007**. 111, 2208-2218.

(50) A. Vishnyakov and A. V. Neimark, *J. Phys. Chem. B*, **2000**. 104, 4471-4478.

(51) S. Urata, J. Irisawa, A. Takada, W. Shinoda, S. Tsuzuki, and M. Mikami, *J. Phys. Chem. B*, **2005**. 109, 4269-4278.

(52) M. Eigen, *Angew. Chem.*, **1963**. 75, 489-508.

(53) M. K. Petersen and G. A. Voth, *J. Phys. Chem. B* **2006**. 110, 18594-18600.

(54) R. Devanathan, A. Venkatnathan, and M. Dupuis, *J. Phys. Chem. B*, **2007**. 111, 8069-8079.

(55) R. Devanathan, A. Venkatnathan, and M. Dupuis, *J. Phys. Chem. B*, **2007**. 111, 13006-13013.

(56) T. A. Zawodzinski, C. Derouin, S. Radzinski, R. J. Sherman, V. T. Smith, T. E. Springer, and S. Gottesfeld, *J. Electrochem. Soc.*, **1993**. 140, 1041.

(57) D. E. Curtin, R. D. Lousenberg, T. J. Henry, P. C. Tangeman, and M. E. Tisack, *J. Power Sources*, **2004**. 131, 41-8.

(58) M. E. Selvan, J. Liu, D. J. Keffer, S. Cui, B. J. Edwards, and W. V. Steele, *J. Phys. Chem. C*, **2008**. 112, 1975-1984.

(59) J. Liu, M. E. Selvan, S. Cui, B. J. Edwards, D. J. Keffer, and W. V. Steele, *J. Phys. Chem. C*, **2008**. 112, 1985-1993.

(60) J. A. Elliott, S. Hanna, A. M. S. Elliott, and G. E. Cooley, *Phys. Chem. Chem. Phys.*, **1999**. 1, 4855-4863.

(61) A. Vishnyakov and A. V. Neimark, *J. Phys. Chem. B*, **2001**. 105, 7830-7834.

(62) D. Rivin, G. Meermeier, N. S. Schneider, A. Vishnyakov, and A. V. Neimark, *J. Phys. Chem. B*, **2004**. 108, 8900-8909.

(63) S. Cui, J. I. Siepmann, H. D. Cochran, and P. T. Cummings, *Fluid Phase Equilib.*, **1998**. 146, 51-61.

(64) H.-C. Li, C. McCabe, S. Cui, P. T. Cummings, and H. D. Cochran, *Mol. Phys.*, **2003**. 101, 2157-2169.

(65) S. P. Gejji, K. Hermansson, and J. Lindgren, *J. Phys. Chem.*, **1993**. 97, 3712-3715.

(66) W. D. Cornell, P. Cieplak, C. I. Bayly, I. R. Gould, K. M. Nerz, D. M. Ferguson, D. C. Spellmeyer, T. Fox, J. W. Caldwell, and P. A. Kollman, *J. Am. Chem. Soc.* , **1995**. 117, 5179.

(67) A. Vishnyakov and A. V. Neimark, *J. Phys. Chem. B*, **2001**. 105, 9586-9594.

(68) W. L. Jorgensen, J. Chandrasekhar, J. D. Madura, R. W. Impey, and M. L. Klein, *J. Chem. Phys.*, **1983**. 79, 926-935.

(69) D. J. Price and C. L. Brooks, *J. Chem. Phys.*, **2004**. 121, 10096-10103.

(70) G. Hummer, D. M. Soumpasis, and M. Neumann, *Mol. Phys.*, **1992**. 77, 769-785.

(71) S. Cui and J. G. Harris, *Chem. Eng. Sci.*, **1994**. 49, 2749-2763.

(72) A. Z. Weber and J. Newman, *J. Electrochem. Soc.*, **2004**. 151, A311-A325.

(73) M. Tuckerman, B. J. Berne, and G. J. Martyna, *J. Chem. Phys.*, **1992**. 97, 1990-2001.

(74) S. Nosé, *Mol. Phys.*, **1984**. 52, 255-268.

(75) S. Nosé, *J. Chem. Phys.*, **1984**. 81, 511-519.

(76) W. G. Hoover, *Phys. Rev. A*, **1985**. 31, 1695-1697.

(77) J. A. Morrone, K. E. Haslinger, and M. E. Tuckerman, *J. Phys. Chem. B*, **2006**. 110, 3712-3720.

(78) S. J. Paddison, R. Paul, and T. A. Zawodzinski, *J. Electrochem. Soc.*, **2000**. 147, 617-626.

(79) S. J. Paddison, R. Paul, and T. A. Zawodzinski, *J. Chem. Phys.*, **2001**. 115, 7753-7761.

(80) R. Paul and S. J. Paddison, *J. Chem. Phys.*, **2001**. 115, 7762.

(81) S. J. Paddison, R. Paul, and K. D. Kreuer, *Phys. Chem. Chem. Phys.*, **2002**. 4, 1151-1157.

(82) T. A. Zawodzinski, T. A. Springer, J. Davey, R. Jestel, C. Lopez, J. Valerio, and G. Shimshon, *J. Electrochem. Soc.*, **1993**. 140, 1981-1985.

(83) K. D. Kreuer, M. Schuster, B. Obliers, O. Diat, U. Traub, A. Fuchs, U. Klock, S. J. Paddison, and J. Maier, *J. Power Sources*, **2008**. 178, 499-509.

(84) F. Mark, M. F. Mathias, R. Makharia, H. A. Gasteiger, J. J. Conley, T. J. Fuller, C. J. Gittleman, S. S. Kocha, D. P. Miller, C. K. Mittelsteadt, T. Xie, S. G. Yan, and P. T. Yu, *Interface*, **2005**. 14, 24-35.

Appendix C

Table 4. 1 Simulation details on the number of molecules for each component in the simulation system at the different hydration levels.

λ (H_2O/SO_3H)	3	6	9	15	22
no. of polymers	40	40	40	40	40
no. of H_2O	1200	3000	4800	8400	12600
no. of H_3O^+	600	600	600	600	600
total no. of particles	22200	27600	33000	43800	56400

Table 4. 2 Densities (g/cm^3) in the hydrated SSC PFSA and Nafion membranes at various water contents λ (300 K and 1 atm).

λ	SSC with different EW				Nafion with different EW			
	678	778	878	978	744	844	944	1144
3	1.91	1.93	1.96	1.97	1.94	1.95	1.96	1.98
6	1.80	1.83	1.86	1.88	1.83	1.85	1.87	1.90
9	1.71	1.75	1.78	1.81	1.74	1.77	1.79	1.83
15	1.58	1.62	1.66	1.69	1.61	1.65	1.67	1.72
22	1.48	1.52	1.56	1.59	1.51	1.54	1.57	1.63

Table 4. 3 Coordination number of each sulfur evaluated from the $S(SO_3^-)$-$S(SO_3^-)$ PCFs within the distance 0-8 Å at various water contents λ.

λ	SSC with different EW				Nafion with different EW			
	678	778	878	978	744	844	944	1144
3	3.74	3.55	3.46	3.19	3.95	3.86	3.71	3.35
6	3.02	2.88	2.80	2.72	3.09	2.98	2.95	2.78
9	2.32	2.18	2.10	2.11	2.32	2.26	2.28	2.16
15	1.62	1.65	1.49	1.50	1.62	1.64	1.57	1.59
22	1.27	1.24	1.22	1.23	1.34	1.28	1.27	1.40

Table 4. 4 Hydration number of each sulfur evaluated from the $S(SO_3^-) – O(H_2O)$ PCFs within the distance 0-4.8 Å at various water contents λ.

λ	SSC with different EW				Nafion with different EW			
	678	778	878	978	744	844	944	1144
3	3.30	3.25	3.22	3.13	3.53	3.57	3.65	3.40
6	6.27	6.09	6.11	5.94	6.58	6.45	6.57	6.46
9	7.41	7.31	7.20	7.18	7.40	7.33	7.42	7.38
15	8.18	8.12	8.02	8.03	7.93	7.93	8.02	7.84
22	8.50	8.50	8.39	8.36	8.17	8.18	8.17	8.12

Table 4. 5 Hydronium ion coordination number of each sulfur evaluated from the $S(SO_3^-) – O(H_3O^+)$ PCFs within the distance 0-4.8 Å at various water contents λ.

λ	SSC with different EW				Nafion with different EW			
	678	778	878	978	744	844	944	1144
3	2.05	2.03	2.03	1.94	1.99	2.00	1.96	1.93
6	1.16	1.20	1.17	1.19	0.98	0.99	1.00	0.97
9	0.82	0.79	0.77	0.80	0.70	0.69	0.72	0.69
15	0.56	0.58	0.56	0.56	0.50	0.49	0.50	0.52
22	0.44	0.45	0.46	0.46	0.40	0.40	0.41	0.43

Table 4. 6 Water coordination number of each hydronium ion evaluated from the $O(H_2O)$ - $O(H_3O^+)$ PCFs within the distance 0-3.2 Å at various water contents λ.

λ	SSC with different EW				Nafion with different EW			
	678	778	878	978	744	844	944	1144
3	1.63	1.62	1.61	1.63	1.81	1.81	1.82	1.78
6	2.81	2.73	2.76	2.72	3.12	3.08	3.10	3.07
9	3.23	3.21	3.19	3.16	3.44	3.43	3.42	3.42
15	3.52	3.47	3.47	3.46	3.67	3.66	3.66	3.60
22	3.65	3.63	3.58	3.59	3.77	3.77	3.74	3.70

Table 4. 7 Coordination number of each water molecule evaluated from the $O(H_2O)$ - $O(H_2O)$ PCFs within the distance 0-5.2 Å at various water contents λ.

λ	SSC with different EW				Nafion with different EW			
	678	778	878	978	744	844	944	1144
3	2.97	2.92	2.78	2.57	2.97	3.02	2.97	2.77
6	6.91	6.94	6.67	6.59	7.20	7.21	7.34	7.12
9	9.62	9.35	9.11	9.10	10.17	10.11	10.10	9.88
15	12.38	12.57	12.23	12.31	13.05	13.13	13.08	12.96
22	14.01	14.18	14.05	14.00	14.66	14.53	14.64	14.70

Table 4. 8 Distance between the centers of clusters calculated from the structure factor (S(q)) based on the Fourier transform of $O(H_2O)$-$O(H_2O)$ PCFs (cutoff distance is 30 Å).

λ	SSC with different EW				Nafion with different EW			
	678	778	878	978	744	844	944	1144
3	18.04	19.74	20.60	20.60	22.17	24.01	22.04	20.38
6	22.18	24.32	24.64	27.12	24.32	26.00	27.92	30.40
9	24.32	27.93	N/A	27.52	N/A	N/A	N/A	N/A
15	N/A	N/A	N/A	N/A	N/A	N/A	N/A	N/A
22	N/A	N/A	N/A	N/A	N/A	N/A	N/A	N/A

Table 4. 9 The distance (Å) water molecules travel during the simulation time.

λ	SSC with different EW				Nafion with different EW			
	678	778	878	978	744	844	944	1144
3	6.83	6.77	6.39	6.08	5.75	5.70	5.84	5.69
6	14.48	14.85	14.27	13.90	14.44	14.83	13.81	13.95
9	21.32	20.43	20.78	20.00	21.58	21.37	22.22	20.27
15	30.18	28.70	28.26	27.62	29.86	29.18	28.68	28.74
22	35.36	33.60	33.57	33.07	35.10	34.57	34.19	33.80

Table 4. 10 Diffusion coefficients (10^{-6} cm^2 s^{-1}) for water in hydrated SSC PFSA and Nafion membranes at various water contents λ.

λ	SSC with different EW				Nafion with different EW			
	678	778	878	978	744	844	944	1144
3	0.63	0.61	0.54	0.46	0.42	0.41	0.42	0.41
6	3.07	3.06	2.87	2.57	3.03	3.26	2.97	2.59
9	7.45	6.19	6.45	5.82	6.81	6.68	7.31	5.77
15	14.2	12.3	12.4	11.3	13.5	12.9	12.3	12.1
22	19.8	17.7	17.3	16.9	19.4	18.4	17.7	17.0

Table 4. 11 Diffusion coefficients (10^{-6} cm^2 s^{-1}) for hydronium ions in hydrated SSC PFSA and Nafion membranes at various water contents λ.

λ	SSC with different EW				Nafion with different EW			
	678	778	878	978	744	844	944	1144
3	0.05	0.06	0.05	0.05	0.05_5	0.06	0.08	0.08
6	0.42	0.39	0.43	0.43	0.54	0.62	0.65	0.56
9	1.51	1.19	1.17	1.09	1.63	1.77	2.09	1.44
15	3.54	2.46	2.81	3.19	3.86	4.19	3.83	3.63
22	5.80	5.14	4.89	4.84	6.10	6.13	6.04	5.01

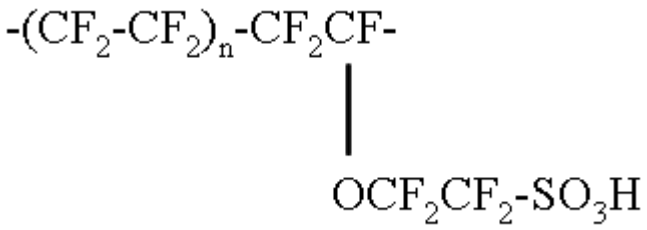

(a)

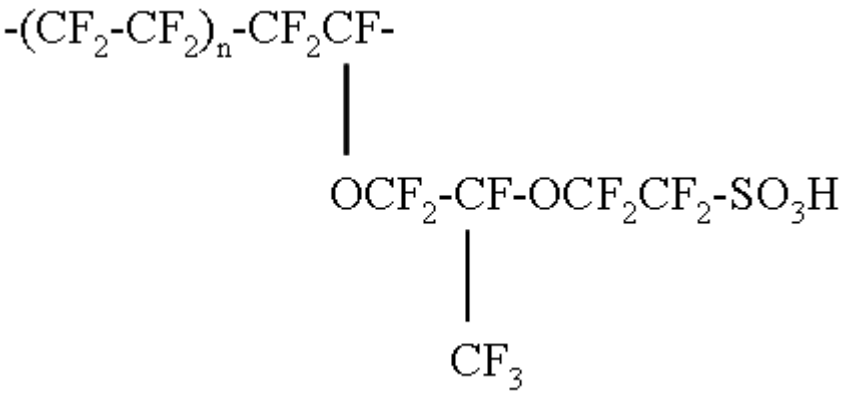

(b)

Figure 4. 1 Chemical structures of the ionomers used in the simulations: (a) SSC PFSA; and (b) Nafion.

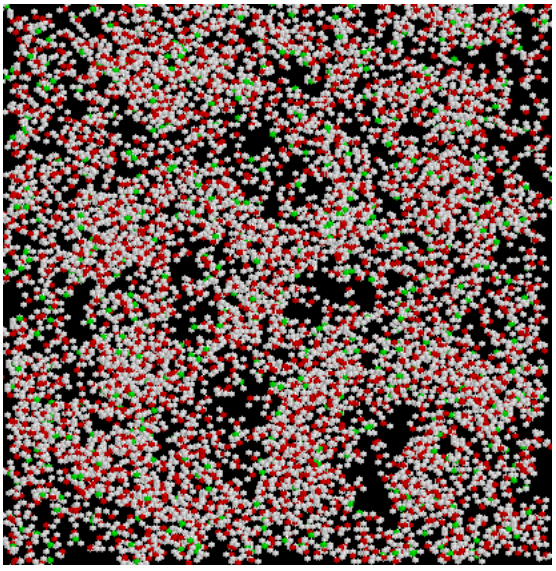

(a)

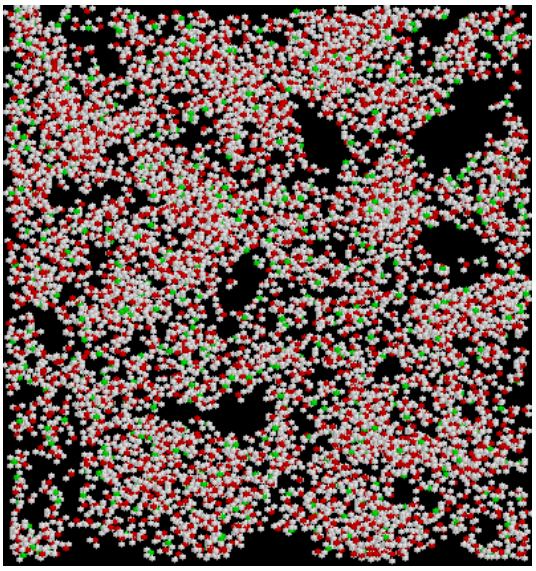

(b)

Figure 4. 2 Snapshots of the final configurations of the SSC PFSA ionomer at hydration level where $\lambda = 6.0$: (a) EW = 678 and (b) EW = 978. Atoms of the ionomer are not shown. Red atoms are oxygen atoms of water molecules, green atoms are oxygen atom of hydronium ions, and white atoms are hydrogen atoms.

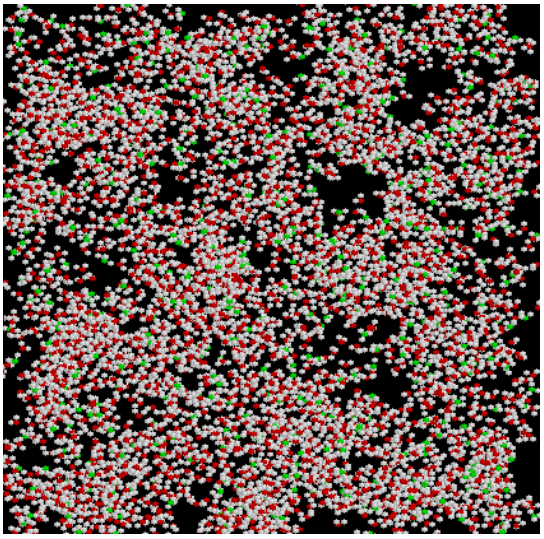

(a)

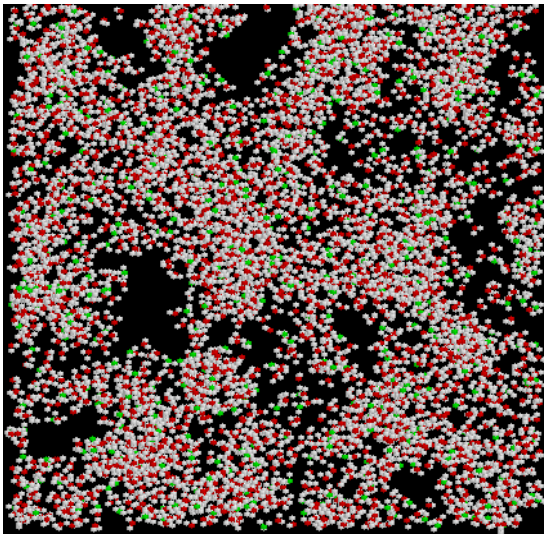

(b)

Figure 4. 3 Snapshots of the final configurations of hydrated Nafion at hydration levels where $\lambda = 6.0$: (a) EW = 844 and (b) EW = 1144. Atoms of the ionomer are not shown. Atomic color scheme is as in Figure 6.2.

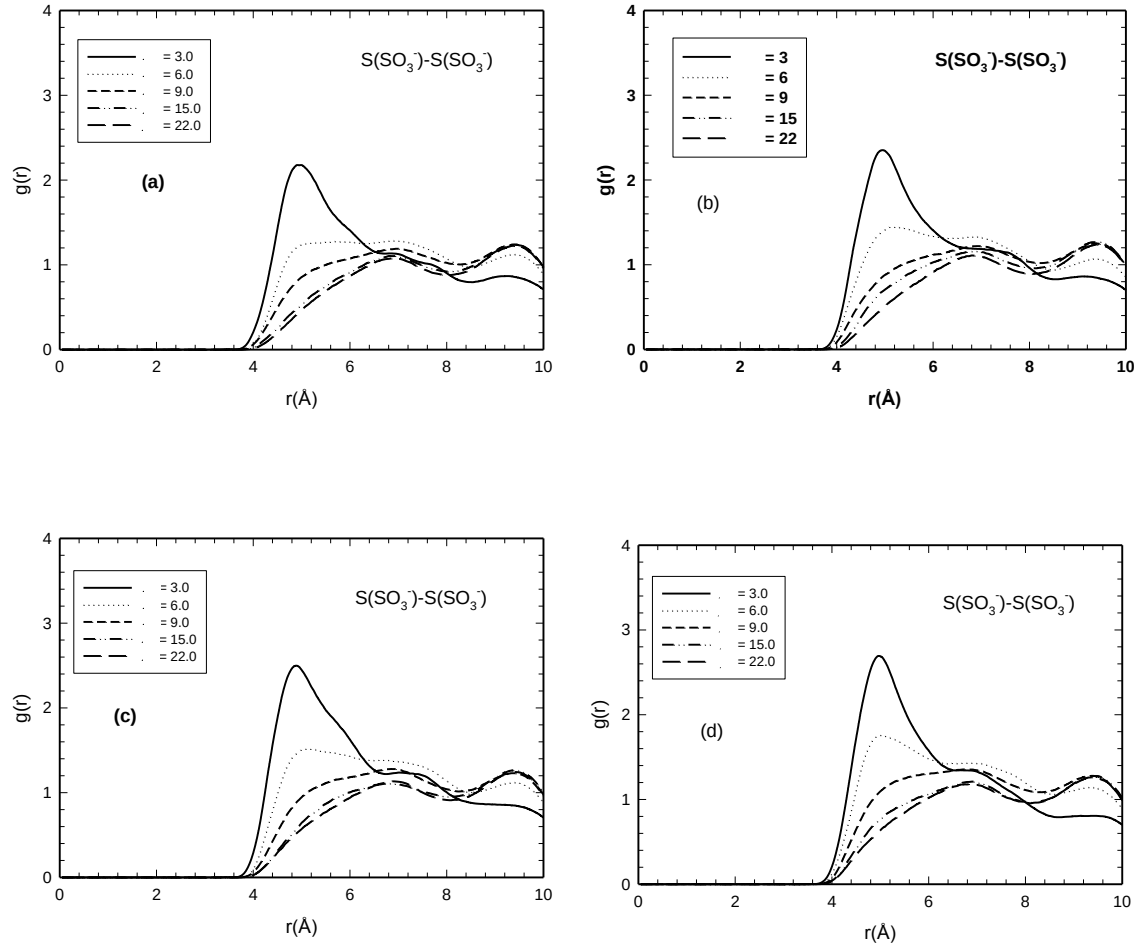

Figure 4. 4 Sulfur-sulfur pair correlation functions for hydrated SSC PFSA ionomer: (a) EW 678; (b) EW 778; (c) EW 878; and (d) EW 978.

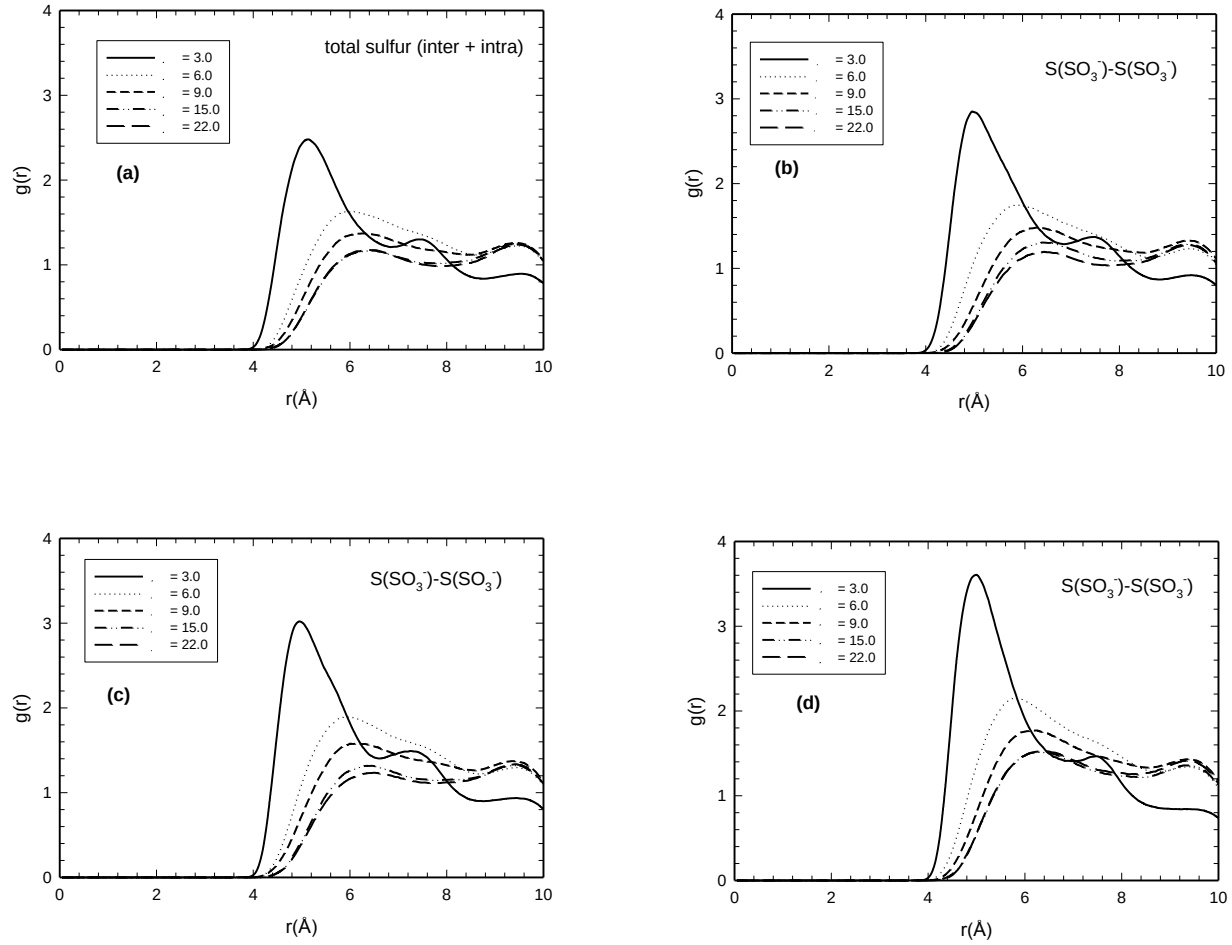

Figure 4. 5 Sulfur-sulfur pair correlation functions for hydrated Nafion: (a) EW 744; (b) EW 844; (c) EW 944; and (d) EW 1144.

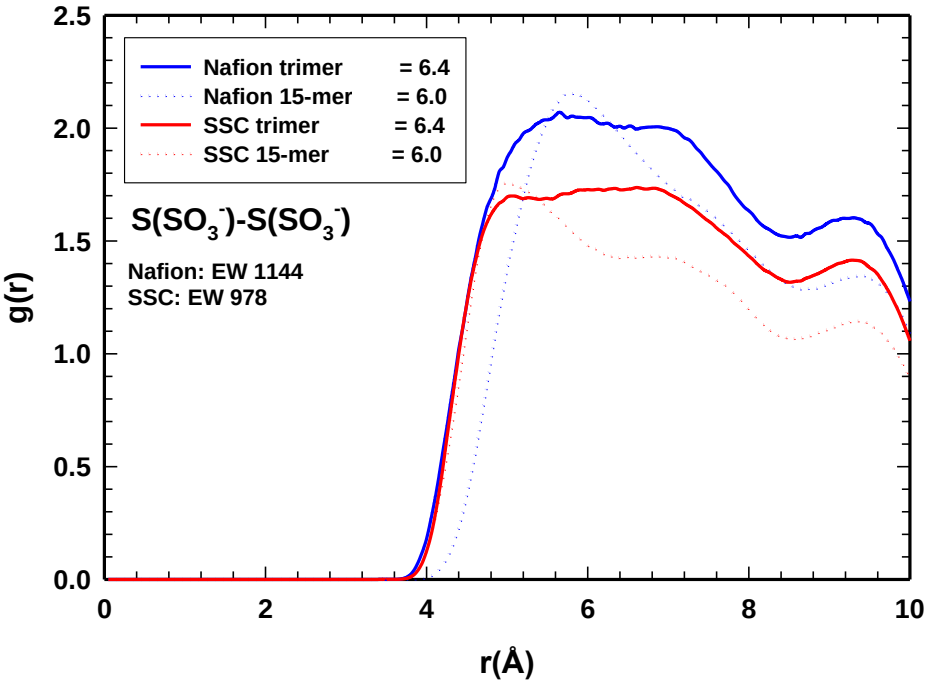

Figure 4. 6 Sulfur-sulfur pair correlation functions for SSC PFSA and hydrated Nafion with different MW.

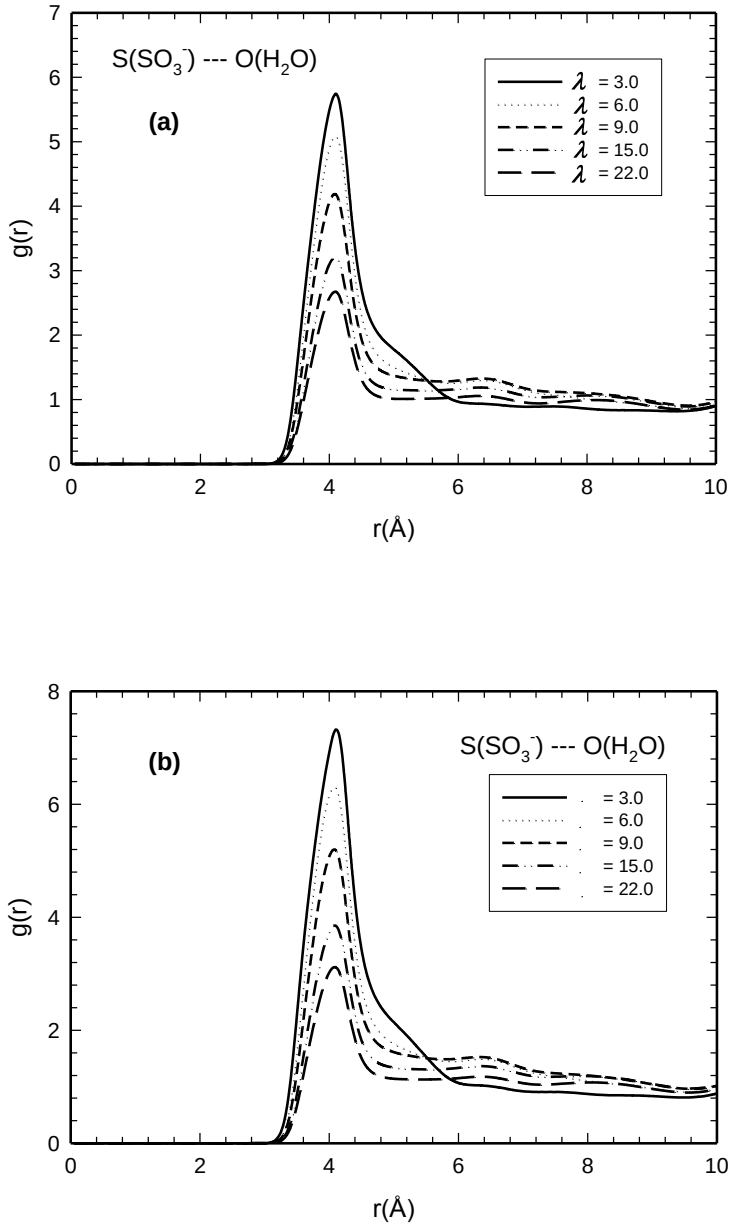

Figure 4. 7 Sulfur-water (oxygen atom of water molecule) pair correlation functions for hydrated SSC PFSA ionomer: (a) EW 678; and (b) EW 978.

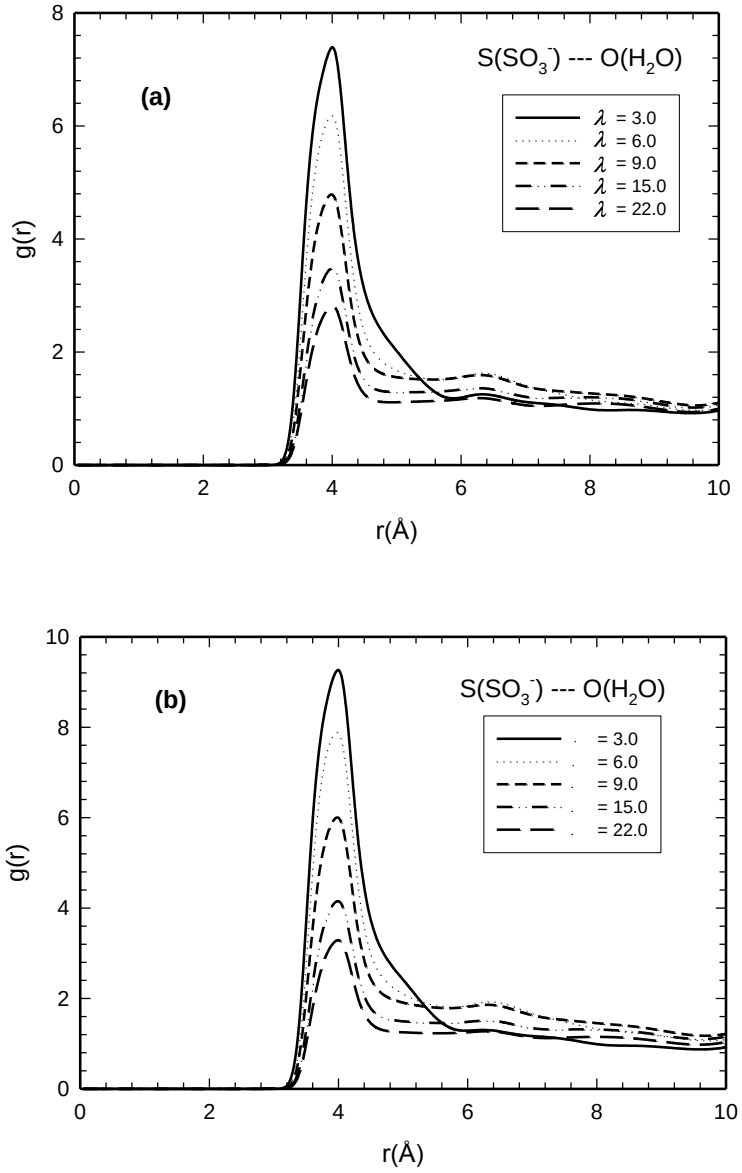

Figure 4. 8 Sulfur-water (oxygen atom of water molecule) pair correlation functions for hydrated Nafion: (a) EW 844; and (b) EW 1144.

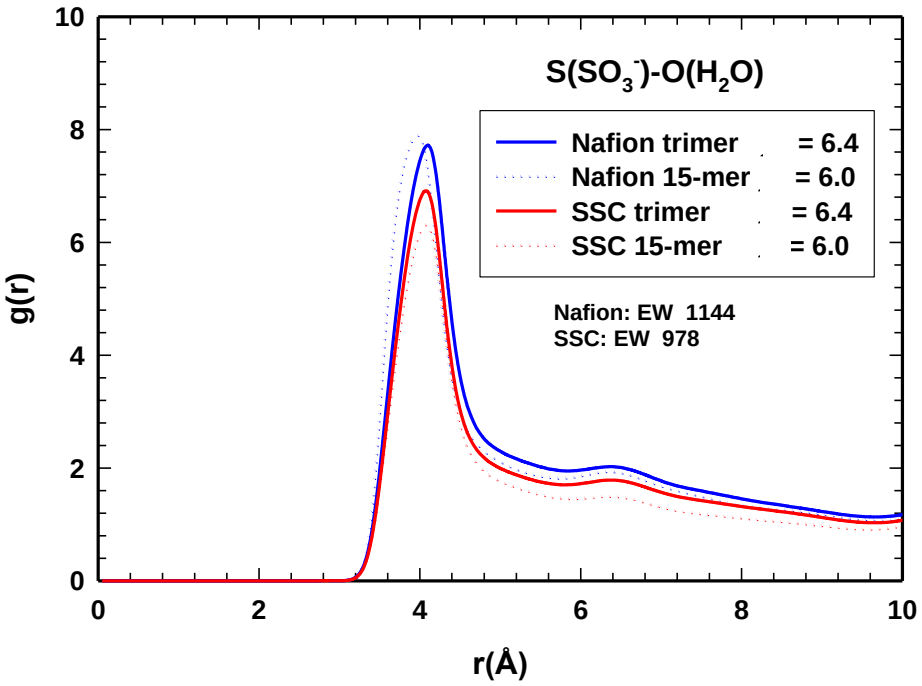

Figure 4. 9 Sulfur-water (oxygen atom of water molecule) pair correlation functions for SSC PFSA and hydrated Nafion with different MW.

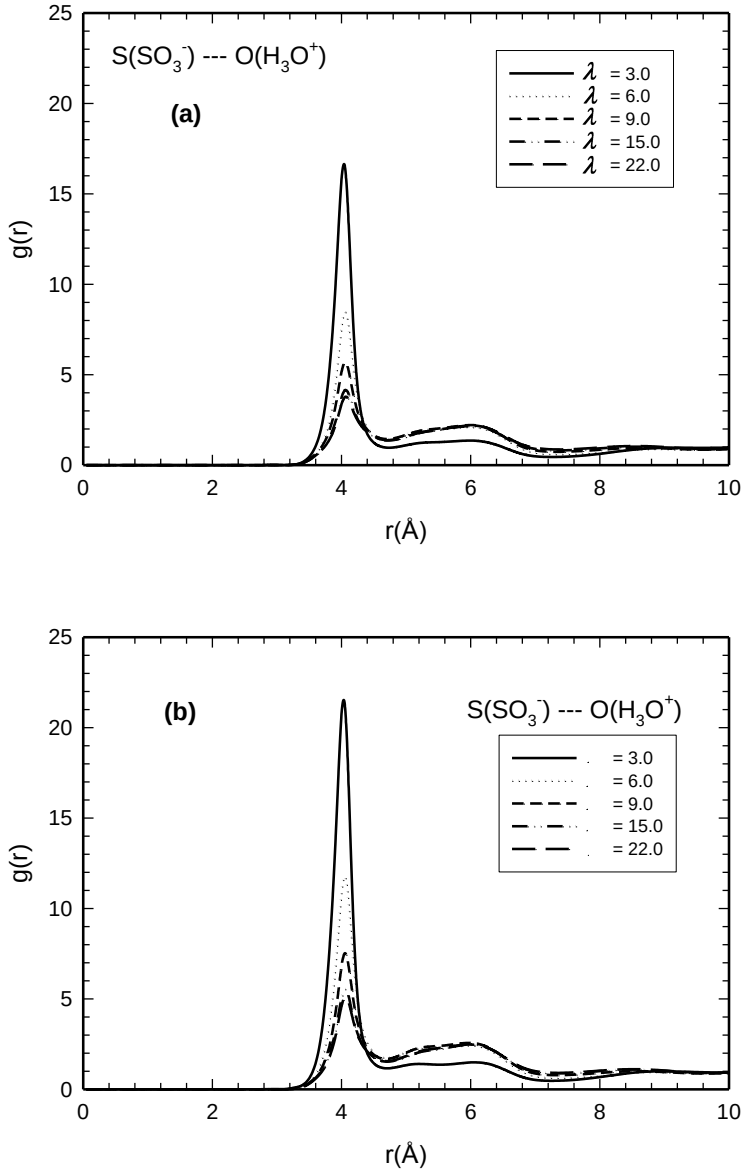

Figure 4. 10 Sulfur-hydronium (oxygen atom of hydronium ion) pair correlation functions for hydrated SSC PFSA ionomer: (a) EW 678; and (b) EW 978.

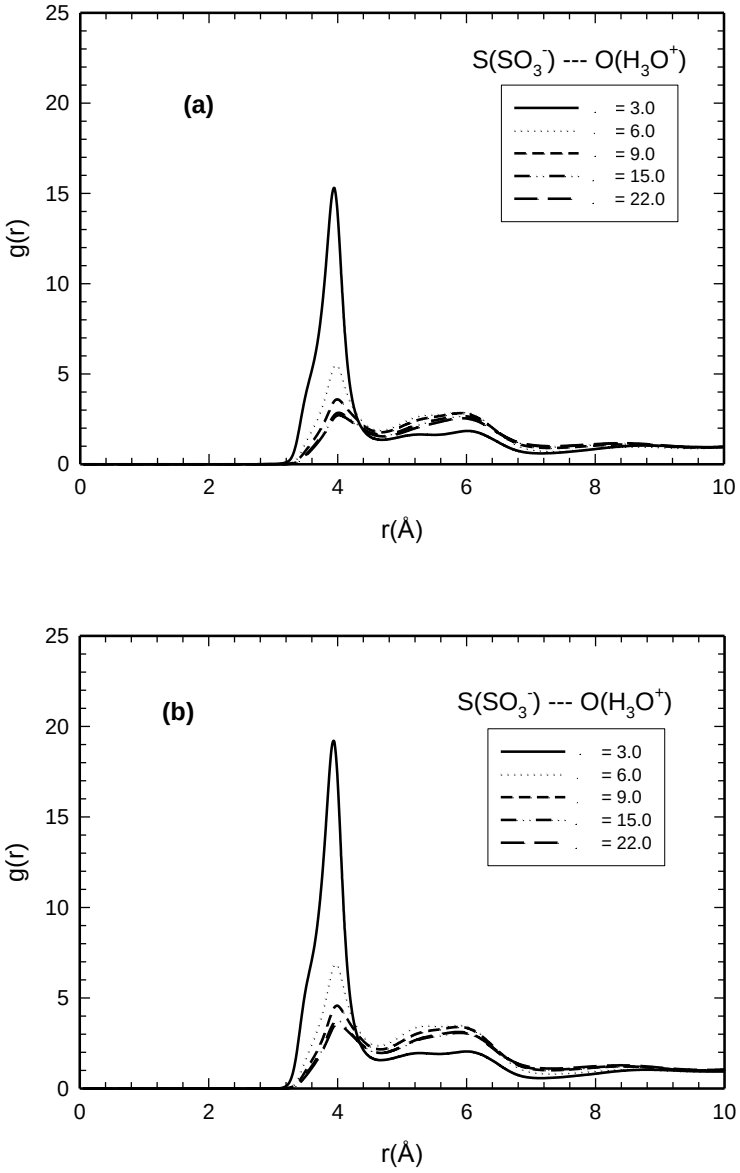

Figure 4. 11 Sulfur-hydronium (oxygen atom of hydronium ion) pair correlation functions for hydrated Nafion: (a) EW 844; and (b) EW 1144.

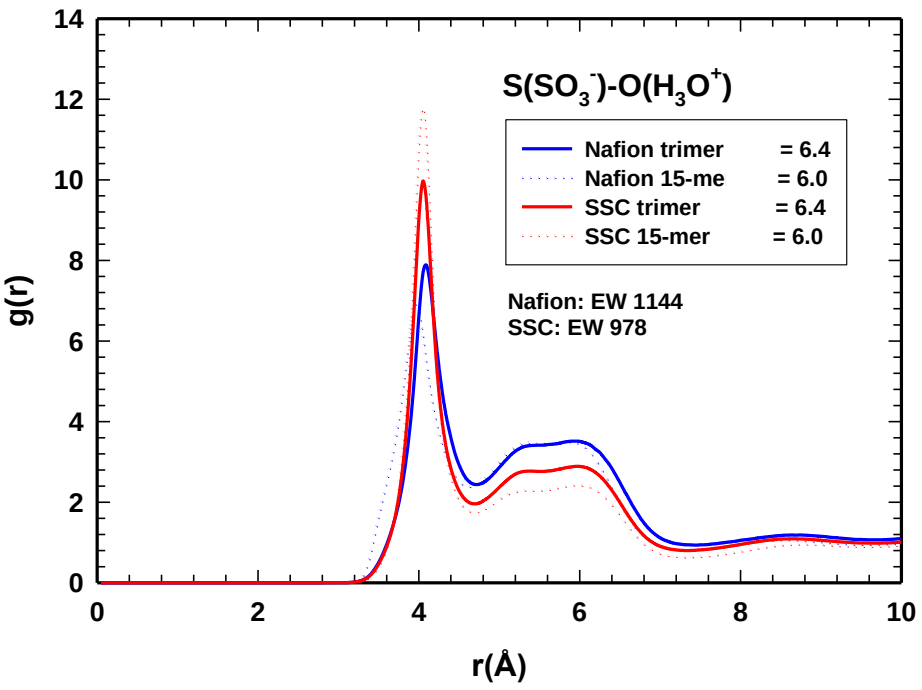

Figure 4. 12 Sulfur-hydronium (oxygen atom of hydronium ion) pair correlation functions for SSC PFSA and hydrated Nafion with different MW.

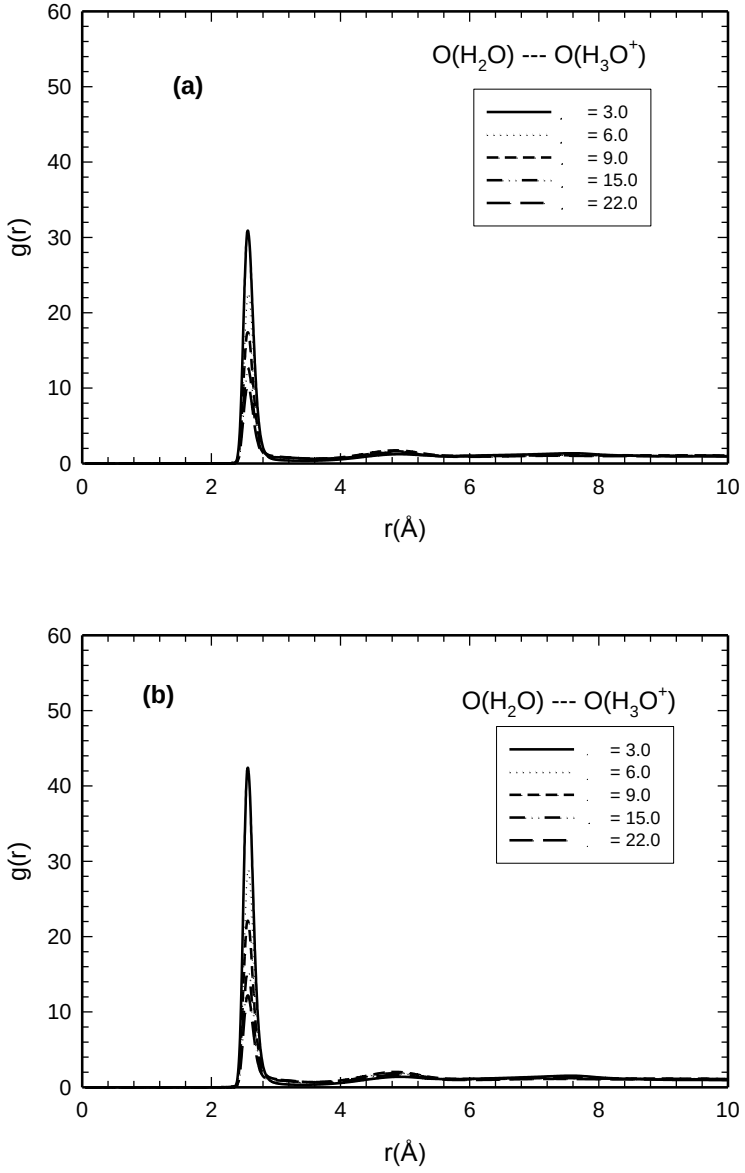

Figure 4. 13 Water-hydrionium (as represented by oxygen of water molecules and hydronium ions) pair correlation functions for hydrated SSC PFSA ionomer: (a) EW 678; and (b) EW 978.

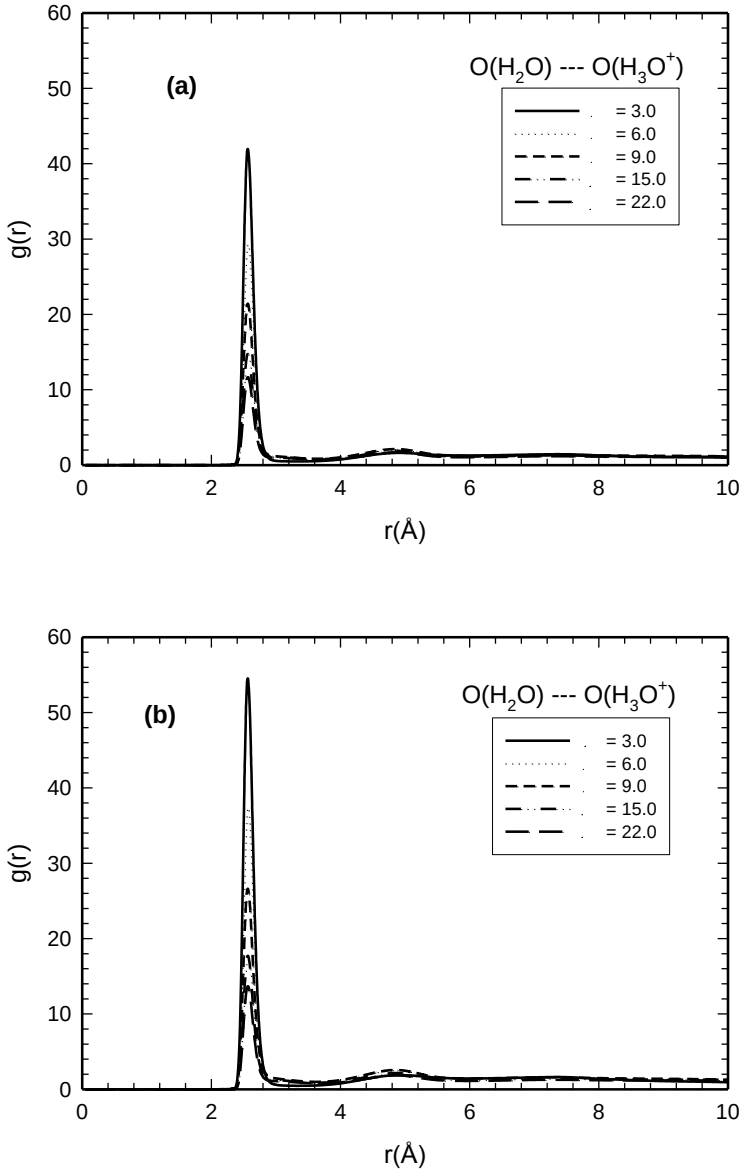

Figure 4. 14 Water-hydrionium (as represented by oxygen of water molecules and hydronium ions) pair correlation functions for hydrated Nafion: (a) EW 844; and (b) EW 1144.

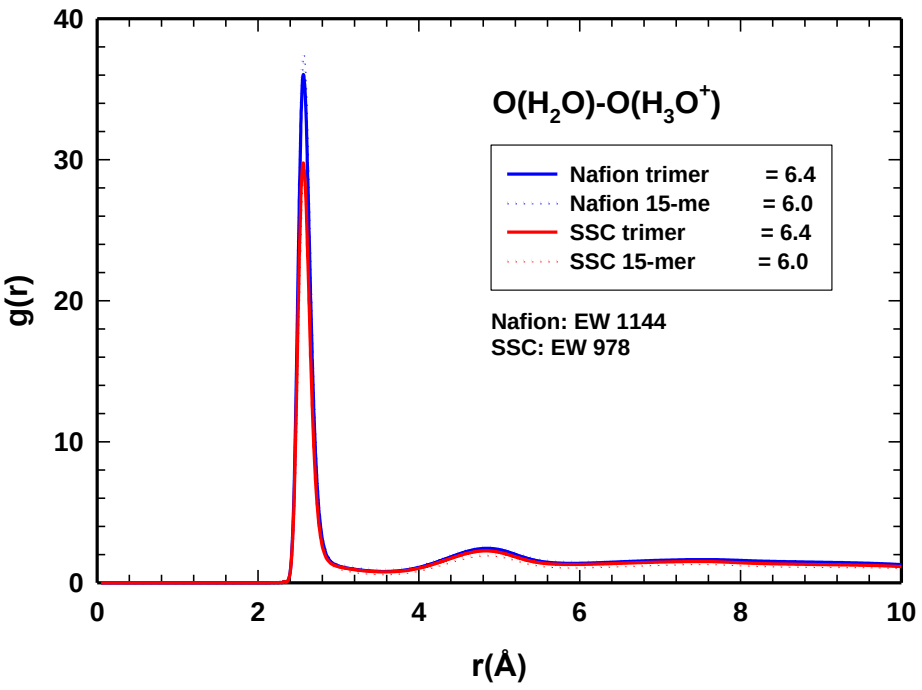

Figure 4. 15 Water-hydrionium (as represented by oxygen of water molecules and hydronium ions) pair correlation functions for SSC PFSA and hydrated Nafion with different MW.

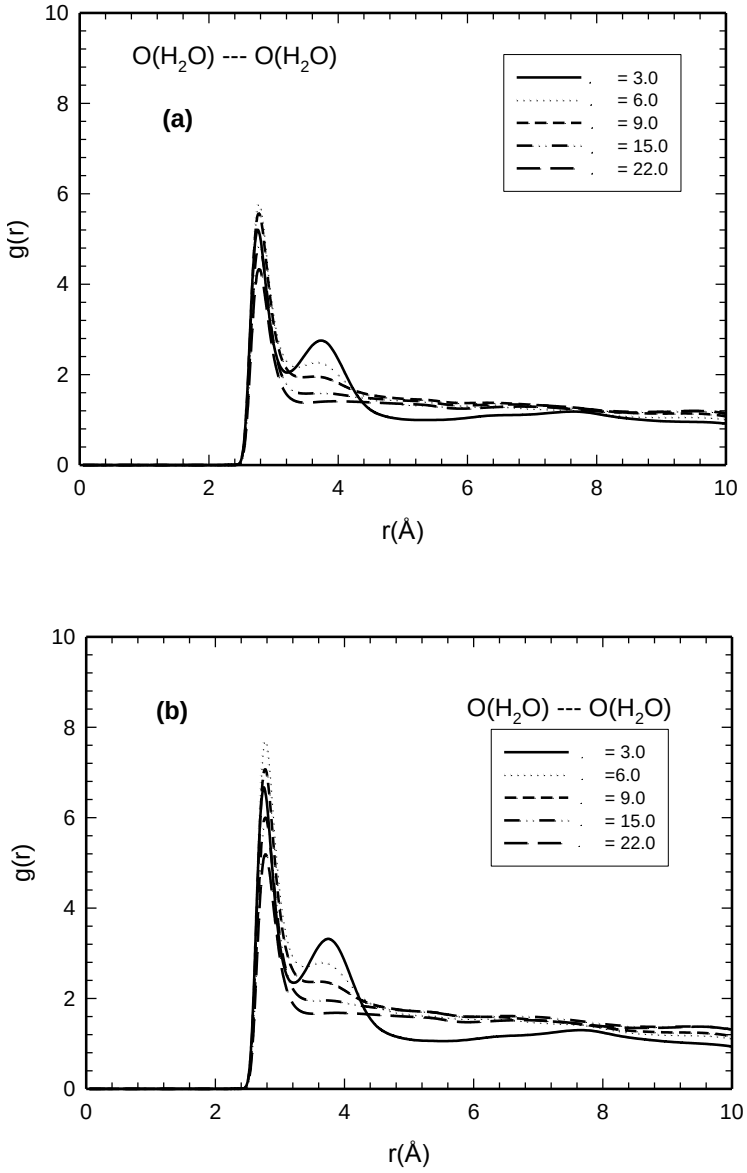

Figure 4. 16 Water-water (as represented by oxygen of water molecules) pair correlation functions for hydrated SSC PFSA ionomer: (a) EW 678; and (b) EW 978.

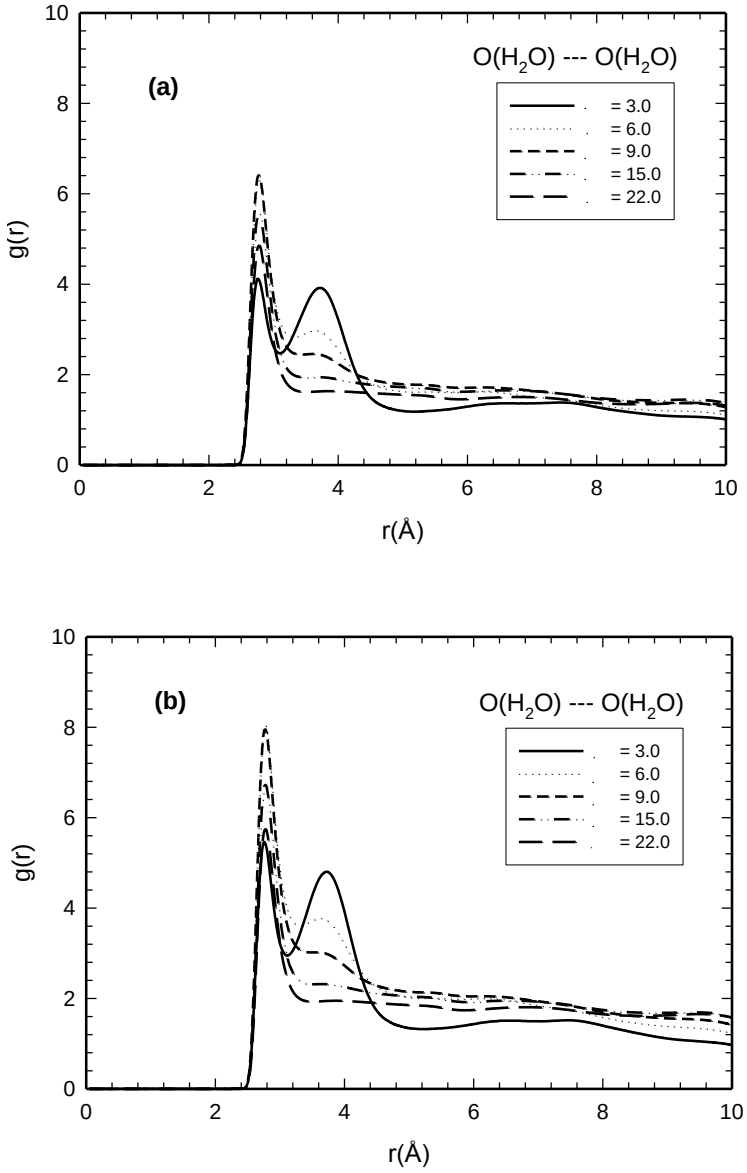

Figure 4. 17 Water-water (as represented by oxygen of water molecules) pair correlation functions for hydrated Nafion: (a) EW 844; and (b) EW 1144.

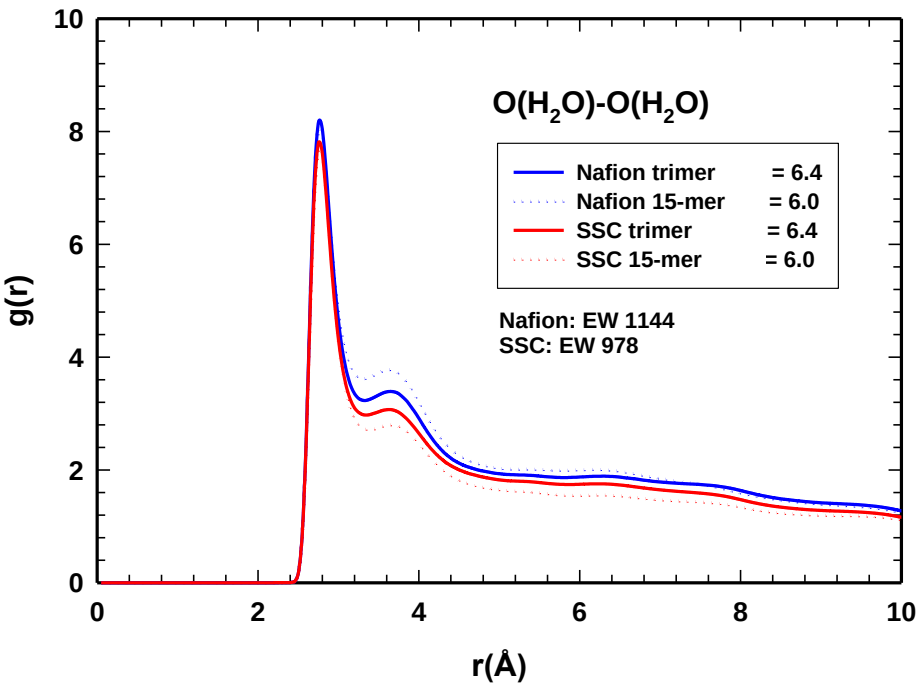

Figure 4. 18 Water-water (as represented by oxygen of water molecules) pair correlation functions for SSC PFSA and hydrated Nafion with different MW.

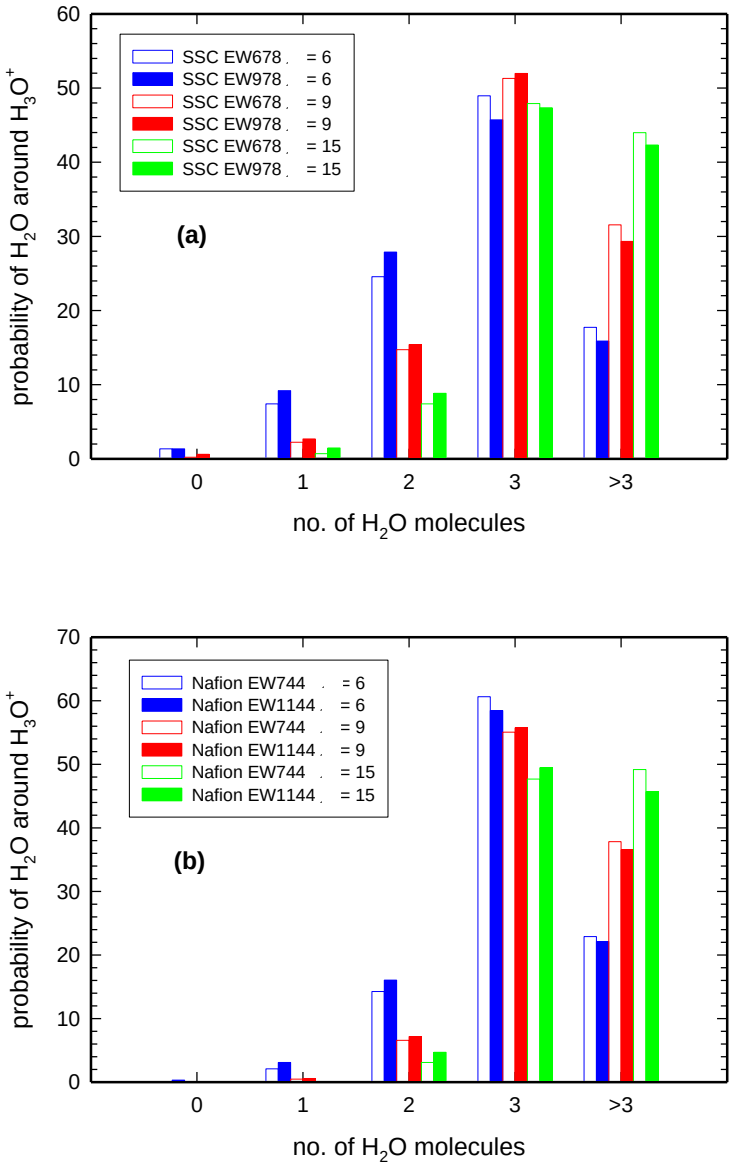

Figure 4. 19 Distribution of water molecules around hydronium ions for: (a) hydrated SSC PFSA; and (b) hydrated Nafion.

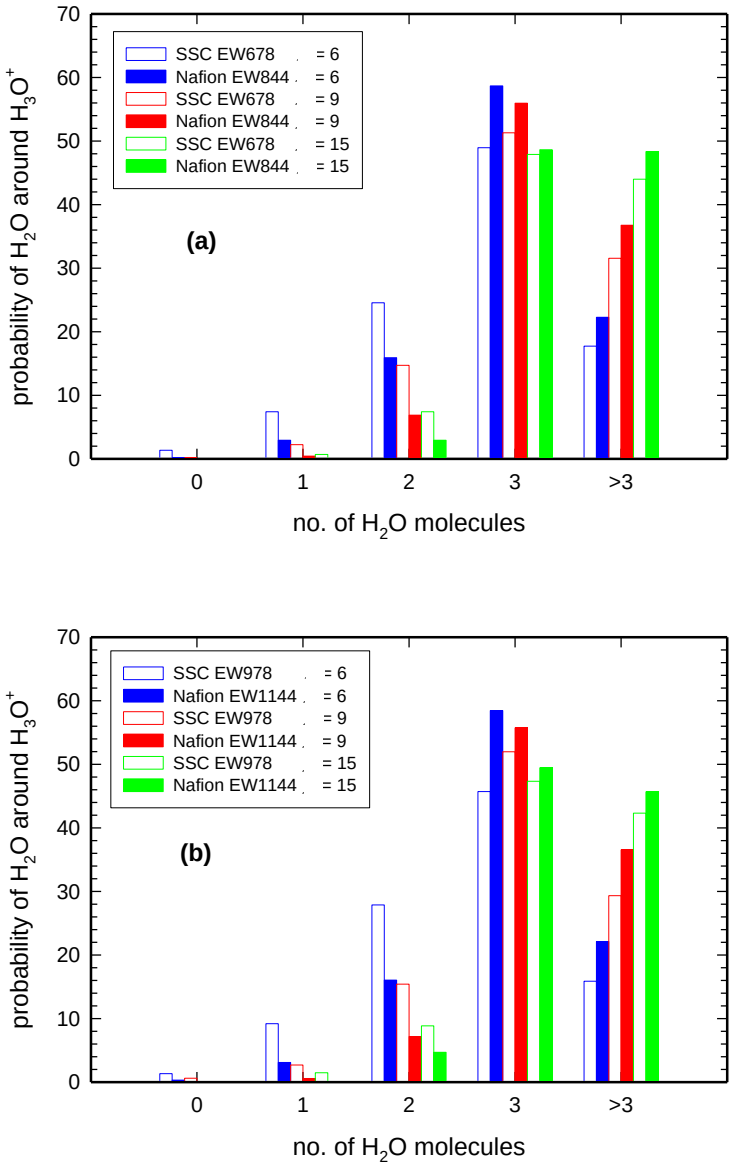

Figure 4. 20 Distribution of water molecules around hydronium ions for hydrated SSC PFSA and Nafion as a function of the side chain length: (a) no. of carbon atoms on the monomer backbone = 10; and (b) no. of carbon atoms on the monomer backbone = 16.

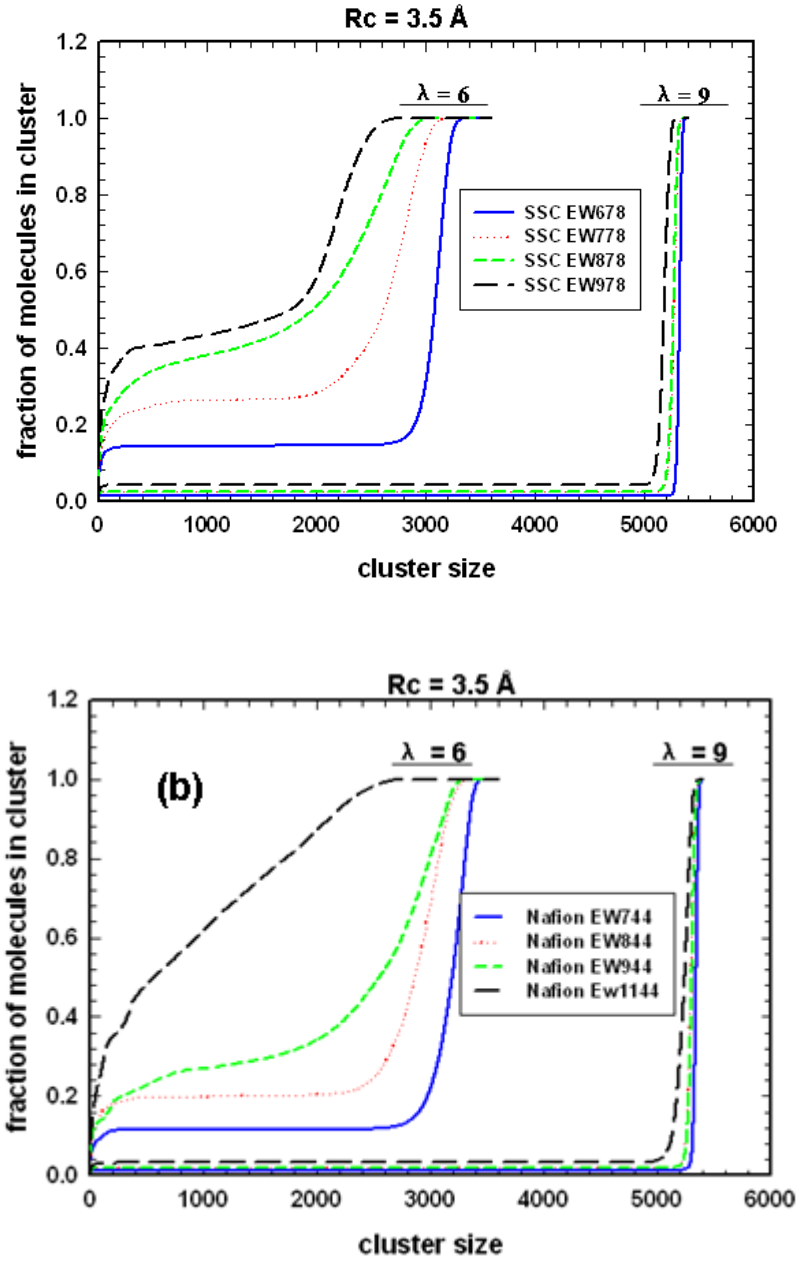

Figure 4. 21 Cumulative number of molecules in clusters for Rc of 3.5 Å: (a) hydrated SSC PFSA ionomer; and (b) hydrated Nafion ionomer.

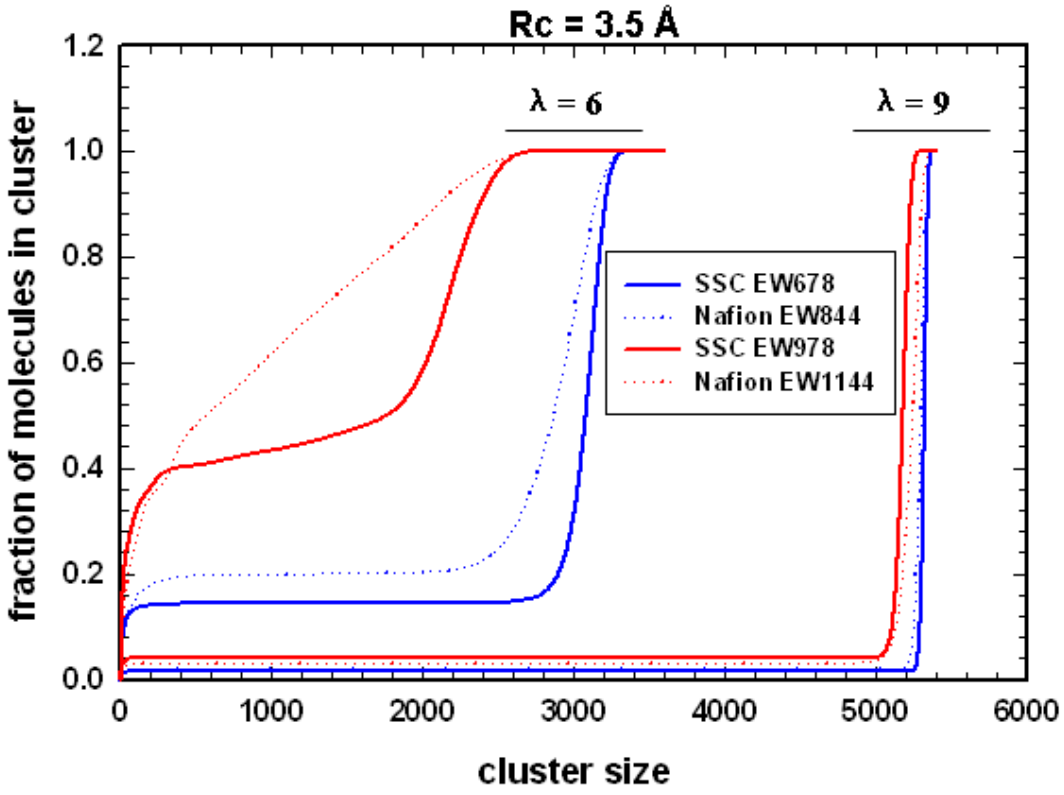

Figure 4. 22 Cumulative number of molecules in clusters for Rc of 3.5 Å to illustrate the effects of the length of the side chain.

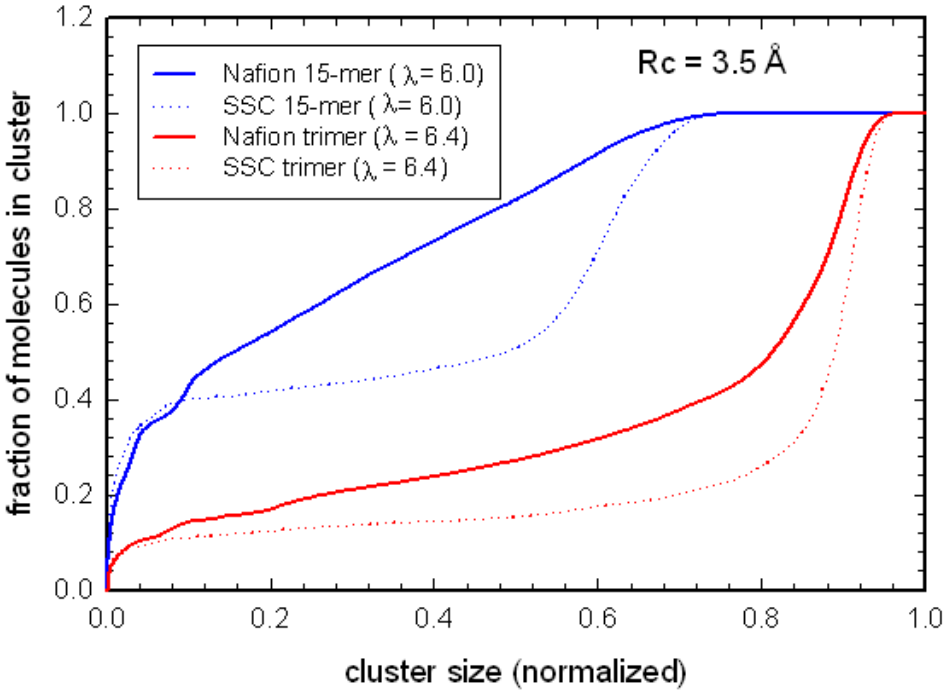

Figure 4. 23 Cumulative number of molecules in clusters for Rc of 3.5 Å to illustrate the effects of MW.

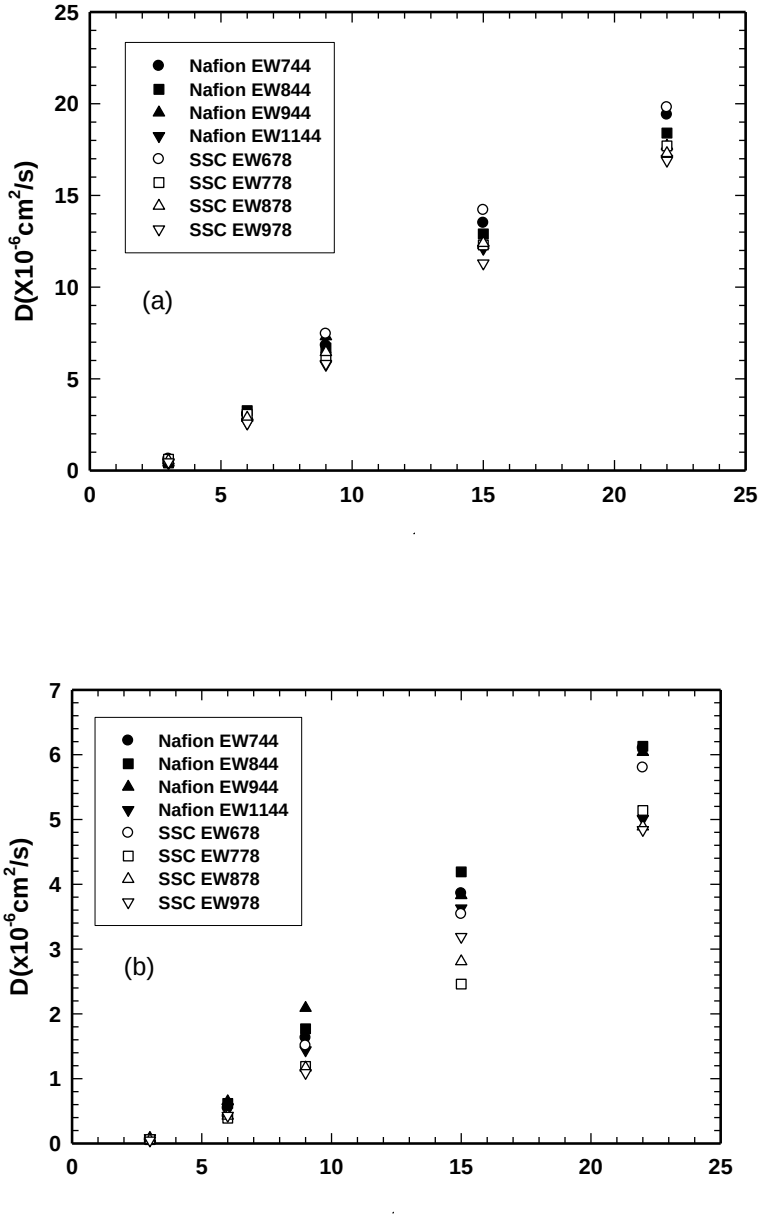

Figure 4. 24 Water and hydroniun ion diffusion coefficients of hydrated Nafion and SSC PFSA ionomers: (a) water; and (b) hydronium ions.

Chapter 5

Molecular-level modeling of the structure and wetting of electrode/electrolyte interfaces in hydrogen fuel cells

This part is a slightly revised version of a paper by the same title submitted to the *Journal of Physical Chemistry C* in 2008 by Junwu Liu, Myvizhi Esai Selvan, Shengting Cui, Brian Edwards, David Keffer, and William Steele:

J.W. Liu, M.E. Selvan, S.T. Cui, D.J. Keffer, B.J. Edwards, and W.V. Steele, "Molecular-level modeling of the structure and wetting of electrode/electrolyte interfaces in hydrogen fuel cells", *J. Phys. Chem. C*, **112**(6) 2008 p. 1985-1993.

The use of "we" in this part refers to the co-authors and the author of this dissertation. My primary contributions to this paper include (1) implementation of the simulation methodology, (2) all of the simulation work and analysis, (3) most of the gathering and interpretation of literature, and (4) most of the writing.

Abstract

Molecular dynamics (MD) simulations were performed to investigate the structural and dynamical behavior of water and hydronium ions at the electrode/electrolyte interface of hydrogen polymer electrolyte membrane (PEM) fuel cells. Specifically, we have studied the hydrated Nafion membrane, humidified for four different water contents, 5, 10, 15, and 20%, at 300 K. We analyzed the three-phase interface where the hydrated PEM is in contact with the vapor phase and with either the catalyst surface (platinum in this paper) or the catalyst−support surface (graphite in this paper). These molecular simulations represent portions of interfaces that exist within the PEM fuel cells. We observed significant wetting of the catalyst surface by a mixture of polymer, water, and hydronium ions but not beyond a monolayer. We observed virtually no wetting of the graphite surface. On the catalyst surface, the degree of wetting of the catalyst surface depends strongly on the level of membrane humidity. The pair correlation functions indicate that the water molecules adsorbed in a monolayer on the catalyst surface form small domains of ordered structures, which are bound by fragments of Nafion on the surface. The diffusion of protons from the catalyst surface into the membrane must proceed across this highly inhomogeneous surface.

5.1 Introduction

A better understanding of the properties of the electrode/electrolyte interface is of practical significance in catalysis, proton transport, water electrolysis, and electrode coatings of Polymer Electrolyte Membrane (PEM) fuel cells, which constitute a promising renewable energy source for automobile applications and portable devices such as cell phones, and laptop computers. Essentially, a PEM fuel cell is composed of an anode, where hydrogen is electro-oxidized, a cathode, where oxygen is electro-reduced, and a perfluorinated polymer electrolyte membrane which serves as a structural framework and transports protons from anode to cathode. The study of the molecular level structure and of the dynamics at the interface between electrode and electrolyte offers new insights into the theory and mechanisms that control the electrochemical and electrocatalytic surface processes.

In recent years, many significant experiments [1-21], classical molecular dynamics simulations (MD) [22-26], and molecular-level simulations [27-30] have been conducted in attempts to understand the structural and dynamical properties of proton transport in the hydrated membrane. Key to the understanding of proton transport in hydrated Nafion is the understanding that hydrated Nafion is composed of two nanophases—a hydrophobic phase composed of the backbone of the Nafion and an aqueous phase composed of the water molecules, the hydronium ions and the sulfonic acid groups at the end of the Nafion side chains. Proton transport occurs through the aqueous nanophase. Numerous idealized models of the morphology of the aqueous phase have been previously presented [4, 5, 9].

More recently, classical MD simulations have been performed to understand the morphology of the aqueous nanophase in Nafion in different solvents, such as water and methanol. Vishnyakov and Neimark [31], for example, found that water does not form a continuous subphase, but forms isolated clusters of about 100 molecules in size. They also concluded that the clusters are connected through short-lived bridges instead of a continuous hydrophilic subphase. By comparison, Urata *et al.* [32] studied the water clustering and concluded that, in the short range distance within 4.6-7.7Å, a continuous aqueous phase bridged the sulfonic acid groups. Cui *et al.* [33] demonstrated through analyses of the water cluster size distributions that the vast majority of water molecules form a single, sample-spanning cluster of water contents at

15 and 20 wt%; however, as the humidity level is decreased, smaller, disconnected clusters are formed. The morphology of the aqueous nanophase can fluctuate in time.

Although much effort has been expended on the molecular-level characterization of proton transport in the hydrated membrane, substantially less work has concentrated on the atomic and molecular-level details of proton transport at the three-phase interface composed of the polymer electrolyte membrane, vapor, and catalyst surface. The electrochemical and electrocatalytic processes occurred at this interface ultimately dictate the overall performance of PEM fuel cells. In aqueous solution, a combination of experiment and simulation has led to a relatively clear molecular-level picture of water close to a Pt electrode b[34, 35]. Rossmeisl *et al.* used *ab initio* density functional theory to calculate the phase diagram for the oxidation and reduction of water over Pt(111) surface[36]. However, this body of work models the electrode in aqueous solution, without Nafion present.

One difficulty in modeling the three-phase hydrated PEM/catalyst/vapor interface is the possible variation in structure due to the manufacturing process and composition of the catalyst zone in the membrane electrode assembly (MEA). The performance of the fuel cell depends upon both the amount of ionomer introduced into the MEA as well as the manner in which was introduced [37]. For example, using gas chromatography and SEM to study Pt/C catalyst impregnated with a solution of Nafion, Broka and Ekdunge report that "it is more likely Pt agglomerates are only partially covered by Nafion" [38]. Using SEM and TEM to study thin-film catalyst layers made by mixing the Pt/C catalyst with a Nafion solution, Cheng *et al.* report that low Pt catalyst utilization can result from catalyst particles being covered by "thick Nafion layers or clumps" [39]. Various groups have varied the Nafion loading in the gas diffusion layer and found an optimum, reflecting the balance between enhanced proton conductivity and hindered gas diffusion at high Nafion content [40, 41].

Using molecular simulation, Lamas *et al.* [42] formulated a model of the three-phase interface to investigate how the configurational and dynamic properties of water in the vicinity of the catalyst surface change with Nafion content. They also reported that the water dynamics adjacent to the catalyst surface vary significantly, according to the degree of membrane hydration.

In this work, we choose to focus on a MEA in which the catalyst surface is not completely covered by Nafion. In Figure 5.1, we present an idealized schematic of the model interface that is used as a basis for the molecular dynamics simulations reported herein. The schematic shows a single unit of the porous electrode. Catalyst particles are distributed on the surface of the pore, and the pore is in contact with the PEM. The specific geometry of this highly idealized schematic is not essential and the schematic is not necessarily drawn to scale, which depends upon the pore size distribution of the electrode; however, the schematic illustrates the specific molecular-level interfaces that are present at the composite electrode/electrolyte interface. Specifically, four systems are isolated. The first system is the "bulk" hydrated membrane, which has been studied extensively via molecular dynamics [23, 31-33, 43-47]. The second system is the interface between the hydrated membrane and the vapor phase. The structure and dynamics of this system were recently reported using MD simulations [48]. The third system is the three-phase interface between the hydrated membrane, the vapor, and the surface of the catalyst support. The fourth system is the three-phase interface between the hydrated membrane, the vapor, and the surface of the catalyst particle. In this work, we report on the structure and dynamics of the third and fourth interfaces, which include the solid surfaces.

The molecular-level environment at the interface is also a function of operating conditions. The temperature and the humidity in the feed stream affect the amount of water in the pore. Under some conditions, the pore can be filled with water, which could completely cover the catalyst particle surface. In this situation, the diffusion of molecular hydrogen to the surface of the catalyst would be dramatically reduced. (At room temperature and pressure, the self-diffusivity of H_2 is 5.6×10^{-1} cm^2/s [49] and the diffusivity of H_2 in water is 4.5×10^{-5} cm^2/s [50].) The increase in mass transfer resistance would be detrimental. However, the catalyst particle would then not require close contact to the PEM, since the hydronium ion could be transported through the aqueous phase.

In this present work, we are specifically examining the three-phase interface. Therefore, we choose to begin with a bare surface and will allow the PEM to relax over it, with the assumption that we are able to maintain a gas phase in the pore. Experimental adsorption isotherms of Nafion indicate that Nafion can be hydrated up to 20 wt% water (the highest loading studied here) through equilibrium with a vapor phase [51].

We present the results of molecular dynamics simulations of hydrated Nafion at four different water contents by weight (5, 10, 15, and 20 wt%) in simultaneous contact with the vapor phase and either the catalyst surface or the catalyst support surface. The catalyst surface is modeled as a [100] Pt surface. The catalyst support surface is modeled as graphite.

The remainder of this paper is organized as follows. In Section 4.2, we briefly describe the methodology and summarize the computational details. The results of the molecular simulations are presented in Section 4.3. In Section 4.4, we provide a discussion of the implications and conclusions of this simulation work on the molecular-level understanding of proton transport in fuel cells.

5.2 Simulation Details and Methodology

Two groups of NVT simulations were carried out at 300K in this work. The first group of simulations was for the membrane/vapor/support system (system 3 in Figure 5.1). The second group of simulations was for the membrane/vapor/catalyst system (system 4 in Figure 5.1). Each group was composed of four simulations which were performed at varying water contents of 5, 10, 15, and 20 wt%. These weight percents correspond to ratios of H_2O/SO_3^- of 4.44, 6.42, 9.63, and 12.83., respectively.

The model of Nafion, water and the hydronium ions used in this work is identical to that of our previous work to model bulk hydrated Nafion [33], that is, each Nafion oligomer is a trimer. The short chain length is a compromise, owing to the fact that long chains have long relaxation times that are beyond the capacity of the simulations. We have previously shown that this model yields consistent results with Nafion chains composed of ten monomers [33]. Philosophically, one has to make a choice between modeling a system with long chains, in which one will not be able to run a simulation of sufficient duration to average out fluctuations due to chain dynamics, or a system with short chains in which the model is more approximate but the resulting statistics are much better.

For Nafion, we used united atoms for CF_3, CF_2, and CF to reduce computational costs. We included bond stretching, bending, torsion, and intramolecular and intermolecular non-bonded

interactions via the Lennard-Jones (LJ) potential and Coulombic interactions. The potential parameters have been reported previously [52] and are taken from Ref. [53].

The water is modeled using the TIP3P model [54, 55] with a flexible OH bond [56]. The model for hydronium ions, H_3O^+, is similar to that of Urata *et al.* [32]. In particular, the partial charges for the oxygen and hydrogen atoms are taken from Urata *et al.* [32]. The bond distance, bond angles, and the force constants are the same as in the TIP3P model [54-56]. Note that this potential does not allow for structural diffusion of the proton. However, we believe that this non-reactive potential is capable of providing realistic static properties, such as configurations, as discussed previously [33].

We modeled the surface of the support phase as graphite, in which the carbon atoms are held rigid and interact with all dynamic atoms in the system through the Lennard-Jones potential with parameters $\sigma_C = 3.4$ Å and $\varepsilon_C / k = 28.0$ K [57]. The positions of the graphite atoms are taken from the literature [58] . The graphite surface is four atomic layers deep.

We modeled the surface of the catalyst phase as [100] platinum, in which the atoms are held rigid and interact with all dynamic atoms in the system through the Lennard-Jones potential with parameters $\sigma_{Pt} = 2.41$Å and $\varepsilon_{Pt} / k = 2336.0$ K [59]. The positions of the Pt atoms are taken from the literature [60]. The Pt surface is six atomic layers deep.

For all interactions, the LJ parameters for cross components were calculated using Lorentz-Berthelot mixing rules. The site-site reaction field was applied for the calculation of the electrostatic interactions [61, 62]. Partial charges for united atom groups were calculated from the summations of the constituent atom values. The backbone was treated as neutral, except for the site to which the side chain is connected through the ether oxygen.

The amount of hydrated membrane material used for these interfacial systems is four times larger than that of our previous bulk hydrated membrane system [33], in order to obtain better interfacial statistics. The size of the current simulation cell is nominally eight times that of the previous bulk hydrated membrane system size, with roughly half of the cell being occupied by the vapor phase, as was done in our strictly membrane/vapor systems [48]. The dimensions of each system are provided in Table 5.1. The dimensions of the solid surface in the z-direction are nominally 60 Å. The dimensions of the cells change to accommodate the integer number of unit

cell dimensions of the catalyst or support surface. The number of each type of molecule used in the simulation is provided in Table 5.2.

The initial conditions of the systems took an equilibrated bulk hydrated membrane from our previous work [33] and placed it next to a vacuum. Because the dimensions of the simulation cell varied according to the integer number of unit cells of catalyst or support surface present, there was a period in which the equilibrated membrane was gradually relaxed into the new aspect ratio of the cell, while maintaining a constant total simulation volume. The solid surface was artificially "grown" into the system gradually over a period of 10ps to avoid overlap with the molecules in the hydrated membrane.

With the solid surface in place, we allow the full system to equilibrate. The water redistributes between the vapor, PEM and solid surface. Thus, it is important to note that the nominal water contents reported in this work are the initial values of the hydrated membrane. This water content will decrease as the water leaves the membrane and enters the vapor phase or adsorbs to the solid phase.

The simulations were equilibrated for 2ns. The data production mode followed for an additional 2ns. We employed the Nosé-Hoover thermostat [63-65], and the r-RESPA method [66] was carried out to integrate the equations of motion with 2fs for the large time step size and 0.2fs for the intramolecular motions.

5.3 Results and Discussion

5.3.1 Membrane/vapor/catalyst Systems

In Figure 5.2 (a)-(d), we present snapshots of the final configurations of the membrane/vapor/catalyst systems for hydrated membranes with initial water contents of 5, 10, 15 and 20 wt% respectively. There are two surfaces visible because the simulations are periodic. However, the size of the system has been chosen to be large enough so that there were no artifacts associated with the periodicity. These snapshots clearly reveal that there is significant wetting of the platinum surface, and that the degree of wetting increases with the water content. The snapshots also show that some fragments of Nafion as well as hydronium

ions adsorb on the Pt surface. The fundamental reason for the adsorption of water, Nafion, and hydronium is the large attractive interaction due to the induced-dipole/induced-dipole term of the Lennard-Jones potential. At all water contents, we do not observe multilayer adsorption, except immediately adjacent to the membrane interface. At higher water contents, the adsorption approaches a complete monolayer of coverage.

The density profile of water in the catalyst system is shown in Figure 5.3. The zero coordinate on the x-axis corresponds to the central location of the membrane/vapor interface. The variation of water density within the interface is a consequence of the fact that the nanostructured segregation of the hydrated membrane into hydrophobic and hydrophilic regions is not uniform on the nanoscale, and also relaxes on a time scale that is greater than the duration of these simulations, as noted before [33]. However, there are several notable features in this plot. First, there is clearly a "dehydrated region" of the membrane near the interface. We observed this dehydration of the interface in the membrane/vapor simulations as well, so we conclude that this is an equilibrium state and is not a transient effect resulting from the catalyst surface extracting water from the membrane interface faster than it can be replenished from the membrane interior. Second, we observe only a monolayer density of water on the catalyst surface.

In these simulations, water is being drawn out of the hydrated Nafion in order to establish an equilibrium between the PEM, the vapor phase and the adsorbed phase. In the vapor phase, we never observe any molecules but water. In other words, as one would naturally expect, there is no hydronium ion or Nafion in the vapor phase. Therefore, we understand that any hydronium or Nafion that appears on the catalyst surface reached the catalyst via surface diffusion. The water can travel to the catalyst surface by moving along the surface or by moving through the vapor phase. The net flux of water from membrane to surface via the vapor phase is much lower than that through surface diffusion. In these simulations, therefore, virtually all of the material on the catalyst arrived via surface diffusion.

The dynamics of wetting are shown in Figure 5.4, which shows the quantitative degree of wetting of the catalyst surface as a function of simulation time up to 4 ns. From these curves, it appears that at lower water contents, the system has equilibrated, with the surface of the catalyst only partially covered by a mixture of water, Nafion, and hydronium ions. At high water

content, the wetting curves in Figure 5.4 still have a significant slope and are gradually continuing to increase in time. At 15 and 20 wt%, the snapshots indicate that there is already a continuous wet path across the catalyst surface. It is likely that in this simulation the surface would be completely wet, if we continued the simulations for a longer duration. We have not continued the simulations because the rate of additional wetting is slow relative to the duration of the simulations.

The reason for the deceleration in the rate of wetting can be partially attributed to a stable structure that forms on the catalyst surface. In Figure 5.5, we show the same snapshots shown in Figure 5.2(c) and (d) (15 and 20 wt% respectively) from an angle normal to the catalyst surface. Here we see the regular structure that the water has formed on the surface. This structure optimizes the degree of hydrogen bonding in a two-dimensional array of water molecules. We observe that each water molecule has four nearest neighbors when the structure is stable. The monolayer coverage of the platinum surface suggests that the wetting of the surface is predominantly through direct transfer of water molecules from the membrane phase to the catalyst surface, not through the vapor phase adsorption. Thus the direct contact between the membrane materials and the catalyst is important.

We can compare the water structure shown in Figure 5.5 with work published structures of water on Pt [34]. While we do see domains of ordered structure, we do not see the same structure. Given the classical nature of this molecular model, it is not surprising that there are differences between this structure and that provided by density functional theory. However, what these classical simulations do provide is a larger scale picture of the distribution of water, hydronium and Nafion on the Pt surface. Accepting these differences, we proceed with an analysis of the material on the Pt surface.

The structure of water on the catalyst surface can be quantitatively characterized through a pair correlation function (PCF). In Figure 5.6, we show the PCF for the oxygen atoms of water with other oxygen atoms of waters (the O_{H2O}-O_{H2O} PCF) in the adsorbed region next to the catalyst surface as a function of water content. We define the adsorbed region to extend 10 Å above the catalyst surface. We observe that the range of the structure increases as the water content increases. Compared with previous work [33], the PCFs show similar profiles, but we find two different behaviors: (i) the four peaks corresponding to the adsorbed water layers

adjacent to the catalyst surface are much more enhanced; (ii) when the distance $r > 4$ Å, the PCFs shown in Figure 5.6 oscillate with distance. In our previous paper [33], the PCFs of the four water contents varied smoothly, displaying a liquid-like structure. In other words, the water on the platinum surface has an enhanced long-range structure.

In Figure 5.7, we show the PCFs for the oxygen atoms of water with oxygen atoms of hydronium (the O_{H2O}-O_{H3O+} PCF) in the adsorbed region next to the catalyst surface as a function of water content. We find that the O_{H2O}-O_{H3O+} PCF at the catalyst surface is very similar to the bulk $g(r)$. The PCFs of the four water contents share the same qualitative behavior as that of our previous paper [33]: the first peak occurs at about 2.6Å, and its height decreases with water content resulting from a decreased binding capacity of hydronium ions to water molecules due to increased humidity. But the height of the PCFs near the platinum surface is enhanced more than that in our previous paper, which means that the degree of hydration (or equivalently, the degree of hydrogen bonding in the system) is enhanced next to the catalyst surface relative to that in the bulk hydrated membrane.

In Figure 5.8, we present a histogram representing the distribution of the number of water molecules around a hydronium ion for all four water contents in the absorbed region next to the catalyst surface. In this case, we include all water molecules with the O atom within 3.2 Å of the O of the hydronium ion. The notable feature in this histogram is that the hydration number is shifted to a higher value with the increased water content. We see that hydronium ions adsorbed to the catalyst surface in the 5 wt% water system are most likely bound to two water molecules. For the 10 wt% and 15 wt% systems, the hydroniums are most likely bound to three water molecules, allowing for the possibility of an Eigen ion to form. In the 20 wt% system, the hydronium ion can be bound to more than three water molecules. One can visualize the four-fold coordination of the hydronium ion at 20 wt% in Figure 5.5(b). We have previously presented these histograms for water in bulk hydrated Nafion [33].

These PCFs and histograms have implications for proton transport. Proton conductivity occurs via both vehicular diffusion of the hydronium ion and structural diffusion described first by the Grotthuss mechanism [67], and more recently as a fluctuation between states known as Zundel ions ($H_5O_2^+$) and Eigen ions ($H_9O_4^+$): see, for example, Refs. [68-71]. Despite the fact

that we use a non-reactive potential, we can still obtain information relevant to the ability of hydronium ions to explore configurations in which they can participate in structural diffusion. The O_{H2O}-O_{H3O+} PCF shown in Figure 5.7 captures the degree of hydration of the hydronium ion. In bulk water, a hydronium ion must be hydrogen-bound to at least three water molecules in order to form an Eigen ion. In quantum mechanical simulations of polymer electrolyte fragments, it has been shown that an oxygen atom of an SO_3^- group at the end of the side chain can participate in structural diffusion by substituting for either one of the oxygen atoms in the Zundel ion or by forming one of the necessary hydrogen bonds in the Eigen ion [72]. Therefore, the hydration of the hydronium ion provides a description of the local environment important for structural diffusion. At the very minimum, hydronium ions that are hydrated by fewer than two water molecules are unlikely to form Eigen ions. Thus, in Figure 5.8, there is a significant decrease in the fraction of hydronium ions on the Pt surface that are in local environments where they can participate in structural diffusion at lower water contents.

5.3.2 Membrane/vapor/support Systems

Additional simulations were performed that contained the catalyst support surfaces, which we have modeled as graphite. In Figure 5.9 (a)-(b), we present snapshots of the final configuration of the membrane/vapor/support system for hydrated membranes with initial water contents of 5 and 20 wt% respectively. Again, we observe two surfaces because the simulations are periodic. Notably, there is no wetting of the surface at either water content. We observed no wetting of the graphite surface at 10 wt% and 15 wt% either (not shown here). The failure of water, Nafion, or hydronium ions to adsorb to the graphite surface can be attributed to the fact that the energetic attraction of a graphitic carbon atom is about 80 times weaker than a platinum atom ($\varepsilon_C / \varepsilon_{Pt} = 0.012$).

The density profile of water in the support system is shown in Figure 5.10. Again, the zero coordinate on the x-axis corresponds to the central location of the membrane/vapor interface. The variation of water density within the interface is a consequence of the fact that the nanostructured segregation of the hydrated membrane into hydrophobic and hydrophilic regions is not uniform on the nanoscale and relaxes on a time scale which is greater than the duration of

these simulations. As was the case with the catalyst surface, there is clearly a "dehydrated region" of the membrane near the interface. We observe virtually no adsorption of water on the support surface.

5.4 Implications and Conclusions

In this work we have studied the molecular-level structure of the electrode/electrolyte interface. We acknowledge that the detail of the electrode-electrolyte environment is a function of the manufacturing procedure, the composition of the MEA, and the operating conditions of the fuel cell. In this work, we have focused on model interfaces that we believe are present in a wide range of MEAs across a range of operating conditions. In this model, the pore contains water vapor.

Regardless of the structure, the catalyst particle must be able to participate in three transport processes: (i) diffusion of molecular hydrogen in a vapor phase to the catalyst surface, (ii) conduction of electrons to the electrode and (iii) diffusion/conduction of protons to the electrolyte membrane. Each of these three transport properties taken independently has an asymptotic optimal configuration associated with it. Because the diffusivity of a gas is orders of magnitude higher than that of a liquid (at room temperature and pressure, the self-diffusivity of H_2 is 5.6×10^{-1} cm^2/s [49] and the diffusivity of H_2 in water is 4.5×10^{-5} cm^2/s [50]), the optimal diffusion of molecular hydrogen would occur on a bare electrode (in which none of the surface is coated with thick layers of water or Nafion). The optimal conduction of electrons requires significant and direct contact between all catalyst particles and the conducting component of the electrode. The optimal conduction of protons requires that all catalyst particles have significant and direct contact with electrolyte in the membrane or leading to the membrane. This optimization procedure is constrained by the desire to minimize the amount of catalyst in the MEA.

The optimization of the performance of PEM fuel cells can benefit from atomic and molecular scale level understanding of the various reactive and transport processes occurred at the electrode/electrolyte interface in the system. We have shown that at higher water contents, the initially bare catalyst surface is likely to be covered by a monolayer which is a mixture of water, Nafion, and hydronium ions. At the anode, the gaseous hydrogen fuel must reach the

catalyst surface, penetrating this monolayer. Furthermore, once the electron and proton of the hydrogen atom have been dissociated, the ability of the proton to form a hydronium ion depends upon the availability of water bound to the catalyst surface. If the surface is dry (as much of it appears to be at low water content), then the relevant surface diffusion process is that of the proton. If the surface is wet, then the relevant surface diffusion process is that of the hydronium ion.

We showed that there is virtually no wetting of the support material (graphite in this work). This observation has implications for effective catalyst utilization. In Figure 5.1, we show two catalyst particles, one immediately adjacent to the polymer electrolyte membrane and one bound to the support but separated by some distance from the membrane. If there is no wetting of the support surface, then there can be no transport of protons (or hydronium ions) across this gap. Therefore, while catalyst particles may be able to adsorb gaseous molecular hydrogen and dissociate it into protons and electrons, if the protons cannot reach the polymer electrolyte membrane, then that catalyst particle cannot contribute to power generation and is ultimately useless. The likelihood of finding a catalyst particle in this state is again a function of the manufacturing process and composition of the MEA. We are currently performing MD simulations to study quantitatively the critical size of the gap between a catalyst particle and the polymer electrolyte membrane across which protons may travel, and the dependence of that critical size on water content.

In conclusion, we performed molecular dynamics simulations of the hydrated polymer electrolyte membrane/vapor/catalyst three-phase interface and the hydrated polymer electrolyte membrane/vapor/support three-phase interface, using Nafion, [100] platinum and graphite atoms. Characterization and analysis of the configurational and dynamic properties indicate that there is no wetting of the catalyst support surface (graphite in this work) and significant wetting of catalyst surface ([100] platinum in this work). The degree of wetting increases on the catalyst surface with the water content, but we do not observe more than a monolayer on the surface. This monolayer is composed of a mixture of water, Nafion, and hydronium ions. At high water contents, the water forms a regular lattice on the catalyst surface. We characterized the structure of water molecules and hydronium ions adsorbed to the catalyst surface by the pair correlation functions (PCFs).

There are two main implications of this work. First, fundamental work is required to study the adsorption and dissociation of molecular hydrogen on catalyst surface with adsorbed layers, such as those described herein. Furthermore, the overall diffusion of protons (including vehicular and structural diffusion) across this surface, as a function of water content, must be investigated at a fundamental level, if one is to quantitatively understand the molecular mechanisms for proton transport at the electrode/electrolyte interface. The second implication of this work is that, because the catalyst support shows no significant wetting, the catalyst particles must be in intimate contact with the hydrated membrane, or with recast hydrated polymer electrolyte membrane in the electrode that provides a pathway for protons to move from the catalyst surface into the bulk hydrated membrane. Work is currently underway to study the critical gap size across which protons can be transported.

5.5 Acknowledgment

The work is supported by a grant from the U. S. Department of Energy BES under the contract number DE-FG02-05ER15723. This research used resources of the Center for Computational Sciences at Oak Ridge National Laboratory, which is supported by the Office of Science of the DOE under Contract DE-AC05-00OR22725.

References

(1) A. Eisenberg, *Macromolecules*, **1970**. 3, 147-54.

(2) M. Falk, *Can. J. Chem.*, **1980**. 58, 1495-501.

(3) E. J. Roche, M. Pineri, R. Duplessix, and A. M. Levelut, *J. Polym. Sci. B: Polym. Phys.* , **1981**. 19, 1-11.

(4) T. D. Gierke, G. E. Munn, and F. C. Wilson, *J. Polymer Sci. B: Polym. Phys.*, **1981**. 19, 1687-704.

(5) H. L. Yeager and A. Steck, *J. Electrochem. Soc.*, **1981**. 128, 1880-4.

(6) M. Fujimura, T. Hashimoto, and H. Kawai, *Macromolecules*, **1981**. 14, 1309-15.

(7) E. J. Roche, M. Pineri, R. Duplessix, and A. M. Levelut, *J. Polym. Sci. B-Polym. Phys.*, **1981**. 19, 1-11.

(8) M. Fujimura, T. Hashimoto, and H. Kawai, *Macromolecules*, **1982**. 15, 136-44.

(9) W. Y. Hsu and T. D. Gierke, *J. Membr. Sci.*, **1983**. 13, 307-26.

(10) M. D. Heaney and J. Pellegrino, *J. Membr. Sci.*, **1989**. 47, 143-61.

(11) M. W. Verbrugge and R. F. Hill, *J. Electrochem. Soc.* , **1990**. 137, 886-93.

(12) Z. e. Porat, J. R. Fryer, M. Huxham, and I. Rubinstein, *J. Phys. Chem.*, **1995**. 99, 4667-71.

(13) A. Lehmani, S. Durand-Vidal, and P. Turq, *J. Appl. Polym. Sci.* , **1998**. 68, 503-508.

(14) G. Gebel, *Polymer*, **2000**. 41, 5829-5838.

(15) P. J. James, J. A. Elliott, T. J. McMaster, J. M. Newton, A. M. S. Elliott, S. Hanna, and M. J. Miles, *J. Mater. Sci.*, **2000**. 35, 5111-5119.

(16) P. J. James, T. J. McMaster, J. M. Newton, and M. J. Miles, *Polymer*, **2000**. 41, 4223-4231.

(17) J. A. Elliott, S. Hanna, A. M. S. Elliott, and G. E. Cooley, *Macromolecules*, **2000**. 33, 4161-4171.

(18) K. D. Kreuer, *J. Membr. Sci.*, **2001**. 185, 29-39.

(19) H.-G. Haubold, T. Vad, H. Jungbluth, and P. Hiller, *Electrochim. Acta* **2001**. 46, 559-1563.

(20) A.-L. Rollet, G. Gebel, J.-P. Simonin, and P. Turq, *J. Polymer Sci. B: Polym. Phys.*, **2001**. 39, 548-558.

(21) S. K. Young, S. F. Trevino, and N. C. Beck Tan, *J. Polymer Sci. B: Polym. Phys.*, **2002**. 40, 387-400.

(22) R. Jinnouchi and K. Okazaki, *J. Electrochem. Soc.*, **2003**. 150, E66-E73.

(23) E. Spohr, P. Commer, and A. A. Kornyshev, *J. Phys. Chem. B*, **2002**. 106, 10560-10569.

(24) T. Li, A. Wlaschin, and P. B. Balbuena, *Ind. Eng. Chem. Res.*, **2001**. 40, 4789-4800.

(25) X.-D. Din and E. E. Michaelides, *AIChE J.*, **1998**. 44, 35-47.

(26) M. Eikerling, A. A. Kornyshev, A. M. Kuznetsov, J. Ulstrup, and S. Walbran, *J. Phys. Chem. B* **2001**. 105, 3646-3662.

(27) S. J. Paddison and T. A. Zawodzinski, Jr., *Solid State Ionics*, **1998**. 113–115, 333-340.

(28) S. J. Paddison, L. R. Pratt, and T. A. Zawodzinski, Jr, *J. New Mater. Electrochem. Sys.*, **1999**. 2, 183-188.

(29) S. J. Paddison, R. Paul, and T. A. Zawodzinski, Jr, *J. Electrochem. Soc.*, **2000**. 147, 617-626.

(30) S. J. Paddison, R. Paul, and T. A. Zawodzinski, Jr, *J. Chem. Phys.*, **2001**. 115, 7753-7761.

(31) A. Vishnyakov and A. V. Neimark, *J. Phys. Chem. B*, **2000**. 104, 4471-4478.

(32) S. Urata, J. Irisawa, A. Takada, W. Shinoda, S. Tsuzuki, and M. Mikami, *J. Phys. Chem. B*, **2005**. 109, 4269-4278.

(33) S. Cui, J. Liu, M. Esai Selvan, D. J. Keffer, B. J. Edwards, and W. V. Steele, *J. Phys. Chem. B*, **2007**. 111, 2208-2218.

(34) H. Ogasawara, B. Brena, D. Nordlund, M. Nyberg, A. Pelmenschikov, L. G. M. Pettersson, and A. Nilsson, *Phys. Rev. Lett*, **2002**. 89, 276102.

(35) I. Benjamin, *Modern Aspects of Electrochemistry*, **1997**. 31, 115-179.

(36) J. Rossmeisl, J. K. Norskov, C. D. Taylor, M. J. Janik, and M. Neurock, *J. Phys. Chem. B*, **2006**. 110, 21833-21839.

(37) M. S. Wilson and S. Gottesfeld, *J. Appl. Electrochem.*, **1992**. 22, 1-7.

(38) K. Broka and P. Ekdunge, *J. Appl. Electrochem.*, **1997**. 27, 117.

(39) X. Cheng, B. Yi, M. Han, Z. J., Y. Qiao, and J. Yu, *J. Power Sources*, **1999**. 79, 75-81.

(40) E. Antolini, L. Giorgi, A. Pozio, and E. Passalacqua, *J. Power Sources*, **1999**. 77, 136-142.

(41) P. Gode, F. Jaouen, G. Lindbergh, A. Lundblad, and G. Sundholm, *Electrochem. Acta*, **2003**. 48, 4175-4187.

(42) E. J. Lamas and P. B. Balbuena, *Electrochim. Acta*, **2006**. 51, 5904-5911.

(43) A. Vishnyakov and A. V. Neimark, *J. Phys.Chem. B* **2001**. 105, 7830-7834.

(44) J. A. Elliott, S. Hanna, A. M. S. Elliott, and G. E. Cooley, *Phys. Chem. Chem. Phys.*, **1999**. 1, 4855-4863.

(45) S. S. Jang, V. Molinero, T. Cagin, and W. A. Goddard, III, *J. Phys. Chem. B*, **2004**. 108, 3149-3157.

(46) A. Venkatnathan, R. Devanathan, and M. Dupuis, *J. Phys. Chem. B*, **2007**. 111, 7234-7244.

(47) M. K. Petersen and G. A. Voth, *J. Phys. Chem. B*, **2006**. 110, 18594-18600.

(48) J. L. Myvizhi Esai Selvan, David J. Keffer, Shengting Cui, Brian J. Edwards, and William V. Steele., *Journal of Physical Chemistry B*, **2007**. submitted.

(49) R. B. Bird, W. E. Stewart, and E. N. Lightfoot, *Transport Phenomena*. Second ed. 2002, New York: John Wiley & Sons, Inc.

(50) D. R. Lide, *CRC Handbook of Chemistry and Physics*. 71 ed. 1990, Boca Raton, FL: Chemical Rubber Publishing Co.

(51) D. R. Morris and X. Sun, *J. Appl. Polym. Sci.*, **1993**. 50, 1445-1452.

(52) S. T. Cui, J. I. Siepmann, H. D. Cochran, and P. T. Cummings, *Fluid Phase Equilib.*, **1998**. 146, 51-61.

(53) W. R. Cannon, B. M. Pettitt, and J. A. McCammon, *J. Phys. Chem.*, **1994**. 98, 6225-30.

(54) W. L. Jorgensen, J. Chandrasekhar, J. D. Madura, R. W. Impey, and M. L. Klein, *J. Chem. Phys.*, **1983**. 79, 926-35.

(55) D. J. Price and C. L. Brooks, III, *J. Chem. Phys.*, **2004**. 121, 10096-10103.

(56) W. D. Cornell, P. Cieplak, C. I. Bayly, I. R. Gould, K. M. Merz, Jr, D. M. Ferguson, D. C. Spellmeyer, T. Fox, J. W. Caldwell, and P. A. Kollman, *J. Am. Chem. Soc.*, **1995**. 117, 5179-97.

(57) G.-W. Wu and K.-Y. Chan, *J. Electroanal. Chem.*, **1998**. 450, 225-231.

(58) S. Picaud, P. N. M. Hoang, S. Hamad, J. A. Mejias, and S. Lago, *J. Phys. Chem. B* **2004**. 108, 5410-5415.

(59) S. Y. Liem and K.-Y. Chan, *Surf. Sci.*, **1995**. 328, 119-28.

(60) S. J. A. Koh, H. P. Lee, C. Lu, and Q. H. Cheng, *Phys. Rev. B* **2005**. 72, 085414/1-085414/11.

(61) G. Hummer, D. M. Soumpasis, and M. Neumann, *Mol. Phys.*, **1992**. 77, 769-85.

(62) S. T. Cui and J. G. Harris, *Chem. Eng. Sci.*, **1994**. 49, 2749-63.

(63) W. G. Hoover, *Phys. Rev. A*, **1985**. 31, 1695-1697.

(64) S. Nose, *Mol. Phys.*, **1984**. 52, 255-68.

(65) S. Nose, *J. Chem. Phys.*, **1984**. 81, 511-19.

(66) M. Tuckerman, B. J. Berne, and G. J. Martyna, *J. Chem. Phys.*, **1992**. 97, 1990-2001.

(67) C. J. T. de Grotthuss, *Ann. Chim. (Paris)*, **1806**. 58, 54-73.

(68) M. Tuckerman, K. Laasonen, M. Sprik, and M. Parrinello, *J. Chem. Phys.*, **1995**. 103, 150-61.

(69) M. E. Tuckerman, D. Marx, M. L. Klein, and M. Parrinello, *Science (Washington, D. C.)*, **1997**. 275, 817-820.

(70) D. Marx, M. E. Tuckerman, and M. Parrinello, *J. Phys.* , **2000**. 12, A153-A159.

(71) N. Agmon, *Chem. Phys. Lett.*, **1995**. 244, 456-62.

(72) S. J. Paddison and J. A. Elliott, *J. Phys. Chem. A*, **2005**. 109, 7583-7593.

Appendix D

Table 5. 1 Size of the three dimensions of the simulation cell for graphite/platinum systems. All units are in Angstroms.

	graphite			Platinum		
water content	*x*	*y*	*z*	*x*	*y*	*z*
5 wt%	115.02	136.10	103.32	113.59	129.82	109.68
10 wt%	119.28	123.09	118.08	117.51	125.55	117.51
15 wt%	119.28	133.70	118.08	121.43	131.97	117.51
20 wt%	123.54	139.35	118.08	125.34	129.38	125.34

Table 5. 2 Summary of the simulation conditions.

	5 wt%	10 wt%	15 wt%	20 wt%
no. of polymers	256	256	256	256
no. of water molecules	2640	4160	6624	9088
no. of hydronium ions	768	768	768	768
total no. of particles	31728	36288	43680	51072
λ (H_2O/SO_3^-)	3.44	5.42	8.63	11.83
simulation time (ns)	4.0	4.0	4.0	4.0
no. of graphite atoms	3024	3584	3584	3712
no. of Pt atoms	4872	5400	5580	6144

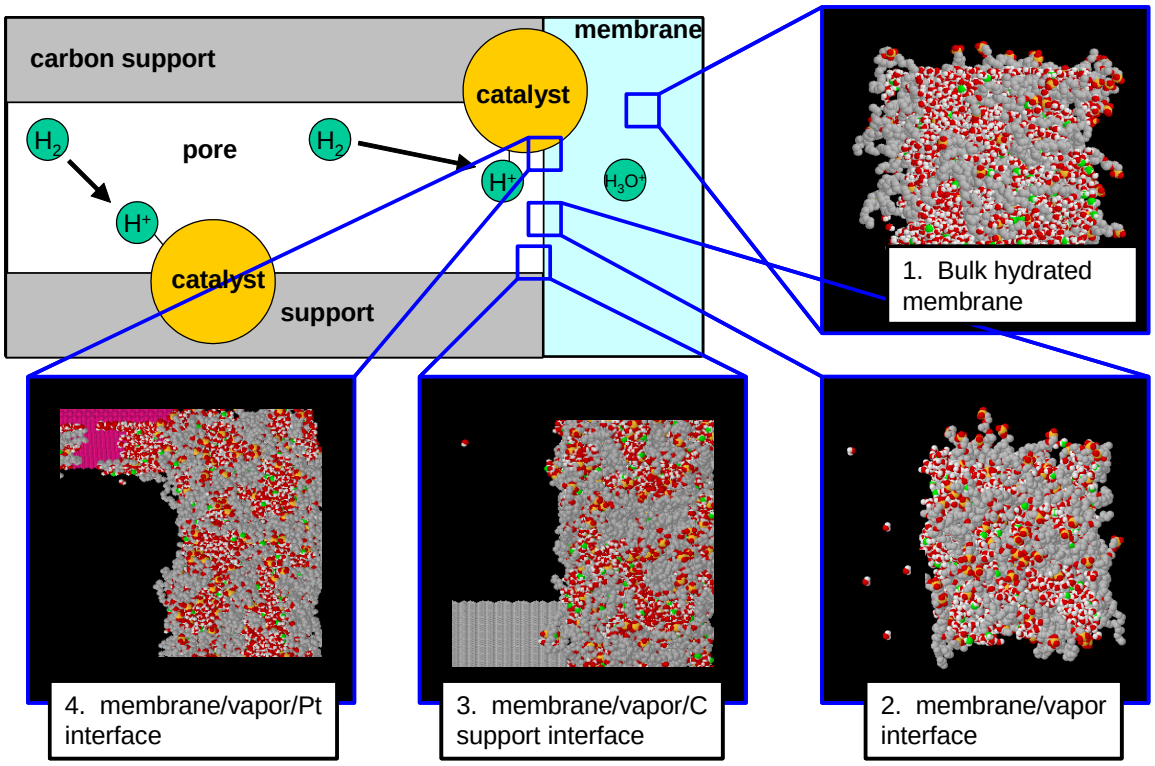

Figure 5. 1 A schematic of the molecular-level interfaces present at the electrode/electrolyte interface of the anode of a PEM fuel cell.

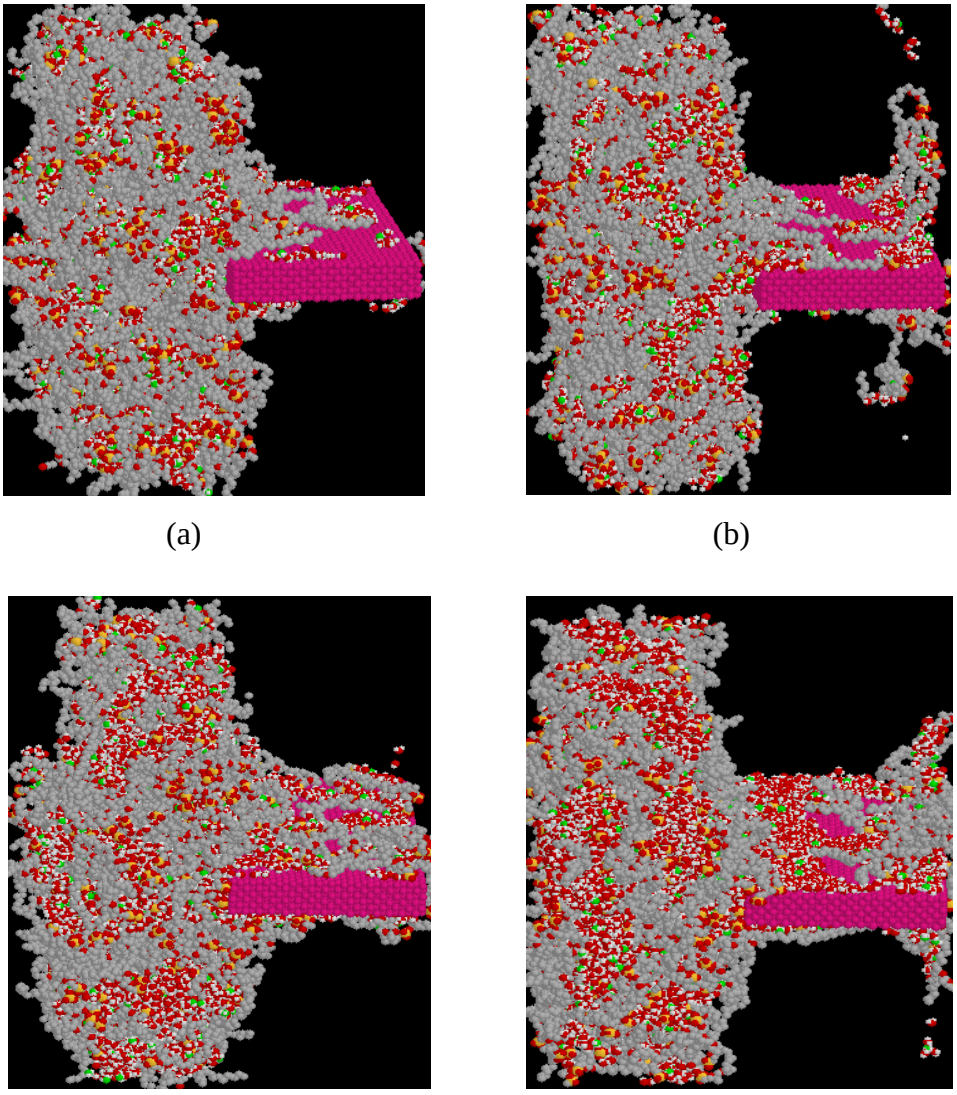

Figure 5. 2 Final snapshots of simulations containing the catalyst surface for water contents of (a) 5 wt%, (b) 10 wt%, (c) 15 wt%, and (d) 20 wt%. The coloring legend is as follows: CF_x groups are gray; sulfur, orange; oxygen of H_2O and SO_3^-, red; oxygen of H_3O^+, green; hydrogen, white; and platinum, pink.

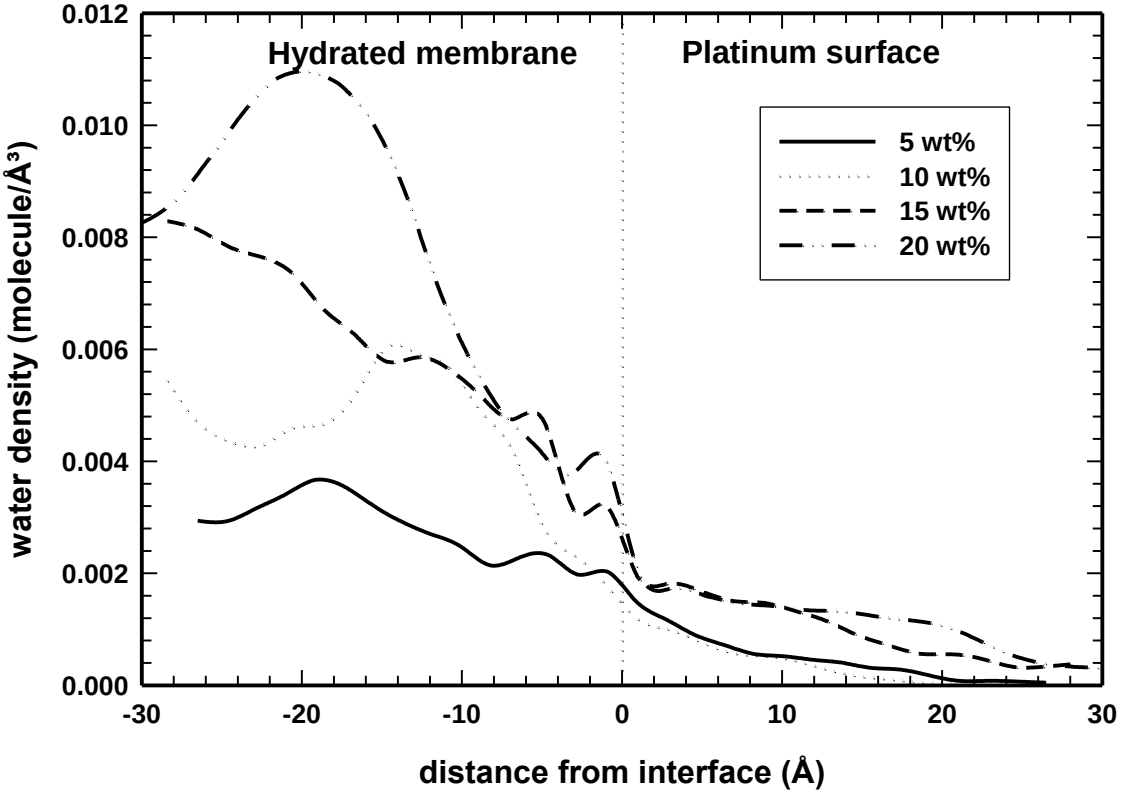

Figure 5. 3 Density profile of water molecules along the z-direction in the simulation cell for the catalyst system.

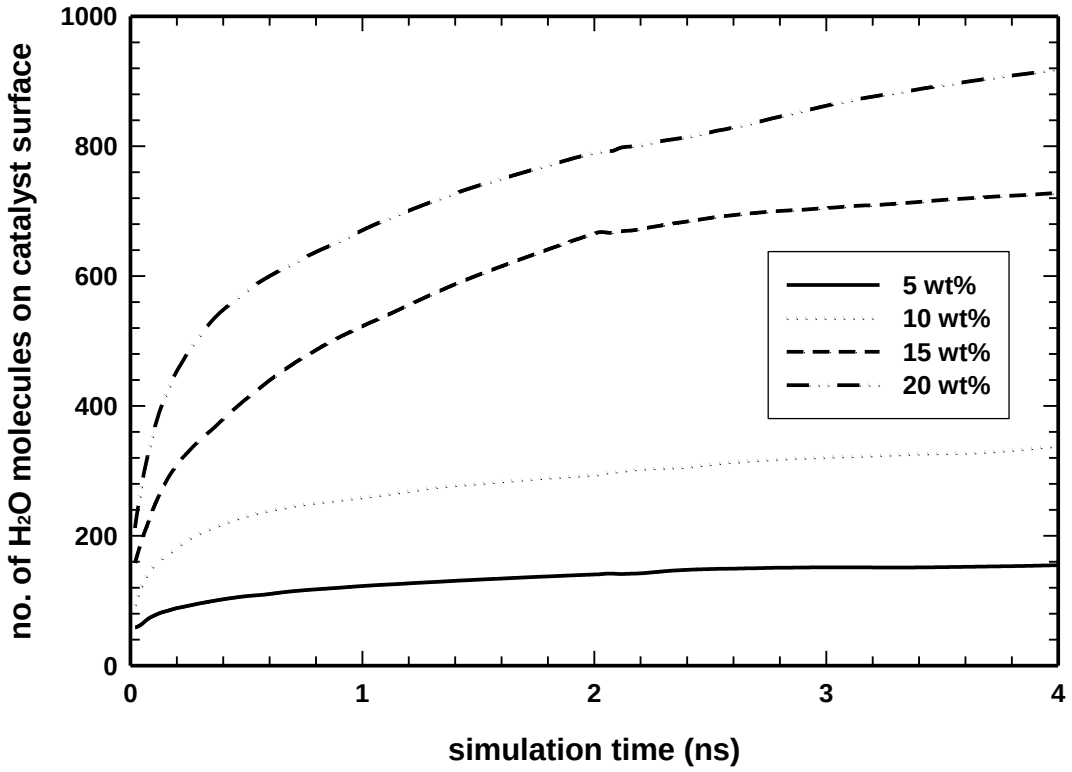

Figure 5. 4 Wetting of the catalyst surface: number of water molecules on the catalyst surface as a function of time.

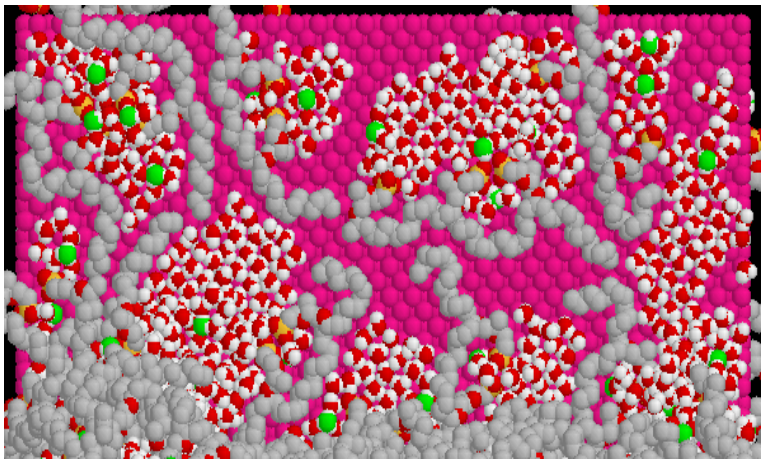

(a)

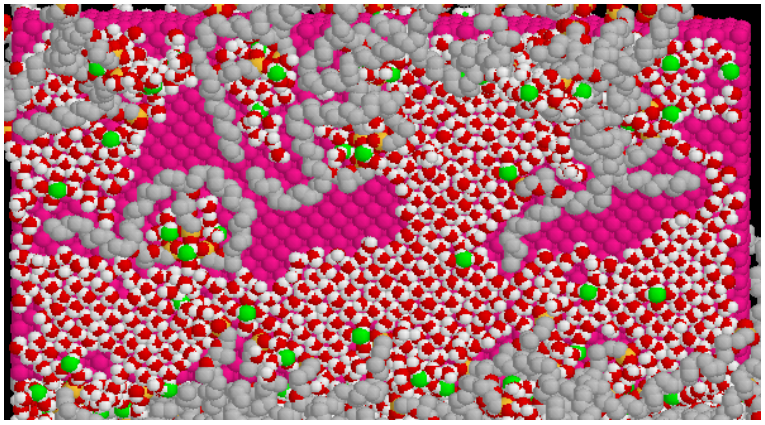

(b)

Figure 5. 5 Final snapshot normal to the surface of simulations containing the catalyst for water contents of (a) 15 wt% and (b) 20 wt%. The coloring legend is the same as Figure 4.2.

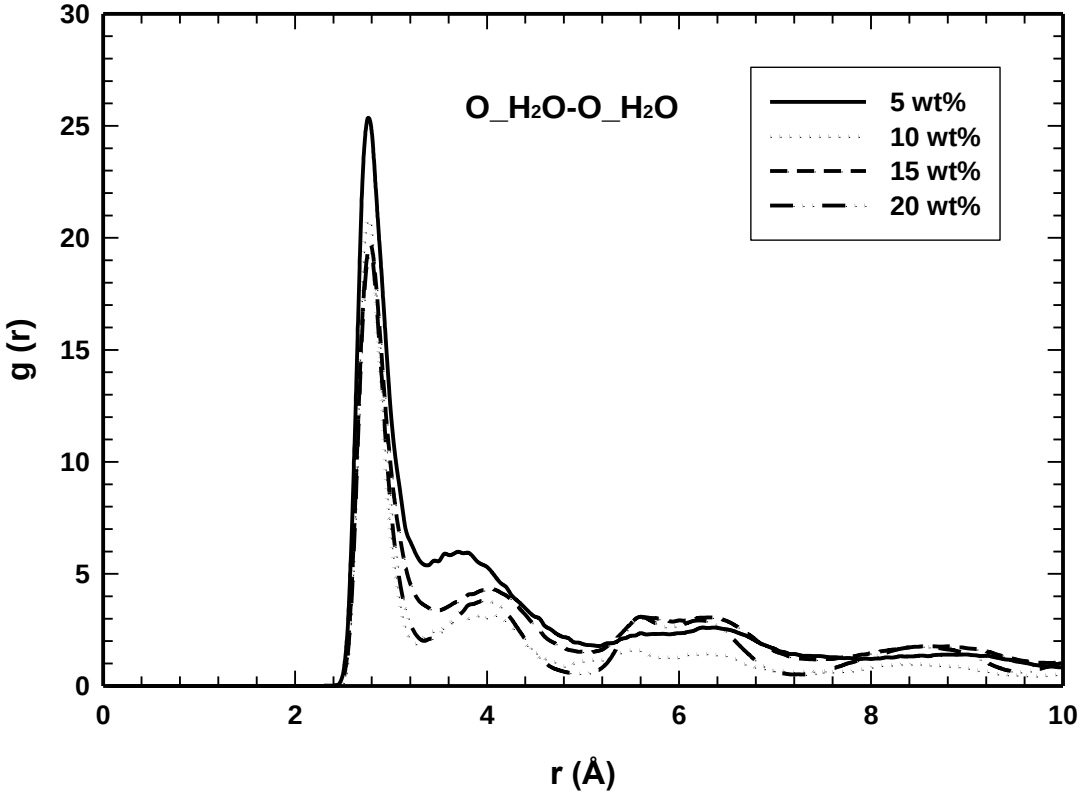

Figure 5. 6 The pair correlation function for the oxygen atom of a water molecule with other oxygen atoms of water molecules (the O_{H2O}-O_{H2O} PCF) in the adsorbed region next to the catalyst surface as a function of water content.

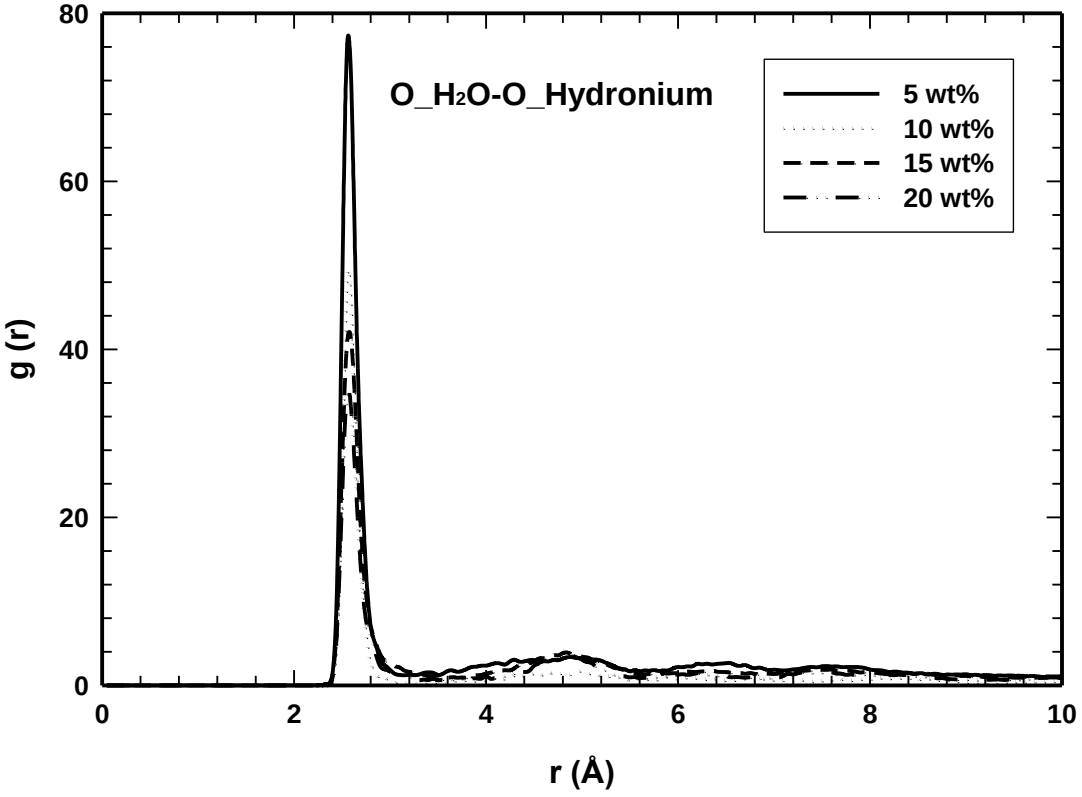

Figure 5. 7 The pair correlation function for the oxygen atoms of water with oxygen atoms of hydronium ions (the O_{H2O}-O_{H3O+} PCF) in the adsorbed region next to the catalyst surface as a function of water content.

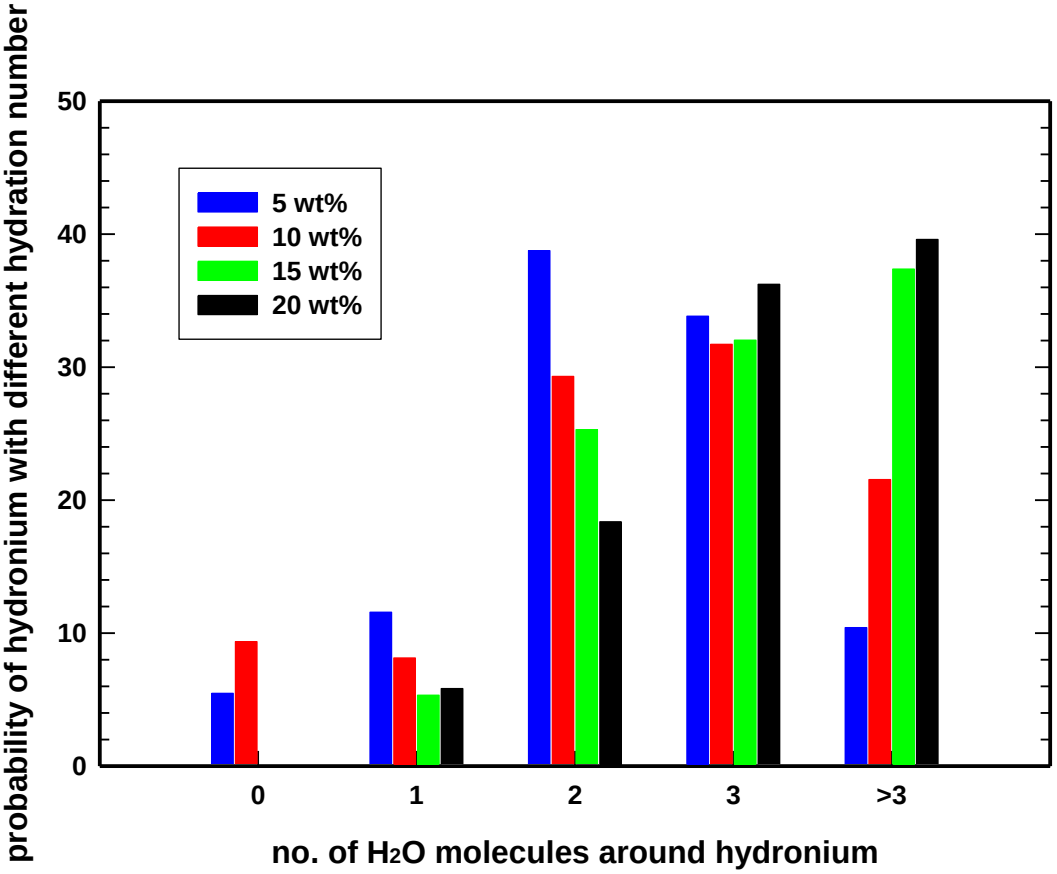

Figure 5. 8 Distribution of water molecules around hydronium ions for all four water contents studied.

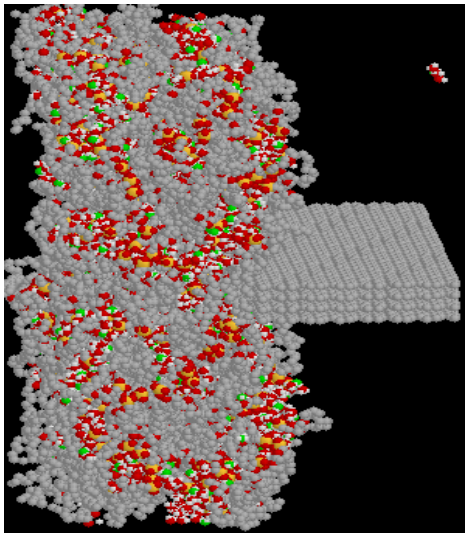

(a)

(b)

Figure 5. 9 Final snapshots of simulations containing the catalyst surface for water contents of (a) 5 wt% and (b) 20 wt%. The coloring legend is the same as Figure 4.2, with the addition that graphitic carbon is gray.

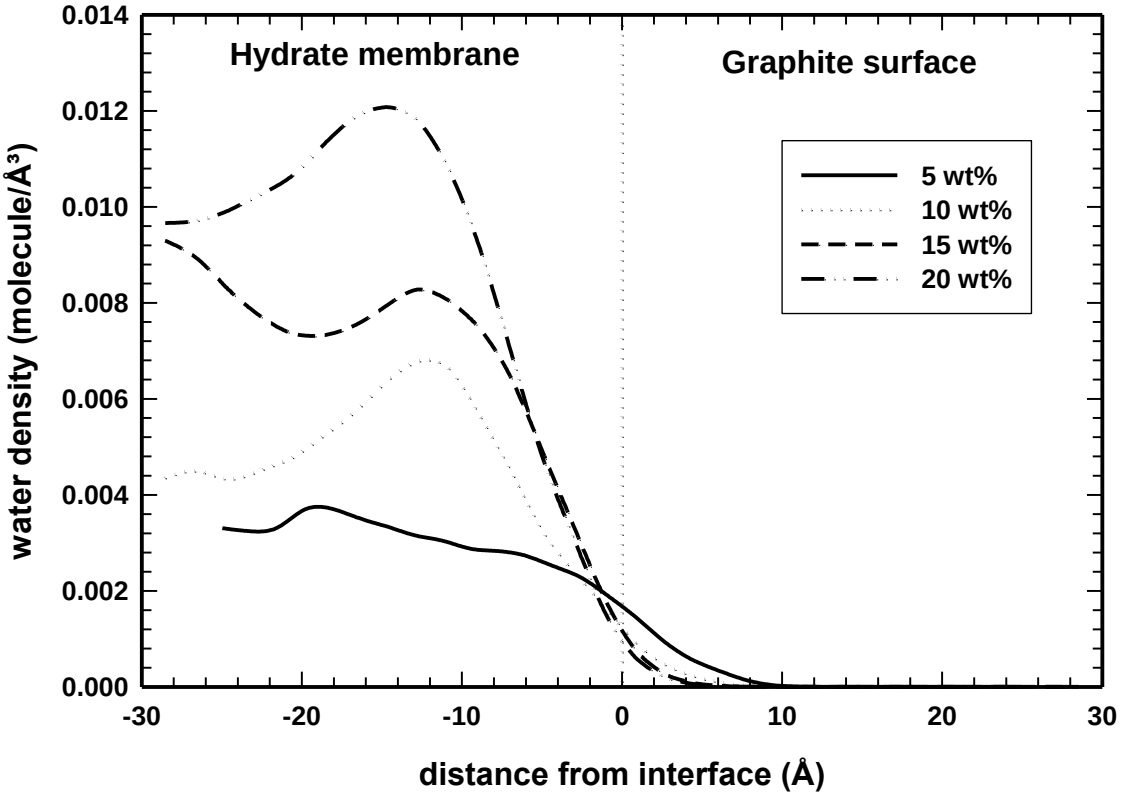

Figure 5. 10 Density profile of water molecules along z-direction in the simulation cell for the catalyst support system.

Chapter 6

Molecular-level investigation of critical gap size between catalyst particles and electrolyte in hydrogen proton exchange membrane fuel cells

This part is a slightly revised version of a paper by the same title published in the *Fuel Cells* in 2008 by Junwu Liu, Shenting Cui, and David Keffer:

J.W. Liu, C.T. Cui, and D.J. Keffer, "Molecular-level investigation of critical gap size between catalyst particles and electrolyte in hydrogen proton exchange membrane fuel cells", *Fuel cells*, 8(6), 2008, 422-428.

The use of "we" in this part refers to the co-authors and the author of this dissertation. My primary contributions to this paper include (1) implementation of the simulation methodology, (3) all of the simulation work and analysis, (4) most of the writing.

Abstract

Molecular dynamics simulations have been performed to study the structure and transport at the electrode/electrolyte interface in hydrogen-based proton exchange membrane fuel cells. We examine the wetting of catalyst surfaces that are not immediately adjacent to a Nafion membrane, but rather are separated from the membrane by a hydrophobic gap of carbon support surface (graphite). A mixture of Nafion, water, and hydronium ions are able to wet small gaps (7.4 Å) of graphite and reach the catalyst surface, providing a path for proton transport from the catalyst to the membrane. However, for gaps of 14.8 Å, we observe no wetting of the graphite or the catalyst surface. Using a coarse-grained model, we found that the presence of a graphite gap of width 7.4 Å slowed down the transport of water by at least an order of magnitude relative to a system with no gap. The implication is that catalyst particles that are not within nominally 1 nm of either the proton exchange membrane or recast ionomer in the electrode leading to the membrane do not possess a path for efficient proton transport to the membrane and consequently do not contribute significantly to power production in the fuel cell.

6.1 Introduction

There is ongoing interest in reducing the amount of catalyst in hydrogen-based proton exchange membrane (PEM) fuel cells, in order to reduce the overall cost of the device. To this

end, numerous efforts have been made to manufacture membrane electrode assemblies (MEAs) that optimise the fraction of catalyst in the system that participates in power generation. The underlying concept in this optimisation is based on the fact that, at the anode, the catalyst must participate in three transport processes: (i) molecular hydrogen must diffuse to the catalyst surface, (ii) electrons must be conducted from the catalyst to the electrode and (iii) protons must be transported to the PEM. Any catalyst particle that does not participate in all three of these transport processes cannot contribute to power generation and is wasted catalyst. The introduction of recast ionomer in the electrode results in a significantly higher fraction of utilised catalyst by creating paths for the protons to be transported from the catalyst surface to the PEM; see for example Ref. [1-4]. Thus, the protons generated from the dissociation of molecular hydrogen on the catalyst surface in the anode can be transported along the recast ionomer to the membrane, assuming that there is a continuous pathway. One parameter that is naturally of interest is the critical size of the gap in this pathway that is sufficient to disrupt proton transport.

The nanoscale structure of the electrode/electrolyte interface is a function of the manufacturing process, including the amount of recast Nafion used in the electrode and the manner in which the catalyst particles are deposited. In Figure 6.1, we present a schematic of the model interface that is used as a basis for the molecular dynamics simulations reported herein. The schematic shows a small portion of the porous electrode. In this graphic, molecular hydrogen diffuses in the gas phase through a pore in the midst of the carbon support. Catalyst particles are distributed on the surface of the carbon support, and the pore is in contact with the polymer electrolyte membrane. The specific geometry of this highly idealised schematic is not essential; however, the schematic illustrates the specific molecular-level interfaces that are of interest at the bulk electrode/electrolyte interface. Specifically for this work, two systems are isolated. The first is a system in which there is an interface between the hydrated PEM, the catalyst surface and the gas-phase of the gas-filled pore. In this first system, the catalyst is immediately adjacent to the hydrated membrane. In the second system, the catalyst is separated from the hydrated membrane by a gap of carbon support. The purpose of this work is to study the impact a gap of this sort has on transport at the electrode/electrolyte interface.

In order to quantitatively analyse the critical gap size, we performed molecular dynamics simulations to model the wetting of catalyst surfaces that are not immediately adjacent to a

Nafion membrane, but rather are separated from the membrane by a gap of carbon support surface. This modeling work is a continuation of a molecular dynamics study that has investigated the structure and transport properties in hydrated Nafion [5], at the interface between Nafion and a water vapour [6], at the three-phase interface between Nafion, water vapour and a catalyst surface (modelled as [100] Pt) [7], and at the three-phase interface between Nafion, water vapour and a carbon support surface (modelled as graphite) [7]. In the previous work, the catalyst surface or the support surface was immediately adjacent to a nominally planar hydrated Nafion surface. The results of the simulations indicate that via surface diffusion a mixture of Nafion, water and hydronium ions wet the catalyst surface immediately adjacent to the Nafion membrane for all water contents studied (5, 10, 15 and 20 wt.-% water). These weight percents correspond to ratios of H_2O/SO_3H of 4.44, 6.42, 9.63 and 12.83, respectively. For the simulations of the graphite interface with Nafion, there was essentially no wetting at any water content.

In this work, in order to maintain consistency with the previous work, we model gaps between the catalyst and the hydrated polymer electrolyte using a [100] Pt surface separated from the membrane by a graphite surface, as shown in Figure 6.1. The purpose of this work is to examine the ability of the Nafion, water and hydronium ions mixture to bridge this gap and consequently provide a path for proton transport from the catalyst surface into the membrane.

Furthermore, we study quantitatively the critical size of the gap between catalyst particles and the polymer electrolyte membrane across which protons may travel, and the dependence of that critical size on water content. We present the results of MD simulations of hydrated Nafion at two different water contents: 5 and 20% water by weight.

The interface between the support surface, catalyst surface and hydrated PEM has not received a great deal of attention from molecular-level modellers. However, there are two molecular dynamics studies [8, 9] in which this interface has been previously modelled. These previous studies have focused on one to three Pt nanoclusters dispersed on carbon support in the presence of water and Nafion oligomers at three water contents corresponding to ratios of H_2O/SO_3H of 5, 24 and 45. At the low water content, they see virtually no connectivity of wet paths between particles. At the two very high water contents, which are well beyond the operating conditions for fuel cells, they observe wetting of the graphite phase and high

connectivity between clusters. Moreover, Goddard et al. [10] use the first-principles based reactive ReaxFF force field to describe the catalytic reactions at the electrodes and the electrochemical processes occurred at electrode/electrolyte interfaces in an attempt to determine the fundamental processes to optimise the fuel cell system performance upon changes in the design. They use finite Pt atom clusters to investigate the dynamic and structural properties of each possible intermediate involved in the electrode reactions and also establish atomistic structural models to understand how the protons are transferred across the membrane–cathode interface, especially, how this is affected by the distribution of water at this interface. This current work differs from the previous work in that it (i) focuses on transport between the catalyst and PEM, (ii) systematically examines the effect of gap size and (iii) maps the results onto a coarse-grained model resulting in a quantitative description of the effects of gap size on diffusivity.

6.2 Computational Details

Canonical ensemble MD simulations were carried out for 5 and 20 wt.-% water content membrane at 300 K in this work. The model of Nafion, water and the hydronium ions used in this work is identical to that of our previous work to model hydrated Nafion [5-7]. The CF_3, CF_2 and CF in Nafion are modelled as united atoms to reduce computational costs. The Nafion has the following intramolecular interactions: bond-stretching, bond-bending, dihedral torsion and non-bonded interactions via a Lennard–Jones potential and Coulombic interactions, with potential parameters taken from Ref. [5, 11]. We model the protonated form of Nafion, in which protons are the charge-balancing cations. In this model, the protons are incorporated into hydronium ions. The number of hydronium ions is exactly equal to the number of sulphonic acid groups, resulting in a charge-neutral system.

The TIP3P model [12, 13] with a flexible OH bond [14] was applied for water. The model for hydronium ions, H_3O^+, is similar to that of Urata et al. [15]. Force constants of O–H bonding and H–O–H bonding are the same as in the TIP3P model [12-14]. We should point out that the potential used for the hydronium ion is a non-reactive model. It is well known that in bulk water proton transport occurs through a combination of structural diffusion, i.e. proton hopping via the Grotthuss mechanism [16, 17], and vehicular diffusion of the hydronium ion. In our model, we

capture only the vehicular component of proton diffusion. This approximation in the model does not have a strong impact on the results drawn from these simulations because we are examining the existence of paths for transport. If the path does not exist, then neither structural nor vehicular diffusion can occur.

For all interactions, the LJ parameters for cross components were calculated using Lorentz–Berthelot mixing rules. The backbone was treated as neutral, except for the site to which the side chain is connected through the ether oxygen. The site–site reaction field was applied for the calculation of the electrostatic interactions [18, 19]. Partial charges for united atom groups were calculated from the summations of the constituent atom values.

We modelled the hydrophobic portion of the surface between the hydrated membrane and the catalyst particles as graphite, four atomic layers deep, in which the carbon atoms are held rigid and interact with all dynamic atoms in the system through the LJ potential with parameters σ_C = 3.4 Å and ε_C/k = 28.0 K [20]. The positions of the graphite atoms are taken from the literature [21]. We modelled the surface of the catalyst phase as [100] platinum, six atomic layers deep, in which the atoms are held rigid and interact with all dynamic atoms in the system through the Lennard–Jones potential with parameters σ_{Pt} = 2.41 Å and ε_{Pt}/k = 2,336.0 K [22]. The positions of the Pt atoms are taken from the literature [23].

The dimensions of the solid surface of the catalyst particles in the *z*-direction are nominally 60 Å. The dimensions of the graphite surface between the hydrated membrane and the catalyst surface change according to the unit number of the graphite surface along the *z*-direction. One unit corresponds to a gap of 7.4 Å and two units correspond to 14.8 Å. The dimensions of the whole simulation cells change to accommodate the integer numbers of unit cell dimensions of the catalyst and graphite surface. The number of each type of molecule used in the simulation is provided in Table 6.1. The amount of the hydrated membrane material used in this work is the same as that of our previous three-phase interfacial system [7]. The dimensions of each system are provided in Table 6.2.

The initial conditions of the systems took an equilibrated configuration of Nafion/vapour/graphite surface from the previous work [7] and replaced the graphite carbon atoms with the combination of graphite atoms and catalyst particles, with the same unit cell of

graphite on each side of Pt surface. With the new solid surface in place, we allow the full system to equilibrate. The water redistributes between the vapour, hydrated PEM and solid surface. The Nafion and the hydronium ions do not enter the vapour phase and therefore can wet the surface strictly via surface diffusion. The simulations were run for 2 ns.

We employed the Nosé–Hoover thermostat [24-26] to control temperature. The r-RESPA method [27] was carried out to integrate the equations of motion with 2 fs for the large time step size (including all intermolecular interactions) and 0.2 fs for the intramolecular motions.

6.3 Results and Discussion

6.3.1 Critical Gap Size

For both water contents, MD simulations were conducted with one unit cell of graphite (7.4 Å) and with two unit cells of graphite (14.8 Å) between the hydrated membrane and the catalyst surface.

Snapshots of final configurations obtained from MD simulations provide direct visual inspection of the structure and dynamics of water molecules and hydronium ions. In Figures 6.2a–d, we present the snapshots of configurations for hydrated membranes with nominal water contents of 5 and 20 wt.-%. For each water content, we show a snapshot for each graphite gap size. There are two solid surfaces visible because the simulations are periodic. However, the size of the system has been chosen to be large enough so that there were no artificial effects associated with the periodicity.

Figure 6.2a shows that for a membrane at 5 wt.-% water, a mixture of Nafion, water and hydronium ions is capable of traversing across the hydrophobic graphite gap and wetting the catalyst surface. This mixture provides a bridge between the membrane and the catalyst particles. This is important because, it has previously been observed that there was no wetting of a graphite surface [7]. Therefore, when molecular hydrogen is dissociated on the catalyst surface, it can form a hydronium ion with water on the surface and diffuse into the membrane across this bridge.

Figure 6.2b shows that for a membrane at 20 wt.-% water, a mixture of Nafion, water and hydronium ions is again capable of traversing across the graphite gap and wetting the catalyst surface. Moreover, there is substantially more material bridging the graphite gap than was observed at the lower water content. In the absence of a graphite gap, we have previously observed that membranes with higher water content will wet the catalyst surface more quickly and to a greater extent than membranes with lower water content [7]. Here we observe the same trend in the presence of the graphite gap.

We next discuss snapshots with a larger graphite gap, 14.8 Å, separating the membrane and the catalyst. Figure 6.2c shows that for a membrane at 5 wt.-% water, there is no wetting of the catalyst surface separated by the larger gap. Of course, this simulation is limited to the nanosecond range. However, in the previous simulations (Figures 6.2a and b) as well as the previous gap-free simulations [7], wetting occurred on the ns time scale. It is true that water, which is able to enter the vapour phase, has potentially two paths to reach the catalyst surface: surface diffusion across the graphite and diffusion through the vapour phase. The accumulation of water on the catalyst surface via vapourphase diffusion is much slower since the density of water in the vapour phase is very low, relative to the membrane. We acknowledge that at much longer time, when thermodynamic equilibrium is reached, there will be a distribution of water between the membrane, vapour and catalyst surface. However, the Nafion and the hydronium ions do not enter the vapour phase. Their path to the catalyst is via surface diffusion. In this simulation, we observe no wetting of the catalyst surface by Nafion and the hydronium ions. Therefore, it appears that, for a membrane at 5 wt.-% water, a graphite gap as small as 14.8 Å is sufficient to block proton transport from the catalyst to the membrane.

Since membranes with higher water contents wet more readily, it is of interest to know if the critical gap size is a function of water content in the membrane. To this end, Figure 6.2d shows that for a membrane at 20 wt.-% water, there is no wetting of the catalyst surface separated from the membrane by a graphite gap of 14.8 Å. Therefore, at least across the range of water contents studied here, we do not observe a dependence of the critical gap size on water content.

In these systems, the non-bonded interaction was truncated at 10 Å. In order to dispel the possibility that the critical gap size was a function of the cut-off distance used in the potential,

we performed additional, independent simulations with a larger cut-off radius. Specifically, we chose a cut-off distance of 20 Å, so that there was a non-zero interaction between the atoms in the catalyst surface and those in the membrane across even the larger graphite gap of 14.8 Å. We repeated these simulations at both water contents and reproduced the results using the larger cut-off distance. Therefore, we believe that there is no simulation artifact in the critical gap size resulting from a finite cut-off distance in the interaction potential.

6.3.2 Wetting Dynamics

For the systems with the smaller graphite gap size, we can quantitatively analyse the dynamics of wetting of the solid surface. In Figure 6.3a, we plot the number of water molecules on the solid surface as a function of time for both water contents. In Figure 6.3b, we similarly plot the number of hydronium ions on the solid surface as a function of time for both water contents. In Figure 6.3c, we plot together the wetting dynamics of water on the solid surface with no gap and with a gap of 7.4 Å. A molecule is defined to be 'on the solid surface' if it resides within the distance of 10 Å over the solid surface. The vast majority of molecules on the surface are immediately adjacent to the surface atoms. The time scale in Figure 6.3 extends to 2 ns. These wetting curves for the two water contents have a significant slope, which means the wetting behaviour will continue if we conduct the simulations for a longer time. However, in the 2 ns time scale, we are certainly able to distinguish whether wetting occurs.

In Figures 6.3a and b, we see the wetting curves are relatively linear in time. At long times, the curves should reach a plateau, when an equilibrium covering of the surface was reached. The degree of wetting by water molecules is higher for the 20 wt.-% water system than it is for the 5 wt.-% system. The same trend is observed for the hydronium ion; more wetting at higher water contents.

In Figure 6.3c, we observe that wetting is significantly slowed in the presence of even this small gap. In the absence of a gap, because of the strong energetic interaction between the catalyst surface and the dynamic particles in the system, the portions of hydrated membrane quickly diffuse across the surface. When the gap is present, the formation of bridges across the graphite gap takes some time to be established and results in a lower transport rate.

In order to quantify the magnitude of the change in the transport rate, we can apply an approximate coarse-grained model and extract an effective diffusivity. If we make the assumption that the transport is purely diffusive, then the partial differential equation describing the temporal and spatial (*z*-axis only) dependence of the water density is given by a material balance including only accumulation and diffusion terms.

$$\frac{\partial \rho_{H_2O}}{\partial t} = D_{eff} \frac{\partial^2 \rho_{H_2O}}{\partial z^2} \tag{1}$$

subject to an initial condition, which states that the initial density in the membrane is a known constant, , and the initial water density on the surface is zero,

$$\rho_{H_2O}(z, t_o) = \begin{cases} \rho_o & for -a \le z \le a \\ 0 & otherwise \end{cases} \tag{2}$$

where *a* is the half-width of the membrane, and subject to the boundary conditions, which state that the density of water infinitely far from the membrane is always zero,

$$\rho_{H_2O}(z \to \infty, t) = \rho_{H_2O}(z \to -\infty, t) = 0 \tag{3}$$

The solution to this partial differential equation is known analytically [28]

$$\rho_{H_2O}(z, t) = \frac{1}{2}\rho_o \left\{ erf\left(\frac{a - z}{2\sqrt{D_{eff} t}} \right) + erf\left(\frac{a + z}{2\sqrt{D_{eff} t}} \right) \right\} \tag{4}$$

In Figure 6.3, we have plotted the number of water molecules on the surface as a function of t. If we assume in our coarse-grained model that any water that has left the bounds of the membrane is on the surface, then from a mass balance, the number of water on the surface at any time *t* is given by a mass balance

$$N_{H_2O}^{surface}(t) = N_{H_2O}^{total} - N_{H_2O}^{membrane} = N_{H_2O}^{total} - \frac{V_{membrane}}{m_{H_2O}} \int_{-a}^{a} \rho_{H_2O}(z, t)\, dz \tag{5}$$

where $V_{membrane}$ is the volume of the hydrated membrane and m_{H_2O} is the mass of a water molecule. Equation (5) can be directly compared to the data in Figure 6.2. We then performed a single variable nonlinear optimization to determine the value of the effective diffusivity, D_{eff}, that produced the minimum root-mean-square between the simulation data and the model. The results are presented in Table 6.3 and Figure 6.3(d).

This model is, of course, approximate and assumes, among other things, a constant effective diffusivity. The assumption of a constant diffusivity is not necessarily valid since the diffusivity of the water within the membrane is almost certainly different from the diffusivity of water on the surface. The model also assumes that all motion is diffusive and specifically, that there is no convection across the surface. This assumption is likely not valid, as indicated by the high value of diffusivities obtained from the model. One could potentially introduce a three parameter model that had a wetting velocity, a membrane diffusivity and an effective diffusivity, which we have not done. Instead, we have chosen to retain a single-parameter model to capture the essence of the effect of water content and gap. We present the effective diffusivities in dimensionless form, relative to the system with 5 wt% water initially in the membrane and with no gap. We feel that these ratios of effective diffusivities provide a useful measure of transport as a function of water content and presence of gap. We have also applied this procedure to the effective vehicular diffusivity of the hydronium ion.

In Table 6.3, by comparing the effective diffusivities of water in the absence of a gap, we see that the effective diffusivity increases with degree of hydration. By comparing the systems with and without gap, we see that the presence of the gap slows water transport by at least an order of magnitude from a system where the membrane is in direct contact with the catalyst. Interestingly, we see that the effect of the gap on the effective diffusivity of water is greater for the system with increased hydration.

The relative effective diffusivity of the hydronium ion compared to that of water in the presence of the gap is curious. In Figure 6.3, we observe a greater degree of wetting by hydronium ions at higher water content. In Table 6.3, we find that the higher water content does indeed have a higher effective diffusivity of the hydronium ion.

6.4 Conclusions

Molecular dynamics simulations were performed to investigate the effect of a graphite gap between the hydrated membrane and catalyst particles on the ability to form paths by which protons can be transported from the catalyst to the membrane. At membrane water contents of 5 and 20 wt.-%, we found that a mixture of Nafion, water and hydronium ions was able to form a bridge across a graphite gap of 7.4 Å width and wet the catalyst surface. The degree of wetting

increased with water content. For a gap size of 14.8 Å, we found no wetting of the catalyst surface for both water contents studied. We explicitly verified that the results are independent of potential cut-off distance. Therefore, we report the critical gap size to be on the order of 10 Å.

Using a coarse-grained model to generate an effective diffusivity, we found that the presence of a graphite gap of 7.4 Å width slowed down the transport of water from the membrane to the surface by at least an order of magnitude relative to a system with no gap. We also found that the transport of hydronium ions across the gap increased with water content.

While these simulations examine the ability of a mixture of Nafion, water and hydronium ions to bridge the graphite gap and wet the catalyst surface, the results have a direct impact on the ability to transport protons from the catalyst to the membrane. When molecular hydrogen adsorbs on the catalyst surface and dissociates into electrons and protons, the protons must find a path to the membrane. The purpose of adding ionomer in the electrode is to provide such a path. In these simulations, the wetting across the graphite gap is forming bridges. These bridges are the paths for proton transport. If there is no bridge, there is no path for proton transport and the catalyst particle is not utilized in the power generation of the fuel cell.

The practical implication of this work is directed towards the optimisation of catalyst in the fuel cell. In order for catalyst particles to contribute to power generation, they must be within nominally 10 Å of the membrane or recast ionomerproviding a path to the membrane.

6.5 Acknowledgement

The work is supported by a grant from the U. S. Department of Energy BES under the contract number DE-FG02-05ER15723. Through the University of Tennessee Computational Science Initiative, this research used resources of the Center for Computational Sciences at Oak Ridge National Laboratory, which is supported by the Office of Science of the DOE under Contract DE-AC05-00OR22725.

References

(1) P. Gode, F. Jaouen, G. Lindbergh, A. Lundblad, and G. Sundholm, *Electrochem. Acta*, **2003**. 48, 4175-4187.

(2) E. Antolini, L. Giorgi, A. Pozio, and E. Passalacqua, *J. Power Sources*, **1999**. 77, 136-142.

(3) K. Broka and P. Ekdunge, *J. App. Electrochem.*, **1997**. 27, 117-123.

(4) M. S. Wilson and S. Gottesfeld, *J. App. Electrochem.*, **1992**. 22, 1-7.

(5) S. Cui, J. Liu, M. Esai Selvan, D. J. Keffer, B. J. Edwards, and W. V. Steele, *J. Phys. Chem. B*, **2007**. 111, 2208-2218.

(6) M. Esai Selvan, J. W. Liu, D. J. Keffer, S. T. Cui, B. J. Edwards, and W. V. Steele, *J. Phys. Chem. C*, **2008**. 112, 1975-1984.

(7) J. W. Liu, M. Esai Selvan, S. T. Cui, B. J. Edwards, D. J. Keffer, and W. V. Steele, *J. Phys. Chem. C*, **2008**. 112, 1985-1993.

(8) P. B. Balbuena, E. J. Lamas, and Y. Wang, *Electrochim. Acta*, **2005**. 50, 3788-3795.

(9) E. J. Lamas and P. B. Balbuena, *Electrochim. Acta*, **2006**. 51, 5904-5911.

(10) W. Goddard III, B. Merinov, A. Van Duin, T. Jacob, M. Blanco, V. Molinero, S. S. Jang, and Y. H. Jang, *Molecular Simulation*, **2006**. 32, 251-268.

(11) W. R. Cannon, B. M. Pettitt, and J. A. McCammon, *J. Phys. Chem.*, **1994**. 98, 6225-30.

(12) W. L. Jorgensen, J. Chandrasekhar, J. D. Madura, R. W. Impey, and M. L. Klein, *J. Chem. Phys.*, **1983**. 79, 926-35.

(13) D. J. Price and C. L. Brooks, III, *J. Chem. Phys.*, **2004**. 121, 10096-10103.

(14) W. D. Cornell, P. Cieplak, C. I. Bayly, I. R. Gould, K. M. Merz, Jr, D. M. Ferguson, D. C. Spellmeyer, T. Fox, J. W. Caldwell, and P. A. Kollman, *J. Am. Chem. Soc.*, **1995**. 117, 5179-97.

(15) S. Urata, J. Irisawa, A. Takada, W. Shinoda, S. Tsuzuki, and M. Mikami, *J. Phys. Chem. B*, **2005**. 109, 4269-4278.

(16) C. J. T. de Grotthuss, *Ann. Chim. (Paris)*, **1806**. 58, 54-73.

(17) N. Agmon, *Chem. Phys. Lett.*, **1995**. 244, 456-62.

(18) G. Hummer, D. M. Soumpasis, and M. Neumann, *Mol. Phys.*, **1992**. 77, 769-85.

(19) S. T. Cui and J. G. Harris, *Chem. Eng. Sci.*, **1994**. 49, 2749-63.

(20) G.-W. Wu and K.-Y. Chan, *J. Electroanal. Chem.*, **1998**. 450, 225-231.

(21) S. Picaud, P. N. M. Hoang, S. Hamad, J. A. Mejias, and S. Lago, *J. Phys. Chem. B* **2004**. 108, 5410-5415.

(22) S. Y. Liem and K.-Y. Chan, *Surf. Sci.*, **1995**. 328, 119-28.

(23) S. J. A. Koh, H. P. Lee, C. Lu, and Q. H. Cheng, *Phys. Rev. B* **2005**. 72, 085414/1-085414/11.

(24) W. G. Hoover, *Phys. Rev. A*, **1985**. 31, 1695-1697.

(25) S. Nose, *Mol. Phys.*, **1984**. 52, 255-68.

(26) S. Nose, *J. Chem. Phys.*, **1984**. 81, 511-19.

(27) M. Tuckerman, B. J. Berne, and G. J. Martyna, *J. Chem. Phys.*, **1992**. 97, 1990-2001.

(28) J. S. Carslaw and J. C. Jaeger, *Conduction of Heat in Solids*. Second Edition ed. 1959, Oxford: Oxford University Press.

Appendix E

Table 6. 1 Summary of the simulation conditions.

	5 wt%	5 wt%	20 wt%	20 wt%
no. of polymers	256	256	256	256
no. of H_2O	2640	2640	9088	9088
no. of H_3O^+ ions	768	768	768	768
total no. of particles	31728	31728	51072	51072
λ (H_2O/SO_3^+)	3.44	3.44	11.83	11.83
simulation time (ns)	2.0	2.0	2.0	2.0
no. of graphite atoms	864	1728	928	1856
no. of Pt atoms	5220	5220	5760	5760

Table 6. 2 Size of the three dimensions of the simulation cell for graphite/platinum systems. All units are in Å.

	7.4 Å gap			14.8 Å gap		
water content	*x*	*y*	*z*	*x*	*y*	*z*
5 wt%	115.02	136.10	125.18	115.02	136.10	139.94
20 wt%	123.54	139.35	132.55	123.54	139.35	147.32

Table 6. 3 Effective Diffusion coefficients (dimensionless).

water content	H_2O with no gap	H_2O with 7.4 Å gap	H_3O^+ with 7.4 Å gap
5 wt%	1.0	7.8×10^{-2}	4.0×10^{-2}
20 wt%	2.6	2.0×10^{-2}	3.3×10^{-1}

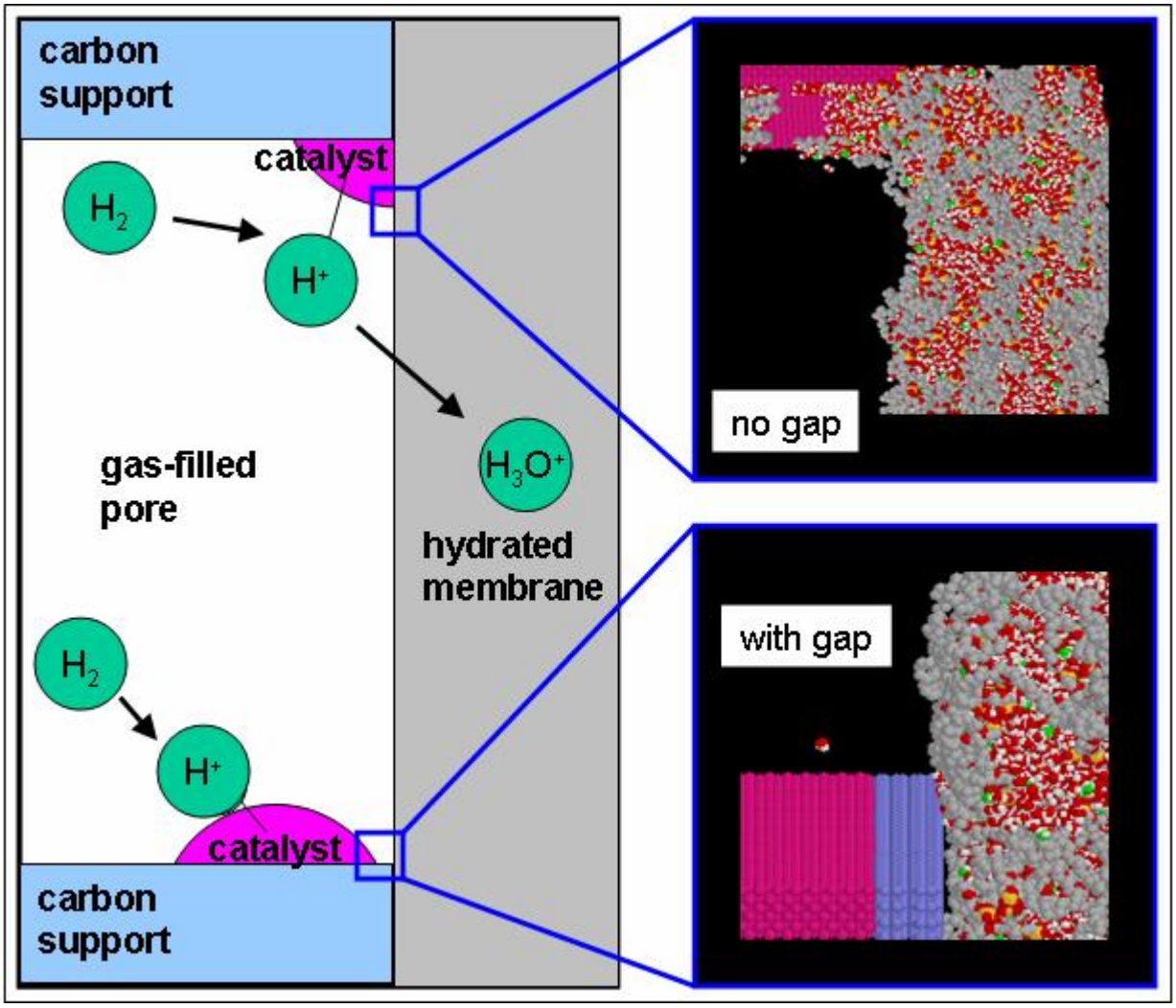

Figure 6. 1 A schematic of the molecular-level interfaces of interest at the electrode/electrolyte interface of the anode of a PEM fuel cell (not to scale).

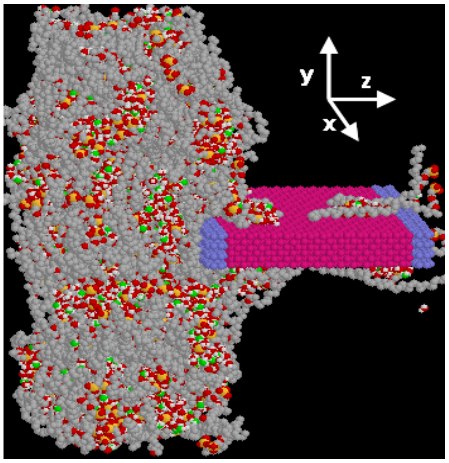

(a)

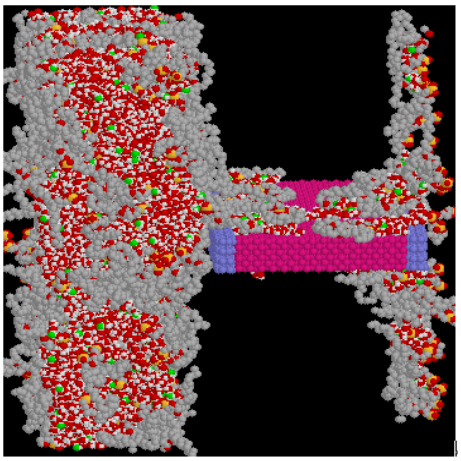

(b)

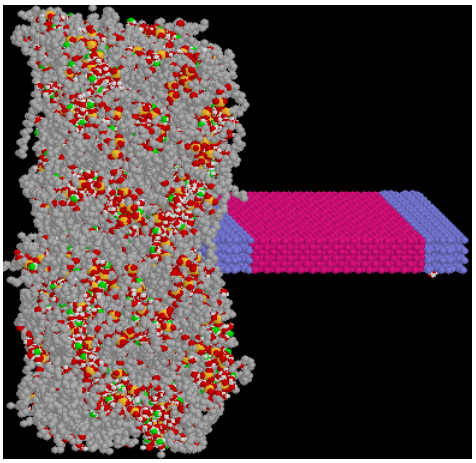

(b)

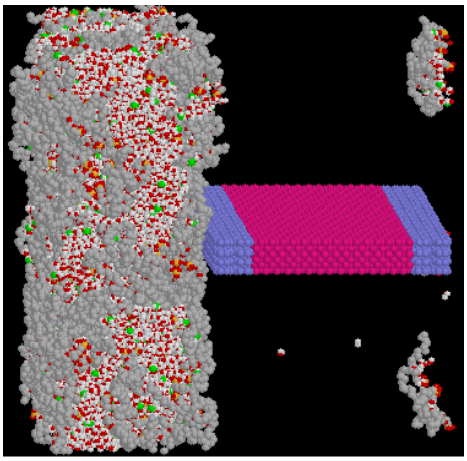

(d)

Figure 6. 2 Final snapshots of simulations containing the catalyst surface and graphite surface for water contents of (a) 5 wt% water and graphite gap size of 7.4 Å, (b) 20 wt% water and graphite gap size of 7.4 Å, (c) 5 wt% water and graphite gap size of 14.8 Å, and (d) 20 wt% water and graphite gap size of 14.8 Å. The color legend is as follows: CF_x groups are gray; sulfur, orange; oxygen of H_2O and SO_3^-, red; oxygen of H_3O^+, green; hydrogen, white; platinum, pink; graphitic carbon, gray.

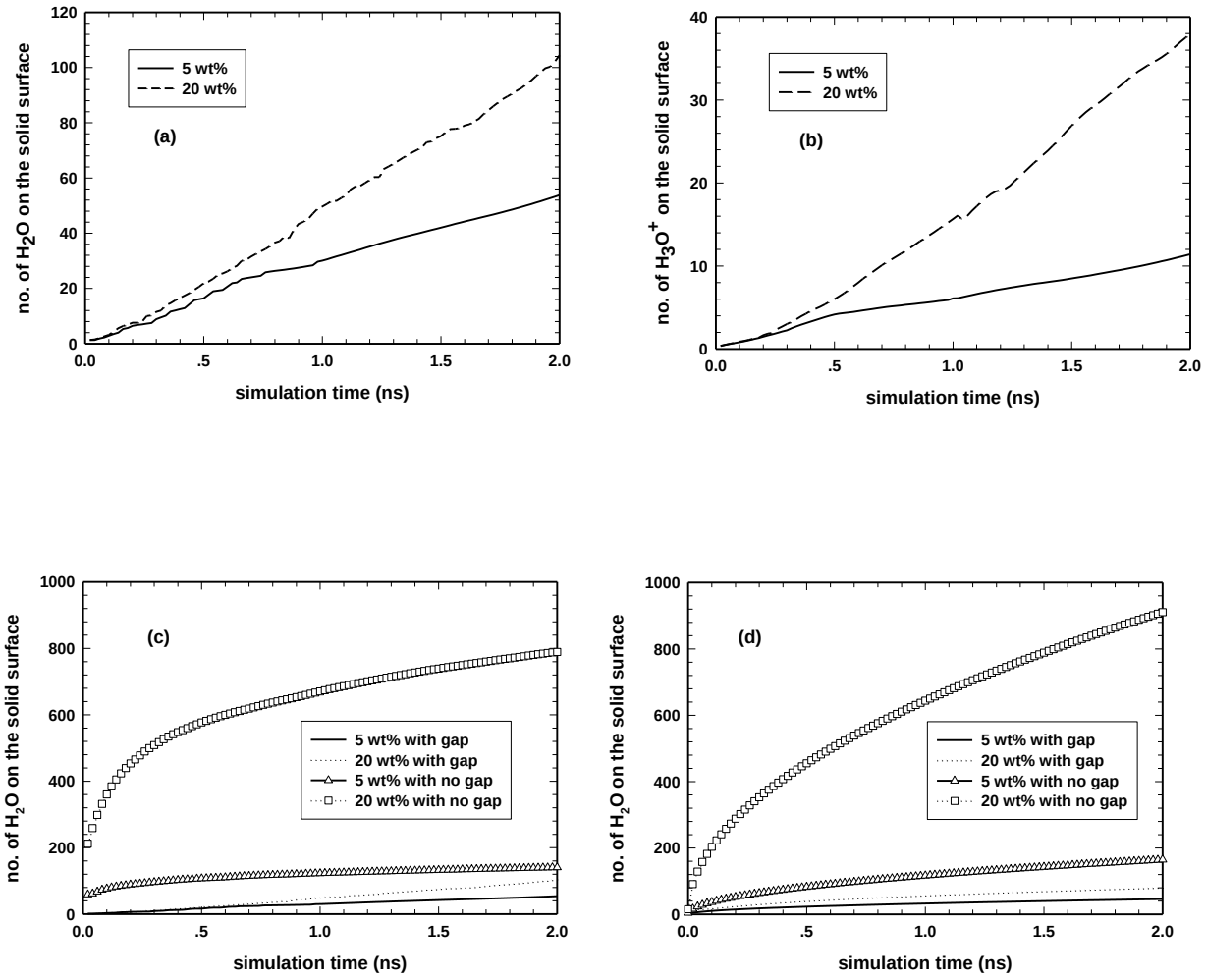

Figure 6. 3 Wetting dynamics of the solid surface for a graphite gap size of 7.4 Å as a function of time. (a) Number of water molecules on the solid surface. (b) Number of hydronium ions on the solid surface. (c) Number of water molecules on the solid surface with no gap and with a gap of 7.4 Å (data are from the MD simulations). (d) Number of water molecules on the solid surface with no gap and with a gap of 7.4 Å (data are from the coarse-grained model).

Chapter 7
Conclusions

Membranes based on perfluorosulfonic acid (PFSA) ionomers are of considerable interest in recent years due to their wide applications as the electrolyte in the fuel cells. Significant research is underway around the world to address the need for the novel membranes with higher proton conductivity, good chemical and mechanical stability, improved durability, and the capability to operate at high temperatures (> 100˚C) without the external humidification of the incoming reactant gases. Although numerous theoretical and experimental studies advanced our understanding of the morphological structures of these materials, it is widely accepted that there is still much more to be understood. One way aiding the implementation of such high-performance materials is tied to the understanding of how the chemical structure of the polymer affects the membrane hydrated morphology and the proton and water diffusion properties.

The chemical composition of the polymer materials has great impact on the hydrated morphology of membranes, such as backbone flexibility and relative hydrophobicity/hydrophilicity limiting and driving the extent of nanoscale phase separation. The hydrophilic regions resulting from the morphological structures form complex and irregular percolation pathways through which transport occurs. Water domain size and the nature of the hydrophobicity/hydrophilicity interface are believed to affect significantly the proton transport properties even though the interdomain aqueous structure is under debate.

One achievement of the present work is to vary several structural parameters of the polymer chemical makeup targeting to probe their effects on the membrane's morphology. Molecular-scale simulations here provide a valuable tool aiming at providing some hints on how to change the molecular structure of the polymer in favor of better connected water domains and efficient proton conduction.

Another important aspect of the present work is the understanding and investigation of the structural and dynamic properties at the interfaces within the membrane electrolyte assemblies (MEAs). The nature and distribution of water at these interfaces plays a vital role in determining the proton conductivity and the fuel cell performance. We focused on the membrane/catalyst and membrane/carbon interfaces to comprehend how the protons diffuse across them as a function of

water contents and how the distribution of the hydrated membrane and the separating distance between catalyst and hydrated membrane affect this conduction process.

In this final chapter of the dissertation, we first summarize each chapter, and then present overall aspects of the current achievement, followed by some future works.

In chapter 2, MD simulations were performed to investigate the structure and dynamics of hydrated Nafion trimers at four different water contents: 5, 10, 15, and 20 wt %. The simulations showed that the system forms a nanophase-segregated hydrophobic regions consisting primarily of the polymer backbone and hydrophilic regions with an inhomogeneous water distribution. It has been revealed that the water clustering strongly depended on the water content. At low water content, only isolated small water clusters were formed. As the water content is increased, it became increasingly possible that a predominant majority of water molecules formed a single cluster, suggesting that the hydrophilic regions became connected.

In chapter 3, MD simulations were performed to analyze the effect of the length of the side chain on hydrated morphology and hydronium ion diffusion in Nafion and the SSC PFSA membranes with the same polymeric backbone. The cluster distributions displayed distinctive differences at the low water contents (λ = 4.4 and 6.4); i.e., hydration of the SSC PFSA membrane tends to produce a more dispersed cluster distributions. At the high water content, the cluster differences between the two systems become very small, even though the SSC PFSA appears to show a slight tendency to be more connected. The simulations indicate that the SSC PFSA tends to induce more distributed aqueous clusters, and thus enhance the connectivity of the clusters through water channels, whereas the Nafion, with a longer and more flexible side chains, is more amenable to form water clusters that are more disconnected than the SSC PFSA. The diffusion coefficient of water and hydronium ions are both slightly lower in the SSC PFSA membrane when compared to Nafion, possibly because our simulations do not include the proton hopping mechanism which may be responsible for the observed higher conductivities in the SSC PFSA membrane.

In chapter 4, MD simulations were performed to investigate the effects of the side chain length, equivalent weight, and the polymeric molecular weight on the hydrated morphology and diffusion properties of water and hydronium ions in the SSC PFSA and Nafion membranes with each ionomer containing 15 monomer units. Membrane hydrated morphologies are studied at

five different hydration levels corresponding to λ ($H2O/SO_3H$): 3, 6, 9, 15, and 22. An increase in side-chain length results in a larger characteristic dimension of the aqueous domain, less local confinement for aqueous species, a more poorly connected global aqueous domain. A decrease in EW results in a larger characteristic dimension of the hydrophobic domain, less local confinement for aqueous species, and a better connected aqueous domain. Connectivity enhances and confinement reduces water mobility. A decrease in EW changes both factors (connectivity and confinement) to favor an increase in diffusivity. An increase in side-chain length changes the connectivity to decrease diffusivity but the confinement to increase diffusivity, which together result in little change in the observed water diffusivity. For the short chains studied, we find these results to be independent of MW.

In chapter 5, we performed MD simulations of the hydrated polymer electrolyte membrane/vapor/catalyst three-phase interface and the hydrated polymer electrolyte membrane/vapor/support three-phase interface, using Nafion, [100] platinum and graphite atoms. Characterization and analysis of the configurational and dynamic properties indicate that there is no wetting of the catalyst support surface (graphite in this work) and significant wetting of catalyst surface ([100] platinum in this work). The degree of wetting increases on the catalyst surface with the water content, but we do not observe more than a monolayer on the surface. This monolayer is composed of a mixture of water, Nafion, and hydronium ions. At high water contents, the water forms a regular lattice on the catalyst surface. We characterized the structure of water molecules and hydronium ions adsorbed to the catalyst surface by the pair correlation functions (PCFs).

In chapter 6, MD simulations were conducted to investigate the effect of a graphite gap between the hydrated membrane and catalyst particles on the ability to form paths by which protons can be transported from the catalyst to the membrane. At membrane water contents of 5 and 20 wt%, we found that a mixture of Nafion, water and hydronium ions was able to form a bridge across a graphite gap of width 7.4 Å and wet the catalyst surface. The degree of wetting increased with water content. For a gap size of 14.8 Å, we found no wetting of the catalyst surface for both water contents studied.

In summary, the present work focused on two parts. The first part was to use MD simulations to investigate the relationship between the polymer electrolyte membrane structure

and the hydration morphology, and the effects of the morphological changes on proton and water diffusion properties in the membrane. We varied three parameters: (1) the equivalent weight, (2) the side chain length, and (3) the molecular weight of the polymer. Firstly, Nafion ionomers with three monomer units (trimer) were investigated to probe the effects of different hydration levels on the cluster size. Secondly, Nafion and SSC PFSA trimers with the same backbone but different pendant side chains were simulated to examine the effects of the side chain length on the morphology and the proton conduction. Finally, MD simulations were performed to investigate the effects of side chain length, equivalent weight, and molecular weight by using the Nafion and SSC PFSA with each ionomer containing 15 monomer units. Since a low EW not only tends to form larger hydrophilic regions, less local confinement, and better connected aqueous domains, thus facilitating proton transport, but also reduces the mechanical strength of the backbone which causes the disintegration or dissolution of the membrane in the water, there may be an optimal EW which can be used to improve the membrane performance. The effect of side-chain length is not pronounced since the connectivity and confinement changes induced are towards opposite direction, which altogether results in little change of water diffusion.

The second part is to probe the structural and dynamic properties of the interfacial systems present in the PEM fuel cells. Firstly, our simulations show that the catalyst surface is likely covered by a mixture of water, hydronium ions, and Nafion PEM but not beyond a monolayer. The hydrogen atoms need to penetrate this monolayer to reach the catalyst surface and dissociate into protons and electrons. The formation of hydronium ions is dependant on the availability of water on the catalyst surface. Secondly, no adsorption of water molecules on the catalyst support surface (graphite) has implications for the effective utilization of catalyst. If there is no wetting of the support surface, then no transport of proton/hydronium ions will occur. Even though the hydrogen fuels will adsorb on the catalyst surface and dissociate into electrons and protons, if the protons can not reach the hydrated PEM, the catalyst particles can not contribute to the power generation. Thus the catalyst surface needs to be within some distance from the hydrated membrane beyond which effective proton/hydronium ions transport will not occur. Finally, we put the hydrophobic graphite carbons between the catalyst surface and the hydrated membrane to investigate the critical gap size through which a bridge can form to facilitate the proton transport.

The gap size is found to be on the order of 10 Å. The results provide a possible way to increase the efficiency of proton conduction and to economize the utilization of the catalyst.

Some future work is presented here on the basis of the achievement of the present work. Firstly, since the hydrated PFSA membranes are inherently inhomogeneous systems and the chemical structure of the polymers has a great impact on the hydrated morphology, thus how the various structure parameters of the polymer such as degree of polymerization, molecular structure, equivalent weight, side chain length, molecular weight, and crosslinking etc., collectively affect the proton and water diffusion properties needs further investigation. The findings of this work provide insight and help in the direction.

Secondly, as for the interfacial systems within the MEAs, fundamental work is required to study the adsorption and dissociation of molecular hydrogen on catalyst surface with adsorbed layers, such as those described herein. Moreover, the overall diffusion of protons (including vehicular and structural diffusion) across this surface, as a function of water content, must be investigated at a fundamental level, if one is to quantitatively understand the molecular mechanisms for proton transport at the electrode/electrolyte interface.

Thirdly, we are now investigating the interfacial properties at the hydrated Nafion/carbon/water and hydrated Nafion/catalyst/water interfaces. We hope to elucidate whether the Nafion membranes can dissolve when they are in close contact with bulk water. The result may have a practical benefit for the operation of fuel cells in reality.

Vita

Junwu Liu was born in Benxi city, Liaoning province, China on October 28, 1973. He was raised in his hometown and went to elementary, middle, and high school there. After graduating from Benxi No.1 high school, he went to the Northwest Institute of Light Industry (now named Shanxi Sci & Tech University), Xianyang, Xian, and received a Bachelor's Degree in Leather Engineering in 1996. After graduation from college, he worked in Xi'men Intex Plastic Co., Ltd for 4 years from 1996-2000. He was a process manager during the first year, then a technical manger during the following three years. He was in charge of the optimization of manufacturing process and supervision of technical department. From 2000- 2002, he worked in Dandong Leather Chemical Insitute as a research and process manger. He was in charge of the R&D of tanning agents, coating materials, and fatliquoring agents used in the leather production. And from 2002-2005, he was employed by China Leather & Footwear Industry Research Institute. He took the responsibility of research and development of tanning and finishing agents and coordinated with the marketing department to facilitate the promotion. He entered into the Ph.D. program in Chemical Engineering at the University of Tennessee, Knoxville, TN in 2005